# Optimising hydrogen based energy storage systems using super capacitors


## A.K. Townsend

**orcid.org/0000-0002-4712-7928**


Dissertation accepted in fulfilment of the requirements for the degree *Master of Engineering in Electrical and Electronic Engineering* at the North West University

Supervisor: Prof R Gouws

Co-supervisor: Mr. C. Martinson

Graduation: June 2021

Student number: 24898813

# EXECUTIVE SUMMARY

One of the greatest challenges when it comes to the efficient energy use in unmanned aerial vehicles is that of the energy storage systems. As drones require minimal weight to have optimal mobility the capacity of the energy source is reduced to decrease the weight. This reduction decreases the flight time of a drone. Batteries overcome the weight issue but have a low power density and perform poorly at peak power demands. A larger power source is found in hydrogen fuel cells that possess a very high energy density, but this comes with an increase in weight and they too have a low power density. A solution to this problem is found in the hybrid combination of these two power sources. However, as they both have low power densities, they still perform poorly at peak power requirements. Super-capacitors are presented as a solution to this problem as they have high power densities and respond significantly better to peak power demands. Previously, super-capacitors have been combined with fuel cells, and in some cases batteries, to improve the functionality of hydrogen vehicles, with small improvements observed and suggestions made to incorporate all three power sources to supply the required load.

The research presented in this dissertation requires the analysis of a hybrid system designed with drone application in mind. Due to the low energy density of super-capacitors many are required to deliver a sufficient voltage level and an increase in the quantity leads to an increase in weight – in some cases – preposterously. This research thus presents the solution of combining the super-capacitors with an appropriate DC-DC converter to assess the effect thereof on the super-capacitors' capacity as well as the operation of the hybrid system as a whole. The proposed DC-DC converter was verified through simulation and validated alongside the entire system through laboratory implementation. A load profile obtained from an existing hydrogen fuel cell drone was used to assess the experimental operation of the system. Six tests were conducted using the different power sources and the load profile. The fuel cell system and super-capacitor bank were all tested individually for the first two tests; the next two tests consisted of combining the super-capacitor bank with the fuel cell and a switching module – these tests consisted of two rounds varying the order of connection; two additional tests were conducted with the inclusion of the DC-DC converter.

From the results obtained through the experimental tests the fuel cell – super-capacitor combination utilizing a DC-DC converter was seen to provide the longest duration of 365 s, the highest energy and power density of 0.70 Wh/kg and 73.5 W/kg, respectively, and an overall efficiency of 96.25%. In obtaining these results the objectives and requirements of this research were met. The findings of this dissertation are not restricted to drone applications as they include outcomes pertaining to super-capacitors and their combination with a DC-DC converter.

Key words: super-capacitor; fuel cell; DC-DC converter.

# ACKNOWLEDGEMENTS

For my parents, I blame you for believing in me and so, I simply had to. For your love, support and provision of sanity and morality, I am forever thankful - no better humans have ever lived.

My gratitude to my supervisor, Prof. R. Gouws and Mr. P. Van Huyssteen for all their assistance and guidance.

This material is based on research/work supported wholly/ in part by DST HySA infrastructure. The findings are that of the author and not that of DST HySA.

# TABLE OF CONTENTS

# LIST OF FIGURES

# LIST OF TABLES

# NOMENCLATURE

## List of Abbreviations

| | |
|---|---|
| AAFC | Aluminium Air Fuel Cell |
| AC | Alternating Current |
| ADC | Analogue to Digital Conversion |
| AFC | Alkaline Fuel Cell |
| ANN | Artificial Neural Network |
| BJT | Bipolar Junction Transistor |
| CCM | Continuous Conduction Mode |
| CSP | Concentrated Solar Power |
| DC | Direct Current |
| DCM | Discontinuous Conduction Mode |
| DLC | Double Layer Capacitor |
| EC | Electric Capacitor |
| EMF | Electromagnetic Field |
| EMI | Electromagnetic Interference |
| ESFC | Electric Storage Fuel Cell |
| EV | Electric Vehicle |
| FC | Fuel cell |
| FET | Field Effect Transistor |
| FPGA | Field Programmable Gate Array |
| GDL | Gas Diffusion Layer |
| HALE | High Altitude |
| HDL | Hardware Description Language |
| HTFC | High temperature Fuel Cell |
| HV | High Voltage |
| I/O | Input/output |
| IDE | Integrated Development Environment |
| IEC | International Electro-technical Commission |
| IEEE | Institute of Electrical and Electronics Engineers |
| IGBT | Insulated Gate Bipolar Transistor |
| IPT | Inductive Power Transfer |
| LA | Low Altitude |
| LED | Light Emitting Diode |
| Li-ion | Lithium-ion |
| Li-Po | Li-Polymer |
| Li-S | Lithium-Sulphur |
| Li-SOCl2 | Lithium-Thionyl-chloride |
| MCFC | Molten Carbonate Fuel Cell |
| MEA | Membrane Electrode Assembly |
| MOSFET | Metal Oxide Semi-conductor Field Effect Transistor |
| MPH | Mild Parallel Hybrid |
| MPT | Microwave Power Transfer |
| NiCad | Nickel Cadmium |
| NiMH | Nickel Metal Hydride |
| PAFC | Phosphoric Acid Fuel Cell |

| | |
|---|---|
| Pb-acid | Lead -acid |
| PEFC | Polymer Electrolyte Fuel Cell |
| PEM | Proton Exchange Membrane |
| PH | Parallel Hybrid |
| PHE | Plug-in Hybrid Electric |
| PID | Proportional Integral Derivative |
| PIH | Plug in Hybrid |
| PLC | Programmable Logic Controller |
| PV | Photovoltaic |
| PWM | Pulse Width Modulation |
| SABS | South African Bureau of Standards |
| SAFC | Solid Acid Fuel Cell |
| SANS | South African National Standards |
| SC | Super-capacitor |
| SH | Series Hybrid |
| SMC | State Machines Control |
| SOC | State of Charge |
| SOFC | Solid Oxide Fuel Cell |
| SPH | Series Parallel Hybrid |
| TSP | Travelling Salesman Problem |
| UAV | Unmanned Aerial Vehicle |
| UV | Unmanned Vehicle |
| WCT | Wireless Charging Technique |
| WPT | Wireless Power Transfer |
| Zn-O2 | Zinc Oxide |

# CHAPTER 1: INTRODUCTION

This chapter serves as the introduction to the remainder of the dissertation, providing essential background information necessary to clarify the purpose of thereof. This chapter includes a problem statement to elucidate the necessity of combining super-capacitors (SCs) with fuel cells (FCs), it provides some background to the problem statement as well as the methodology with which the problems are addressed. This chapter also outlines the scope of the project that is conducted in this dissertation, providing research questions and success factors with which to verify and validate the project and ends with a conclusion highlighting the contents of this chapter.

## 1.1 Background

The world is becoming more technologically reliant and this is increasing the requirement for autonomy and mechanization, where human error can be reduced [1]. There are many applications involving visual condition inspections where humans have become expendable due to inaccessibility, stealth requirements, safety considerations and viability, applications where the purpose necessitates minimal noise and a small size [2]. An Unmanned Vehicle (UV) is a vehicle that operates without the need of a physical pilot/driver on board. Any and all communication with the vehicle is done via on-board computers and a remote control of sorts [3], [4]. UVs can offer the aforementioned characteristics, but still require a surface to operate on and many of the aforementioned applications lack the availability of such surfaces. Unmanned Aerial Vehicles (UAVs) however, do not require a continuous surface of operation, as they are aloft and are therefore ideal for these applications.

UAVs have a couple of advantages and disadvantages, the former including, low operating costs, good camouflage, good mobility and has simple and easily available technology compared to manned aircrafts [5]. UAVs can also be beneficial where the use of manned aircrafts is impractical, expensive or risky. All of the above make UAVs a very efficient and economical alternative to manned aircrafts [6]. Most UAVs are relatively small, mobile and very quiet and offer less interference due to wind direction or speed changes, they also offer a wide range of applications. There are however some disadvantages, they can have a limited capacity due to their size and each type of UAV has variously limiting flight times [7] and unfortunately, the smaller UAVs do not solve the mechanization issue to the required extent as they have one predominant flaw, the power supply is inadequate [8]. It is notable to mention that the larger drones, mainly used in military applications, do have an adequate power supply, however, due to this they're much larger, noisier and significantly less mobile. Another major complication drones have is that if one issue is improved another issue is created. For example, increase the power supply capacity for a longer flight then the size and mobility of the drone is suddenly at a disadvantage [9]. A power supply is directly proportional to a longer flight endurance and an adequate one along with mobility and being minimally affected by the

surrounding environment is imperative when choosing a UAV [10]. There are many different power sources available on the market, such as batteries, solar power, FCs, combustion engines, etc., most of which can be applied to drones. Over the years some of these power sources have been disregarded as they have more disadvantages than advantages regarding this specific application, some of these include having a too large weight or size, being restricted to specific movements or simply not having a large enough energy density. Figure 1.1 depicts a Ragone plot of selected energy sources illustrating the power density with respect to the energy density. These help to give a better understanding of why some sources are preferred over others.

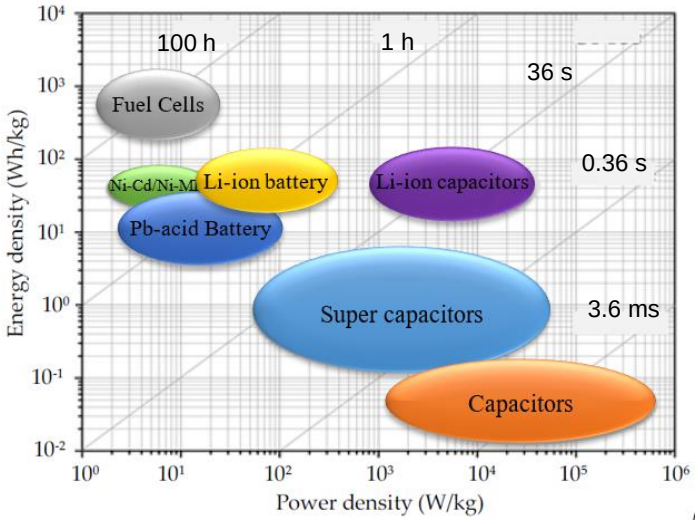


**Figure 1.1: Ragone plot of selected energy sources (adapted from** [11]**)**

The power density refers to the amount of power contained within the volume capacity of a source that it can provide at a specific instance, whereas the energy density refers to the energy (Wh) contained within the volume capacity of a source, therefore how long it can provide a specific amount of power. From Figure 1.1 it can be seen that SCs can provide a large amount of power (80-75 000 W/kg) but for a short period of time (energy density: 0.9-0.1 Wh/kg). FCs can provide a small amount of power (1.5-20 W/kg) for a larger period of time (energy density: 200-3 000 Wh/kg). Li –ion batteries are similar to FCs as they too can provide a small amount of power (15-400 W/kg) for a relatively long period of time (energy density: 20-150 Wh/kg) [11].

Currently the demand for UAVs is mainly consumed by military applications, however in recent years the demand in commercial, recreational and public applications has increased tenfold and it is expected to exponentially shift more in this direction [12], [13]. The use of UAVs in criminal, theft and poaching surveillance is one of the major applications [14], another being for the application in scientific monitoring (water sampling, landslides, volcanic activity) and transmission line surveillance [15]–[18]. At present combustion engines remain the most popular power supply for UAVs although electrical systems offer a higher efficiency, can be more reliable, have low to no greenhouse gas emissions and minimal noise [2]. This gives an indication as to why these systems are becoming more prevalent. Electrical systems extends to batteries, FCs and solar power, amongst others, and

will be further explained in section 2.2 of this dissertation. Below is a Table that contains the flight times of different UAV's and their respective power sources.

**Table.1.1: UAV Flight time (adapted from[41])**

| UAV | Flight time hours : minutes | Power source |
|---|---|---|
| **Boeing Condor** | 58:11 | Gasoline |
| **General Atomics GNAT** | 40:00 | Gasoline |
| **TAM-5** | 38:52 | Gasoline |
| **RQ-4 Global Hawk** | 33:06 | Gasoline |
| **QinetiQ Zephyr Solar Electric** | 336:22 | Solar |
| **DJI Mavic 2 Zoom** | 00:31 | Battery |
| **Hydrogen drone** | 77:00 | Hydrogen FC, estimated using [1] |

From the table it is quite obvious that the drones that run solely on battery power are far inferior to those powered by solar and gasoline. Solar and gasoline do however have disadvantages compared to a battery. The gasoline powered drones require an engine that is quite heavy, making the drone much larger compared to the other two [19]. Solar powered drones require vast expanses of solar panels [20], again making the physical aircraft much larger [21]. The battery powered drone is much lighter and can be manufactured significantly smaller than the other two aircrafts, but it is seen that the battery powered drone only lasts a fraction of the time of the other drones [22].

## 1.2 Problem statement

Since drones have become more prevalent, many researchers have been evaluating the efficiency of drones and methods to increase the flight times thereof [23], [24]. There are mainly two options in achieving this goal, replace the power source with one of a greater capacity or refuel the power source sporadically [25]. The latter requires the use of refuelling stations, which in itself presents more problems; the UAV will be required to land periodically and refuel throughout its flight, decreasing the actual usable flight time; stations will be required along the flight path, limiting the range and path, decreasing mobility and increasing complexity. All of this increases the overall costs unnecessarily. The former option in increasing the flight time includes more possibilities that can be simpler to implement and ultimately more cost effective. To name a few: the capacity can be increased through replacement with the same power source (or a different one) with a larger capacity, or the existing power source can be combined with another to exploit the benefits of both (Hybridization). All of these options [26] have their respective advantages and disadvantages, which will be discussed in more detail in section 2.1.

FCs have advantages including [27], no direct pollution, no sound, the refuel/ recharge time of a hydrogen FC is only limited to the availability of hydrogen in the environment and the speed of the acquisition of the hydrogen. According to [20] a hydrogen FC, compared to a similar Lithium Polymer

(Li-Po) battery, has an increase in energy density by a factor of 150, which is also superior to the gasoline powered UA; however, a hydrogen FC has the disadvantage of a lower power density than that of the gasoline UAV, meaning that peak power requirements drain the FC significantly, limiting the applications and flight time [27], [28]. Hydrogen FCs are often combined with Li-Po batteries to improve the power density however, batteries have a similarly low power density. Thus, although the addition of a battery can increase the endurance of the system and improve peak power performance, it does not increase them to the desired point and both power supplies are still significantly drained during these peak power instances, still limiting the flight time of the system.

SCs have a very large energy capability with a fast release aspect, this means that the capacitor can provide very large amounts of current over very short periods of time. However, SCs are very large in size (and weight) when compared to Li-Po batteries of equivalent capabilities, making the drones quite large in size again. Although the SCs have small energy densities compared to batteries they offer the quick bursts of energy during the peak power demands and can store energy quickly that would otherwise be lost [20]. Thus, the addition of SCs to any of the energy sources mentioned should lead to much better efficiencies of UAV's especially during peak power requirements.

As SCs are relatively new they are quite expensive and little research has been done pertaining to their application in combination with FCs. The available hydrogen FC is currently being used in combination with a Li-Po battery of similar power- and energy densities. It is thus beneficial to examine how the use of SCs, with Li-Po batteries, can affect the functionality of a FC. This dissertation proposes the project of analysing these hybrid combinations with the future expectation of replacing the power source of a hydrogen FC UAV.

## 1.3 Objectives

The objectives of this project are categorized under two headings, primary- and secondary objectives. The former will have the main objectives of the project pertaining to the aim thereof, while the latter will contain the more detailed objectives required to complete the primary objectives.

### 1.3.1 Primary objectives

A FC system is available for use in this project, that is designed (and controlled) to use a Li-Po battery to supplement power when required by the FC. The goal of this project is to investigate the effect of adding a SC bank to this combination. As this design is for a drone, weight and size considerations will be made. Thus, a boost DC-DC converter will be required to increase the voltage capabilities of the capacitor bank such that the weight and power characteristics of the battery can be matched.

### 1.3.2 Secondary objectives

In order to fulfil the primary objectives, the following secondary objectives will first need to be met:

1. A SC bank is required that combines SCs in a configuration that matches the energy, weight and size requirements similar to that of the Li-Po battery and the FC system. The energy requirements for peak power instances will need to be calculated such that sufficient energy is stored in the bank for the duration of the load requirement. The voltage of the bank will need to match the continuous voltage of the FC and the current supply would need to be sufficient to adjust to the power requirements accordingly.
2. As this experiment is for the future combination with a drone, the size and weight considerations are of utmost importance – it will need to be determined whether the weight of the capacitor bank will exceed that which is feasible and thus require a DC-DC converter to allow for the reduction in the size of the bank. The power and energy conservation rules will apply in investigating the best converter to combine the banks with the FC. For this the converter should be able to boost, be uni-directional and able to withstand the high-power requirements. A few options for this application exist and will therefore be examined to determine the most suitable.
3. As the capacitor bank will vary in voltage output the converter will need to be designed to self- adjust the duty cycle according to the input in order to provide a constant output.
4. In order to fully understand the effect of this combination other combinations of the sources will be required to use as a basis of reference. These combinations will be the sources individually (FC-battery combination, SCs without DC-DC converter, SCs with DC-DC converter) and the FC & SC combination.

## 1.4 Scope of the study

This project is focussed on investigating the effect of the combination of SCs with an existing hydrogen FC through the use of a DC-DC converter and the load profile of an existing hydrogen drone. The scope of this project is divided into four key areas which will be discussed below.

### 1.4.1 Super-capacitor bank

A load profile of a hydrogen drone will be obtained and used to determine the characteristics required for the SC bank. The FC, having a high energy density, will be used to supply the load when a constant (average) power is required. The SCs will be implemented to provide additional power and energy to the FC when the load has instances of peak power requirements. This is due to the SCs ability to deliver bursts of energy (that is large amounts of power for a very short period of time). The configuration of the SC bank is based on the maximum duty cycle of the DC-DC converter (70%) as well as the maximum voltage that each SC can supply (2.7 V). The FC available will also be used to determine the energy and power requirements of the SC bank. The SC bank will also be required to

be under a certain weight as the application of this power source pertains to use in drones and drones are heavily affected by weight variances in terms of balance of the drone.

### 1.4.2 DC-DC converter

As the SCs have a minimum voltage of 2.7 V each, they will be combined in a configuration that will allow the DC-DC converter to operate in its allowable region, where the duty cycle does not exceed 70%. The FC system is currently designed to function bi-directionally towards the battery; therefore, the battery can supply the necessary power and when depleted below a certain percentage the battery will be recharged by the FC. Ideally the DC-DC converter for the SCs should function in the same manner, however, as the FC system available is designed for continuous operation and it is connected to an “unlimited” supply of hydrogen, it will be difficult to examine the effects of the replacement of the battery with the SCs, as the system will continuously provide power and recharge when required. Therefore, it is desired that the DC-DC converter be uni-directional such that it only allows current to flow from the SCs to the FC/ load. This will allow the SCs to deplete to their recommended voltage such as which would occur once the hydrogen storage runs out. This area of operation will give a better idea of how the system will function with this combination. The FC system is designed to indicate and return once the hydrogen storage needs to be refuelled.

Therefore, for this project it is desired to see how much hydrogen is used for each combination and each repetition of the load profile thus determining the duration of the power source with a specific amount of hydrogen stored. The DC-DC converter is required to be a uni-directional boost converter, such of which exists a few configurations which will be examined for efficiency in this application. The converter is desired to have minimum components and a small circuit to allow the entire system to match the weight characteristics of the existing Li-Po battery configuration.

### 1.4.3 Control system

In this section the control method (i.e. Fuzzy Logic, Artificial Neural Network, etc.) and the control device (i.e. microcontroller) will be researched. It is important to determine which method and device will allow the system to operate seamlessly and with minimal delay, as this system is being designed for optimal flight time. This system will be designed such that the energy use will be maximized throughout the entire system. These methods will be included in the literature study, but as they, in themselves, create a project this will not be the main focus. The main focus of this section will be the use of the controller with the switch. A number of microcontrollers will be researched with weight, size and functionality in mind. Some criteria that the microcontroller will need to fulfil includes high switching frequency, Pulse Width Modulation (PWM) enabled pins, user simplicity, personal preference and open source code availability.

### 1.4.4 Power source combinations

In order to actually examine the effect of the SC combination with the FC effectively, some other combinations' results will be required. These results can then be used as bases of reference, such as the hydrogen usage, the response to peak current requirements, the repetition quantity and size and weight characteristics.

## 1.5 Research Methodology

The research process of this project will be conducted in different phases namely: literature survey, design and simulation of the system and implementation, tests and results of the system. The literature survey will help to discover the respective components required and the tests that need to be conducted on the final system, the simulations are required to compare component values for maximized results and finally the tests will help determine whether the system is setup as best it could be. These phases will all be verified and validated in order to determine whether the correct system was built and also whether it was built correctly.

### 1.5.1 Technology and Literature review

A broad literature study will be conducted and documented in the dissertation in order to ensure that all aspects of the project have been researched and that the possible solutions to the proposed problem have been investigated leading to the best solution. The literature survey will include journal articles, conference proceedings and book references relating to each topic. Any case studies regarding the topics will also be investigated to determine how the topic has previously been approached.

### 1.5.2 Design and Simulations

After the literature survey has been completed the information can be used to design the system that will eventually be built to conduct the tests and make a conclusion regarding the problem statement. The first step in this design is the conceptual design which contains trade-off matrices that help to determine the best component from a list of options for the specific application. Once this study has been completed the detail design of the system can be done. After the system has been designed and before it can be built simulations will be used to determine the relevance of the design and to finer tweak any component values. Once the simulations produce the desired results the components will be ordered so that the system can be built. As this system will require the use of a microcontroller the software will also need to be developed and tested before it is implemented into the final system. For both the software and simulations mathematical simulation software will be used such as Matlab®'s simulation tool Simulink® and LTspice®.

### 1.5.3 Implementation, Tests and Results

Once the system has been simulated, the desired results achieved and all the components have been acquired the system will be built so that relevant tests can be conducted to determine whether the system is in working order and also to determine whether the system will be able to solve the proposed problem. The results from the tests will be used to determine, mainly, whether the system is a relevant solution to the proposed problem but also how the system could be improved to possibly be a viable solution.

### 1.5.4 Key Research Questions

The following questions will be used as a guide in completing the literature study and aid in completing the design of the system.

1. How does the SC bank affect the operation of the FC?
2. Was the SC able to improve the provision of the peak power requirements of the system?
3. Which combination of SCs and FC provided the longest flight time?
4. Which combination of SCs and FC had the best power- and energy density?
5. Is the system better or worse than the current system?

### 1.5.5 Verification and Validation

The Verification and Validation process are very crucial to the completion of this dissertation to determine whether the goals and objectives of the project have been reached. These two processes are complementary, where Validation refers to whether the right project was built, and verification refers to whether the project was built right. If one of these processes are not done correctly then both are incorrect. These two processes will be used throughout the project at different stages as shown in Figure 1.2 below.

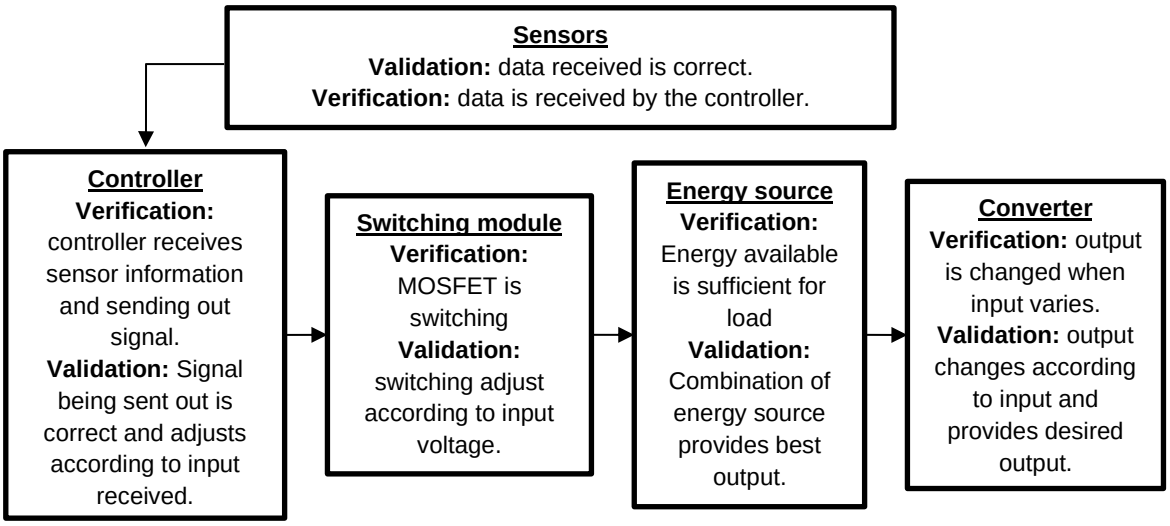


**Figure 1.2: Verification and Validation Process**

## 1.6 Publications and Peer Reviews

An effort was made to receive feedback on the relevance of the topic of this dissertation in the field of power electronics and energy. Two articles were submitted of which one has been accepted and another is under review. Citations of the publications are given below with the full texts available in Appendix A.

1. A. Townsend, I. N. Jiya, C. Martinson, D. Bessarabov and R. Gouws, “A comprehensive review of energy sources for unmanned aerial vehicles, their shortfalls and opportunities for improvements”, in *Heliyon 6.11 (2020) Elsevier*, pp. 1-22, doi.org/10.1016/j.heliyon.2020.e05285, ISSN: 2405-8440. [Published]

   **Article abstract:**

   *Unmanned Aerial Vehicles were first introduced almost 40 years ago and their applications have increased and diversified substantially since then, in both commercial and private use. One of the UAVs main issues when it comes to mobility is that the power sources available are inadequate, this highlights an area for improvement as the interest in drones is on the increase. There exist many different types of power supplies applied to UAVs, however each has their own limitations and strengths that pertain to weight contributions, charging and discharging times, size, payload capabilities, energy density and power density. The aim of this paper is to review the main power sources available for UAVs, determine their shortfalls, compare the power sources with each other and offer suggestions as to how they can be improved – hence identifying where the gap lies for developing better alternative power sources.*

   **Sections of dissertation contributed to article:** section 1.1, 2.2, 2.3.1, 2.3.3, 2.3.4, 2.3.5.

2. A. Townsend, C. Martinson, D. Bessarabov and R. Gouws, “Effect of super-capacitors on the operation of an air-cooled hydrogen fuel cell”, in *Heliyon (2021) Elsevier*, pp. 1-27, ISSN: 0360-3199. [Submitted]

   **Article abstract:**

   *One of the greatest challenges associated with efficient energy use in unmanned aerial vehicles (drones) is that of the energy storage systems – more specifically it’s weight and capacity. Current hydrogen fuel cell drones have very promising flight durations but have a low power density thus performing poorly at peak power demands. Supercapacitors are known to have high power densities and respond significantly well to peak power demands. For this research it is desired to evaluate how supercapacitors can affect the operation of an existing hydrogen fuel cell system, when combined. This study will include the evaluation of the viability of a DC-DC converter used to reduce the size (and subsequently, weight) of a supercapacitor bank. It also evaluates whether specified switching of the sources has an effect. Using data generated from the experiment it was determined that the DC-DC converter (with efficiency >94%) reduced the efficiency (by 0.5%) and duration (by 3.8%) of the supercapacitor bank whilst increasing the*

*weight (by 16.7%). It was also seen that the method of selective switching offered no benefit over that of a self-selecting system, where the former obtained 223 s of usability and the latter 365 s. However, comparing all the results it was observed that the addition of a supercapacitor bank allowed for an improvement in energy- and power density, of the hydrogen fuel cell system, from 0.65 Wh/kg to 1.19 Wh/kg and from 69.7 W/kg to 125.7 W/kg, respectively.*

**Sections of dissertation contributed to article:** sections 1.2, 2.2, 3.1, 3.2.1, 3.2.5, 4.1.1.1, 4.1.1.2, 4.2.2, 4.3.3, 4.3.4, 4.4, 5.4.

## 1.7 Dissertation Overview

This dissertation is composed of five chapters and one appendix, Chapter 1 gives a background overview and introduction to the dissertation, Chapter 2 involves the literature study – looking at the alternative solutions to the problem mentioned in Chapter 1 and discusses the different aspects of the project. The design of the project will be discussed in Chapter 3, distinguishing between the conceptual design, those aspects that still need to be decided upon, and the detail design, showing the preliminary idea of how the project will look and function. The detail design includes the simulations of the circuit, the circuit board's design, the pseudo code of the Arduino program and the calculations required to determine the SCs size. In Chapter 4 the system will be physically built, integrated and tested to determine whether it solves the problem statement. Chapter 5 will contain an overall summary of the dissertation, the verification and validation of the project and any recommendations for further improvements or adjustments to the performance of the system.

## 1.8 Conclusion

This chapter served as the introduction to the dissertation, detailing the problem statement, giving a brief background leading to the problem statement and discussing the objectives necessary for completion of this project. These aspects are all important as they give the dissertation a structure that can be followed throughout. The key research questions mentioned in this chapter will be used to determine whether the objectives have been met and they will be assessed using the validation and verification of each chapter in this dissertation. A summary of the dissertation was also provided in this chapter.

Chapter 2 will give a more detailed overview of the project by presenting a literature study that will highlight key points of the dissertation in order to give a better understanding of the problem statement. These key points will also be used to develop the solution to the problem statement.

# CHAPTER 2: LITERATURE STUDY

This chapter contains the majority of the research required for this project. It contains the literature study of the major components of this project, shown in Figure 2.1. This figure outlines the subsections of this chapter and contains the topics that are discussed. Each block in the figure is researched in depth referencing published documents pertaining to them. Some of the topics are linked to each other and these interactions are shown in Figure 2.2. These interactions will help to distinguish between the different options under each topic as well as give an indication of how this research can be verified and validated.

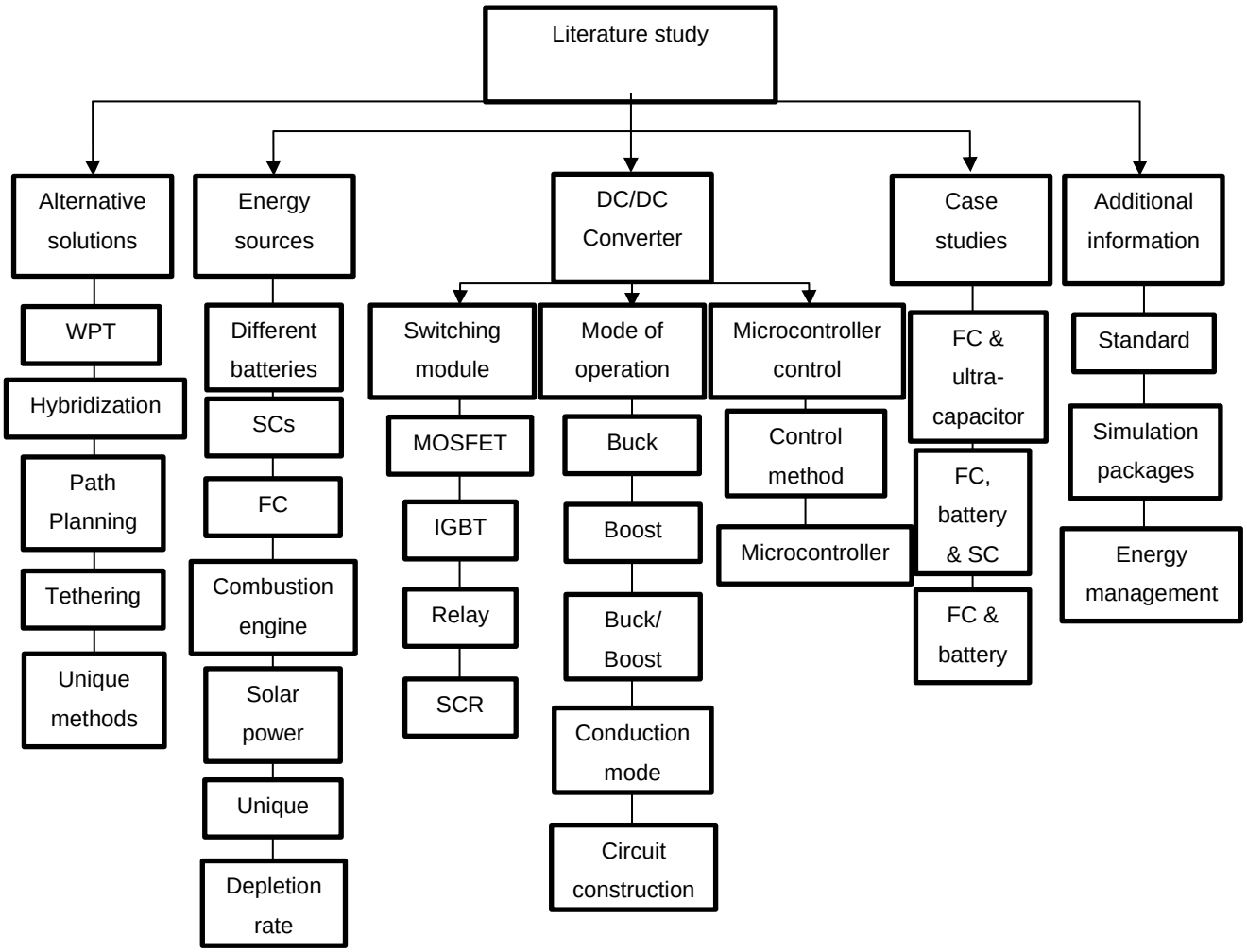


**Figure 2.1: Literature review plan**

## 2.1 Alternative Solutions

Drones have many different applications in which they could be used. However, their use therein is often disregarded due to certain aspects that make them unwarranted. These aspects include: the flight time, ease of transport, the requirement of a licence to fly it and a specified technician to maintain the craft. All of these factors can be ignored, even if slightly, if the flight time was to be improved. As this is also the problem statement of this dissertation this will be the main focus of the research of alternative solutions. There are some possible solutions to improve the flight time of

these power sources, i.e. Wireless Power Transfer (WPT) (gust soaring, Photo-voltaic (PV) arrays, Laser and battery dumping), Electromagnetic field (EMF)-based techniques, Hybridization. These techniques will be discussed in order to determine their relevance to the topic.

### 2.1.1 Wireless Power Transfer

The WPT utilizes magnetic resonant coupling of two parallel planar circular coils, one being the on-board receiver and the other being on the base station acting as the transmitter [29]. The idea of WPT has been around since the days of Hertz and Tesla, however, ambient power density at high frequencies is too low for practicality. In recent years this issue has been addressed with the development of solid-state electronics and the availability of wide band gap transistors and diodes, allowing the WPT systems to be designed for significantly higher frequencies whilst reducing the size of the system and increasing its efficiency [30]. The development of this technology could potentially remove the necessity of batteries, requiring periodic replacements, this can therefore reduce costs of maintenance [31]. One of the big limitations of drones is the reduced autonomy and need for human interaction to recharge the battery, to overcome this a base station can be created that allows automatic recharge of the batteries [32]. The base station can recharge the batteries either through a wired or a wireless system, the former tends to be more energy efficient but less reliable due to mechanical contacts that are exposed to the elements leading to extra maintenance and therefore decreasing efficiency. The wireless method allows a system to be used that has a slightly lower efficiency than the wired one but with a significant improvement regarding reliability.

WPT is a collective term referring to a number of methods of transmitting power by means of physical fields. This technique involves transmitting electromagnetic energy from the source to a receiver without the use of connecting cables. WPT can be divided into 2 main types, radiative (Far field WPT) and non-radiative (near-field WPT). The former having low efficiency but a long transmitting distance and the latter being more efficient over small and medium transmitting distances. Non-radiative can further be split into inductive- and resonant coupled WPT. Far field WPT is microwave power transfer (MPT) and is used to transfer large amounts of power between two locations. A WPT system requires a transmitter and receiver, the former connected to a power source converting electrical power into a time-varying electromagnetic field. The latter receives the field power and converts it back into electrical power to be consumed by the load.

Near field WPT refers to an area within one wavelength of the transmitting antenna. The oscillating electric and magnetic fields between the antennae are separate and power is transferred via electric fields using capacitive coupling or electrostatic induction, or via magnetic fields using inductive coupling or magnetic induction through coils of wire. Inductive coupling is used for short range transfers (in the centimetre range) and boasts a very high efficiency at very high-power transfers. However, the distance plays a significant role in decreasing those values.

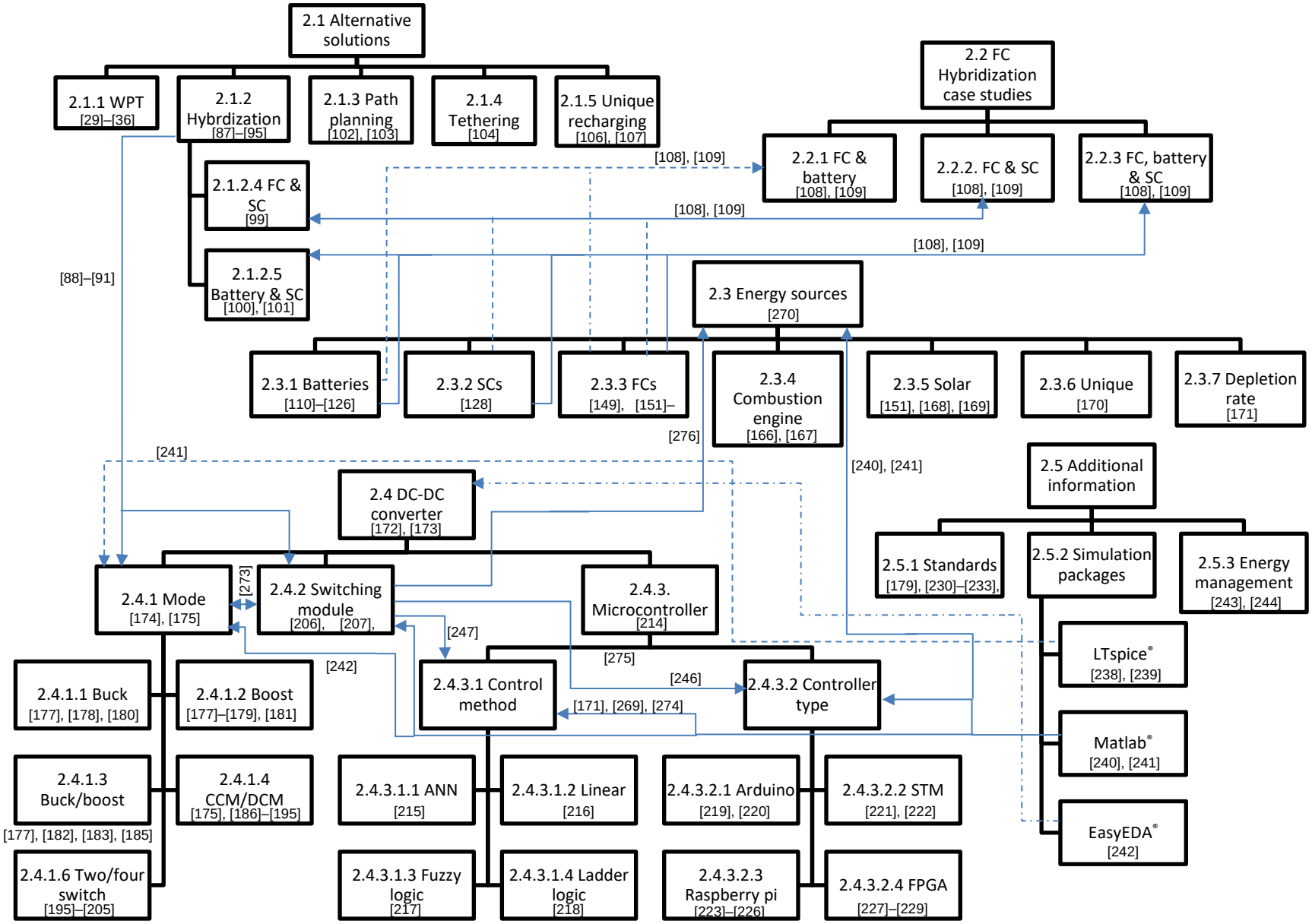


**Figure 2.2: Interactions between different subject areas**

Resonant coupled WPT has the advantage over inductive in that it can transfer larger amounts of power over greater distances [26], [33]–[35].

The main disadvantages of this system are linked to misalignments due to imperfect landing of the drones, the size of the system and the weight thereof. The misalignment of the coils increases the gap between them decreasing the coupling factor and reducing efficacy of this method [36]. To overcome these shortfalls the base station can be equipped with a positioning system that automatically aligns the coils which in turn decreases the weight of the on-board system as well as increasing efficiency of the system as a whole [29].

#### 2.1.1.1 Near field wireless power transfer

Near field WPT (otherwise known as Wireless Charging Techniques – WCT) is a technology that transmits power through an air gap to electric devices in a way to address the bottleneck effect of energy of portable battery-powered devices. This technology has many applications therefore encouraging its advancement. The advantages include increased user-friendliness, renders much smaller designs, increases product durability, enhances flexibility and can provide power almost instantaneously, as required, making these devices more efficient [37]–[40]. There are a number of power sources that include the use of WCT such as, gust-soaring, PV arrays, laser beaming and battery dumping (these will further be discussed from 2.1.1.1.1 – 2.1.1.1.4 below). WCT has two main methods which will be explained in this section. First the principle of Electromagnetic wireless charging will be explained using Figure 2.3 below.

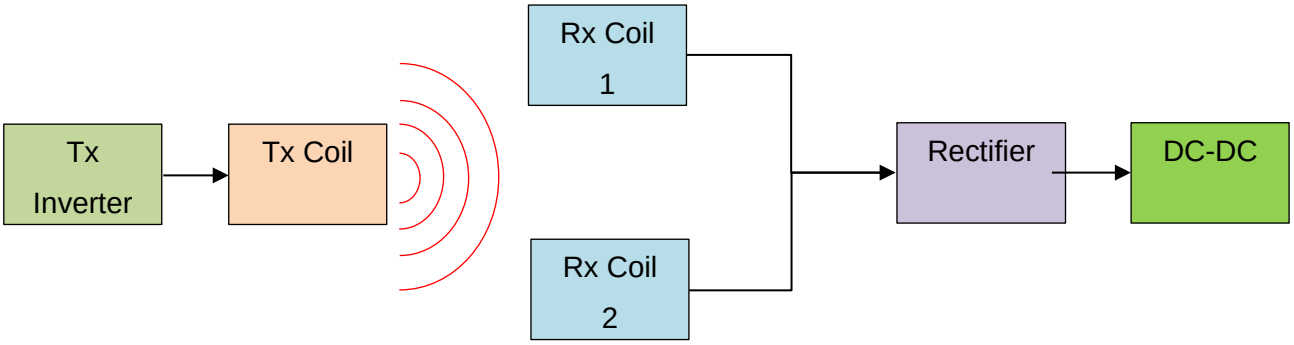


**Figure 2.3: Wireless charging operation (adapted from**[41]**)**

This method of charging is based on the principle of magnetic induction between two coils (a transmitter- and receiver coil) and their respective magnetic fields. DC electricity is transformed into AC to generate an electromagnetic field in the transmitter coil which in turn generates a magnetic field in the receiver coil that gets transformed back to DC. The obvious advantage of this method over conventional charging is that there are no cables that need to be connected before the charging can occur[42]. Other advantages include: charging initiating as soon as contact is made and the power transmissions being unaffected by a material (other than metal) placed between the transmitter and receiver coils [42]. Disadvantages include: extended charge periods (+- 50% longer than conventional methods) [42], a charging pad is required and the range of the craft is limited. The

second method uses Capacitive Power transfer and will be explained, with reference to Figure 2.4, below.

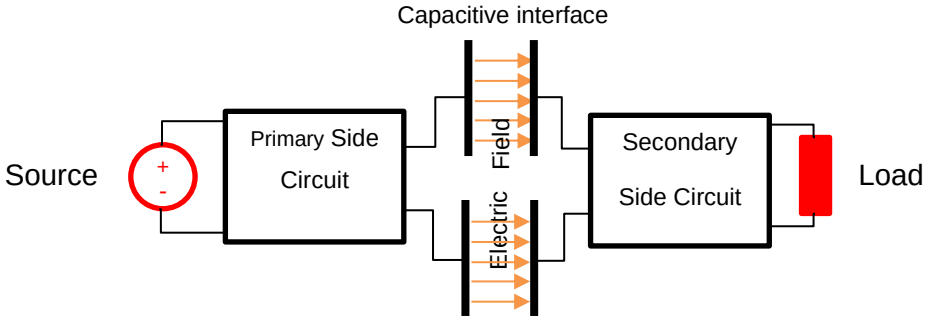


**Figure 2.4: Capacitive Power Transfer operation (adapted from** [43]**)**

The primary circuit consists of an inverter, filter, matching circuit and transformer. These all help to convert the power on the primary side to a power that can be transferred to the drone via the landing pad. The secondary side circuit consists of a full-wave rectifier, DC-DC converter and the necessary charging circuit. For this method to work the drone lands on the secondary side's capacitive plate causing a connection to the primary side completing the circuit and allowing the drone to charge. This method utilises the electric field rather than the magnetic field therefore does not require bulky magnetic materials. The principle here allows for a much larger landing surface for the charge connection to occur [43]. Advantages of this method include a reduction in Electromagnetic Interference (EMI), a reduction in power losses and lower manufacturing costs [43]. Disadvantages include: physical limitations, grounding instability, a change in impedance matching and field fringing [43].

#### 2.1.1.1.1 Gust-soaring

A UAV is governed by three forces when in flight, lift, drag and weight; lift – relative to the wind, drag – parallel to the wind and weight – pointed towards the earth's centre regardless of the UAVs trajectory. While the UAV is in flight it is possible for the wind to be in a direction that is not parallel to the flight path making it possible for the lift force to affect the energy state. The effect of the lift on the energy depends on the flight path relative to the wind. While the UAV ascends or descends the lift causes a thrust force that can increase the energy profile. UAVs can gain kinetic and potential energy through its velocity and height respectively [44]–[47]. Gust soaring is a method of energy storage that uses the principle of adjusting the trajectory of an object in order to capture the energy caused by uplifting airflow. This energy can then, in turn, be used to recharge the energy storage device of the UAV [45], [48]–[50].

Biometric behavioural engineering has long been a key factor when it comes to scientific discoveries. The term refers to applying the adaptive strategies of animals, in the real world, to the development of scientific technology. The main concept is to observe the actions of a creature to modify and optimize it for scientific use [51]. In the scope of this section this method has been used to observe the flight of birds (especially the larger ones) and their ability to remain aloft without expending energy

through flapping their wings. Energy expenditure through flapping increases with the size and the wingspan of the bird, for this reason larger birds have developed soaring techniques through utilizing energy form wind motions, in turn reducing their energy consumption [52]. Scientists have observed this behaviour and utilized it in many an aircraft paying special attention to UAVs.

There are generally two main types of soaring, static and dynamic. Basically the former involves flying through air that is rising relative to the surrounding air and the latter uses trajectories through the distributions of wind speed to increase kinetic energy [52]. Figure 2.5 will be used to describe these methods further.

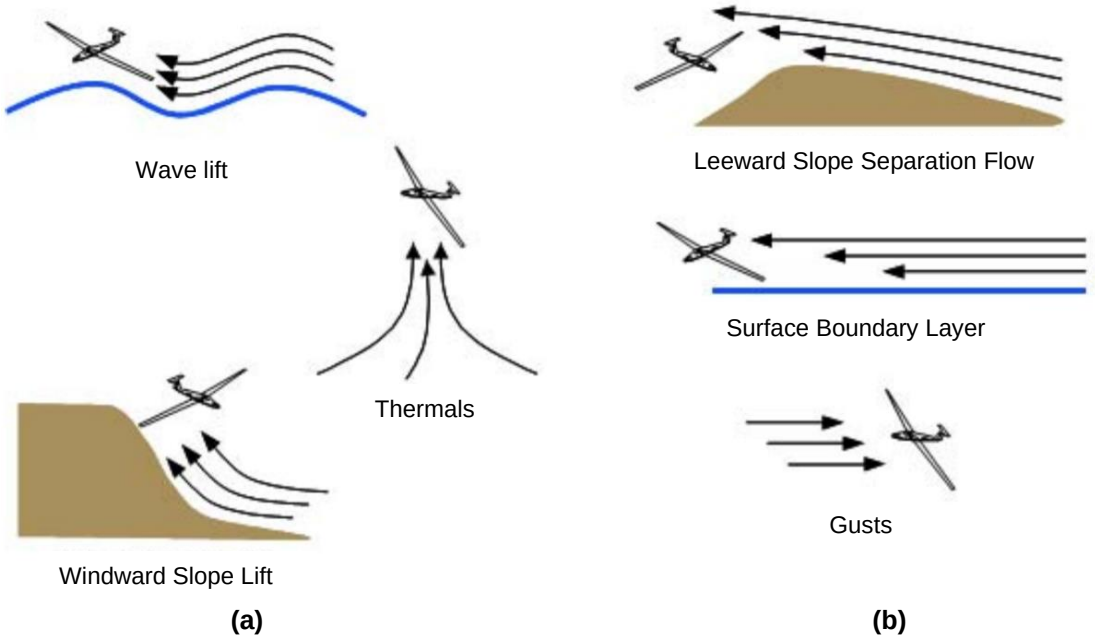


**Figure 2.5: Examples of (a) static soaring and (b) dynamic soring (adapted from [114])**

In a motionless atmosphere without variable wind gradients, it would be impossible to sustain gliding flight, however, the atmosphere is in near-constant motion making this phenomenon possible. When a mass of air experiences an increase in its upwards velocity, compared to the still-air surrounding, it an updraft is observed. Updrafts can be caused by thermals (the rising of hot air into the atmosphere), slope lift (when wind traverses an orographic uplift) or wave lift (updraft caused by atmospheric waves), shown in Figure 2.5 (a), and cause an aircraft to experience an upwards force competing with the natural gravitational force in flight, causing the aircraft to rise without expending energy [51]. This is known as static soaring, basically the use of vertical wind gusts, and has been investigated for use with a UAV in a few instances. Dynamic soaring is perceived to be much more complex as it uses horizontal wind gusts and has therefore received much less attention. This method utilizes what is known as a horizontal shear to sustain flight. Energy is absorbed from air masses that have varying velocities at different horizontal layers of the atmosphere, examples are shown in Figure 2.5 (b). Dynamic soaring is achieved where there is a rapid change in the horizontal wind velocity and can allow a UAV to gain kinetic (forward motion) and potential (elevation increase) energy from a single cycle [47].

This method makes use of the environmental conditions that would otherwise go to waste, but unfortunately is only suitable for fixed-wing type UAVs and this requires the drone to be dependent on the environmental conditions and can thus not remain in one position for a long period of time, which is a requirement for most drone applications.

#### 2.1.1.1.2 Photo-voltaic arrays

One way to achieve a long endurance flight form a UAV is to employ the use of solar power. Solar power is desirable as it is clean energy without pollution and is technically “free”, all it requires are PV cells to capture and convert the energy into a usable form. Solar powered UAVs capture the radiation from the sun and convert it, photo-electrically, in the daytime in order to power the operating system of the drone whilst in flight [53]. Any excess energy is then stored in the batteries and used for night flight, therefore if the daytime consumed energy is smaller than the available energy during the day continuous flight can be obtained [54]. PV arrays can be combined with WPT to provide an eco-friendly method of charging an Electric Vehicle (EV) or UAV. PV cells convert the solar energy into electricity while on the move, the PV array then functions as the primary power source and also to charge the batteries through inductive power transfer technology [55]–[58]. This method includes using the PV cells to power the drone and recharge the battery while the solar irradiation is available and switching to battery use when the irradiation is insufficient [59]–[62].

This method uses the sun, a free, natural resource of power, thus making it very economic. However, the drone is heavily dependent on the solar irradiation which can limit the applications thereof to mainly daytime applications or those which require an alternative source of power supplemented by the PV-arrays. Also, PV-arrays are only applicable to the fixed- wing drone type [26]. These drones require large wingspans for maximum solar energy exploitation, again limiting applications. This method is mainly used for High Altitude Long Endurance (HALE) missions as this allows the UAV to fly above any obstruction that blocks the sun allowing for optimal photo electric conversions and radiation absorption, increasing flight duration [63].

#### 2.1.1.1.3 Laser

Drones can be charged in flight without the necessity to land, increasing the safety and efficacy of the UAV. For this a primary power source is installed in a ground station transmitting a laser-beam to the drone’s optical receiver. When the battery reaches depletion an aerial power-link is established between the UAV and the ground station. These ground stations are usually placed on rooftops of high buildings or on cell phone towers in order to avoid obstructions [63]. This WPT method uses electricity from a source such as grid power that is converted into light via a laser, shaped and directed to a remote PV receiver. The receiver then converts the light back into electricity which then charges the battery on board the UAV. Power and energy density are critical for many remote power applications, if the power drawn is smaller than the power density the payload of a UAV is increased

and a higher energy density implies a longer endurance. With a laser power system, the energy source is left on the ground where generation is easier and cheaper.

In UAV Power link technology power-beams are used to power drones equipped with a laser receiver. This technology has the capability of a flight time of up to 48 hours. This system can provide almost unlimited flight endurance if there is a laser transmitter available. The range of these systems is limited by the source of irradiance, which can be increased depending on the quality of the laser, and also by line of sight. This method is heavily affected by weather and the environment [64], [65]. Most of the above mentioned power sources can be used in either fixed-wing or rotor-type UAVs with the exception of pure solar as this requires the larger expanse of space that a rotor-type UAV does not have [20]. These drones can achieve more than 12 hours of flight making them quite feasible [66]. Advantages of the laser method include a much longer duration of flight, compared to non-laser types, and the ability to be applied to both types of UAVs. Disadvantages include requiring an energy source that is mobile and close to the UAV, limiting the applications. Lasers also present a health-hazard to the users and to the environment surrounding its use [26], [66]. The drone has to operate in a limited vicinity close to the ground station and also within the legal height regulations of the Federal Aviation Administration, thus limiting its operating range. Also, each drone requires its own dedicated laser source as one source cannot supply multiple drones [63].

Another method of employing the laser-beam technique is through the use of two drones, one for low-altitude (LA) and one for high-altitude (HA). The LA UAV is quite small in size and thus energy constrained giving it a limited flight time. However, this can be amended through the use of solar power, but the LA UAV is of such a small size and flies at such a low altitude that it cannot gather enough solar power. Introduce the HA UAV, this UAV is much larger and flies at a much higher altitude allowing it to sufficiently exploit the solar energy available. Essentially, the HA UAV uses the solar power to operate and can store any excess power that can later be shot via laser beam to the LA UAV when required. The LA UAV is equipped with a panel that can withstand the intense laser beams and convert them as desired. The downside of this is that the laser beam is quite intense and very harmful to the human body and if the laser misses the LA UAV panels can be very detrimental to anyone that encounters it. That is why the aforementioned laser powered drone with a ground station is preferred as the laser is pointed upward and away from human contact [67].

#### 2.1.1.1.4 Battery dumping

Most papers describing UAV performance base the model on the fact that the battery has a fixed weight that remains unchanged during charging and discharging. There exists, however, a solution to extend the endurance by dumping the section of the depleted battery out of the aircraft while in flight. The theory is that if the weight of the battery can be reduced, similar to the fuel consumption of a combustion engine, the endurance can be increased. One possibility is to divide the battery into battery packs and dump the depleted ones out of the aircraft, only one battery from the pack will be

connected to the system at a time. However, the system itself increases the weight of the craft while improving the power consumption therefore cancelling the benefit obtained from the variable battery weight. The focus of this dumping system therefore needs to rather be related to the endurance of the flight. The centre of gravity of the aircraft needs to be taken into consideration as well so that this dumping effect does not alter it too much. It is seen that the efficacy of this system increases if the battery is divided into more packs, conversely, there is a point where the hardware for the amount of packs can become too heavy and decrease the benefits thereof [68]–[70].

This method increases flight duration, but the system required to allow for this dumping method increases the initial weight and cost of the drone, decreasing the proposed efficiency of this method. It was found that this method can be feasible if the right quantity of batteries is chosen, however what the author failed to mention was what happens to the batteries after being dumped. The main question is whether the batteries are retrieved or not. If retrieved, they can be retrieved with the help of another device, stationary or mobile, or by the drone pilot. Stationary device(s) can be used and placed along the path onto which the batteries can be dropped, a mobile device can follow the drone (on the ground or in the air) to collect the batteries or the position of where each battery is dropped can be recorded for later retrieval by the pilot. All of these methods add to the cost and decrease the efficiency of the drone and may allow this method to, in fact, become unfeasible. If the batteries are not retrieved there are other concerns involved, environmental pollution, cost of renewing the batteries and type of battery being used to facilitate the disposal thereof, to name a few. All of which, again, affect the final cost and efficiency of the system.

A variation of this method, battery swapping, exists which entails landing the drone on a platform that is equipped with an automatic system to disconnect and remove the depleted battery from the drone and replaces it with a fully charged one. This method reduces the human participation in the process as well as reducing time wasted charging drone batteries [70], [71]. Allows continuous operation, weight is significantly reduced and power management system is not required. However, the drone needs to land during flight, decreasing efficiency, the system has a high operational cost and the cooperation between the landing station and the drone increases complexity [63], [70], [72], [73].

#### 2.1.1.2 Electro-magnetic field-based technique – High Voltage power line charging

This method is mainly used for the inspection of High Voltage (HV) power lines as the inspections can be extremely expensive when using helicopters and are also quite dangerous when inspectors have to climb up the power line tower to inspect live conductors. UAVs offer the advantage of being faster than a manual inspection and far less expensive than employing a helicopter [74]. To be feasible the UAV needs to have good position control, tracking, obstacle avoidance and be as energy independent as possible. For this it also needs to be able to traverse along the entire length of the

power line, which poses a significant challenge in terms of the discharge rate of the battery [75], [76]. As the electrical power lines offer a good source of power it is possible to harness this power to charge the drone when discharged. This is done through utilizing the EMF surrounding the conductors in order to wirelessly charge the UAV [77].

There are mainly two techniques in using the power lines to charge the UAV, power line perching and WPT. Power line perching involves the drone landing on the current carrying conductor and charging from it [78], [79]. For this, the drone needs to be able to navigate in the vicinity of the power line and it needs to have a means of converting the HV power to a lower voltage that the drone can use. The first issue comes in where the readings of the navigational equipment close to the transmission line are severely biased by the EMF. When the drone lands it will fasten itself to the conductor with a special connector that represents a magnetic core. Once the core is closed around the conductor it forms an electromagnetic closed-loop circuit used to transfer energy to the secondary circuit on-board the drone to charge the battery [78].

WPT will use the EMF surrounding the current carrying conductors which contain enough energy to recharge a medium scale UAV [33], [80]. There are two main techniques under WPT, Inductive Power Transfer (IPT) and Resonance Coupled WPT (RC WPT). The first is more well-known and widely used and basically entails the use of two strongly coupled coils that transfer power wirelessly from one to the other [34]. A magnetic core is utilized in this process and streamlines the magnetic flux, significantly improving the efficiency of the transfer. If the core is removed the wireless link remains loosely coupled but can still transfer power, this method is more desirable for UAV use as it weighs much less than when a magnetic core is involved. IPT can transfer power in the kW range, but the transmission distance is limited to several centimetres, it is also very vulnerable to external EMF therefore requiring a form of shielding in order to improve performance. Another major drawback is that the coils need to be precisely aligned as efficiency is dependent on the coils being as closely aligned as possible [81], [82].

RC WPT is a newer approach entailing two loosely coupled coils operating at the same resonant frequency which allows them to transfer significant amounts of power from one to the other whilst being at a considerable distance from each other. A study showed that a transmission of 80 W of power was possible at a distance of over two meters [83]. This method therefore remains effective at a transmission distance of around several meters. RC WPT does not require EMF interference protection since the coils operate in resonance mode, it provides a WPT opportunity from multiple sources and dynamic charging with a moving receiver [34]. It does however have the downfall of a typical operating frequency in the range of 10 kHz to 200 MHz while the operating frequency of the power line is only 50-60 Hz [83].

This technique involves a fixed –wing UAV perching on a power line and recharging using the EMF around the HV conductor [84], [85]. For this method it is important that the insulation of the conductors is sufficient and well-kept as a direct physical transfer of power must not be possible [86]. This method allows the UAV to easily recharge whilst on the move but proposes a problem in maintaining a strong coupling and high efficiency of the power transfer.

### 2.1.2 Hybridization

Hybrid systems contain two or more types of power sources, generally one is used to generate the other or one is preferred and the other is used at specific times to improve efficacy. The principle behind this is that one of the power sources has more advantages than the other in normal conditions, whereas the other provides specialized advantages which are beneficial at certain times during operation. This helps improve the energy and fuel efficiency of the system and minimize pollution [87]–[89]. From the above sections it is evident that some of the power sources have advantages over the others and vice versa. There are disadvantages of some of the sources that can be resolved or improved by using alternate sources. This is where the concept of hybridization comes into consideration. By combining two or more power sources their advantages can be combined and their disadvantages can be minimized. However, special attention needs to be given to the method of hybridization.

There are generally five categories of hybrid vehicles, parallel (PH), mild parallel (MPH), power split or series parallel (SPH), series (SH) and plug in hybrid (PIH). PH can function using either of the sources used in the hybrid or one individually, when both are used the use is split equally. MPH prefers the use of one and use the other when assistance is required. SPH can utilize both in varying ratios, i.e. 100% of both or 60% one and 40% the other; therefore, one can regulate the efficiency. Generally, SPH also only uses the one power source, either when assistance is required or when the power requirements are really low in order to decrease fuel usage. SH uses the one power source (electric power) as its main power source and utilizes the other to (petrol/diesel generator) to recharge the main source, thus the second power source is not connected to the main power system. PIH uses the main power source permanently and uses grid power via a plug to recharge, thus avoiding the use of the combustion engine for this purpose. The use of the combustion engine is then up to the discretion of the driver, making this option the more pure of the five [90]–[94].

The type of hybrid used depends on many aspects including, cost, availability, user preference and application. Some areas in the world are far from a reliable source of energy, therefore utilizing renewable energy sources becomes imperative, but these sources tend to have low energy density and poor stability. To combat this, the renewable source is combined with something of a less renewable nature or another renewable source [95]. Another advantage of hybrid systems is the reduction in one’s carbon footprint. In order to meet the needs of both energy and power hybrid

power supplies are becoming more popular. A couple hybrid power supplies are explained under their respective headings below.

#### 2.1.2.1 Solar Hybrids

These systems include the combination of PV and CSP systems with each other or other forms of power generation such as diesel, wind or biogas. This hybridization allows the system to modulate power output depending on the demand or to reduce fluctuations caused by the solar power [96]. Solar power-hybrid drones deliver astonishing endurances. Tethered systems also fall under these types of drones. These are systems that allow an unlimited flight time within the small radius. These types of UAVs are used more for military or industrial application and are therefore not of interest for this paper.

#### 2.1.2.2 Gasoline – electric hybrids

Gas-electric hybrids are mainly used for regenerative breaking, duel power or less idling. As the vehicle slows down for breaking the energy is used to recharge the batteries, depending on the driving circumstances the power can be divided between the dual sources or the vehicle can be shut off and restarted easier using an electric motor when the car comes to a stop [97]. For UAV applications these types combine the quick reactions of an electric motor with the advantages of gasoline powered flight.

#### 2.1.2.3 Plug-in hybrid electric (PHE)

This system uses a combustion engine to supplement the electric engine when the battery levels are too low. The electric motor is powered mainly using PV-arrays. The main shortcoming to this hybrid system is the necessity of the combustion engine [98].

#### 2.1.2.4 Fuel cell and super-capacitor hybrid

This system combines an aluminium air FC (AAFC) and SCs to form the power source. AAFCs have a higher energy density than most other batteries, but have a lower power density, therefore on its own, the AAFC is not a viable driving source of power. As mentioned in section 1.1 SCs have a high-power density, fast charge and discharge, but a poor energy density. This makes them ideal for supplementing the AAFC. There are three stages in power supply of this system, stage 1 involves only the use of the AAFC when there is a low power demand, stage 2 uses both AAFC and SC for larger power demands and stage 3 is one that occurs continuously, known as regenerative breaking, where the SC is charged through the use of energy that is usually lost when the system idles [99].

#### 2.1.2.5 Lithium-ion battery and super-capacitor hybrid

The Li-ion battery has many advantages over other batteries including, high voltage, light weight, low self-discharging and long cycle life. The shortcoming of Li-ion batteries is that if they are used in

a high-power demand application, their performance in terms of weight, cost and lifetime degrades tremendously. By adding the SCs, the battery can satisfy the average power demands while the SCs satisfy the peak power demands during acceleration or breaking [100].

For a more detailed comparison of the hybridization solution refer to the published article [101].

### 2.1.3 Path planning

Drones are used in the application of field surveillance where path planning is actually ideal. However, a path needs to be determined such that the entire terrain can be surveyed with minimal overlapping. This method can allow the drone to have a more precise flight pattern allowing for more efficiency or more use out of the drone for the specific charge output. This method entails determining the path that will most optimally scan the area in question [102]. Path planning has the advantages of fewer power losses due to erratic motions and pre-determining a path that can optimize the battery life. Disadvantages include, knowing and determining the optimal path before use, the requirement of trained personnel and this method also requires complex coding.

The above-mentioned path planning uses the Travelling Salesman Problem (TSP) algorithm with focussing mainly on the distance travelled by the drone. Another method of path planning exists, Energy Efficient path planning, this method takes energy consumption of the drone at specific points into consideration. This method helps determine the amount of power consumed by the drone at specific speeds, at certain degrees of a turn and the distance travelled. Lower speeds result in longer use of drone and increased degrees of turning angles reduce the power usage of the drone. All of this allows the path of the drone to become more energy efficient than the conventional TSP method [103].

### 2.1.4 Tethering

For this method one end of the tether is connected to a spool driven by a DC-motor and the other end is connected to the drone, as seen in Figure 2.6. The tether allows the drone to continuously be powered as long as it is connected to the tether. This allows for fully autonomous flight of the drone [104].

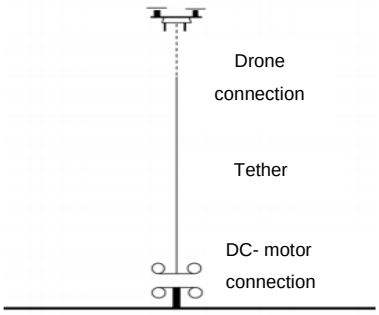


**Figure 2.6: Drone tethering (adapted from** [105]**)**

The advantages of this method include an uninterrupted flight and an increase in power as the power supply can be virtually any size and capability [104]. Disadvantages of this method include a limited flight range and an imperative necessity that there be tension in the cord [104].

### 2.1.5 Unique recharging methods

Passive take-off aquatic drone: this drone works on the principle of flying short distances, in the direction of large bodies of water, landing on the water and recharging using built-in solar panels before taking off again [106].

Another unique method of powering a UAV or prolonging the flight time is by using what is known as drone-swarming. This is a continuous energy replenishment method allowing a large group of drones to achieve perpetual flight by recharging more depleted drones in the swarm using freshly recharged drones. The configuration of the swarm can determine the efficacy thereof [107].

## 2.2 Fuel cell hybridization case Studies

For this section of the literature study a couple of case studies will be looked at with emphasis on those that pertain to this project.

### 2.2.1 Fuel cell and battery combination

Many studies have been done using this particular type of combination, these case studies will be used to assess the specific energy management of each as well as the outcomes and suggested improvements. In [108] a 35 kW FC is combined with a Li-ion battery of 346.5 V, where the FC utilizes a DC-DC converter in order to boost the voltage to (250 – 400 V) in order to use a smaller FC to reduce costs and vehicle mass; the battery, however, does not use a converter as it delivers the required voltage. In this study the battery stores regenerative braking energy (when battery is less than 98% charged), supplements the FC during extra power requirements as well as very low power requirements (the FC is inefficient below a certain power level – 7.55% of the total) and is only charged via the FC when the State of Charge (SOC) is less than 50%.

Charging the battery through regenerative braking instead of the FC increases fuel economy. From this study it is seen that the FC & battery combination has a slightly lower efficiency when compared to the FC, SC & battery combination, even though the weight of the former system is significantly less. An advantage of the FC & battery combination is that it is more cost effective due to the absence of the SCs and the bidirectional DC-DC converter. A major disadvantage is that the battery life is much shorter than that of the FC, SC & battery combination as the battery is continuously charged/discharged throughout the operation of the vehicle.

In [109] a PEMFC of 500 W, 40 A, 13 V is combined with a lead-acid battery of 33 Ah, 48 V to supply a FC vehicle. The FC will utilize a boost converter to optimize the characteristics and boost the output

voltage to that of the battery. The battery will not use a converter in order to minimize costs and improve efficiency of the system. The FC will be the main energy source and when the power demands are large, decrease below the specified level of the FC or regenerative breaking energy is present in the system the battery will be utilized. This configuration leads to a significant degradation in the battery lifetime as the battery is constantly supplementing the FC, there is no method to improve this issue without altering the setup (i.e. the use of an additional SC bank to rather supply the peak power demands). The FC is also used to recharge the battery throughout the operation. This system does improve the efficiency and fuel consumption of the FC however it leads to an additional consideration in lifetime of the battery as this is significantly reduced due to the charge/discharge of the battery throughout the operation of the system.

In [108] the combination consisted of a battery pack used in conjunction with a FC; the former used when there is a high power demand and the latter as the main source of power. It can also be seen in this configuration that the battery will receive the surplus energy that is not absorbed by the load during low load power. The system worked well with the exception of equipment having lower precision than desired causing a higher error rate and, on occasion, the incorrect operation of the hybrid power system. The system had an overall high efficiency (>90%) with lower hydrogen fuel consumptions.

### 2.2.2 Fuel cell and super-capacitor combination

The combination of the FC & SC has had a few previous studies and experimental combinations, but all had some form of a limitation, these limitations will be of importance. In [108] a 35 kW FC was combined with a SC bank to supply a FC vehicle. The FC utilizes a boost DC-DC converter to increase its voltage to that required by the motor (250 – 400 V) such that a smaller FC can be used to reduce vehicle mass and overall costs. The SC bank consists of 27 SC-packs are used in series comprising of six 2.5 V, 350 F cells in series, thus 405 V, 2 F capacity. The SCs do not use a DC-DC converter in order to reduce costs and weight of the system and improve efficiency. The SCs store the regenerative braking energy and only provide extra power when it is required (during accelerations). Best fuel economy is achieved when the sum of kinetic energy in the vehicle and the potential energy of the SCs is kept constant. This study shows that the FC & SC combination cannot compete with the FC & battery combination as the SC bank does not have enough energy storage to provide for the peak power requirements. It is suggested that a few SC banks be combined in parallel to increase the energy storage capabilities, however, this increases the weight of the system tremendously decreasing fuel consumption to an infeasible point lower than the FC & battery combination.

In [109] a PEMFC of 500 W, 40 A, 13 V is combined with a SC bank of 292 F, 500 A, 30 V to theoretically power a FC vehicle. The FC will utilize a uni-directional boost converter while the SCs

will utilize a bi-directional converter to facilitate the power requirements and the storage of the regenerative breaking energy. For this setup, the FC will be the main supply of power and when peak power demands are observed or regenerative breaking energy is increased above 0, the SC bank will be utilized. The FC will also be used to recharge the SCs throughout the operation. This setup does allow for FC downsizing, increased efficiency characteristics as compared to only FC use and energy recovery through regenerative breaking. The downside of using only SCs as the auxiliary power source is that the system could malfunction during start-up as the FC requires 5-10 minutes of constant power. For both of these case studies the future adjustments would be to either increase the SCs energy characteristics or to look into a hybrid system that includes the use of a battery to absorb the bulk of these constant power requirements.

### 2.2.3 Fuel cell, battery and super-capacitor combination

Fewer studies have been done into the use of the power sources in this combination than in the prior two combinations. These case studies will be used to assess the viability of the combinations as well as defining some limitations observed leading to room for improvement.

In [108] a 35 kW FC is combined with a SC bank (405 V, 2 F) and a Li-ion battery (346.5 V) to supply a FC vehicle. The FC utilizes a boost converter such that the FC required can be smaller and thus more cost effective and the battery will use a bi-directional converter in order to be recharged while the system is in use. In order to minimize mass of the system it is determined that only one of the additional power sources (batteries or SC) will use a converter. The SC will be used to supply power only during peak power requirements and will accept regenerative braking energy only if the SCs are below 400 V; the batteries will continuously supplement the FC during normal operation, will also be used to store regenerative braking energy (when the SCs don't) and will also be used when the power requirements are too low for the FC (< 7. 55%), thus, the bi-directional converter is chosen to be used in conjunction with the batteries for its charge/discharge.

The SCs are used to lengthen the lifetime of the batteries and are therefore monitored to remain within the required 250 – 400 V of the load motor. One major advantage of this setup is that the degradation of the battery is delayed due to it not undergoing high current charge/discharges. The battery in this setup is only used for peak power when the SC is discharged, whereas it is used for all peak power requirements in the FC & battery combination. This setup does have the downside of being much heavier (due to the SC pack addition) and also more expensive (due to the addition of the SCs and the bidirectional converter), however, it still has a lower fuel consumption compared to that of the FC & battery setup.

In [109] a combination of a FC – used as the main source of power, batteries – used to provide boost power over moderate durations and SCs – providing a fast acting source to smooth rapid transients and reduce the degradation of the FC and battery. This system was tested using a flight simulator in

order to get a desired flight profile and performed adequately during all stages of the simulation. These sources are used in conjunction to supplement each other. The battery removes a significant load off of the FC allowing the FC to have a much lower voltage drop throughout the simulation. The SC allows for a much smoother power curve providing significant energy absorption to the system. Thus, it provides considerable load smoothing to the FC and has the expected benefit of increasing the lifetime and durability of not only the FC but also the battery.

## 2.3 Energy sources

As the main focus of this project pertains to energy sources it is necessary to understand the operation and use of relevant types. The sources that will be reviewed will include those mainly used in the application of UAVs, but the ones specific to this project will receive more attention. The depletion rate of the sources as well as the weight and energy considerations of this project relating to each source will also be researched. A comparison Table of the main power sources for UAVs will also be given at the end of this section. The first five energy sources have been discussed with reference to the published work [101].

### 2.3.1 Different battery types

The first documented battery, or more specifically the lead-acid battery, has been around for over 150 years and although still similar to the original, the technology has been significantly refined over the last 100 years [110]. These refinements include, a sealed construction, lower-maintenance, simplified designs, extended cycle life, improved degradation, higher charge acceptance, etc. [111]. Different batteries have different solvents, membranes and/or electrode materials. These differences allow the battery to be lighter, more efficient, have a larger power or energy density, have a smaller volume or charge faster and the characteristics determine the best application.

There are many different types of batteries used on-board UAVs, each of which has its respective advantages and disadvantages. The types include: Lead acid (Pb-acid), Nickel cadmium (NiCad), Nickel Metal Hydride (NiMH), Alkaline, Li-Po, Lithium Ion (Li-Ion), Zinc Oxide ($Zn\text{-}O_2$), Li-air and Lithium-Thionyl-chloride ($Li\text{-}SOCl_2$) [112]. The most common batteries for drones are Li-Po and Li-Ion. $Li\text{-}SOCl_2$-batteries have two times higher energy density per kg compared to the aforementioned and Li-air batteries can be up to seven times higher, however, they are unfortunately not so widely available and are much more expensive than Li-Po and Li-Ion. Another variation of Li-batteries, Lithium sulphur (Li-S), also offer a higher density compared to Li-Ion at a reduced cost making them the obvious choice to replace Li-Ion batteries in the near future.

The most suitable type of battery is determined by comparing the power density, energy density, weight, volume, cycle life, cost, safety and maintenance (to name a few criteria) of the different options. Each of the criteria affect different aspects of the drone, power density affects the acceleration capabilities, energy density determines the range, cycle life determines how often the battery will need to be replaced, weight and volume affect the range of the system and cost affects availability [113]. Pb-acid, NiMH and Li-ion batteries are the most popular for EV applications as they are capable of meeting the requirements of EV's. Li-ion batteries have a liquid composed of a lithium salt and non-aqueous organic solvent as electrolyte, electrodes with a crystalline structure with a proportion of lithium inserted inside of it and a porous membrane, as shown in Figure 2.7 [114].

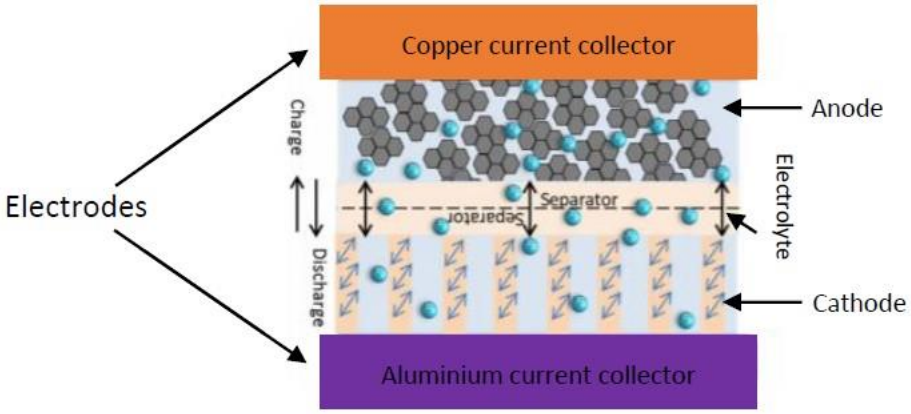


**Figure 2.7: Basic construction of a Li-ion battery (adapted from** [114]**)**

This allows Li-ion batteries to be able to deliver high energy and power per unit of battery mass; they are also lighter and more compact than the other rechargeable batteries. Other advantages include high energy efficiency, no memory effects and a comparably long cycle life. The one major shortcoming of these batteries is the cost which is significantly more than the other two. Table 2.1 below compares a few categories of the mentioned battery types, this table is obtained from the published article [101].

For cost comparisons between the different types to be relevant it is necessary to choose a reference point. That point was chosen as the capacity of the battery, namely: 2 Ah, however, due to availability the closest values to this chosen value were used and in the case of the Zn-$O_2$ battery, the largest value was used. Li-air batteries could cause a significant increase in the range of EV's as they have a very high energy density, almost comparable to that of gasoline. They can hold 5-10 times the energy of a Li-ion battery with the same weight or twice the energy for the same volume. For comparison they have an estimated energy density of around 2000-3500 Wh/kg, which is much higher than any other known battery. A small lithium-air battery has already been designed with a 600 mAh/g density compared to the 100-150 mAh/g density of a Li-ion battery of the same size [115], [116]. Amongst all of these advantages lie a few disadvantages, a rechargeable version of this battery presents a challenge as they have a very limited number of recharge/discharge cycles, they

have a very slow recharge rate and they are extremely dangerous if water vapour is present in the oxygen, as lithium reacts violently with this.

**Table 2.1: Comparison of different battery types (combined from** [113], [115]–[119]**)**

| | Battery Type | | | | | | | | |
|---|---|---|---|---|---|---|---|---|---|
| | **Pb-acid** | **NiMH** | **Li-ion** | **NiCad** | **Alkaline** | **Li-Po** | **Zn-$O_2$** | **Li-air** | **Li-$SOCl_2$** |
| **Nominal cell voltage (V)** | 2.1 | 1.2 | 3.6-3.85 | 1.2 | 1.3-1.5 | 2.7-3 | 1.45-1.65 | 2.91 | 3.5 |
| **Energy density (Wh/kg)** | 30-40 | 60-120 | 200-265 | 40-60 | 85-190 | 100-265 | 442 | 11140 | 500-700 |
| **Power density (W/kg)** | 180 | 250-1000 | 250-340 | 150 | 50 | 245-430 | 100 | 11400 | 18 |
| **Cycle life** | <350 | 180-2000 | 400-1200 | 2000 | NA, non-rechargeable | 500 | 100 | 700 | NA |
| **Charge/ Discharge efficiency (%)** | 50-95 | 66-92 | 80-90 | 70-90 | 45-85 | 90 | 60-70 | 93 | 6-94 |
| **Self-discharge rate (%)** | 3-20 | 13.9-70.6 | 0.35-2.5 | 10 | <0.30 | 0.3 | 0.17 | 1-2 | 0.08 |
| **Rating** | 12 V 2 Ah | 12 V 2 Ah | 3.6 V 2 Ah | 12 V 1.8 Ah | 1.5 V 2.2 Ah | 3.7 V 2 Ah | 1.4 V 300 mAh | NA | 3.6 V 2.2 Ah |
| **Costs (US$/Wh)** | 0.6975 | 0.8546 | 0.9361 | 2.6778 | 1.6727 | 2.3095 | 0.3095 | NA | 0.5492 |
| **TRL**** | 9 | 9 | 9 | 9 | 9 | 9 | 9 | 6 | 9 |

*Available for purchase on 18/05/2020 [119]–[126], relative for comparison

**Technology Readiness Level [127].

Li-Po batteries are preferred over most other batteries in portable devices and electric transportation (EV and their hybrid counterparts) due to their superior energy density, power-to-energy balance and long cycle life [113], [117], [118]. The main advantages of battery powered drones relate to being capable of charging almost anywhere, transported generally without limitations and easily recharged by simply replacing the battery pack. The disadvantages include small amounts of recharge cycles and comparably low energy density.

### 2.3.2 Super-capacitors

A capacitor consists of electrodes (anode and cathode) separated by an electrolyte [128]. The variations of capacitors are differentiated through the type of electrodes and electrolyte used. Electrostatic capacitors store charges through dielectric polarization, their energy density is not very high, however the power density is, making them good for applications requiring short duration, high efficiency and high output power. To further investigate super-capacitors, they will be defined using their general classification, common applications, equivalent circuits and future trends. These will be discussed respectively below.

#### 2.3.2.1 Super-capacitor classification

SCs can be classified into three categories, electric double layer capacitors (EDLC), pseudo-capacitors or electrochemical capacitors (EC) and hybrid capacitors (HC). EDLCs involve a separation of charges at the interface of the electrodes and the electrolytes; the capacitance is proportional to the area of the electrode material [129]. ECs function on the principle of fast Faraday

redox reactions, therefore relying on high reversible redox reactions occurring on the electrodes surface or inside the electrodes to produce the specific capacitance. HCs are a combination of the former two SCs containing two electrodes, one exhibiting electrostatic capacitance and the other electrochemical [130], [131]. All three of the categories can exhibit a ratio of electrostatic and electrochemical capacitance, where the proportion of each determines the behaviour [129], [132].

#### 2.3.2.2 Applications

The breakdown potential of the electrolyte in SCs limits the voltage of a single SC to a maximum of 3 V. In order to increase the effective working voltage, multiple SCs need to be combined in series. This combination simultaneously reduces the effective capacitance. Therefore, different connection topologies need to be examined to find the best resultant voltage and capacitance for the application.

Regardless of the topology a compromise will always be required in terms of either total voltage or total capacitance and due to SCs weight (and size) increasing with increase in capacitance another compromise will need to be considered [131]. The charge and discharge of SCs occurs very quickly compared to batteries, due to their energy– and power densities, and they have almost unlimited recharge cycles. All of these characteristics make SCs ideal for a quick charge and discharge application – which is usually that of a hybrid storage system [133]. The SCs in the hybrid system will be used to supplement a main power source as they cannot maintain sustained power demands [129], [134].

#### 2.3.2.3 Equivalent circuits

In order to simulate and therefore predict the behaviour of a super-capacitor an equivalent circuit model is required. There are generally three main classifications – a classical RC model, a three-branch model and a transmission line model [135]. These respective classifications can be seen in Figure 2.8.

The classical RC model is very simple to implement and resultantly insufficient in characterizing a SCs terminal behaviour. The three branches of the three-branch model represent respective time ranges of seconds, minutes and time ranges longer than 10 minutes [136]. However, as SCs energy storage is usually used in applications in the range of seconds thus rendering the other branches pointless and thus reducing this model to that of the classical RC [137]. The transmission line model is very effective as an equivalent circuit however it utilizes impedance spectroscopy analysis which cannot show the effect of large currents and it is also a complex model [138], [139].

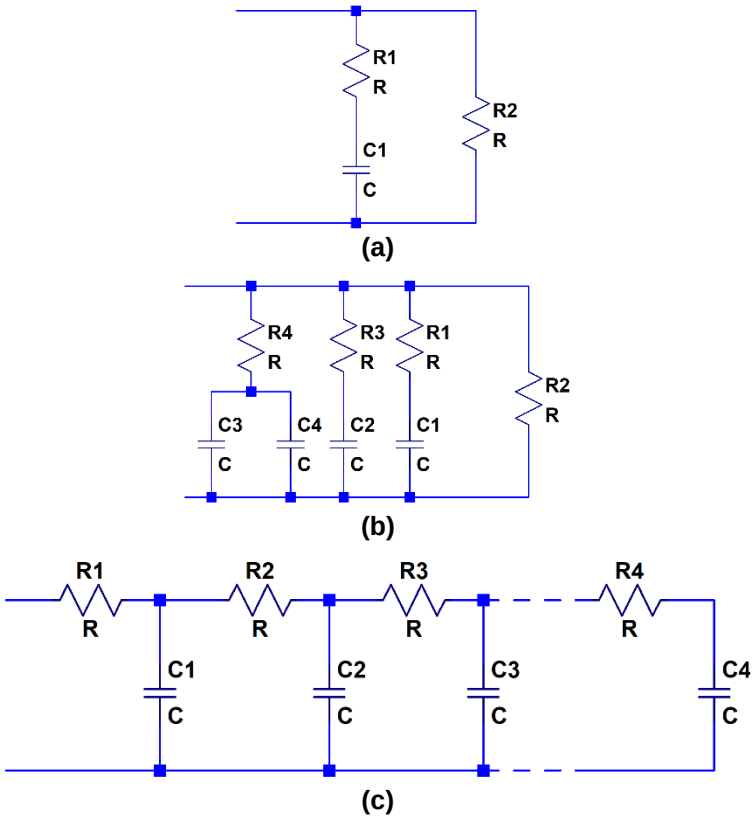


**Figure 2.8: SC equivalent circuits - (a) Classical RC, (b) Three-branch and (c) Transmission line models (adapted from** [139]**)**

#### 2.3.2.4 Future applications and technologies

What makes SCs so attractive is their ability to charge quickly, their high current capabilities and their almost unlimited quantity of recharge cycles [140], [141]. The main downfalls comprise of the low voltage per cell, the low energy density thereof and the physical size of a single cell, restricting applications to mostly that of hybrid systems in the automotive field. This open the door to many possibilities for improvements, some of these future trends are listed below.

- Graphene SCs: graphene is a single layer of carbon that has an astounding tensile strength (more than that of steel) whilst remaining remarkably thin [142]; it is also flexible and highly conductive [143]. Capacitance is limited by relative surface area and to overcome this SCs make use of activated carbon – activated carbon contains nano-pores and porosity increases relative surface area. Graphene also contains nano-pores however it has significantly more than activated carbon, so much so that a fraction of the size of the graphene is required to achieve the same relative surface area as that of activated carbon [144]. This allows for the reduction in the size of SCs to the point where they can be used on micro PCBs [145]. With reduction in the size of SCs, the field of application expands ten-fold including, pacemakers, cell phones and virtually any application using capacitors or requiring energy bursts [146].
- SC batteries – also known as super-batteries: combine the positive aspects of batteries with those of SCs. This creates a battery with a significantly smaller size, the capability to recharge faster (than conventional batteries) and increases the recharge cycles to a capability close to

that of standalone SCs [147]. Applications would include any application requiring the capabilities of a battery and the ability of fast charge and discharge [148].

### 2.3.3 Fuel Cells

A Polymer Electrolyte FC (PEFC) operates in a similar manner to that of a battery. With reference to Figure 2.9, there are two electrodes (anode and cathode) separated via a membrane and connected using an electrolyte. A fuel is supplied to the one electrode (anode) and an oxidant to the other (cathode). The fuel and oxidant react with the electrolyte as well as with each other causing electrons to flow in the external circuit from the one electrode to the other inducing a voltage. This chemical process produces two types of by-products, one from the fuel and one from the oxidant. A hydrogen FC has a fuel of hydrogen and oxidant of air, thus producing water and air as by-products. These FCs have an energy density of up to 150 times that of a Li-Po battery [20]. In recent advancements a hand-launchable fixed-280 wing UAV has been developed that is capable of a 10-hour flight with a distance of 500 km.

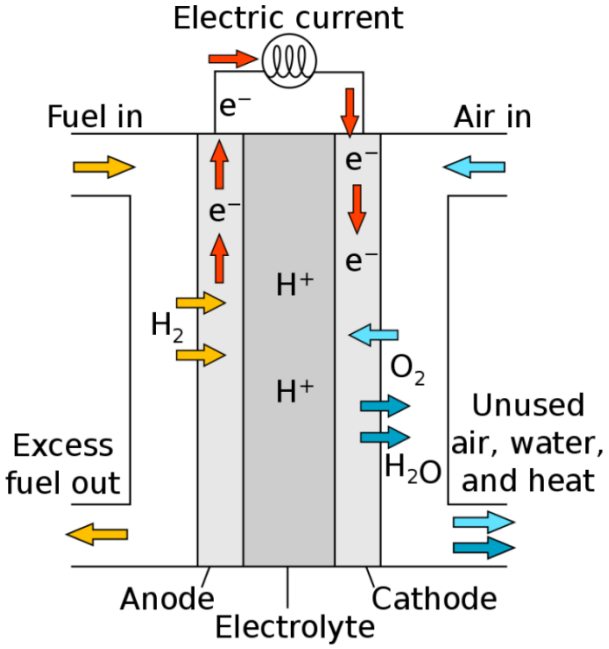


**Figure 2.9: Basic structure of a PEFC (adapted from** [149]**)**

Another drone design uses the hollow structure of its body to store hydrogen instead of air allowing the elimination of the weight contributed by the usual storage of the hydrogen. As renewable fuel vehicles become more popular, alternative power sources to batteries are being investigated, one of which has to do with FCs. For the implementation of hydrogen FCs in vehicles FCs are required to have a high-power density, rapid response to loads and a hydrogen supply infrastructure. FCs can be divided into different categories, i.e., Proton Exchange Membrane (PEM) FC (also known as Polymer electrolyte fuel cell [150]), Phosphoric Acid FC (PAFC), Solid Acid FC (SAFC), Alkaline FC (AFC), High temperature FC (HTFC) and Electric storage FC (ESFC).

PEMFCs consist of a stack of bi-polar plates containing a Membrane Electrode Assembly (MEA) which contains the electrodes, their catalysts, the hydrated membrane and the gas diffusion layer

(GDL). A platinum catalyst on the anode side separates the hydrogen ($H_2$) into two protons and two electrons, the former moving through the membrane, with the use of water (from water-based, acidic polymer membrane electrolyte), to the cathode and the latter utilizing the GDL to move through a conductor and generate a current [151]. Once on the cathode side the protons use the cathode catalyst to once again bond with oxygen and form water [152].

PAFCs contain two porous gas diffusion electrodes (composed of carbon or cloth) with a porous electrolyte matrix. The electrodes are composed of a porous substrate on the gas feed side and a reactive catalyst layer facing the electrolyte, the reactions are similar to those explained for the PEMFC. For the PAFC hydrogen is the fuel and liquid phosphoric acid is the electrolyte [153]. This FC has a few drawbacks including: the phosphate ion being absorbed at the catalyst surface hindering the electrochemical reaction, an acid loss when operated at high temperatures for extended periods of time, the platinum catalyst particles migrating and forming larger particles on the electrode reducing the active surface thereof and at high voltages a gradual carbon corrosion becomes present [154].

SAFCs utilize a solid acidic material as the electrolyte. Solid acids are chemical intermediates between salts and acids, at low temperatures they act like salts and have an ordered molecular structure, while at higher temperatures they undergo a phase transition to become a highly disordered super-protonic structure like acids. This increases conductivity and allows for increased efficacy of the FC. These FCs are very similar to the PEMFCs, in structure and operation, however the electrolyte of the PEMFC is a water-based acidic polymer membrane, therefore it is constantly in the liquid state, where the SAFC has an acid that transitions from solid to liquid when required. This type of FC can function using hydrogen gas obtained from a variety of different fuels, increasing their areas of application [155], [156].

AFCs have a liquid potassium hydroxide (KOH) solution as electrolyte separating the electrodes [157]. They are one of the first developed FC technologies and use non-precious catalysts for the electrodes, nickel or the anode and activated carbon for the cathode. As with the PEMFC the hydrogen divides into its protons and electrons at the anode and the electrons then move towards the cathode in the external circuit inducing a current [158]. Different to the PEMFC, the hydroxyl (OH-) moves from the cathode to the anode producing water and heat on that side of the FC. This FC is advantageous as it has a high efficiency, lower costs and a simple structure, however their shortfalls include quite a short operating life due to the KOH eroding the FC parts and purified oxygen is required in the system as it is very intolerant to carbon dioxide [157].

HTFCs have two main types, Solid oxide FCs (SOFC) and Molten carbonate FCs (MCFC). The former uses a solid ceramic inorganic oxide as the electrolyte and a solid ion exchange membrane for ion exchange [159]. SOFCs are not limited to the more common flat shape and are often in the

shape of a rolled tube, they only operate at high temperatures allowing for the use of more inexpensive catalysts and can be run on a variety of fuels, without the need of purification [160].

MCFCs also require high operating temperatures but use a mixture of molten potassium and lithium carbonate as an electrolyte [161]. They use inexpensive nickel catalysts as the electrodes and are capable of internal reforming, allowing them to convert other fuels into hydrogen, directly [162]. This FC functions similar to the other FCs but has advantages over the others including, a higher resistance to impurities, the catalysts comprise inexpensive non-precious metals, they attain high energy efficiency and also high fuel efficiency [150].

The final FC is the ESFC which is a conventional battery that includes the use of hydrogen and oxygen as alternative inputs for charging the battery. PEMFCs require relatively low operating temperatures while maintaining high efficiency, power density and rapid response to load changes, which makes them the preferred variation for EVs or other applications requiring a light weight power source that is small in size [163]–[165]. FCs used on-board drones contain a buffer Li-Po battery that is used to supplement the power when peak power is required. This allows the FC to have a longer usage time per flight as it isn't drained during the peak power instances. However, these batteries cause the system to be heavier and decrease the life of the aircraft as batteries have a limited cycle life. This cycle life is less than that of the FC. Another detrimental issue is that the FC constantly recharges the battery once it is depleted below its optimal voltage. This significantly decreases the cycle life of the battery although it allows for convenience of the user.

Advantages of FCs on drones include no direct pollution, no sound, large energy density and an almost instant charge. Disadvantages are related to the size being slightly larger than conventional battery-powered drones, operating costs are dependent on the availability of hydrogen gas [22] and the size of the hydrogen gas tank limits the build of the drone. The hydrogen tank needs to be taken into consideration when balancing the drone remembering that the weight decreases as the tank empties.

### 2.3.4 Combustion Engine

Both petrol and diesel engines fall under the term combustion engines and consist of relatively the same components, an engine block containing (amongst others) a combustion chamber, pistons, fuel injectors, and an intake and exhaust valve. A two-stroke engine, the most commonly used combustion engine, consists of two strokes and four stages, intake, compression, power and exhaust. One of the main differences between petrol and diesel engines is that the former have spark plugs, whereas the latter do not require this due to diesel self-igniting when under extreme pressure. Diesel engines, do however, sometimes require a glow plug to heat up the diesel before it enters the chamber as diesel engines can have complications when starting in cold weather. Other differences include petrol engines having a faster rotational speed compared to diesel as they have lighter

pistons, connecting rods and crankshaft (lower compression ratios) and due to petrol igniting easier than diesel. However, petrol engines have lower efficiency than diesel engines; this includes thermal efficiency [166].

Kerosene, Methanol, Ethanol and LPG Propane are all variations of the petrol-powered solutions available and some of them have a remarkable performance, one performance of a gasoline-powered fixed wing UAV being more than 20-hours with one full tank of gasoline [166]. The weight of drone is continuously decreased in flight due to the weight of the fuel decreasing, therefore increasing the range. Diesel engines have the highest effective efficiency of all the combustion engines, they can also operate on a variety of fuels, some of which have high energy density and are safer for the environment and the external system requires lower voltages allowing for better environmental adaptability [167]. Diesel engines are in general more robust than petrol engines but this also leads them to be heavier and bulkier which is counterproductive when used on-board a drone. The advantages of combustion engines drones comprise of longer flight time, robustness, small, lightweight and having a good specific fuel consumption. The disadvantages comprise of being heavier compared to battery-powered drones and require more complex maintenance [19].

### 2.3.5 Solar power

The conversion of sunlight into electricity is most commonly done by converting light into electric current through the PV effect. This current is then either directly used or stored in a battery and the battery provides power to the system. There are two main technologies used for solar power, PV systems or CSP. The former being a direct conversion of sunlight into electricity and the latter being used to make steam that allows a turbine to generate electricity [151], [168], [169]. Solar panels are generally used on-board fixed-wing drones as they require a large surface for the panels, but also used to extend the range of a rotor-type drone (used to assist the main power of the rotor-type). Solar powered drones are quiet, have low operational costs, low maintenance costs and an excellent carbon footprint, however, in order for them to be efficient a large area is required for the panels, therefore increasing the size of the drone tremendously and the panels also require sunlight to operate.

### 2.3.6 Unique power source

Ionic wind powered drone. This drone does not use any batteries or moving parts, it is only powered using ionic wind and the principle of electro-aerodynamic thrust. Due to there being no moving parts the plane is completely silent. Electro-aerodynamic thrust is a principle based on thrust or wind produced by passing a current between a thin and thick electrode, if the applied voltage is sufficient the air between the electrodes will produce enough thrust to propel a small aircraft [170].

### 2.3.7 Depletion Rate

With reference to Figure 1.1, the Ragone plot, the depletion rate of the different power sources can be deduced. SCs are seen to have a higher power density and lower energy density which means that they can supply high levels of power immediately for short periods of time, the lower the power required the longer the duration of the supply. FCs are seen to have a much higher energy density and lower power density, thus they can supply the energy for much longer periods of time, but the higher the power requirement the shorter the supply. Figure 1.1 contains diagonal lines that represent the duration each power source can last before entering depletion. Theoretically, if we were to combine the FCs with the SCs the energy and power density would exceed that of the mentioned batteries and the Li-ion capacitors. This would be ideal as the FCs can supply power for as long as it is supplied with fuel and could therefore also be used to recharge the SCs allowing the system to last much longer [171].

### 2.3.8 Cycle life

There are many factors that affect the longevity of the efficient use of energy sources with depth-of-discharge (DoD) and c-rates being two of the more important factors that affect the cycle life. DoD refers to the capacity that an energy source can discharge, expressed as a percentage of the source's maximum capacity. C-rate refers to the rate at which an energy source discharges with respect to its maximum capacity. DoD indicates the voltage minimum whereas c-rate indicates the current maximum of the source. Energy sources can operate outside of these limits but in order to preserve the longevity is it inadvisable. Both of these ratings are specific to the energy source and are advisable to not exceed as this places unnecessary strain on these sources which will degrade the capacity of the energy source significantly, reducing these ratings and thus reducing the cycle life of the source. If the energy source is operated within the specified ratings it will provide the user with the expected cycle life.

## 2.4 DC-DC converter

Due to the system being a hybridization of two power sources a device will be required to match the characteristics of the sources such that a smooth transition can occur between the use of either source. There are two main power conversions, namely, AC and DC and there are multiple ways to achieve conversions from- and to the desired one. As this project involves the interfacing of DC systems the focus will be on DC-DC conversions. There are two main ways to achieve the interface, either use two DC/AC converters back-to-back (DC/AC/DC) or use a DC-DC converter [172], [173]. The former increases the robustness of the converter as DC volts can be blocked in the AC section and AC transformers can enable higher conversion ratios with relatively low losses. There are many different DC/AC/DC topologies, however, for this project the focus will be on DC-DC converters as the project needs to be lightweight to not interfere with the balancing of the drone too much and

transformers can increase the complexity and weight of the system tremendously. This section of the literature study will focus on the main considerations required before such a system can be built. These considerations include the topology, the conduction mode, the switching module and the microcontroller type (and control method) required for the converter. These will be discussed below.

### 2.4.1 Mode of operation

In order to explain the different operations of the DC-DC converter a basic circuit for a two-switch buck/boost converter is given in Figure 2.10 below. This figure was drawn on LTspice® and will be altered according to the desired topology of each subsection.

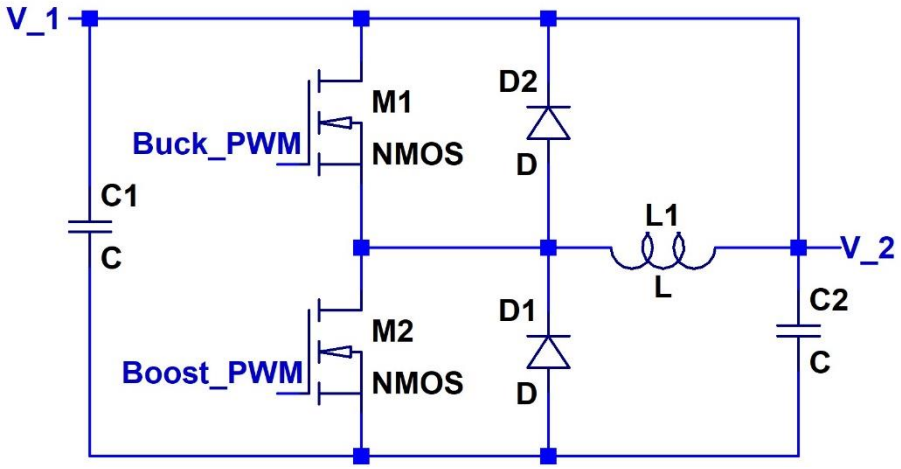


**Figure 2.10: Basic circuit for a buck/boost converter**

DC-DC converters consist of a charge and discharge phase, where the inductor “charges” and “discharges” through the circuit. The switching of the Metal Oxide Semi-conductor Field Effect Transistor (MOSFETs – determined by the PWM signal sent to each switch) determines which phase the converter is in and it is vital that only one switch is closed at a time. If any overlapping of the switching occurs a short circuit will be observed and the system will blow. An inductor is a form of a decreasing resistor in a circuit, this is due to it being a conductor wound around a magnetic core. The core induces EMI in the conductor which opposes the flow of current, but as the current flow strengthens, the EMI decreases allowing more and more current through – this phenomenon is known as the inductance.

The charge and discharge phases of an inductor are controlled by the potential difference across the inductor – as long as there is a potential difference the inductor will remain in the specific phase. Potential difference is an indicator of the direction of flow of current. Starting with a forward flow of current, as the inductor charges the potential difference across it will decrease. There is a point where the input to the inductor is equal to the output and the potential difference is zero. After this point the voltage of the output will become larger than that of the input thus swopping the polarity of the inductor.

An inductor is designed to function in a specific frequency range and this determines the charge and discharge rate of the inductor. Equation (2.1) (obtained from equation (19.1) in [174]) will help show the connection between the frequency and the current,

$$Current\ (I) = \frac{charge\ (Q)}{time\ (t)} \quad \textbf{(2.1)}$$

Time is the inverse of frequency and thus current is proportional to frequency – the higher the frequency, the larger the current capabilities. An inductor is chosen according to the frequency of operation of the circuit and this in turn determines the maximum current allowance of it. If the load current increases above that allowed by the frequency range, the inductor will charge and discharge at a faster rate. This becomes an issue when the circuit contains other switching elements. Another switching element (which was also designed for the specific frequency), can prohibit the inductor from changing polarity to allow the charge and discharge thereof. This prohibition causes the inductor to get stuck in a phase after it has either fully charged or discharged. If it is stuck in the charge phase the EMI is at its lowest, essentially causing the inductor to become a conductor, decreasing the inductance tremendously [175] – this leads to losses in the form of heat, decreasing the efficiency thereof exponentially. This area where the inductor gets stuck in a phase is referred to as the point of saturation. Saturation is not as detrimental for the discharge phase as EMI is at its highest then and the inductor will simply not conduct, thus causing losses in the form of time. An example of this point is given in Figure 2.11.

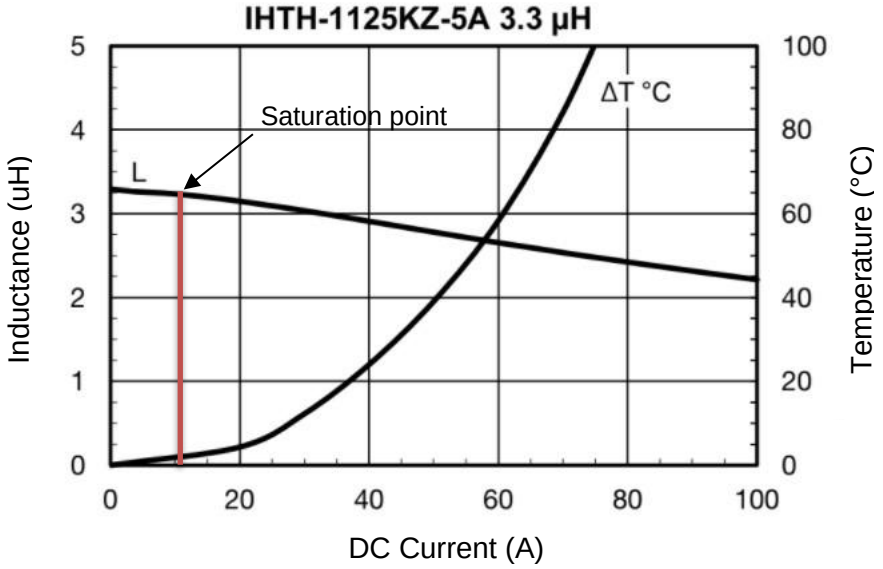


**Figure 2.11: Example of inductor performance graph (adapted from** [176]**)**

The figure depicts the saturation curve of a 3.3 µH inductor. This curve shows that after the point of saturation the inductance decreases drastically whilst the temperature increases exponentially. This shows that the inductor can operate at levels higher than 10 A, but it is not advised due to this temperature rise. Temperature is a form of needless losses as in a circuit as it causes power dissipation at that point. This initial stage up to the saturation point of an inductor is the charge stage thereof and in order to avoid the saturation of the inductor it must discharge through some form of a

load. The charge and discharge stages of the inductor will be explained further under the respective headings of buck-, boost-, and buck/boost operation.

#### 2.4.1.1 Buck

The charge and discharge stages of the inductor for a buck converter will be explained using Figure 2.12 below.

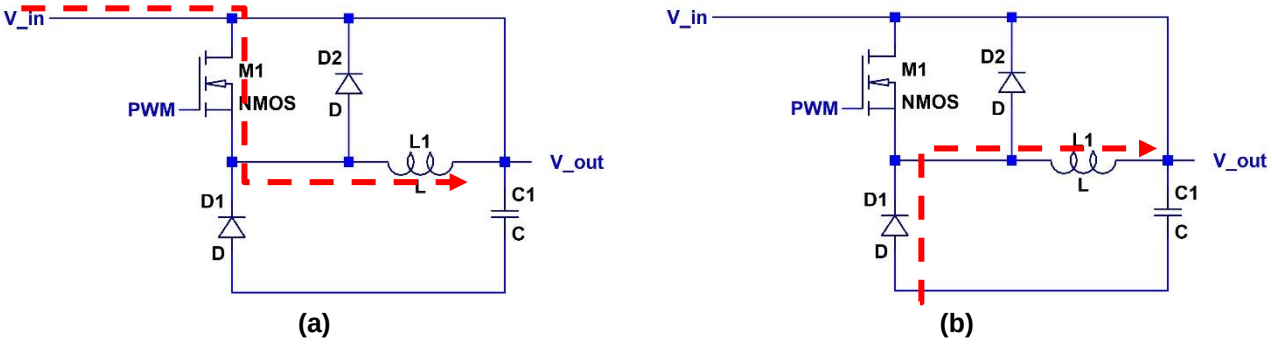


**Figure 2.12: (a) Charge and (b) discharge stages of buck converter**

The buck converter consists of two modes, charge and discharge, when $M_1$ is closed and when $M_1$ is open, respectively, this is determined by the PWM signal – a square wave that repeats at a specific frequency. During the charge stage ($M_1$ is closed and $D_1$ & $D_2$ are not operating) the inductor will charge up to a percentage of the input voltage determined by the duty cycle of the PWM signal, given by the equation (2.2) (obtained from equation (5) in [177]),

$$D = \frac{V_o}{V_{in}} \tag{2.2}$$

Before the inductor saturates the switch will open and $D_1$ will connect the inductor to ground allowing it to discharge towards $C_1$ and the output. This operation of the inductor limits the output voltage to that accumulated by the inductor during its charge stage, therefore causing the buck/ step down in voltage of the system [178]. The function of $C_1$ is to stabilize the output voltage and to filter out AC components in the voltage due to the switching operation of the inductor.

This mode of converter is preferred where there is a power supply that needs to be decreased to a specified voltage and where the supply voltage will not decrease below that specified voltage [179]. As this converter only functions in a single direction it is classified as a uni-directional converter. Many DC-DC converters are uni-directional and have many more applications as their circuitry is much simpler and does not contain as many components as a bi-directional converter [180].

#### 2.4.1.2 Boost

The charge and discharge stages of the inductor for a boost converter will be explained using Figure 2.13 below.

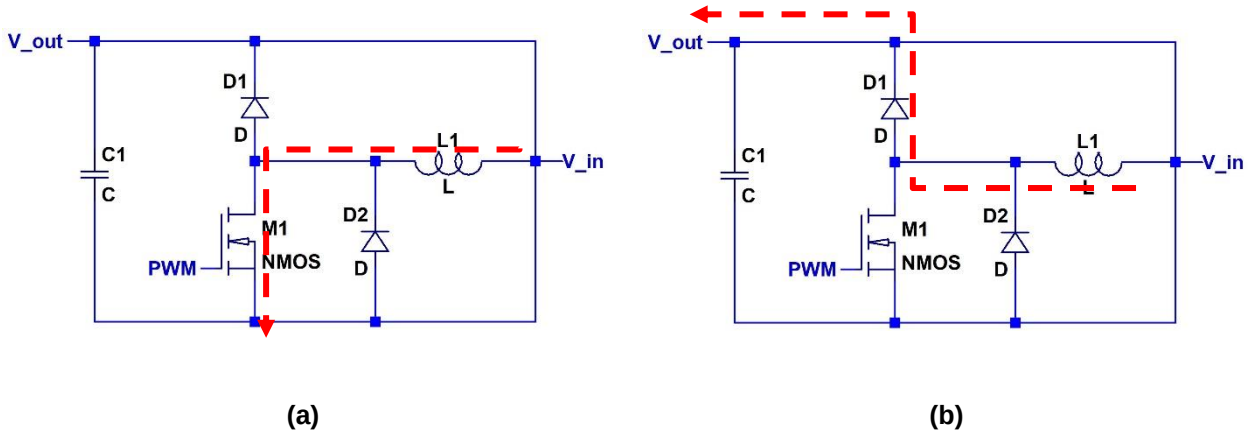


**(a)** **(b)**

**Figure 2.13: (a) Charge and (b) discharge stages of boost converter**

The boost converter similarly consists of two modes, charge and discharge, when $M_1$ is closed and when $M_1$ is open, respectively, this is determined by the PWM signal, a square wave the repeats at a specific frequency. During the charge stage ($M_1$ is closed and $D_1$ & $D_2$ are not operating) the inductor will charge up to a percentage of the input voltage determined by the duty cycle of the PWM signal, given by the equation (2.3) (obtained from equation (5) in [177]),

$$D = 1 - \frac{V_{in}}{V_o} \tag{2.3}$$

Before the inductor saturates the switch will open and $D_1$ will connect the inductor to $C_1$ and the output allowing it to discharge while simultaneously allowing the input voltage to flow directly to the output of the system. This operation of the inductor causes the output voltage to be the combination of the input voltage and the percentage stored in the inductor during mode 1. This leads to the boost/ step-up in voltage of the system [178]. The function of $C_1$ is to stabilize the output voltage and to filter out AC components in the voltage due to the switching operation of the inductor.

This mode of converter is preferred for applications where the power supply is lower than the preferred voltage and does not exceed this voltage [179], [181]. As this converter only functions in a single direction, like the buck converter, it is also classified as a uni-directional converter.

#### 2.4.1.3 Buck/boost

For the operation of the buck/ boost converter Figure 2.10 will be referenced. This converter has 4 modes of operation shown in Table 2.2.

**Table 2.2: Buck/boost converter Mode breakdown (adapted from** [182], [183]**)**

| | $M_1$ | $M_2$ | $D_1$ | $D_2$ |
|---|---|---|---|---|
| **Mode 1** | ON | OFF | OFF | OFF |
| **Mode 2** | OFF | OFF | ON | ON |
| **Mode 3** | OFF | ON | OFF | OFF |
| **Mode 4** | OFF | OFF | ON | ON |

This converter functions as a buck converter from left to right and as a boost from right to left, respectively. Mode 1 & 2 indicate the buck operation and mode 3 & 4 indicate the boost operation. Both buck and boost mode operate in the same manner as discussed above except that the equation for the duty cycle differs given in equation (2.4) (obtained from equation (12) in [177]),

$$D = \frac{V_o}{V_{in} + V_o} \quad \textbf{(2.4)}$$

This converter differs from the aforementioned buck and boost converters as it can function in both directions, classifying it as a bi-directional converter [184]. The design of bi-directional converters is also more complex as they need to take into account the flow of current in both directions and the requirements of each side. This leads to additional components, more complex switching, and increased power losses. The buck/boost converter offers a lower efficiency and larger footprint than the uni-directional buck or boost converter, although it can operate in both directions therefore simplifying circuits requiring both [185]. A buck/boost converter can also be applied where a negative output voltage is required from a positive input with respect to ground [182], [183].

#### 2.4.1.4 Conduction Mode

The charge and discharge functionality of the inductor is known as the conduction mode. There are two main modes of conduction, Continuous Conduction Mode (CCM) and Discontinuous Conduction Mode (DCM). When selecting an inductor for a DC-DC converter it is important to decide which of the two modes the converter will function in. Figure 2.14 will be used to explain the two.

Ideally it is desired that the charge and discharge of the inductor occur without any “dead times” as these lead to decreases in efficiency of the converter. “Dead times” refer to moments when the inductor is stuck in either charge or discharge phase [186]. For this to occur all the variables in the converter need to be precise; these variables refer to: switching frequencies of all components, the PWM signal of the switch(es) and the characteristics of the inductor. All of the components in the circuit that switch operate at a specific switching frequency, these need to be faster than that of the inductor due to losses in the circuit. The PWM signal supplied to the switch also operates at a specific frequency, which again needs to be faster than that of the inductor.

Finally, the characteristics (switching frequency, peak current capability, and inductance) of the inductor need to match the requirements of the circuit (voltage output and load current). Another consideration is that of the input voltage, does it vary or is it continuous? If the input voltage remains constant all of the above requirements can be calculated accordingly such that the inductor switches before it enters saturation and just before it is fully discharged – this allows for CCM, where there is no point that the inductor is not operating. If the input voltage varies all of the above requirements need to vary with it, which is a difficult task as most of the requirements are fixed values of components. Therefore, most of these values can be overestimated to accommodate their largest

requirement, respectively, with the exception of the PWM signal sent to the switch which can be altered via the system accordingly.

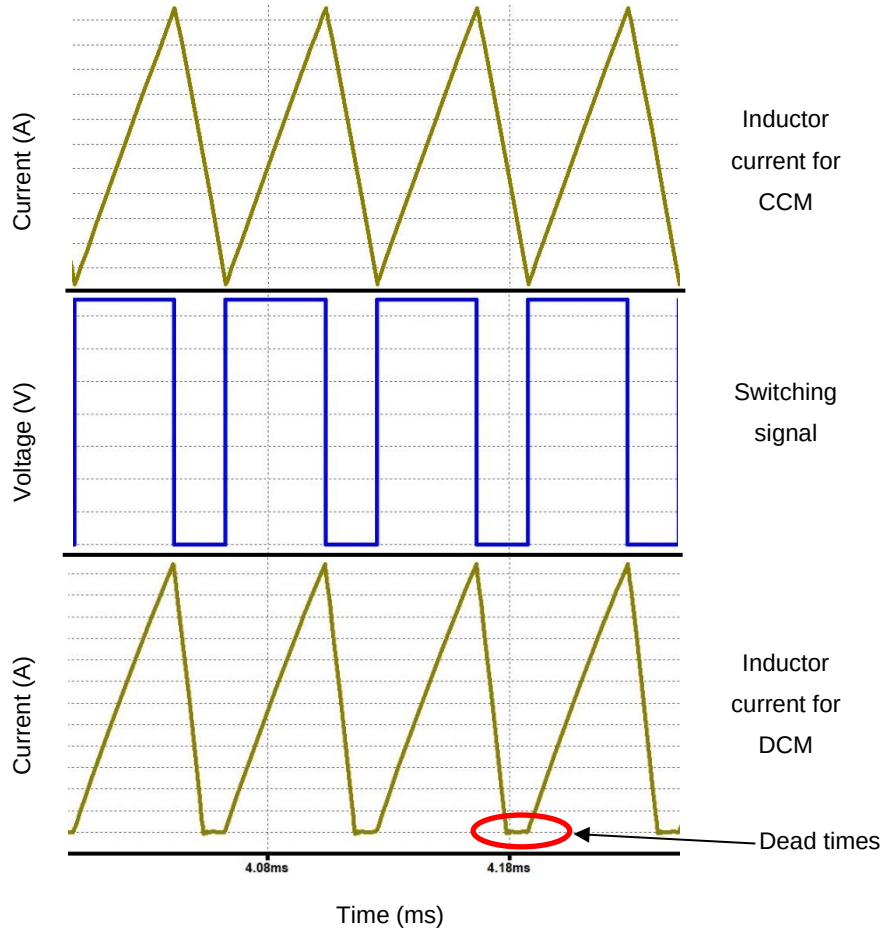


**Figure 2.14: Conduction mode graphs**

However, due to the PWM adjustments not occurring instantaneously the inductor might still experience “dead times” when it is fully discharged and the system is slightly slower. This is the DCM shown in Figure 2.14 – where the inductor will not conduct for a short period of time while discharged. The dead time is also indicated in the figure and if the vertical grid is followed into the switching signal graph it can be seen that the dead time occurs after the inductor has fully discharged and the switching signal is still off. A final consideration as to why these dead times can occur is whether the load on the output varies as well. A larger load can cause the inductor to discharge faster, again causing DCM [175].

A buck or boost converter can operate in either CCM or DCM, whereas a buck/boost converter’s conduction mode is dependent on the buck or boost functionality [187]. Some converters tend to operate in the DCM/CCM boundary – which refers to general operation in CCM until a dead time occurs due to a varying input voltage or load requirement where the converter will switch to DCM. This boundary operation leads to an increased ripple component in the inductor current leading to a large conduction loss and an overall decrease in efficiency, therefore it is desired to reduce this boundary occurrence such that the converter remain in CCM for the majority of the operation of the

converter or that the dead times are as short as possible [188]–[192]. Advantages of CCM include less power and efficiency losses due to dead times and therefore a more precise output voltage. Disadvantages include the requirement of a stable continuous input voltage and a continuous load, therefore limiting applications and a more complex and precise design. Advantages of DCM include a simpler design, can be used with both a varying input voltage and a varying load and disadvantages include a lower efficiency and increased power losses [193], [194].

#### 2.4.1.5 Circuit construction

The most common construction of DC-DC circuits are that of the two-switch or four switch converters. In both cases the switches can refer to any type of switching module and they are specifically chosen according to the desired operation of the converter. There also exists Flyback [195], Cuk [196] SEPIC/Zeta [197], coupled inductor [198], tapped inductor [199], switched capacitor [200] and Negative Coupled Inductor [201] converters, but as these are more complex and require an increasing amount of components compared to the two-and four switch, these will not be discussed due to the size requirements of the proposed solution. The two-and four switch construction will be discussed below [202].

##### 2.4.1.5.1 Two switch

This construction is shown Figure 2.10, Figure 2.12 and Figure 2.13. The two switches refer to the amount of switching devices used for the general operation of the converter for either buck or boost mode. In Figure 2.10 this refers to $M_1$ & $D_1$ in buck mode and $M_2$ & $D_2$ in boost mode. In Figure 2.12 and Figure 2.13 this refers to $M_1$ & $D_1$ as these respective switches control the flow of current in these circuits. Although bi-directional, this converter can only function as a buck from left to right or as a boost right to left [203].

##### 2.4.1.5.2 Four switch

This type of construction is also known as an h-bridge construction and is shown in Figure 2.15.

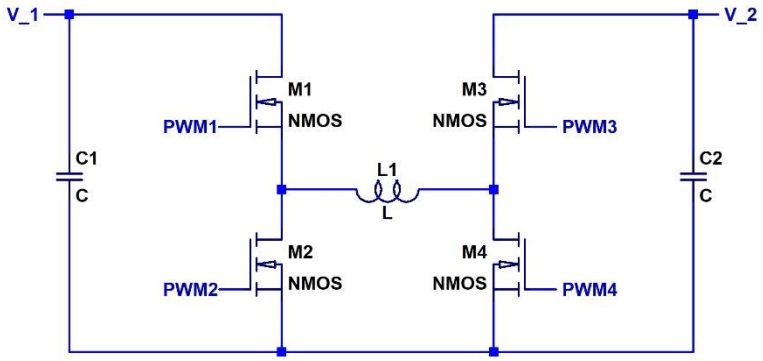


**Figure 2.15: Four switch DC-DC converter construction**

This particular four switch construction is bi-directional and can function in both buck and boost mode in both directions [204]. Figure 2.16 will be used to explain the boost mode operation of the four-switch converter.

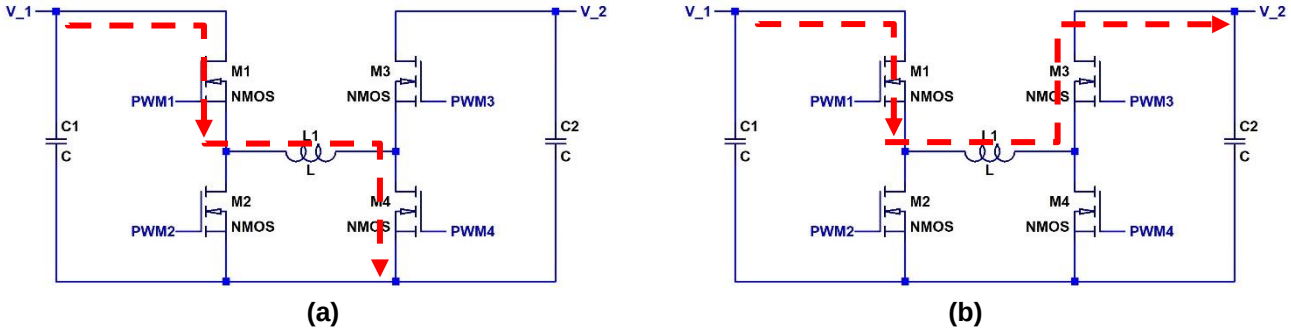


**Figure 2.16: Four switch buck mode (a) charge and (b) discharge stage**

In boost mode $M_1$ is always closed, $M_2$ is always open and $M_3$ & $M_4$ will have inverted PWM signals. As with the two-switch circuit it is imperative that $M_1$ & $M_2$ and $M_3$ & $M_4$ never be closed at the same instance as this will cause the system to blow. The PWM signals sent to $M_3$ & $M_4$ are determined through the use of equation (2.4). Similar to the two switch boost converter the inductor will charge (when $M_1$ & $M_4$ are both closed) to the percentage determined by the duty cycle of equation (2.4) and discharge (when $M_1$ & $M_3$ are closed) allowing the full input voltage ($V_1$) and the discharged voltage to flow towards $V_2$ as the boosted output voltage. Figure 2.17 will be used to explain the buck mode operation of the four switch DC-DC converter.

In buck mode $M_3$ is constantly closed, $M_4$ is constantly open and $M_1$ & $M_2$ have inverted PWM signals. The PWM signals and the duty cycle is determined in the same manner as with the boost mode above. The inductor will charge to a percentage of the input ($V_1$) when $M_1$ & $M_3$ are closed and will discharge the accumulated voltage when $M_2$ & $M_3$ are closed, supply $V_2$ with the smaller output voltage. The buck and boost mode work in the same manner when operating in the reverse direction [205].

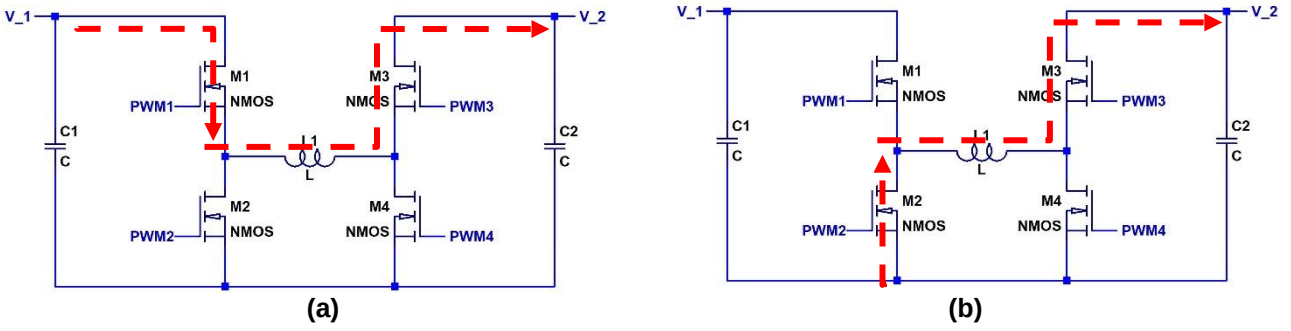


**Figure 2.17: Four switch buck mode (a) charge and (b) discharge stage**

Advantages of the two-switch construction include a simpler design, less components, less interference due to the components and their switching elements and also simpler coding of the PWM signals. The switches elements are also suggested to operate under 70% duty cycle this means that the two switch converters, when operating as a uni-directional device, can deliver a larger

variance between the input and output voltage when compared to the four switch. The main disadvantage of the two-switch converter is that it can only function in one mode and one direction, therefore limiting applications.

The four-switch converter has the advantage of bi-directional multi-input operation broadening the areas of application. Disadvantages include lower efficiency, smaller variations of input to output voltage ratio, more complex design and therefore more components and complex code for the PWM signals required [203].

### 2.4.2 Switching Module

The DC-DC converter to be used in this project will contain one or more switching elements and it is necessary to research the different types in order to determine which would be best suited for the application. For the application it is necessary to understand how each works in order to understand how the operation will affect the external circuit and vice versa. This will also give an indication of additional circuitry required for optimal operation of the switching device. The most common switching devices used in a DC-DC converter include transistors, relays, diodes and Silicon Controlled Rectifiers (SCRs). Each of these will be further researched below.

Bipolar Junction Transistors (BJTs), Field Effect Transistors (FETs), MOSFETs, Power MOSFETs and Insulated Gate Bipolar Transistors (IGBTs) are a few of the different types of transistors available on the market, but how do they differ from each other and why is one preferred over the other? With regards to a DC-DC converter picking the switch depends on the application, the input & output voltage & current requirements, the power requirements, the switching frequency capabilities, the size restrictions, the efficiency, the positioning of the component and parasitic interference caused by the component and how it will affect other components in the circuit. These are just a few considerations that will be discussed for each transistor as well as for the other switches in this section.

There are two types of transistors, n-type and p-type, the most common difference is that an n-type is normally open until a signal closes it allowing current to flow and a p-type is normally closed and a signal will stop the flow of current. BJTs are bi-polar as they use both holes and electrons simultaneously to operate; they are constructed using two PN-junctions to form three terminals; BJTs have a low gate impedance and are therefore current controlled. The FET does not contain a PN-junction its main current carrying path, instead it is constructed using an N-type or P-type semiconductor; the FET is uni-polar and functions using either the holes alone or electrons alone to conduct; it is a voltage controlled device as the voltage level applied to the gate controls the conductivity of the channel.

A MOSFET is a type of FET with a gate insulated from the current carrying channel; the insulation causes a miller capacitance and increase gate inductance above that of a FET [206]. An IGBTs construction combines a MOSFET to control the input and a BJT as the switch, this leads to the IGBT having an extra substrate layer that creates a carrier overflow and therefore requires a reverse biased freewheeling diode in parallel help the flow of current in the substrates [207]. A MOSFET is preferable for low current, low voltage, high frequency applications whereas an IGBT is designed for high voltage, high current but low frequency applications.

A power MOSFET is specifically designed for higher power levels (higher voltage due to the N-channel doping and higher current due to a larger channel width) and also has a better efficiency than both IGBTs and normal MOSFETs and is thus preferred in DC-DC converters. MOSFETs can switch at higher frequencies but this is limited by the charge/discharge of the input and miller capacitances present in the MOSFET structure [206]. The major flaw of an IGBT is that the additional substrate causes a significant decrease in switching speed at turn-off, this flaw is very complicated to reduce [207]. To further compare BJTs, MOSFETs and IGBTs Table 2.3 will be used – the information in the table was obtained through comparing the different components under the references listed.

**Table 2.3: BJT, MOSFET and IGBT characteristic comparison (obtained from** [208]–[211]**).**

| | **Current capability (A)** | **Voltage capability (V)** | **Power capability (W)** |
|---|---|---|---|
| **BJT** | <500 | <1k | <100k |
| **MOSFET** | >500 | <1k | <500k |
| **IGBT** | >500 | >1k | <800k |

MOSFETs are solid state switches and therefore have no moving parts whereas relays contain moving parts. Relays are metal switches controlled via a magnet and therefore can cause an EMI in the external circuit; due to the magnetic components, relays require more power to switch than a transistor does, however as they have much larger power capabilities than transistors. One major downfall when used in DC-DC converters is that a relay is either on or off and cannot control the flow of current or percentage thereof through it. They also have a very low switching frequency and unfortunately have the very high likelihood to latch causing malfunctions in the circuit [212].

Another disadvantage when used in DC-DC converters is that the coil requires quite a large amount of power to energize and remain energized whilst in use, this causes increase and unnecessary power losses in the circuit. An SCR is a uni-directional semiconductor, can handle extremely large currents, is a current controlled device that only switches off when the current equals zero but it works best in AC applications [213]. A diode is also a uni-directional semi-conductor therefore blocking reverse current and it can operate at very high frequencies but it cannot vary the amount of current flowing through it.

### 2.4.3 Microcontroller control

The DC-DC converter will require a method of controlling the switch which will be done through the use of a PWM signal. This signal can be sent from a variety of sources however as the system requires a method of adjusting the PWM according to the input to the converter a device will be required that can offer this. This device will be required to measure the input to the converter and apply a few calculations in order to deliver a signal to the switch that will in turn allow the converter to deliver a desired output. This functionality requires input and output (I/O) pins as well as pins enabled to supply a PWM signal – hence, a microcontroller. A couple of considerations will need to be made in terms of the physical size, the operating frequency, user complexity, open-source code availability, I/O pin capabilities, analogue to digital conversion (ADC) accuracy and integration with the remainder of the circuit. Beginner preference will also be included under user complexity [214]. As this system will adjust according to the varying input a control method will be desired, specifically one that is intelligent, a few of these will be discussed in this sections as well as some suitable microcontrollers.

#### 2.4.3.1 Control Method

The DC-DC converter will be adjusting the duty cycle of the switch according to the input voltage measured. It is a good assumption that some errors will occur due to inaccuracy of the microcontroller measurements and also due to delays of measurements made. This is all expected as the microcontroller will operate in a “loop” and will therefore only complete each task in the written order, thus causing a slight delay in measurements and an equally slight inaccuracy of measurements read and actual values at a specific moment. These inaccuracies lead to calculated values based on past input values leading to a deviation in the output value to that which is desired. This is where intelligent control methods come in. Intelligent control methods allow a system to calculate expected error values or deviations and apply these values to the calculations leading to more accurate outputs and smaller deviations. A few methods to include these error values are given below.

##### 2.4.3.1.1 Artificial Neural Network (ANN)

Computing system inspired by the biological neural network. This system learns to perform tasks by considering examples and is generally not programmed with task-specific rules. The more examples given the better the identification results. General applications include pattern or sequence recognition and system control. This method allows a system to adjust and improve continuously improving efficiency tremendously. However, it involves complex programming with a requirement of large quantities of training for optimal accuracy which in turn requires considerable computing resources to store all this information [215].

2.4.3.1.2 Proportional – integral – derivative controller (PID)

This is a linear control method and involves a control loop feedback mechanism used in applications that require continuous modulated control. The controller calculates an error value as the difference between the desired point and the measured point and applies a correction based on proportional, integral or derivative terms. It automatically applies the accurate and responsive correction to control the function. The more the program is run the smaller the error becomes. This method is significantly easier to program than ANN, no internal state measurements are required, tuning of this method occurs through trial and error, this method is also highly efficient and requires very few computing resources. This method is however, not suited for non-linear processes and does not function well under a changing/varying input environment [216].

2.4.3.1.3 Fuzzy Logic

This method uses logic control (similar to PID) for complex systems involving a varying input. Logic control functions on the principle of a measurement either being true or false, fuzzy logic accepts measurements that are partially true and applies an algorithm to produce the desired output. This algorithm allows the controller to appear linear. Advantages of this method include the use of simple math, it allows for a varying input value, returns highly precise results and has a quick operating speed. Increased accuracy requires more algorithmic levels leading to more complexity, the result isn't immediate and therefore can deviate from that which is expected, this method does not adjust/learn from deviations/errors and there is a restriction on the number of input variables [217].

2.4.3.1.4 Ladder Logic

The programs in this language resemble ladders and is based on the physical logic of relay circuits. This method is mainly used to program Programmable Logic Devices (PLCs) but can be applied in theory in other applications. This method has the advantage of self- documentations as the program is in the form of documentation, it is easily debugged and very user friendly. However, as the system uses single logic levels it can become unmanageably long and it can also require complex algorithms [218].

#### 2.4.3.2 Microcontroller type

In order to apply the desired control method a microcontroller will be required. From personal experience and preference an Arduino, STM32, Raspberry and FPGA board will be examined as they are the simpler microcontrollers to program, i.e. they operate in easy to use environments and simple languages. There are also more open-source resources available and many external devices are easily integrated with these boards. In picking the correct board attention will be given to the size thereof, the number of I/O pins, operating voltage and current requirements, I/O pin functionality, operating frequency and ease of use.

#### 2.4.3.2.1 Arduino boards

The Arduino boards are very simple to use with an open source community, there are many different examples of many different applications and the code is freely available to anyone. Various boards are available but the smaller boards are of interest as the system to be designed needs to be as small as possible, therefore the Arduino Nano will be focussed on. [219]. Advantages of the Nano include sufficient number of I/O pins, low operating power requirement (7 V), PWM enabled pins, and the Integrated Development Environment (IDE) is extremely user friendly. Although the switching frequency is high (62.5 kHz), it is much slower than the other boards, the I/O pins have a very low current capability (40 mA) and the board is also very susceptible to static [219], [220].

#### 2.4.3.2.2 STMicroelectronics boards

The family consists of many different series' of boards whose use depends on the application. Some of these boards are compatible with the Arduino environment and most support the mbed IDE. With regards to the size requirement the STM32F 103 C8 will be considered. These boards are cheap, have low power requirements (4 V), have a better performance compared to the Arduino boards, have a sufficient amount of I/O pins with 150 mA tolerance, the size is comparable to that of the Nano and they have a fast operating frequency (36 MHz) [221]. These boards do however use a more complex programming environment, integration with external devices can be more complex than with the Nano and certain functionalities are restricted for specific boards [222].

#### 2.4.3.2.3 Raspberry Pi boards

A series of small single-board computers to promote the teaching of basic computer science. Several generations of the board have been released but due to size restrictions the Raspberry Pi 0 will be examined here. These boards have significantly faster processing speeds (>400 MHz), it has a sufficient number of I/O ports with 50 mA capabilities and low operating power requirements (5 V) [223]. This board is compatible with many different IDE's and open source firmware is also available as well as being compatible with other boards' IDE's [224], [225]. This board cannot run complex multi-tasking and requires Linux to program, making this board not as user friendly as the above two boards [226].

#### 2.4.3.2.4 FPGA

A Field Programmable Gate Array Chip (FPGA), the TinyFPGA BX board, is an integrated circuit designed to be configured by the user after being manufactured, this is done using Hardware Description Language (HDL). Many of these chips can be reprogrammed to implement different logic functions making flexible reconfigurable computing, similar to that performed in computer software, possible [227]. This board has a low power requirement (1.4 V), sufficient amount of I/O pins with 300 mA tolerance and a 16 MHz switching frequency capability [228]. The programming of these boards require a considerable amount of compilation time although programming is simple and easily

understandable. These boards are however, initially expensive, require knowledge of HDL and programming resources are limited to that available on the FPGA IC [229].

## 2.5 Additional information

Some additional information was required to be researched for this dissertation. This information pertains to standards, simulation packages and energy management strategies. They will be researched to ensure compliance where necessary and to determine the relevance thereof in this dissertation.

### 2.5.1 Standards

As this is an electrical project it is necessary to research the standards that can be related to it in order to determine compliance and relevance to the project. These standards include IEEE, SANS, SABS and IEC. Each of these will be discussed briefly showing relevance to this project.

#### 2.5.1.1 IEEE – Institute of Electrical and Electronics Engineers

A professional association formed through an amalgamation of the American Institute of Electrical Engineers and the Institute of Radio Engineers. This is the world's largest association of technical professionals with objectives of educational and technical advancement of electrical and electronic engineering, telecommunications, computer engineering and allied disciplines [179], [230], [231].

The organization is composed of computer scientists, software developers, information technology professionals, physicists and associated professionals. Their main focus is to foster technological innovation and excellence for the benefit of humanity with a vision of being globally recognized for their contributions of technology and technical professionals in improving global conditions. Within the organization there is a separate unit that recommends policies and implements programs intended for maximum benefits of the members [232]. This organization has the purpose of consolidating ideas dealing with electro-technology, they publish technical work, sponsor conferences and seminars, give accreditation and develop standards [233].

As this project entails the use of power sources, electronics and some mechanical structures the IEEE Std 1662-2016 for power electronics [234] will need to be adhered to where applicable.

#### 2.5.1.2 SANS – South African National Standard

A standard that specifies the performance requirements of a specific product. These standards are either locally written or created by adopting an international standard [232].

The code that will be brought into consideration for his project is the SANS 10142 -1, which is the wiring code that covers fixed electrical installations of up to 1000 V AC and 1500 V DC. A second part to this code has been developed for higher voltages, but this project will not entail these voltages

and this code will be disregarded, [232]. This code is aimed at ensuring people, animals and property is protected from hazards that can arise from the operation of an electrical installation under both normal and fault conditions. This protection is provided against shock current, overcurrent, and fault current, overvoltage, under voltage, excessive temperatures and electric arcs. In order to provide this protection the designer should be aware of the characteristics of the power supply, the nature of the demand and the operating environment of each part of the installation [235]. All of the above mentioned has a direct connection to the project at hand as this project will contain wires between the components and different sections of the system. Also, this project is meant to be integrated into a drone, making it commercial and increasing the importance of this code. SANS 1652 for power electronics will also be looked at where applicable for this project.

#### 2.5.1.3 SABS – South African Bureau of Standards

A certification body that is accredited by SANS. This is not a standard, but rather a testing and certification body allowed to sample and test products to certify them according to SANS standards [233]. This organization is responsible for maintaining South Africa's database of standards and developing, revising, amending and withdrawing standards. Therefore, with reference to the SANS 10142-1 standard above, the SABS will be process of testing the project for legibility under the wiring code.

#### 2.5.1.4 IEC – International Electro-technical Commission

A not-for-profit, quasi-governmental organization with members from National Committees that appoint experts and delegates to participate in the technical and conformity assessment work of the IEC. They are the leading global organization that publishes consensus-based international Standards and manages systems for electric and electronic products, systems and services. The publications made by this organization serve as a basis for national standardization [236]. For this project the IEC 62477-2:2018 standard for power electronics [237] should be adhered to where applicable.

### 2.5.2 Simulation Packages

This dissertation comprises of a project that will involve the physical build of a DC-DC converter. DC-DC converters can be complex and it is therefore necessary to simulate the design before it is built to determine whether the component values are acceptable. To this end four simulation packages will be utilized, LTspice®, Matlab® Simulink® and JLCPCB®. LTspice® is a powerful simulation package as it contains many libraries and the option to alter component values or create new components through minimal effort [238], [239]. This simulation package does represent the real-world conditions to a point, but does have a few discrepancies, thus this will be used for the preliminary simulations of the circuits where after Simulink® will be used to verify and make final adjustments to the component values. This second stage of simulation is required as Simulink® has

the option of more variable changes of a component compared to LTspice®. Both simulation packages have various graphs that can be plotted and exported for external use [240], [241].

Another advantage of Simulink® is its ability to be integrated with a microcontroller, both the Arduino and STM32 boards can be integrated with the Simulink® software. This allows the simulation to be able to include operation of the microcontroller as well as using the simulation software to program the intelligent control of the microcontroller. This will give a better simulation of the circuit with fewer differences compared to the actual circuit.

After the simulations' component values are approved the circuit will be designed using EasyEDA® and JLCPCB®. Shenzhen JIALICHUANG Electronic Technology Development is the largest Printed Circuit Board (PCB) prototype enterprise in China and a high-tech manufacturer specializing in quick PCB prototype and small batch production. This company allows the design of the PCB through EasyEDA®, the purchase thereof and the purchase of the components to be used on the PCB all at a very reasonable (lower) price without the need to buy ridiculous quantities of the components [242]. The interface of the program used to design a PCB is very user friendly and simple. This program allows the design of each level/layer of the circuit board and the traces that will be used to connect the components on the board. Once the PCB is designed to the desired specifications the board can be proofed by the system to determine any physical errors, which can be attuned before the board is produced. It is desired that the circuit for this project be printed as this will simplify the build process and decrease needless human errors.

### 2.5.3 Energy management strategies

As this project requires the control of power from multiple sources energy management strategies are also required, for this section two strategy bases will be briefly touched on – optimization based and rule based. Their relevance to the project will be assessed through this research.

#### 2.5.3.1 Optimization based

Based on the optimization theory and is useful in finding the optimal policy [2]. This strategy has two sub-categories, global and real time optimization. The former consisting of dynamic programming and Pontryagin's minimum principal and the latter consisting of $\lambda$-control and predictive control. Global optimization has the advantage of optimal performances but the disadvantage of real time implementation, the use thereof is therefore benchmarked. Real-time optimization offers a compromise between performance and real time implementation. Both of these categories require complex mathematical algorithms making them inefficient for this projects application [243].

#### 2.5.3.2 Rule based (SMC – State Machines Control)

Rule based energy management entails controlling the working range of parameters through setting a threshold for the pre-set rules. This method reduces the vehicle energy loss, has a simple structure,

has a small amount of competition and a high efficiency. It is best suited for real time energy management [243]. Rule based strategies can further be divided into deterministic and fuzzy rules. The former using filtering and thermostat control and the latter using fuzzy logic and neural networks. This option has the advantage of being real-time based but the disadvantage of having no optimal performances. The principle of frequency energy management is shown in Figure 2.18.

For filtering, the low-and high dynamics of the traction current are separated through the use of a filter, where the battery is preferred for the low dynamics and the capacitors for the high dynamics. The other category under rule-based optimization is much more complex than what is required for this project and will thus be omitted from this study [243]. The load profile is sent through a low pass filter where the lower frequencies switch the FC on and the higher frequencies switch the SC on [244].

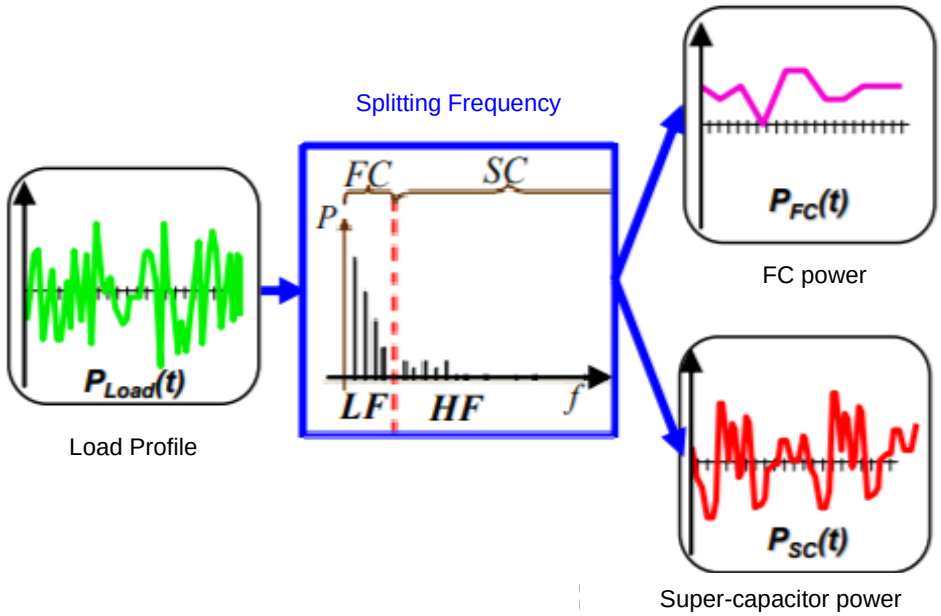


**Figure 2.18: Frequency Energy Management Principle (adapted from** [244]**)**

## 2.6 Conclusion

In this chapter a thorough literature study was compiled pertaining to the main components of this project, these components and their interactions with each other were presented in a diagram in Figure 2.2. Alternatives to the proposed solution were reviewed to determine whether the proposed solution is viable. The main energy sources related to a drone were reviewed to understand the problem statement as well as make a cognisant decision as to the best combination. These energy sources were examined paying close attention to the application in mind. The DC-DC converter was researched in depth such that each stage could properly be understood such that the operation can be designed for optimal efficiency with respect to the desired application. Components such as the switching module, the microcontroller and the inductor were highlighted as the main components requiring the most attention for the design phase of this converter. Some additional research was

conducted into the simulation packages to be used in this project as well as standards that could come into practice during the course of the project.

The case studies reviewed in this chapter as well as the research done for the DC-DC converter will be used to assess the viability of the proposed solution and to verify and validate the results presented later in this dissertation. The bulk of this chapter has been summarized and published in an article given in Appendix A with reference [101]. Chapter 3 is the design and simulation chapter of this dissertation and will contain the conceptual and detail design of the DC-DC converter, and the system as a whole, and the information gathered in this chapter will facilitate the final choices required for the design as will be seen in Chapter 3.

# CHAPTER 3: DESIGN

This chapter consists of two parts, the conceptual design and the detail design. The conceptual design contains the trade-off matrices made using the literature study that will allow for decisions to be made on the ideal components for each application. The detail design section contains the simulations, circuit diagrams and SolidWorks® drawings required in order to verify that the system will work before it is built. The layout for this chapter is shown in Figure 3.1, which details the content of the two parts of this chapter.

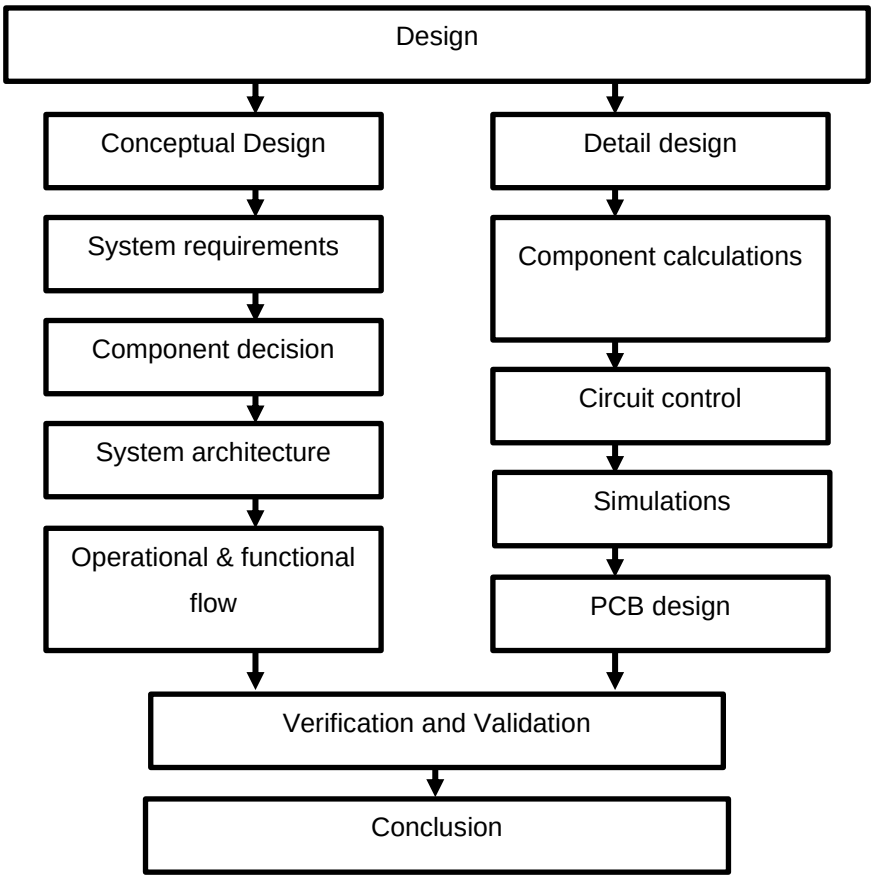


**Figure 3.1: Layout plan for Chapter 3**

## 3.1 Conceptual Design

The general concept of the proposed solution for this project is outlined using Figure 3.2. The shaded blocks highlight the main focus of this project, the SCs, the controller, the DC-DC converter and the load switch. The FC system to be used contains its own DC-DC converter and controller – this existing controller controls when the FC requires a power supplementation as well as controlling the operation of the FC, therefore, this controller will not be altered and an additional controller will be used to control the auxiliary circuit (shaded blocks). The solid lines represent the flow of power within the circuit while the striped lines represent the flow of control (either measurements or signals). The controller receives the power requirements from the programmable load which is used to control the load switch (ON or OFF) – this switch remains closed (ON) for the majority of the tests as it is only desired to remotely control when the SCs are available for certain tests.

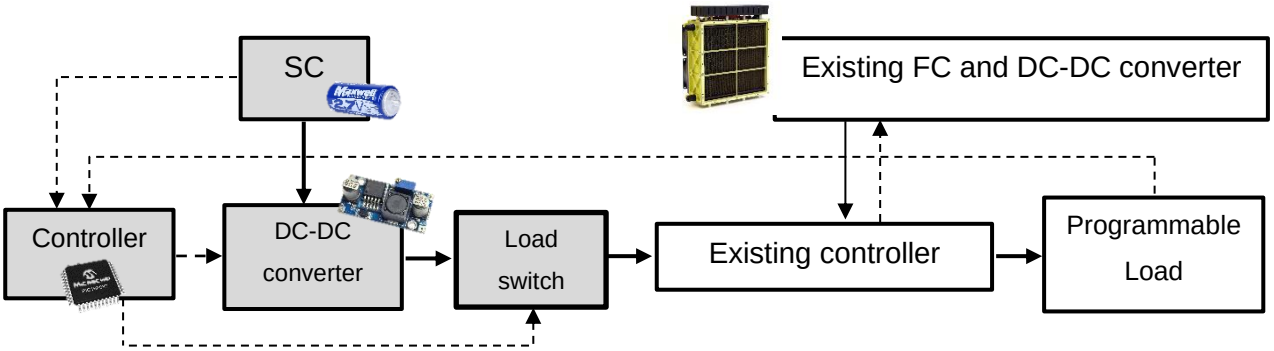


**Figure 3.2: Conceptual design of proposed hybrid system**

The SCs send a signal of SOC to the controller which is used to calculate the duty cycle required for the desired output of the DC-DC converter, this is sent as PWM signals to control the converter. The existing FC system has a constant voltage rating and it is desired to match the SCs voltage with this rating; as the SCs deplete their voltage decreases to a level below this required voltage; to avoid this, a DC-DC converter will be used to boost the voltage of the SCs, to that of the FC system. The DC-DC converter will also be used to limit the current provided by the SCs to the converters capabilities; the DC-DC converter will be uni-directional such that the SCs can only provide power and not use it. When the load has a power requirement above that which the FC system can provide, the SCs will be utilized. For the initial tests there will be no control over the use of the SCs, thus allowing them to continuously contribute to the load when required.

### 3.1.1 System Requirements and Design Specifications

This section is compiled of a number of specifications that the project must pertain to in order for it to be a viable solution to the problem stated in section 1.2. These requirements will also be used to verify and validate the final project at the end of this dissertation.

(i) A prototype of the DC-DC converter needs to be built in the laboratory.

(ii) The available FC system is rated for 1 kW at a constant 50 V and thus 20 A. the provided load profile (further discussed in section 3.2) shows a maximum power requirement of 1200 W, therefore the SCs should be designed to supply the extra requirement of 200 W. As a safe initial estimation this value will be increased to 500 W to account for the multiple uses of the SCs, their quick release ability and the safe operation of the FC under its maximum rating. The DC-DC converter must therefore be able to deliver 50 V, 10 A with a maximum power of 500 W.

(iii) DC-DC converters have various duty cycle limits that affect the efficiency and operation thereof. Therefore, the operational duty cycle range of the DC-DC converter needs to be able to deliver the peak load requirements (50 V, 10 A).

(iv) An intelligent controller will need to be designed in order to increase/improve efficiency.

(v) The effective combination of the power sources needs to be achieved.

### 3.1.2 System Architecture

Figure 3.3 below shows the system architecture that represents the general operation of the system. This is the system that will be used to operate the programmable load (PL). The PL will send a signal to the controller that will mainly consist of the current drawn by the load, this current will then be used to determine whether the SCs are required and the use of the SCs will occur via the switching module. The FC will be continually used and the SCs will supplement the FC when required. When the SCs are in use their power will flow through a DC-DC converter that increase the voltage to match that of the FC and both the FC and SC will power the load in order to obtain results.

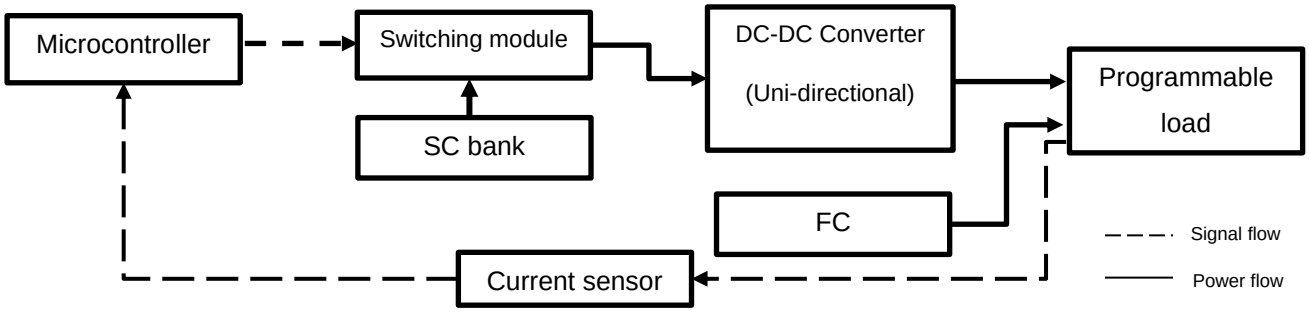


**Figure 3.3: Basic System architecture**

### 3.1.3 Operational and Functional flow

An operational flow diagram can be seen in Figure 3.4, this gives a description of the overhead operation of the system.

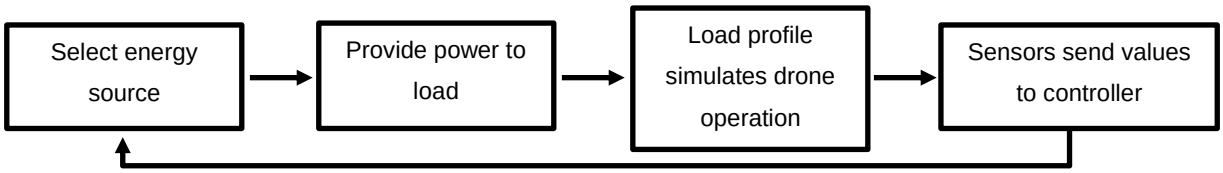


**Figure 3.4: Operational flow diagram**

The operational flow diagram shows the main operation of the power sources from selection to ultimately providing power to the load. Figure 3.5 gives an elaboration of the operational flow diagram.

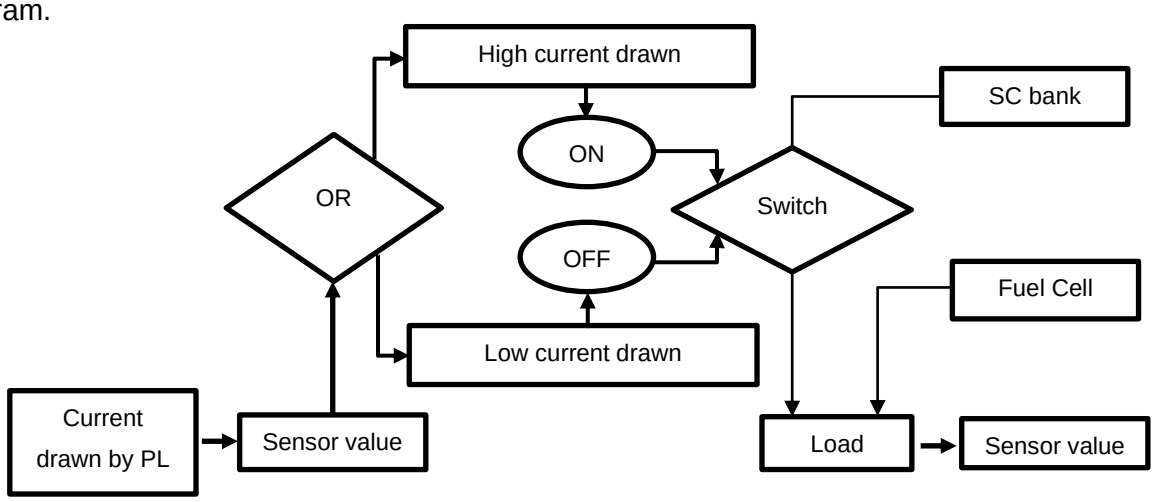


**Figure 3.5: Functional flow diagram**

The selection of the SC bank is dependent on the value obtained by the sensor. This will predictably improve the performance and flight time of the system. A more detailed diagram of the system architecture can be seen in Figure 3.6.

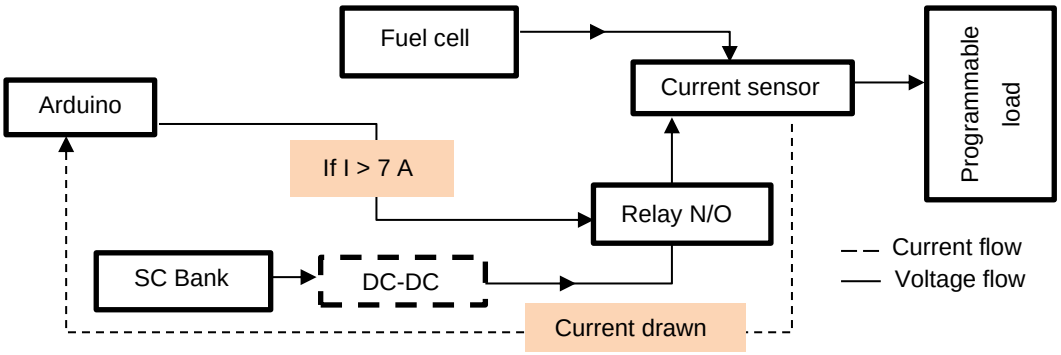


**Figure 3.6: Detailed System architecture**

## 3.2 Detail Design

In this section the extra circuitry required in order to replace the buffer battery section will be designed. The conceptual design of the proposed final system is shown in Figure 3.2.

### 3.2.1 Super-capacitor calculations

The SC bank that is used for this project will need to be designed according to some required specifications to meet the needs of the load. The considerations and calculations required for this end are discussed in this section.

#### 3.2.1.1 Weight and energy considerations

The system will be designed as a testing station which, in the long term, will be able to be implemented onto a pre-existing drone requiring minimal alterations. This pre-existing drone consists of the drone itself, FC stack (with its control system), the buffer battery and the hydrogen storage tank. The buffer battery serves as an additional power source that can provide the system with a large amount of current without affecting the operation of the system. The general operation of the existing hydrogen FC drone is shown in Figure 3.7 below.

The system mainly operates on the FC stack that has a built-in DC-DC converter that allows for a regulated voltage output. When the system requires a current level that is too large for the FC the buffer battery is employed in order to provide this current. The current requirements of the FC become too large when it causes the system to have a significant voltage drop, which in turn can lead to a system failure. The current requirements are at this abovementioned level when the UAV takes off or lands, encounters strong winds or needs to start up in cold conditions.

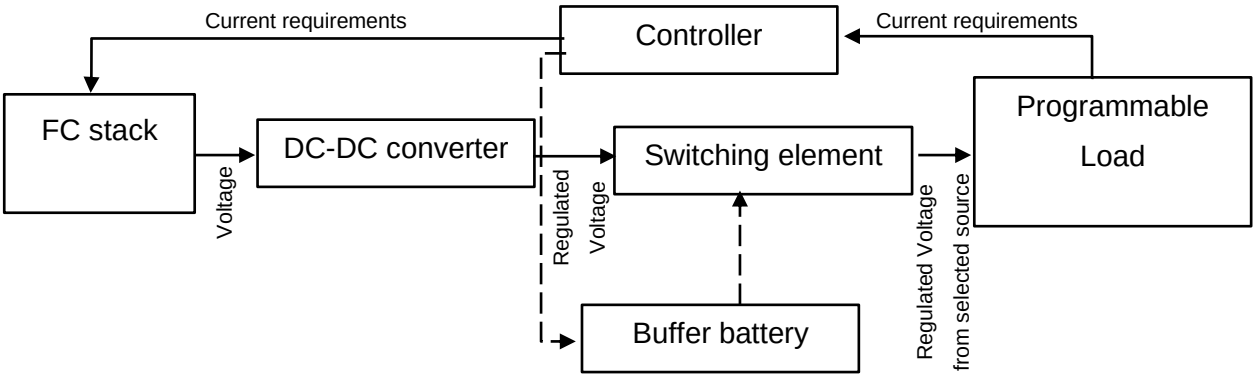


**Figure 3.7: FC operational diagram**

For this project the temperature applications will not be considered. As the system already contains a controller and switching element for the different sources this will not be designed. From the case studies in section 2.2 it is shown that the battery is used at the lower end and peak power requirements of the load, supplementing the FC and it is suggested that the battery continue providing power at the lower end of the load requirement (supplementing the FC) and a SC bank be utilized for the peak power requirements. The idea is to add a SC bank of equivalent capacity of the battery to the existing FC system and to evaluate the effect thereof on it. In order to do this the capacity of the battery will need to be matched, this is done using the equation (3.1) (obtained from equation (19.9) in [174]),

$$Battery\ capcity\ rating = \frac{(Energy\ density)(battery\ weight)}{battery\ nominal\ voltage} \quad \textbf{(3.1)}$$

For this two 12s Li-Po batteries will be used with weight of 0.4 kg, rated voltage of 48 V and energy density of 160 Wh/kg, each. Using these values, the battery capacity rating is calculated as 1.33 Ah per battery. Therefore, the SC bank needs to have a current rating of 2.66 Ah and be less than or equal to 800g in weight. This is a requirement that will allow for minimal adjustments to the hydrogen drone whilst increasing the energy capacity of the drone. The calculations of the capacitors in order to keep within these limits will be done in the next section.

#### 3.2.1.2 Equivalent super-capacitor characteristics

In order to determine the required values for the SCs, the load profile provided for the experimental tests will be examined. This load profile is seen in Figure 3.8 below.

In this load profile there is a horizontal line indicating when the proposed system makes use of the buffer battery to supplement the FC. This occurs when the system requires more than 1 kW of power to operate. The FC system (including the buffer battery) provided for this experiment has a rating of 1 kW, however, as the FC is used for research and experimentation in the HySA laboratory, through the years of operation the system has degraded to a point where it is suggested to be used to supply a maximum of 450 W.

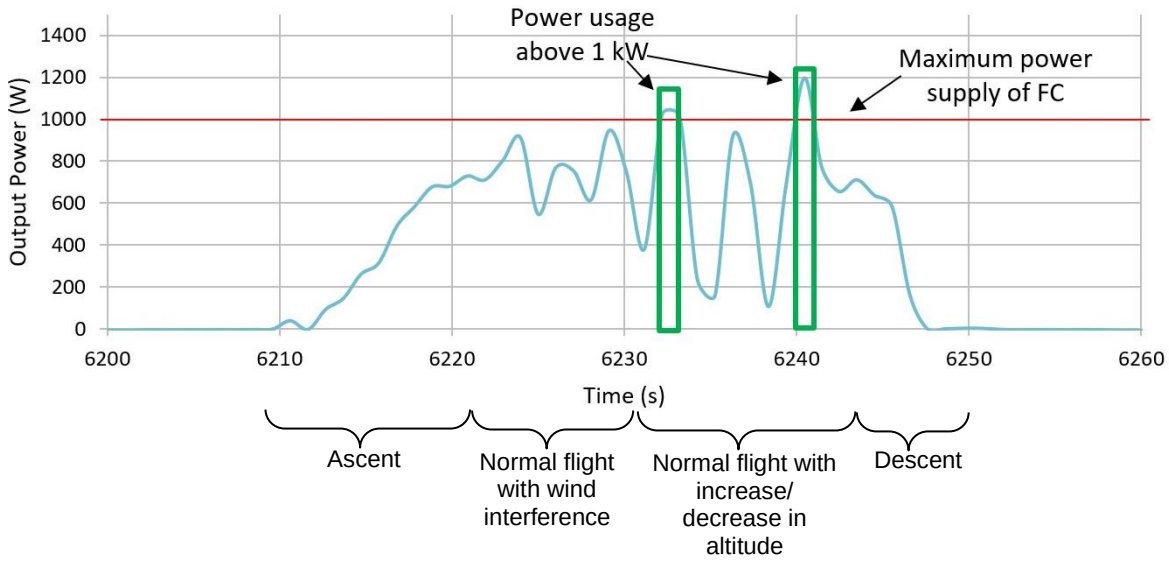


**Figure 3.8: Full Load Profile**

As the system can supply 50 V, this leaves a maximum current supply of 9 A. While testing the new load profile (450 W maximum) it was discovered that with a maximum demand of 9 A from the load, the FC system supplied a maximum of 350 W, therefore the load profile has been reduced accordingly. This new load profile is shown in Figure 3.9.

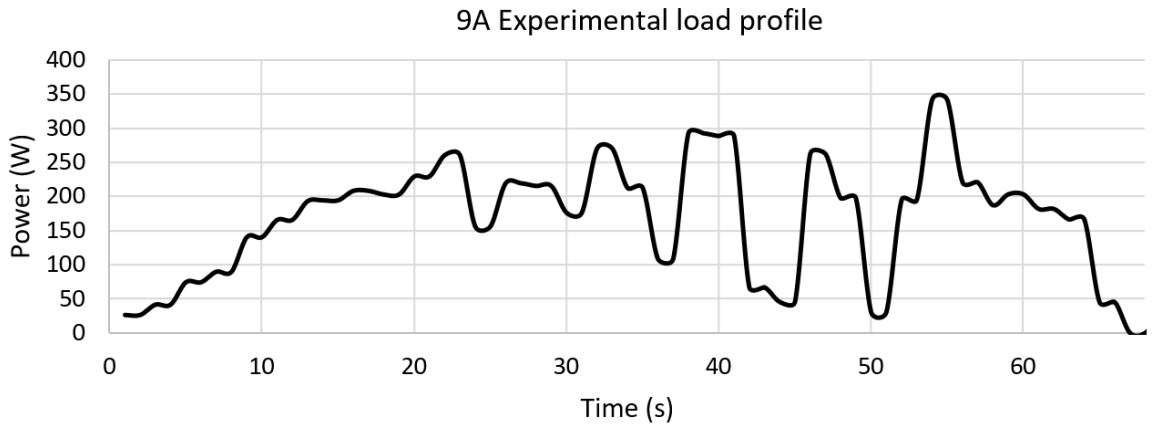


**Figure 3.9: Reduced 9A load profile**

The SC bank will be designed for the full load profile, as it will allow for an easier transition when a larger FC system is available, and the DC-DC converter will be designed for the 9 A load profile as it is desired to be combined with the available FC system.

As mentioned, the FC system requires a buffer battery, the particular system to be used uses two of these batteries in parallel. For the new system the buffer batteries will be replaced with a SC bank. This SC bank will need to match the characteristics of the buffer batteries in order for the system to require minimal adjustments. These characteristics are (per battery): the weight (≤ 0.4 kg), the energy density (≥ 160 Wh/kg), the rated voltage (≥ 50 V) and the capacity rating (≥ 1.66 Ah).

If the buffer batteries were to be simply replaced by an equivalent capacitor system these requirements will allow the system to operate in a similar fashion without compromising the efficiency

thereof. As they are in parallel, the combined weight increases to 0.8 kg, the combined voltage and energy density remains the same whereas the combined current rating increases to 2.66 Ah, In order to determine the values of the capacitors, these characteristics will need to be converted to the applicable unit, Farad. To do this the capacity rating is first converted to ampere-second, thus converting to Coulomb, using equation (3.2) (obtained from (19.2) in [174]),

$$Capacity\ rating\ (C) = 3600(Capacity\ rating\ (Ah)) \quad \textbf{(3.2)}$$

Using the capacity rating of 2.66 Ah the capacity is converted to 9 576 C. Next, the capacitance can be calculated using equation (3.3) (obtained using equation (18.10) in [174]),

$$Capacitance\ (F) = \frac{Capacity\ rating\ (C)}{Voltage\ (V)} \quad \textbf{(3.3)}$$

Using the calculated capacity rating and voltage rating of 50 V, the total capacitance is calculated as 191.52 F. The nominal voltage of a SC is 2.7 V, thus 19 cells will be required in series to reach 50 V. In series the total capacitance can be calculated using equation (3.4) (obtained from equation 6.28) in [245]), which can be rewritten to calculate the capacitance per cell,

$$Total\ series\ Capacitance = \frac{Capacitance\ per\ cell}{number\ of\ cells} \quad \textbf{(3.4)}$$

This equation works under the assumption that all connected capacitors have the same capacitance, thus the required capacitance per cell will be 3 638.88 F. The largest SC available is 3400 F with a rated voltage of 3 V per cell. With these values only 17 cells will be required, reducing the capacitance per cell to 3 255.84 F, therefore the 3 400 F cells will be sufficient. According to the Maxwell datasheet [246] the weight of one 3 V, 3 400F SC is 496 g, therefore the combined weight would be 8.43 kg, which is far above 800 g.

In order to combat this weight, issue the system can be designed to accommodate SCs that satisfy the increase in power above 1 kW, but that cannot provide the entire load independently. Also, the DC-DC converter can be used to increase the voltage requirements from a lower level to the desired 50 V. This will allow for the SCs to be much smaller and also to recharge much faster, allowing the system to be more efficient. From the load profile it can be seen that the maximum power consumed is around 1200 W, this needs to be supplied by the capacitors and FC simultaneously. However, the SCs have the tendency to supply most of the energy when used thus if we assume that the SC bank will be required two times on the load profile (this is indicated on Figure 3.8 by the green blocks) each period lasting two seconds, we can assume that the average power supplied by the FC will be around 400 W and the capacitor banks will need to supply the remainder of the power, namely 600 W for the first instance and 800 W for the second instance. Using the equation (3.5) (obtained from (equation (1.3) in [245]) the energy requirements values can be determined,

$$Energy\ (J) = (Power\ (W))(time\ (s)) \quad \textbf{(3.5)}$$

For the first instance of a 600 W requirement, 1 200 J will be required and for the second instance of 800 W, 1 600 J will be required, giving a total of 2 800 J. This value is initially rounded up to 3 000

J and we also assume that this is only 80% of the requirement, thus 100% would require 3 750 J. The SC size can be calculated using equation (3.6) (obtained from equation (18.15) in [174]),

$$Energy\ (J) = \frac{1}{2}CV^2 \quad \textbf{(3.6)}$$

The maximum duty cycle of a boost DC-DC converter is around 70%, thus the SCs will only be able to be boosted with a 70% increase in the maximum voltage. To calculate the minimum allowable voltage for the boost converter equation (3.7) (obtained from equation (5) in [245]) is used,

$$V_{in} = (1 - D)V_{out} \quad \textbf{(3.7)}$$

This equation is a rewritten in the form of equation (2.3). Using $V_{out}$ = 50 V and $D$ = 0.7, $V_{in}$ (the minimum required input voltage) is equal to 15 V. However, SCs have an allowable voltage drop, for efficient life time usage, of 20%, therefore the 15 V will be the 80% SOC of the SC bank at which the converter will be able to boost the input voltage for the entire 20% discharge of the SC bank; 100% SOC of the SCs will therefore be 18.75 V. To achieve this total voltage around seven cells of 2.7 V each will be required, this value is rounded up to 8 cells; the total voltage will be 21.6 V. To determine the required capacitance of the SC bank – equation (3.6) can be rewritten to form equation (3.8), shown below,

$$C = \frac{2(Energy(J))}{V^2} \quad \textbf{(3.8)}$$

The 3 750 J calculated above is the energy required at the output of the DC-DC converter. Using the law of energy conservation, the output energy of the converter will be a percentage of the input energy, this percentage is determined by the efficiency of the converter (assumed to be 90%). Therefore, the required input energy can be determined using equation (3.9) (obtained from equation (6.10b) in [174]),

$$E_{in} = \frac{E_{out}}{\eta} \quad \textbf{(3.9)}$$

For this equation ŋ refers to the efficiency constant of 0.9 and results in a minimum required energy at the input of 4 167 J. Using this energy requirement and the minimum voltage of the input (80% of the SC bank maximum voltage – mentioned as the most efficient SC operating range) above, the total capacitance is calculated and rounded up to 28 F. the minimum voltage of the SCs is used as this will ensure that the SCs have enough energy for the requirement for the entire range of its discharge. Using equation (3.4) and 8 cells the capacitance per cell is calculated as 224 F. To verify that this value is correct the energy it can supply will be calculated and compared to the requirement mentioned above, this is done using equation (3.6) The input energy is calculated as 6 532 J (with 28 F total capacitance) which is larger than the 4 167 J requirement at the input, thus a value larger than 224 F per cell can be used in the system. For this project the capacitance per cell was chosen to be 360 F, which delivers 10 498 J (more than sufficient to account for losses in the system); according to the datasheet [247] each one of these SCs weigh 71.4 g, giving a total of 571.2 g, which is well under the weight of the two batteries of 0.8 kg, leaving sufficient weight for the circuitry.

### 3.2.2 Arduino Program

For the system it has already been established that a microcontroller will be required for the control of the DC-DC converter, in section 2.4.3.2 a few microcontrollers were reviewed and it has been decided that the Arduino Nano will be favoured for this application. This is mainly due to user preference and ease of acquisition. A program will need to be written to control the different elements thereof. This program will be responsible for the correct operation of the DC-DC converter and can thus be seen as an integral part of the system. The program cannot be simulated however the logic flow thereof can be described and this description is seen in Figure 3.10.

The logic flow shows that the microcontroller will distinguish between two states, one where the current drawn by the load is 0 and the other where a current is drawn. When a current is drawn the DC-DC converter will operate increasing the input voltage to that which is desired otherwise it will not operate. The intelligent control aspect of the converter will be a combination of a few of the reviewed methods. The Arduino program will utilize a switch-case which resembles the functionality of ladder logic; it will also use a method resembling that of fuzzy logic as the input voltage values vary and the region that the value falls under will determine the state of the switch-case used.

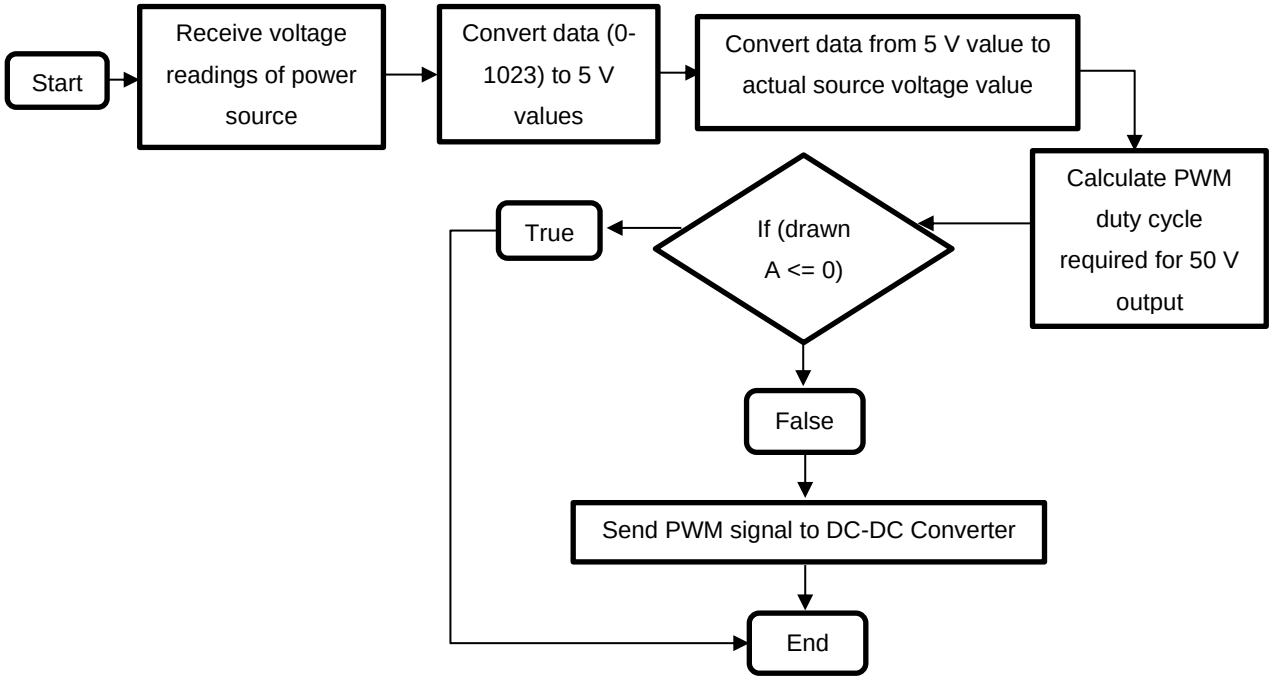


**Figure 3.10: Microcontroller program logic flow diagram**

### 3.2.3 DC-DC Converter Circuit

In this section of section 3 the DC-DC converter circuit of the system will be designed and simulated in order to determine whether the circuit will work accordingly and also to adjust the component values to achieve the desired results before the system can be built. The DC-DC circuit along with the SC circuit will be designed on a PCB in order to increase simplicity of the system, this is seen in section 3.2.4. The circuit diagram and the operation of the DC-DC converter is explained below using

Table 3.1 and Figure 3.11. The table summarizes the two modes of the converter as well as the state of all the switches present in the design.

**Table 3.1: DC-DC and switch operation (adapted using Table 2.2)**

| Mode | M2 | D3 | D4 |
|---|---|---|---|
| **1** | ON | OFF | OFF |
| **2** | OFF | ON | ON |

It is desired that the battery be recharged by the FC but the SC should only be recharged through regenerative breaking as the SCs have the rapid recharge ability required for rapid bursts of energy caused by the regenerative breaking. The SCs require a large amount of energy that, if supplied by another power source, will degrade that source at an increased rate. There is no regenerative breaking present in the load (it is provided by a programmable load) and thus the SCs will not use or require the bi-directional functionality of a DC-DC converter. The DC-DC converter is going to operate as a boost converter in order to boost the power supplied by the SC bank so that it matches that of the FC.

The converter consists of two modes, the charge and discharge of the inductor. Mode 1, represented by the red line in Figure 3.11, is the charge mode of the inductor where current flows through the MOSFET to ground. During this stage the polarity of the inductor is opposite to that of the flow of current through the circuit due to the potential difference across the inductor and the voltage being higher at the input and lower at the output. However, as the inductor charges the potential difference across it decreases to a point where the input equals the output, thus allowing the potential difference to equal zero.

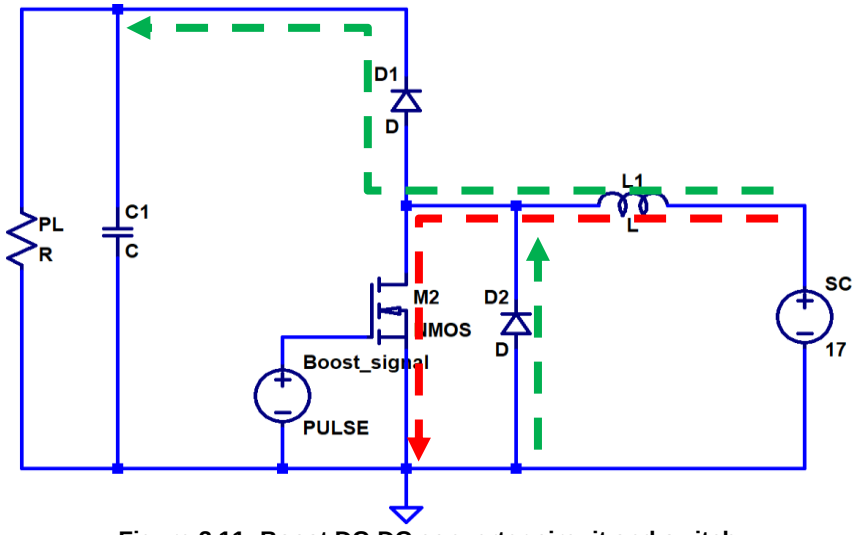


**Figure 3.11: Boost DC-DC converter circuit and switch**

It is ideal for the inductor to start discharging before reaching this point, which can only occur if the polarity is once again switched and this occurs once the MOSFET is switched off during Mode 2. If the MOSFET is not switched off and the polarity of the inductor remains the same as in Mode 1, the inductor will enter saturation where the inductance decreases, the conductance increases and the

inductor essentially behaves as a short circuit. The point of saturation is determined by the frequency, peak – current and voltage requirements of the circuit. These calculations will be done in this section of the dissertation.

Mode 2, represented by the green line, is the discharging stage of the inductor. As mentioned above, this stage starts once the MOSFET is switched off. During mode 2, $D_2$, the freewheeling diode, enters reverse bias mode and helps the n-channel of the MOSFET to separate allowing the MOSFET to switch off more efficiently ensuring it is off for Mode 2. $D_1$ is also on and allows the inductor to discharge towards the output capacitor and the programmable load (PL). The inductor can once again saturate at this point, but as it has already completed its full charge and discharge pulse the avoidance of this point is not as imperative as before. The aforementioned saturation in mode 1 causes a large power loss in the inductor in the form of heat as the inductor is a short circuit at this point, this ultimately affects the efficiency of the converter.

Saturation in mode 2 does not cause this power loss as the inductor is already discharged and as there is no 'clear' path to ground it does not act as a short circuit to ground, thus not causing a detrimental power loss. This saturation allowance of mode 2 is what defines this converter as a Discontinuous Conduction Mode (DCM) DC-DC converter. The converter can be designed for Continuous Conduction Mode (CCM) – where saturation doesn't occur at either end of the inductor charge or discharge stages – but as the voltage input to the circuit varies, causing the duty cycle and PWM of the system to vary, the system will, at some point, enter DCM. CCM is ideally reserved for applications where the input does not vary continuously.

The proposed circuit design is shown in Figure 3.12 below. This is the proposed design that will be used to create the boost DC-DC converter to increase the SC voltage to that of the FC system. The respective sections of this circuit will be designed in detail according to the desired specifications. The labelled sections of the figure will be individually calculated below in order to optimize the function of the converter.

#### 3.2.3.1 Switching Elements

For the proposed DC-DC converter to operate accordingly three switches are required, one that can operate with a PWM signal to vary the flow of current ($M_1$ – preferably a n-type MOSFET), another to block the flow in a specified direction ($D_1$ – a diode) and the final one ($D_2$) to be placed in parallel with $M_1$ and operate as a reverse biased freewheeling diode. The function of $M_1$ and $D_1$ have been explained above; $D_2$ has yet to be explained. The operation of an NMOS relies on the creation of a n- channel between the drain and source to allow the flow of electrons, when the NMOS is switched off the n-channel needs to be removed in order for conduction to cease.

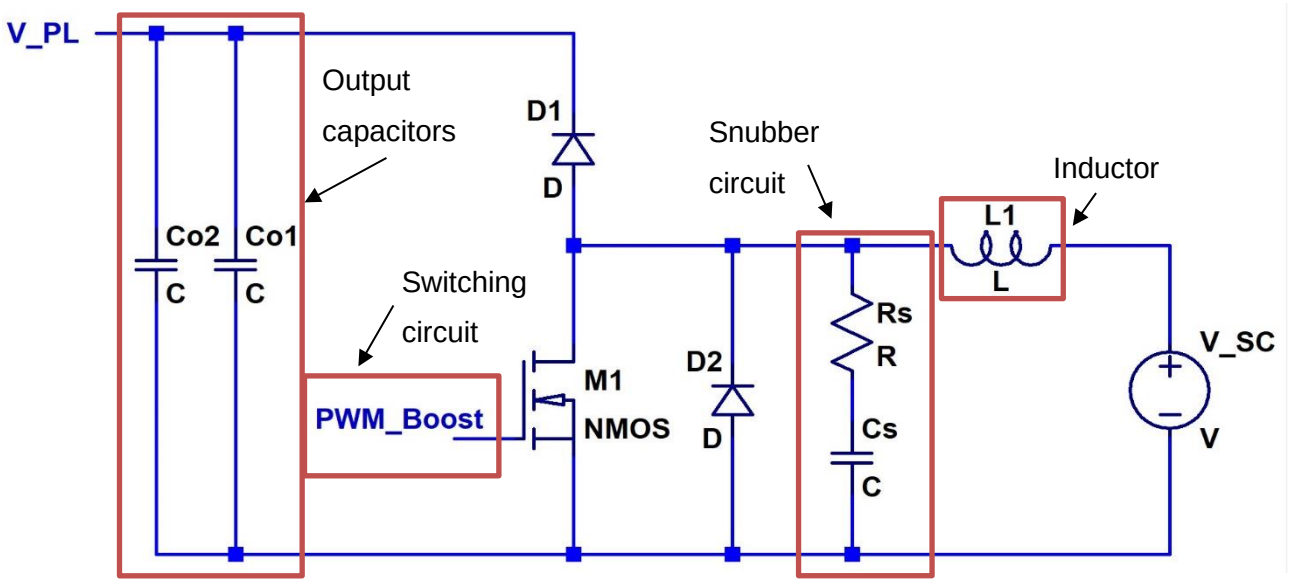


**Figure 3.12: Proposed DC-DC converter circuit design**

This removal does occur naturally in the NMOS however in circuits where there is a switching frequency present this removal needs to occur relatively fast in order for all the components to be in the correct state at the correct time. Therefore, the diode is used to eradicate any excess electrons, in turn switching the NMOS off faster. The only considerations required for this diode is that it be able to withstand the power conditions of the circuit, be a fast switching diode and that the voltage drop across the diode be less than that of the NMOS. $D_1$ is also required to be a fast switching diode that can withstand the power conditions of the circuit.

Table 3.2 below summarizes the specific characteristics of the switches from section 2.4.2 for the required application.

**Table 3.2: Summary of distinguishing characteristics of switching modules**

| | BJT | FET | MOSFET | Power MOSFET | IGBT | Relay | Diode | SCR |
|---|---|---|---|---|---|---|---|---|
| **Switching frequency (kHz)** | <62.5 | <62.5 | <62.5 | >>62.5 | >62.5 | <<62.5 | >>62.5 | >62.5 |
| **Size** | Smallest | Smallest | Medium | Medium | Large | Largest | Smallest | Large |
| **Degree of control** | PWM enabled | PWM enabled | PWM enabled | PWM enabled | PWM enabled | Either open or closed | Either conducts or doesn't | Latches on |
| **Parasitic interference** | Low | Low | Medium-Large | Medium-Large | Medium-Large | Very large | Medium-Large | Low |
| **V & I characteristics** | Small | Small | Lower than IGBT, higher than BJT & FET | Higher than IGBT & MOSFET | Lower than power MOSFET, higher than MOSFET | Very large | Large | Very large |
| **Efficiency (%)** | Lower than MOSFET | Lower than MOSFET | Good | Good | Lower than MOSFET | Good | Good | Good |
| **Power losses** | Low | Low | Medium | Medium | Medium | Very large | Medium | Medium |

*populated using [248]–[255]

In the table the size refers to the physical size of the component itself as well as the additional circuitry required for proper operation (compared to each other). Degree of control refers to whether the device can control the percentage of flow through it or not. Parasitic interference refers to any capacitances or inductances that can be induced and affect the external circuitry and power losses refers to any power losses caused due to the operation of the device. These characteristics are referenced to that which is desired for the proposed solution.

The switching frequency should be larger than 62.5 kHz; the size should be as small as possible to reduce weight; the degree of control should allow the use of PWM; as there are other components in the circuit it would be preferable that the switch cause minimal parasitic interference; the current and voltage capabilities should be as close to or larger than 100 A and 100 V as possible; the switch should have at least 70% efficiency; the losses across the switch should be as low as possible.

From this table it is seen that the power MOSFET is superior to the other switches as it is able to handle the high-power requirements of the circuit, has a fast switching frequency, it has low power losses (and external interference) and it is capable of PWM control. Therefore, a MOSFET will be favoured as the switching element of this DC-DC converter. The switching of the MOSFET will however require an external circuit as the Arduino's I/O pin cannot supply the required power to switch it, this circuit as well as its design will be explained in the next section (switching circuit).

#### 3.2.3.2 Switching circuit

Figure 3.12 highlights a section labelled Switching circuit, this circuit is used to enhance the PWM signal sent from the Arduino as well as to isolate the Arduino from the main circuit to protect it from the larger voltages and currents present in it. The entire switching circuit is used to drive the MOSFET $M_1$. The design of the switching circuit is shown in Figure 3.13. This circuit comprises of a photo-coupler ($U_1$ – used to isolate the Arduino from the remainder of the circuit) and some additional components used to improve performance and reduce malfunctions. $D_1$ & $D_2$ are the current steering diodes of this circuit and have the only requirement of being fast switching diodes (used to redirect current spikes towards the capacitors); $C_1$, $C_2$ & $C_3$ are used to filter the supply voltage ($V_{cc}$) of the photo-coupler, therefore two will be ceramic and the other electrolytic (this will filter both the high and low frequency components of voltage).

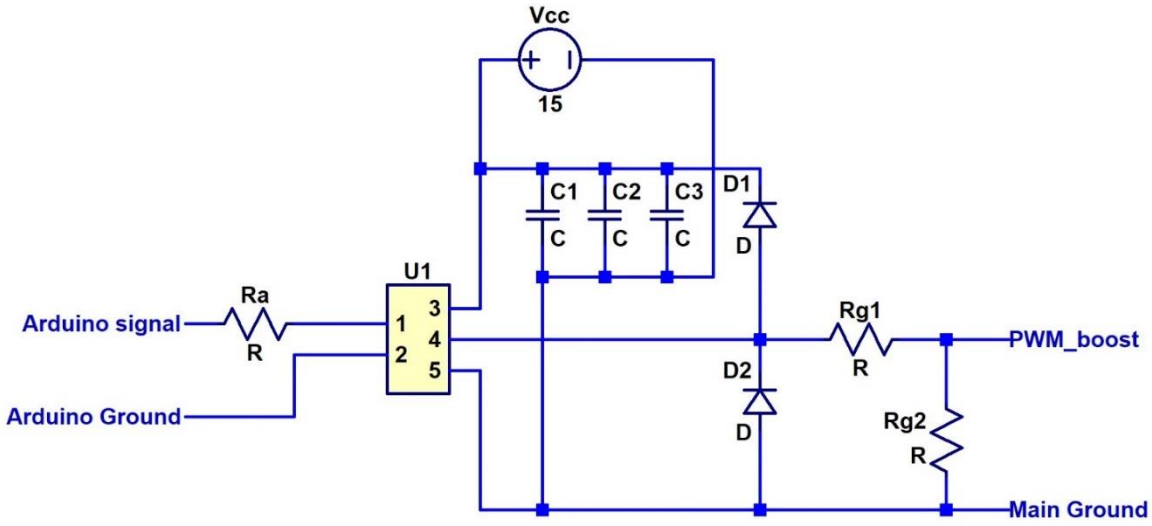


**Figure 3.13: Secondary circuit used for switching of the NMOS**

A photo-coupler is used in this circuit as it is the combination of an opto-coupler and a MOSFET driver and therefore will reduce the number of components and thus the efficiency losses in the circuit. $R_a$ is used to protect the Arduino I/O pin from reverse currents, as it can only handle an absolute maximum 40 mA. The Arduino pin can output a maximum of 5 V, which is larger than the possible output of the photo-coupler, thus equation (3.10) (obtained from equation (19.4) in [174]) is used to determine the size of the resistor,

$$R_a = \frac{V_{max}}{I_{max}} \tag{3.10}$$

The maximum current is used as 20 mA in order to keep ensure the protection of the pin. Using the equation $R_a$ is calculated as 250Ω. $R_{g2}$ only need be large enough to discharge the input capacitance between the gate and source, for this end a 10 kΩ resistor is sufficient. The principle for determining $R_{g1}$ is the same as that of $R_a$ where the Resistor needs to be able to absorb reverse currents flowing towards the photo-coupler, but the pin of the photo-coupler has a larger reverse current capability than what can be sent from the gate and thus $R_{g1}$ can be kept quite small only to absorb the remaining energy on the gate when the signal is switched off.

#### 3.2.3.3 Inductor calculations

All of the equations used in this section are obtained from [182], [184], [256], [257] unless otherwise specified. The main equations will be derived using Figure 3.11. The two modes of operation were discussed in section 3.2.3 using Table 3.1 and allow Figure 3.11 to be reduced to the circuits shown in Figure 3.14.

For mode 1 the MOSFET is on allowing the inductor to have a direct connection to ground as shown in Figure 3.14(a) and in mode 2 the MOSFET is off allowing the diode to conduct towards the capacitor and load, shown in Figure 3.14(b). Using Kirchhoff's voltage and current laws an equation can be determined for the voltage across the inductor and the current through the capacitor of each circuit.

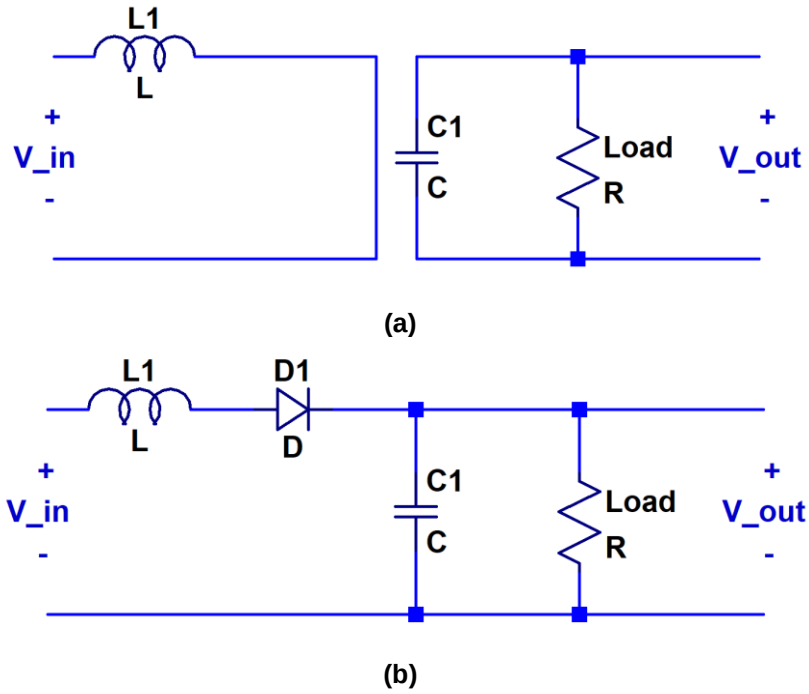


**Figure 3.14: Inductor equivalent circuits for (a) Mode 1 and (b) Mode 2**

Equation (3.11) represents the voltage across the inductor and equation (3.12) represents the current through the capacitor in Figure 3.14(a).

$$V_L = V_{in} \tag{3.11}$$

$$i_C = -\frac{V_{out}}{R} \tag{3.12}$$

Equation (3.11) shows that the inductor is in series with the input voltage and has no other influences, thus having the same voltage ($V_L$) as that of the input ($V_{in}$). The capacitor in Figure 3.14(a) is in series with the load ($R$) and therefore has the same current flowing through it ($i_C$) as that of the load but in the opposite direction, using Ohm's law this current is determined as Equation (3.12). Equation (3.13) and (3.14) represent the voltage and current of the inductor and capacitor of Figure 3.14(b).

$$V_L = V_{in} - V_{out} \tag{3.13}$$

$$i_C = i_L - \frac{V_{out}}{R} \tag{3.14}$$

Using Figure 3.14(b) it can be seen that the voltage across the inductor is influenced by the output voltage ($V_{out}$); the current flowing through the capacitor is seen to be influenced by the inductor current ($i_L$) in the circuit.

Interpreting Figure 3.14 and equation (3.11) - (3.14), a waveform can be drawn to show the behaviour of the voltage across the inductor during operation, this waveform is shown in Figure 3.15. Mode 1 of the DC-DC converter is shown from time 0-DT and mode 2 from time DT-T.

To determine the average voltage across the inductor for one cycle, the area under the graph for mode 1 and 2 is summated, the equation used is shown as equation (3.15).

$$V_L = V_{in}DT + (V_{in} - V_{out})(1 - D)T \tag{3.15}$$

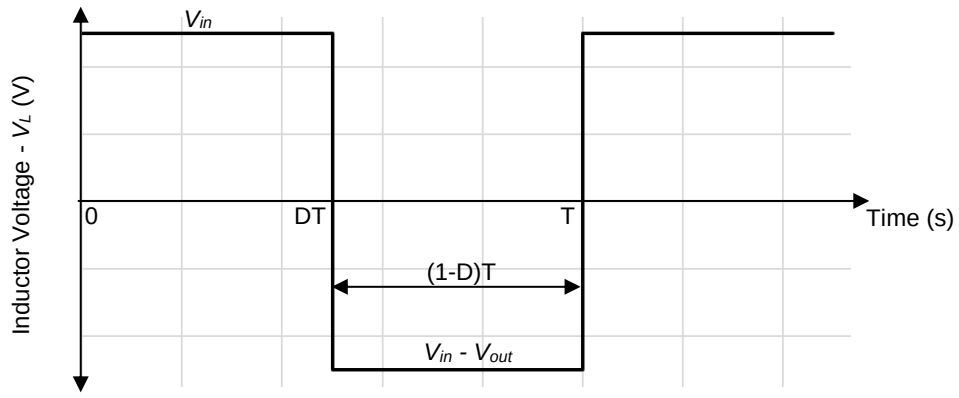


**Figure 3.15: Inductor voltage derivation waveform**

The average voltage across the inductor is ideally equal to zero therefore equation (3.15) is equated to 0 and rewritten to isolate *D.* The resulting equation is given in equation (3.16).

$$D = 1 - \frac{V_{in}}{V_{out}} \tag{3.16}$$

Equation (3.16) is the equation used to determine the duty cycle (*D*) of the converter. In order to determine the equation used to obtain the required inductor value Figure 3.16 will be used – this figure represents the waveform of the current flowing through the inductor while in operation. Mode 1 is represented in the segment of time 0-DT and mode 2 in the segment of time DT-T.

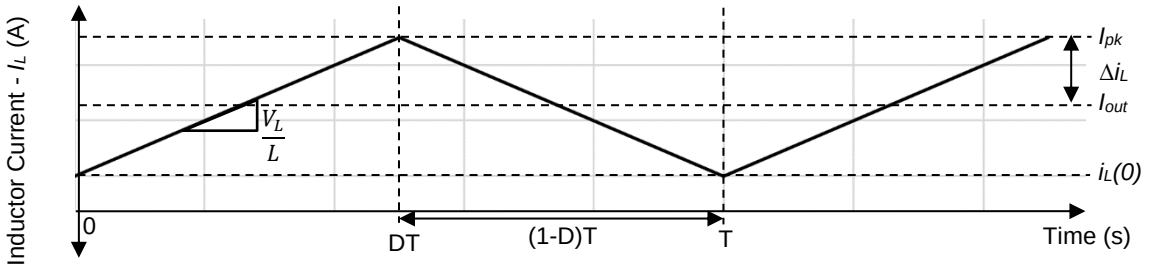


**Figure 3.16: Inductor current derivation waveform**

To determine the area under the graph for mode 1, equation (3.17) is used.

$$V_L = L\frac{di_L}{dt} \tag{3.17}$$

This equation can be rewritten to determine the slope of the graph ($di_L/dt$) and the result is shown in Figure 3.16. This term for the slope can be rewritten in the form $2\Delta i_L/DT$ where $\Delta i_L$ represents half of the area under the slope in the segment for mode 1 and as such when multiplied by 2 can be used to determine the area under the graph given by equation (3.18).

$$2\frac{\Delta i_L}{DT} = \frac{V_L}{L} \tag{3.18}$$

This term is rewritten to isolate the inductance *L* shown in equation

$$L = \frac{V_{in}DT}{2\Delta i_L} \tag{3.19}$$

*T* represents the period and can be rewritten as $1/f_{sw}$, also, using the laws of conservation of power in an ideal environment, the input power equates to the output power both with general equation *P = VI*. This power equation can be written as in equation (3.20)and rewritten to form equation (3.21).

$$V_o I_o = V_{in} I_{in} \quad \textbf{(3.20)}$$

$$I_{in} = \frac{V_o I_{out}}{V_{in}} \quad \textbf{(3.21)}$$

Knowing that $I_L$ is equal to $I_{in}$, determined using Figure 3.14, and using equation (3.16) to substitute $V_{in}/V_{out}$, equation (3.21) is rewritten and used in equation (3.19) to form equation (3.22) to be used to determine the minimum value of the inductor for a DCM DC-DC converter.

$$L > \frac{D(V_{in})(1-D)}{(2f_{SW} I_{out})} \quad \textbf{(3.22)}$$

In this equation, $L$ refers to the inductance, $f_{SW}$ refers to the switching frequency (chosen as 62 500 Hz as this is the highest frequency the microcontroller can supply), $I_{out}$ refers to the maximum output power required by the load (9 A), $V_{in}$ refers to the maximum input voltage of the converter (21 V from SCs) and finally $D$ refers to the minimum duty cycle of the converter calculated using equation (3.16). $V_{in}$ refers to the maximum input voltage (21 V) and $V_{out}$ refers to the desired voltage output of the converter (50 V). The maximum duty cycle (using the minimum input voltage – 17 V) can also be used to determine the inductor value however the largest value of the inductor using the minimum and maximum duty cycles is preferred to be used as it results in a better functioning converter avoiding the saturation point. For demonstration purposes both inductor values will be calculated and simulated in section 3.2.3.6. Using equations (3.16) and (3.22), $D_{min}$ is calculated as 58%, giving an $L_{max}$ of 4.55 µH and $D_{max}$ is calculated as 66% giving an $L_{min}$ of 3.44 µH.

Before the inductor can be acquired the peak current that will be passing through the inductor needs to be calculated. This value is compared to the saturation current of the inductor to ensure that the inductor will not enter saturation for the entire range of current requirements of the converter. As the converter is a boost converter the voltage output is larger than the voltage input, but the power needs to remain relatively the same throughout the converter with a general efficiency of 90%, this accounts for power losses in the system. For conservation of power equation (3.23) (obtained from equation (6.10c) in [174]) can be used to give a rough estimate of the power input requirements,

$$P_{in} = \frac{P_{out}}{\eta} \quad \textbf{(3.23)}$$

For this equation $P_{out}$ refers to the required output power (maximum of 450 W) and n refers to the efficiency of the system (0.9), using these values the input power should be around 500 W. the general equation to determine the power of a circuit is given by equation (3.24) (obtained from equation (19.9a) in [174]),

$$P_{in} = V_{in} I_{in} \quad \textbf{(3.24)}$$

With $V_{in}$ referring to the minimum input voltage (17 V) as this results in the largest current requirements for power preservation, equation (3.24) can be rewritten to determine the maximum $I_{in}$ requirements in equation (3.25),

$$I_{in} = \frac{P_{in}}{V_{in}} \quad \textbf{(3.25)}$$

Using equation (3.25), the estimate of maximum input current is determined as $I_{in}$ = 30 A. However, to account for more losses in the system a more accurate value is acquired using equation (3.26),

$$I_{pk} = \frac{V_{in(\max)} D}{f_{SW} L} \quad \textbf{(3.26)}$$

This peak current is calculated as $I_{pk}$ = 43 A, which is obtained using $L_{max}$ as the L-value.

### 3.2.3.4 Output Capacitor calculations

All of the equations used in this section are obtained from [182], [184], [256], [257] unless otherwise specified. The output capacitor of the system is a parallel combination of two capacitors and is used to reduce the voltage ripple caused by the charge and discharge curve of the inductor, this ripple is desired to be 1-5% of the output voltage [194], [257], [258]. By reducing the ripple voltage, the output voltage can be stabilized to give a smoother DC output. To determine the output capacitance required the waveform of the current through the output capacitor shown in Figure 3.14 will be observed. This waveform is shown in Figure 3.17.

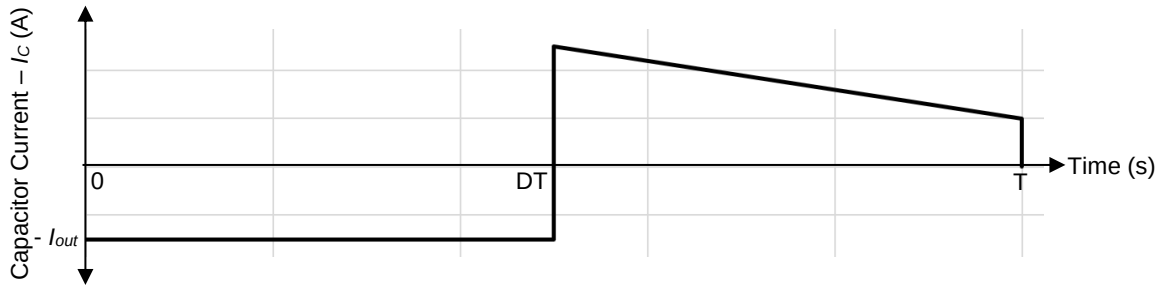


**Figure 3.17: Capacitor current derivation waveform**

Once again, the two modes of operation are represented through time segments 0-DT and DT-T. The slope of the waveform is determined using equation (3.27).

$$i_C = C_{out} \frac{dv}{dt} \quad \textbf{(3.27)}$$

Isolating the capacitance $C_{out}$ and knowing $I_C = I_{out}$ this equation is rewritten in the form of equation (3.28).

$$C_{out} = \frac{I_{out} \Delta t}{\Delta v} \quad \textbf{(3.28)}$$

$\Delta t$ is rewritten as $DT$ and $T$ is rewritten in the form $1/f_{sw}$. This allows equation (3.28) to be rewritten in the form of equation (3.29).

$$C_{out} > \frac{I_{out} D}{\Delta v f_{SW}} \quad \textbf{(3.29)}$$

Here, the ripple voltage is chosen as 1% of the output voltage (50 V), thus 0.5 V, giving a $C_{out}$ of 202 µF. In order to stabilize the output further, this capacitance can be divided amongst a few capacitors in parallel adding a ceramic capacitor to filter out the higher frequencies as the lower frequencies are filtered out using aluminium electrolytic capacitors; the parallel combination of these capacitors should equal the value calculated for $C_{out}$. Capacitors with low ESR values and large capacitances

are preferred for this application as they decrease the overshoot in the output voltage as well as the ripple [194].

#### 3.2.3.5 Snubber circuit calculations

Whenever MOSFETs are used in a circuit a phenomenon known as switching losses occur. When a MOSFET is switched between the on and off states a rise and fall time is seen which is the time it takes for the MOSFET to completely switch on or off. In order for these rise and fall times to occur quickly power is drained from the system to pull the switch up or down. This power is the switching loss mentioned above. Although it seems like these losses cannot have a large effect on the circuit, when the power in the circuit is increased these losses can have a large effect. These losses can cause the MOSFET to only have a maximum efficiency of 70%, where after it will fail. In order to combat these losses a snubber circuit can be inserted over the MOSFET that will allow for a soft – start and –stop of the MOSFET while diverting any losses into the snubber circuit and directing it back into the main circuit and its operation, therefore decreasing overall losses.

Snubber circuits are classified as either active or passive, the latter including resistors, diodes, capacitors and inductors and the former including those as well as transistors and switches thus requiring more complex circuitry than that of the passive type. A passive snubber can include either inductors or capacitors (in conjunction with a resistor) or both. Capacitors are usually used to snub the voltage across the switch while inductors are used to snub the current, if the values of the components are correctly chosen, the switching losses can be reduced up to 40% [259]. For application in this project an RC snubber will be used and the values are calculated below. A similar method was followed as that found under the Quick Snubber Design section of the CDE application guide [260].

To simplify the design of the snubber circuit the capacitor value was chosen to be small enough such that the resistor could be of a large value such that the power rating need not be large. To obtain a formula to calculate the resistor value, equation (3.6), used to determine the energy stored in a capacitor, will be used. Equation (3.30) (obtained from equation (19.9b) in [174]), used to calculate power, can be rewritten to determine the resistance. Power is defined as the energy use over a period of time (*E/T*) and *1/T* is rewritten as $f_{SW}$, therefore, power is also $Ef_{SW}$. Using this, rewriting equation (3.30) to isolate *E*, equating the result to equation (3.6) and once again isolating *R,* equation (3.31) is obtained.

$$P = \frac{V^2}{R} \tag{3.30}$$

$$R = \frac{2}{C * f_{SW}} \tag{3.31}$$

For this final equation the capacitor value will be chosen as 4.7 nF giving a resistor value of 6.8 kΩ rounded up to 10 kΩ.

### 3.2.3.6 Simulation

To simulate the designed DC-DC circuit, LTspice® and Simulink® will both be used. Simulink® will be used to verify the LTspice® simulation, this is due to Simulink® having more adjustable parameters of the components. LTspice® contains a variety of each of its components, allows the user to adjust specific parameters of the component and also has the option of importing the Spice™ model of a specific component. However, all of this variety is limited to a maximum of five parameters and also to those Spice™ models available (usually more generic components). Simulink® allows for the adjustment of a wider range of parameters of each component, thus, using the datasheet of the specific component a more accurate functionality of that component is achieved. Through this the entire circuit simulation will return a more accurate representation of its real time operation.

#### 3.2.3.6.1 LTspice® simulations

Using LTspice® the circuit can now be simulated to determine the correct operation and to fine tune the values of the inductor and output capacitor. The circuit that will be used to simulate these values is shown in Figure 3.18 below.

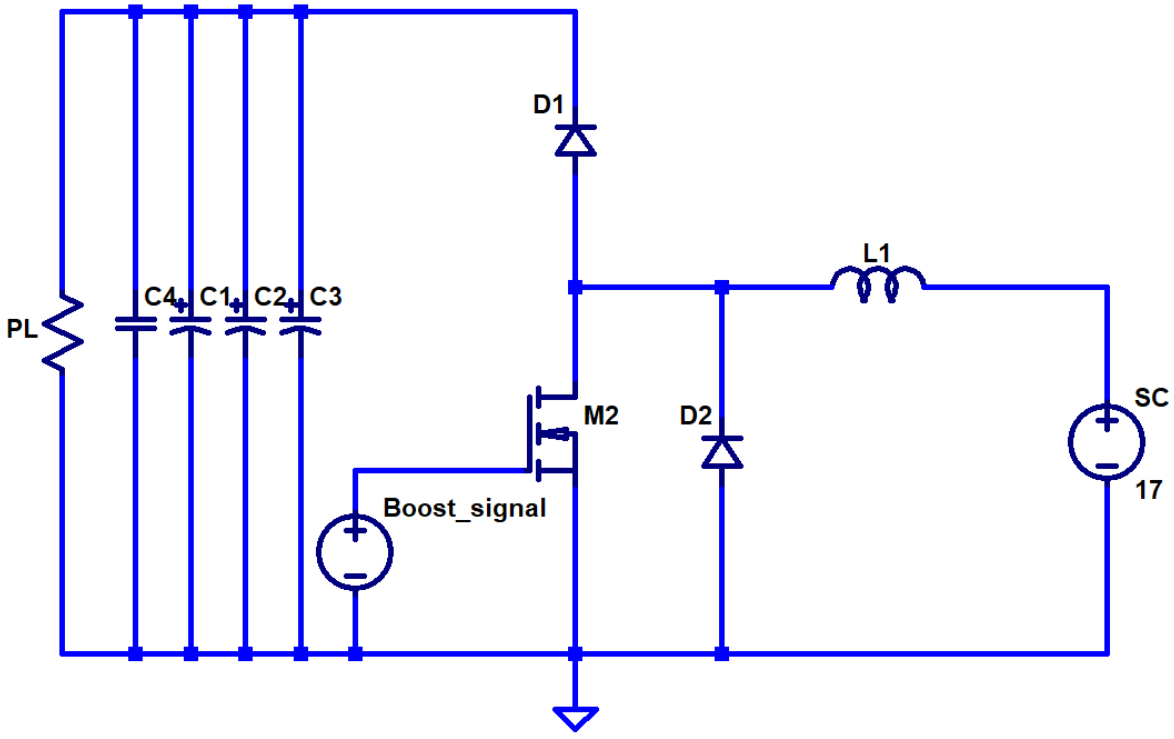


**Figure 3.18: LTspice® simulation model**

In the figure $C_1$ – $C_3$ represent the electrolytic capacitor combination of the output capacitor value calculated and $C_4$ represents the additional high frequency ceramic capacitor filter. In order to simulate the circuit efficiently a resistor will be used to represent the load, this is calculated using the output current (1-9 A) and voltage (50 V) values and equation (3.32) (adapted from equation (3.10)),

$$R_{load} = \frac{V_{out}}{I_{out}} \tag{3.32}$$

Using the maximum and minimum current values $R_{load}$ must be 5-50 Ω.

Using the above calculated values, the circuit can be simulated and the results can be analysed. The first analysis will be done using $L_{min}$ = 3.44 µH = $L_1$, $C_{out}$ = 288µF ($C_4$ = 47µF, $C_1$ = $C_2$ = $C_3$ = $C_{out}$/3 = 96 µF and $D_{max}$ = 66%). First the transient analysis of the output voltage and the current through the inductor will be discussed. Figure 3.19 displays the transient analysis of the voltage present across the output capacitor for an extended period of time used in order to show the initial ramp of the output voltage until it stabilizes. The graph also shows the values between which the voltage ripples, once stabilized.

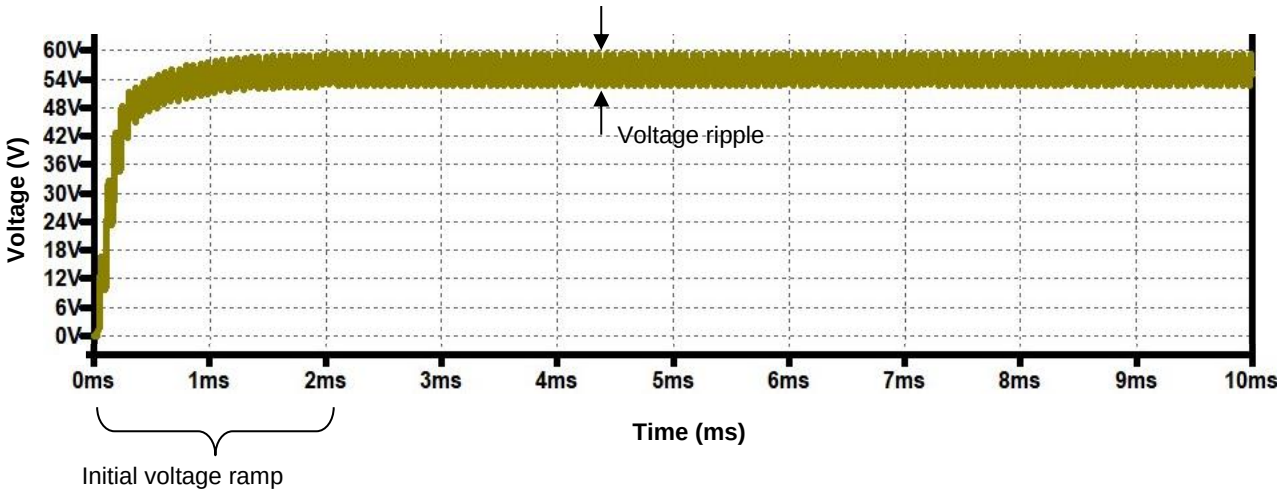


**Figure 3.19: Transient analysis of output voltage with *L* = 3.44 µH and *D* = 66%**

In the figure it can be seen that the initial voltage ramp occurs in around 2 ms, this is due to the system being off before this point and no charge having been stored anywhere in the circuit, it is also seen that there is no overshoot. Both this and the rise time can be attributed to the size of the capacitors (high capacitance and low ESR) on the output and more specifically that of the ceramic capacitor, as the capacitors dampen the effect of an overshoot and the ripple voltage [194].

The size of the inductor can also affect the stabilization time as the inductance is inversely proportional to the ripple current and the smaller the ripple current, the smaller initial current spike (overshoot), thus if the inductance is too small the initial spike will be larger causing the voltage spike to consequently be smaller and the capacitors to have a larger, and possibly an over-, dampening effect. The voltage is seen to ripple between 51-60 V (9 V), which is 16.4% of the output voltage (averaging at 55 V) and the desired ripple voltage is recommended to be 1-5% of the output voltage [194], therefore 0.55-2.75 V. The simulated value is much larger than desired and therefore unacceptable but it can be adjusted through altering the values of the ceramic and electrolytic capacitors on the output. Using a 66% duty cycle and input voltage of 17.5 V the desired output is calculated using equation (2.3) as 51.47 V, showing a 6.4% deviation from the measured value; this can be remedied through the adjustment of the inductor and capacitor values.

The next Figure, Figure 3.20, shows the transient analysis of the current through the load of the system. The period used to analyse the waveform is chosen again to show the initial ramp of the current and the point at which it stabilizes therefore also including the current ripple of the waveform.

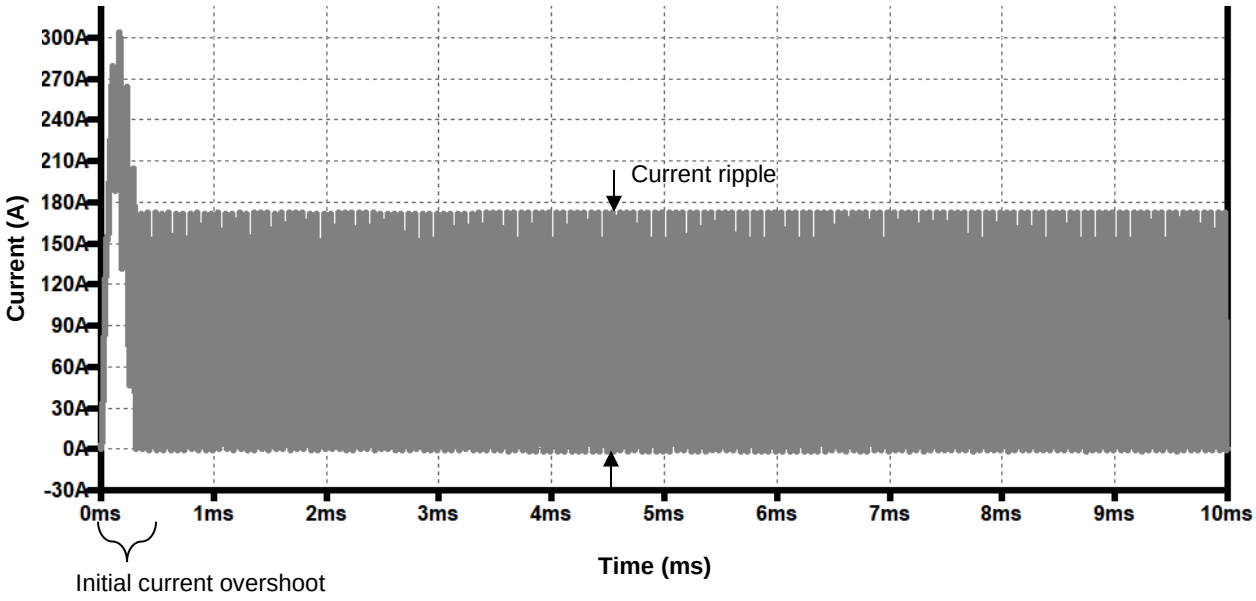


**Figure 3.20: Transient analysis of inductor current with *L* = 3.44 µH and *D* = 66%**

In the figure the current overshoot is due to the system being off prior to this point and the first initialization of the circuit causes this. It is then seen that the current stabilizes and ripples for the remainder of the analysis. The ripple current is measured as 0-172 A (172 A). It is desired that this value be 20-40% of $P_{out}/V_{in}$ [194], [256], [257], therefore with a desired $P_{out}$ of 1 kW and $V_{in}$ of 17 V, the desired ripple current is 23.5 A, which is significantly smaller than that measured. However, the output current is larger (15 A) than the required 9 A, which can be attributed to the size of the inductor being smaller than required but is not an issue as load will only receive what is required.

The final figure for analysis is Figure 3.21, which is a combination of the output voltage- and inductor current- ripples compared to the boost signal of the MOSFET. This graph only shows a portion of the transient analysis as it is desired to show the charge and discharge of the specified components as compared to the switching of the MOSFET. From Figure 3.21 it can be seen that when the MOSFET switches on the inductor current increases and when the MOSFET switches off the current decreases to 0. This is desired and expected as it demonstrates the charge and discharge of the inductor.

It can also be seen that the inductor reaches saturation on its lower end, indicating that the circuit is operating in DCM. The inductor does not saturate at its upper end which is desired as it will not lead to excessive power loss in the form of heat, however it can be seen that the rise and fall curves are slightly rounded and less linear – this will lead to a similar rounding effect in the voltage waveforms, such that is seen on the graph. The voltage waveform is following a general pattern of charge and discharge opposite to that of the inductor which is desired as the inductor discharges during mode 2 allowing current to flow towards the output and therefore increasing the output voltage. What is not desired, however, is that the voltage waveform has a “kink” in the descent of the waveform showing that one of the capacitors is filtering a larger portion of the output than desired.

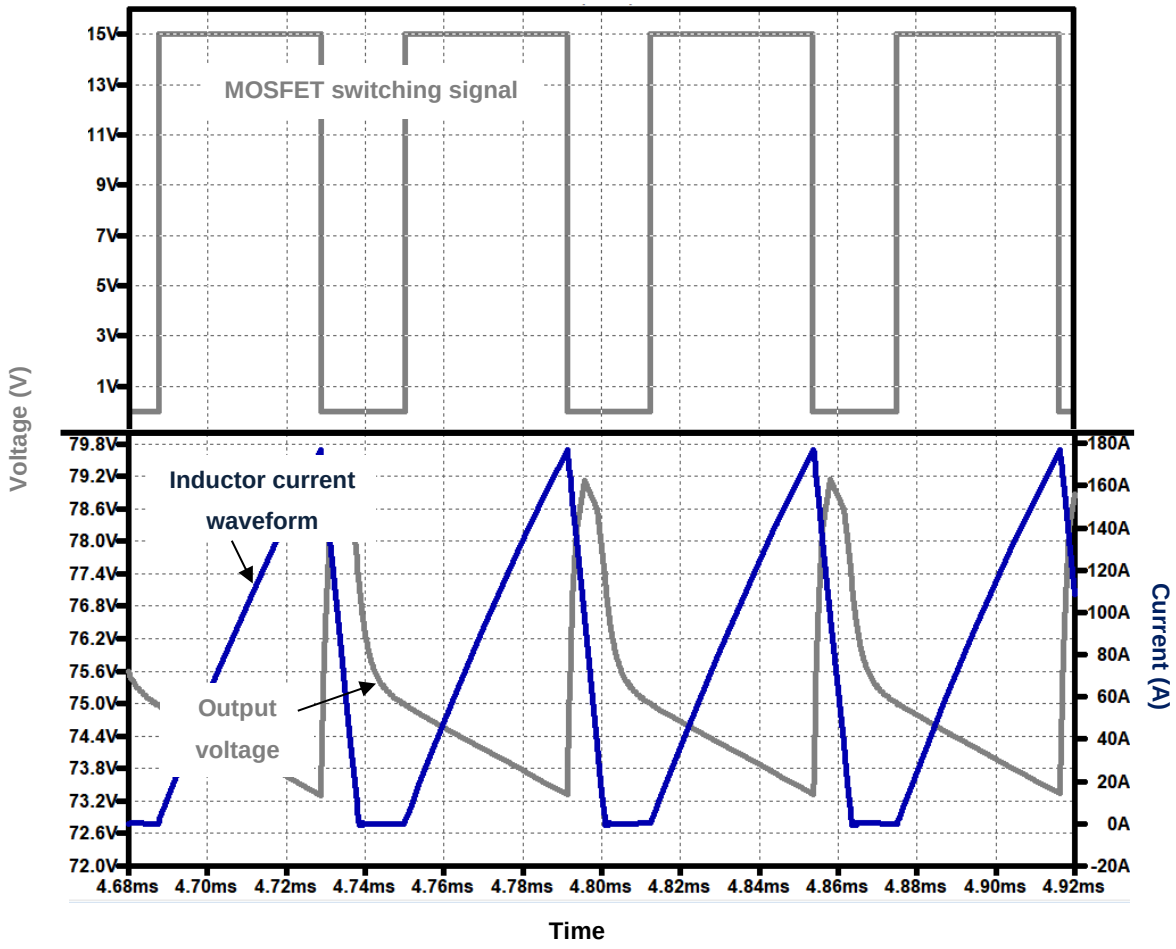


**Figure 3.21: V & I ripples present in inductor and output capacitor**

These undesired outcomes can be remedied through the selection of a larger inductor (decreases the output current as well as creating a more linear charge and discharge pattern) and also through finer tuning of the output filter capacitors. For the next simulation the inductor value will be increased to 5 µH with all the other values the same as before. Figure 3.22 shows the transient analysis of the voltage across the output capacitor and is used to show the voltage ripple on the output, as well as the initial voltage before the voltage stabilizes.

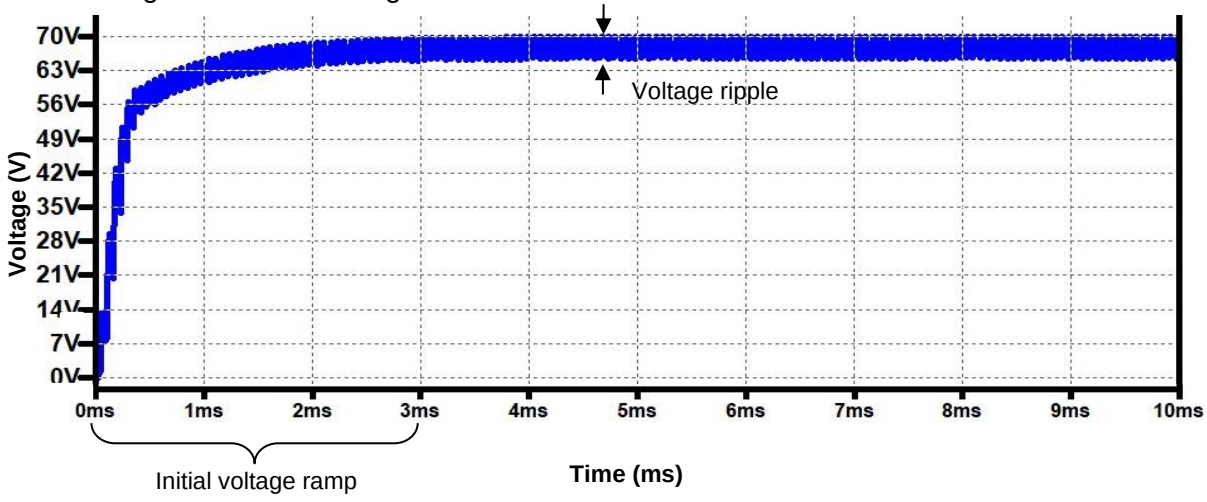


**Figure 3.22: Transient analysis of the voltage across the output with *L* = 5 µH**

From the figure it can be seen that the initial voltage ramp occurs within 3 ms, slightly longer than in the previous case. The voltage ripple is seen to fluctuate between 65.4-70 V (4.6 V), comparing this to the average output voltage (66.8 V), the ripple has a percentage of 6.9%.This is larger than that of the previous case and the desired 1-5%. This shows that the inductor value also plays a role in the ripple voltage; the capacitor values will be altered next to obtain the appropriate ripple percentage. The output voltage (66.8 V) which gives a deviation of 29.78% from the calculated 51.47 V – this is a much larger deviation than with the smaller inductor value thus showing its relevance and the capacitor values will be altered next to finer tune this deviation.

Figure 3.23 displays the transient analysis of the current through the load and will be used to examine the effect of the inductance on the ripple current and the initial current ramp.

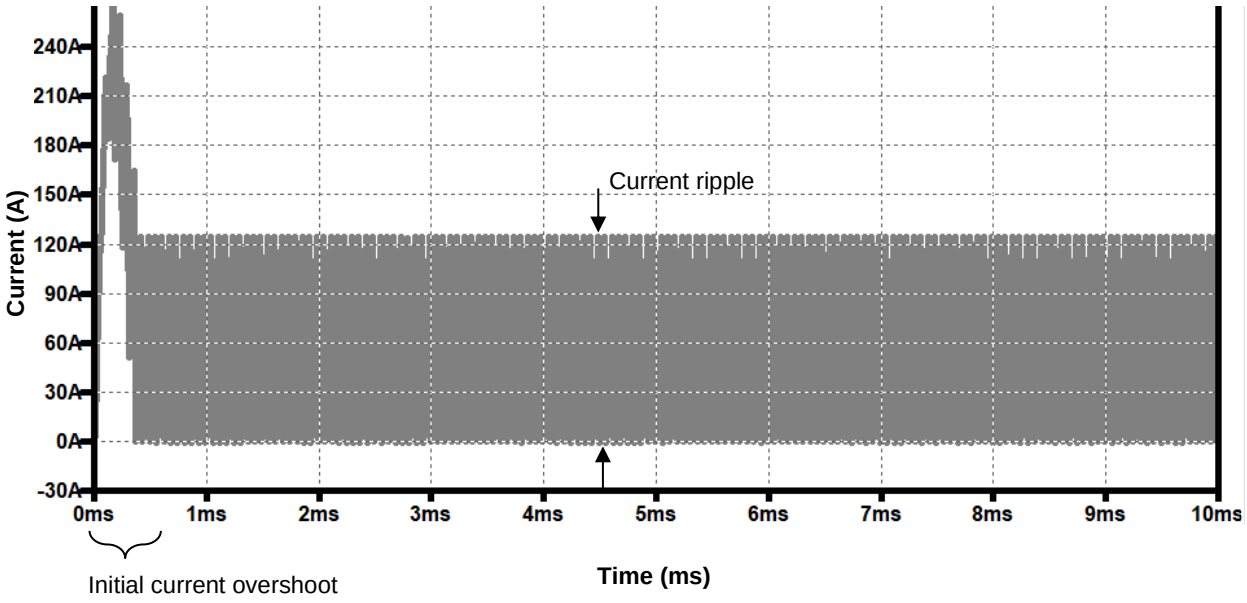


**Figure 3.23: Transient analysis of current through the inductor with *L* = 5 µH**

From the figure it can be seen that the current ripples from 0-124 A (124 A), which is a value closer to the desired 23.5 A, as compared to the previous simulation, but still significantly much larger. This will be attempted to be rectified in the next simulation. The output current is also larger than the required 9 A, but this is not an issue as it only shows that the system can provide a larger current than required.

Figure 3.24 shows the portion of the transient analyses where the current through the inductor and the voltage across the output capacitor stabilize as compared to the switching of the MOSFET. This figure is used to analyse the waveforms of the aforementioned current and voltage to determine correct operation and values of the components. It is evident from the figure that the inductor is charging and discharging as it should with the switching of the MOSFET, it can also be seen that the waveform is slightly more linear than before resulting in a slightly more linear waveform of the voltage.

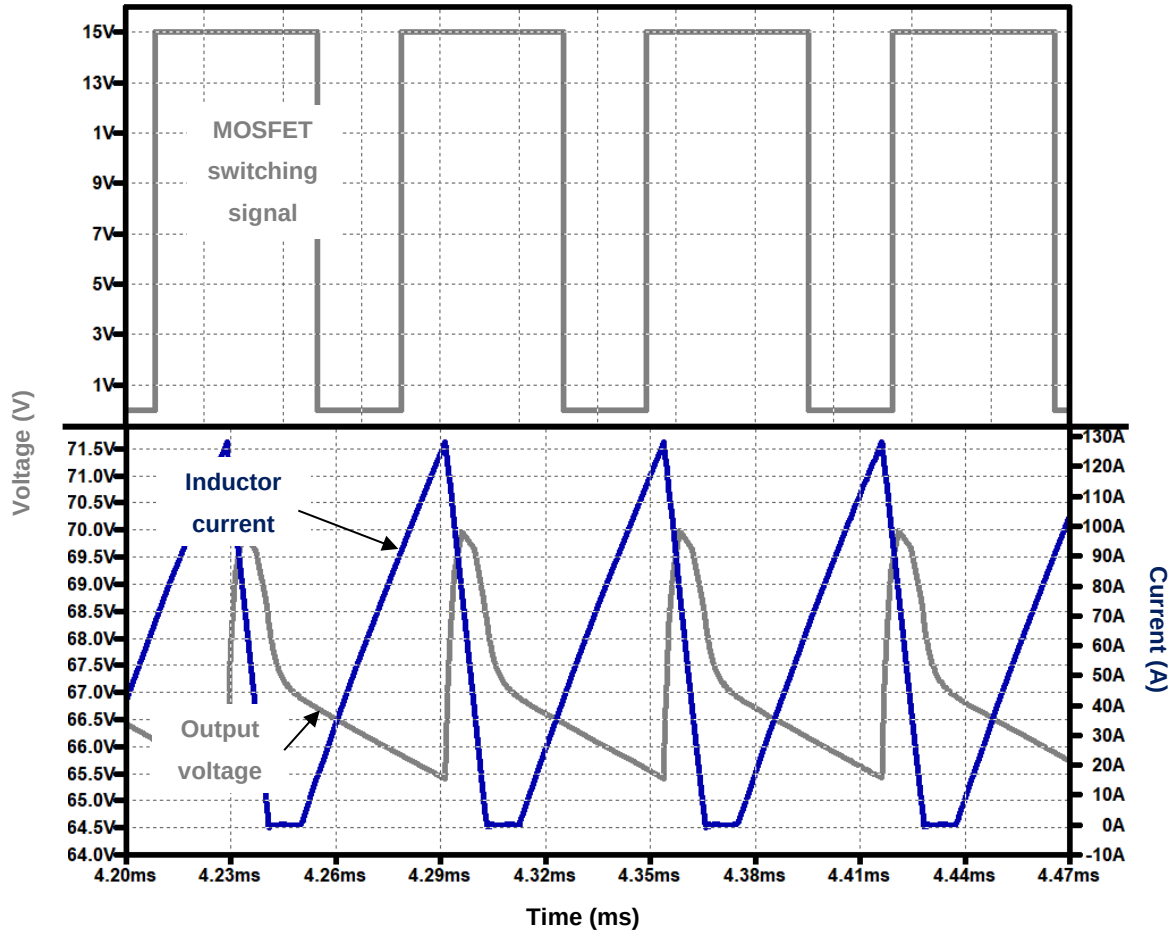


**Figure 3.24: V & I ripples present in inductor and output capacitor with *L* = 5 µH**

The saturation of the inductor is of a larger extent (~0.15 ms) than before (~0.010 ms). The voltage waveform is very similar to that of the previous simulation with the exception of it being less rounded. This shows that the voltage waveform is more dependent on the output capacitors than the inductance. For the next simulation the capacitor values will be altered to obtain more desirable waveforms.

#### 3.2.3.6.2 Simulink® Simulations

The circuit used to verify the LTspice® simulations in Simulink® is shown in Figure 3.25. The circuit used in Simulink® is a replica of that used in LTspice® (Figure 3.18).

The analysis of the circuit output will contain a few similar graphs as well as some extra graphs to explain the desired operation in a more in-depth approach which is possible with the Simulink® outputs as they are more accurate than those of LTspice®.

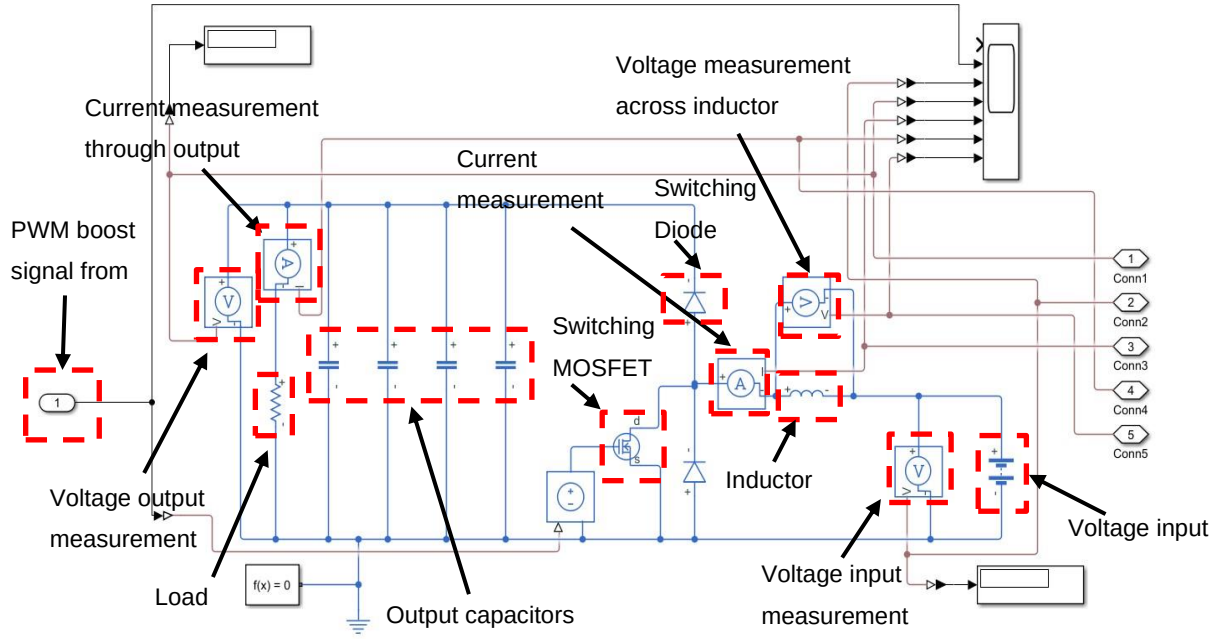


**Figure 3.25: DC-DC converter simulation circuit used in Simulink®**

Figure 3.26 below depicts the transient analysis of the voltage across the output capacitor of the circuit.

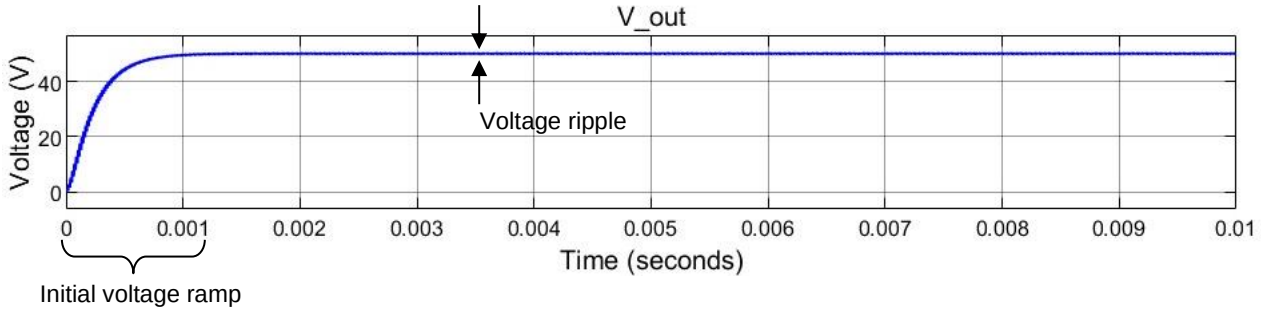


**Figure 3.26: Simulink® circuit transient analysis of Voltage output**

For this simulation the duty cycle is set at 64% and the input voltage is 21.5 V; all other values are the same as in the LTspice® simulations for the $L_{max}$. The initial voltage ramp is the same from both simulation packages but the voltage ripple is 50-50.7 V (0.7 V) (closer view shown in Figure 3.27, $C_{out}$ = 320 µF), comparing to the output voltage (50.3 V) – a 1.39% ripple is obtained. This value is significantly less than that obtained from LTspice® and is also within the acceptable range of 1-5%.

This value can be finer tuned, if desired, by adjusting the output capacitor values. For illustration purposes the output capacitor values have been varied to assess how the value affects the ripple voltage. The resultant waveforms are shown in Figure 3.27. The waveforms showing the output ripple voltage of the chosen output capacitance are indicated using the combined capacitances given next to each waveform. The 320 µF waveform is the waveform obtained using the calculated output capacitance, whereas the remaining two waveforms use capacitance values chosen arbitrarily. It is evident from the various waveforms that an increase in the total capacitance leads to a smaller ripple voltage of 1.09% (50.15-50.7 V) of the average 50.4 V.

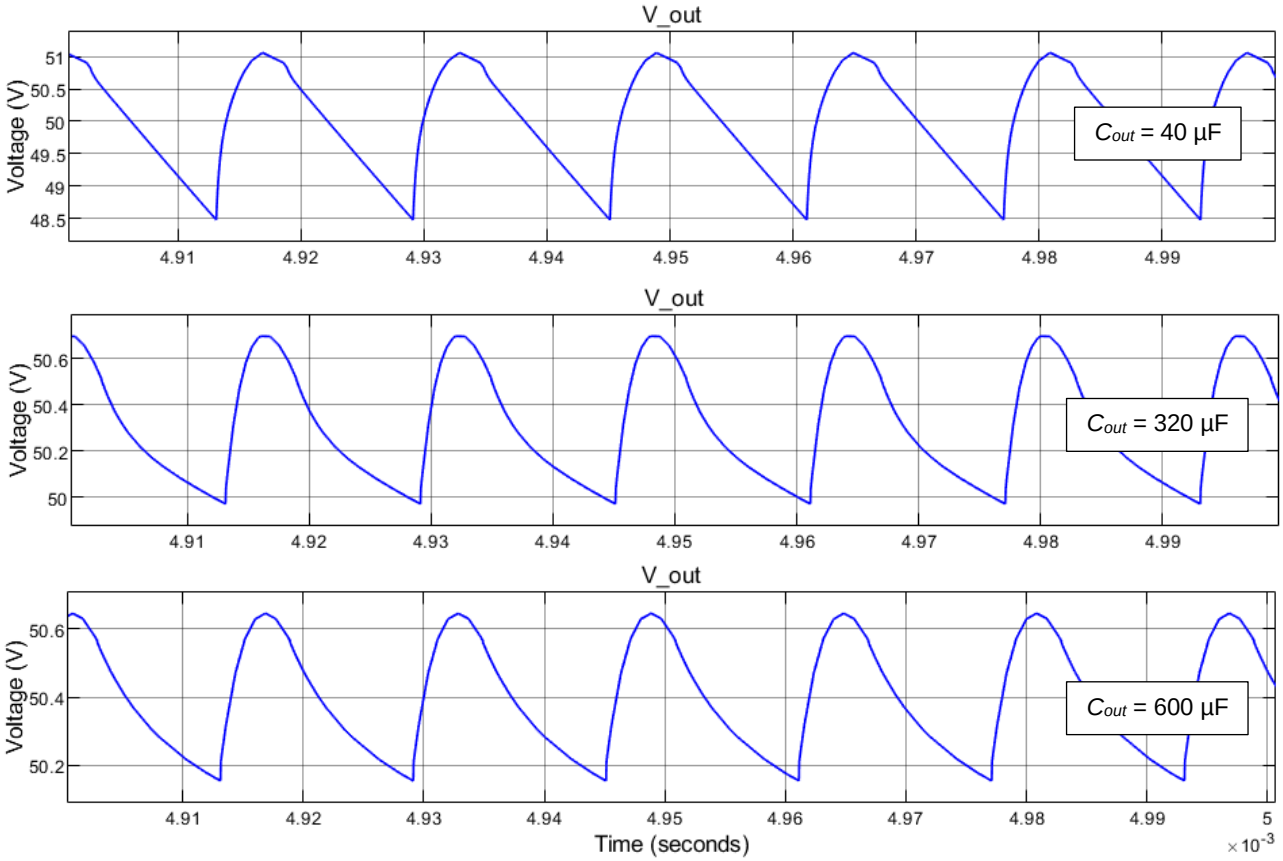


**Figure 3.27: Output ripple voltage variation with output capacitor size variations**

A decrease in the output capacitance alternatively leads to an increase in the ripple voltage – 5.04% (48.5-51 V) of the average 49.55 V. Therefore, if it was desired to improve the voltage ripple, the output capacitance need only be increased, however, the initial ripple of 1.39% is well within the desired value such that this adjustment is needless. Using equation (2.3) the desired output voltage is calculated as 59.2 V; the measured value therefore deviates 15% from this value, however the system is designed for a 50 V output and this value can thus be accepted. Figure 3.28 depicts the transient analysis of the current measured through the load of the Simulink® circuit.

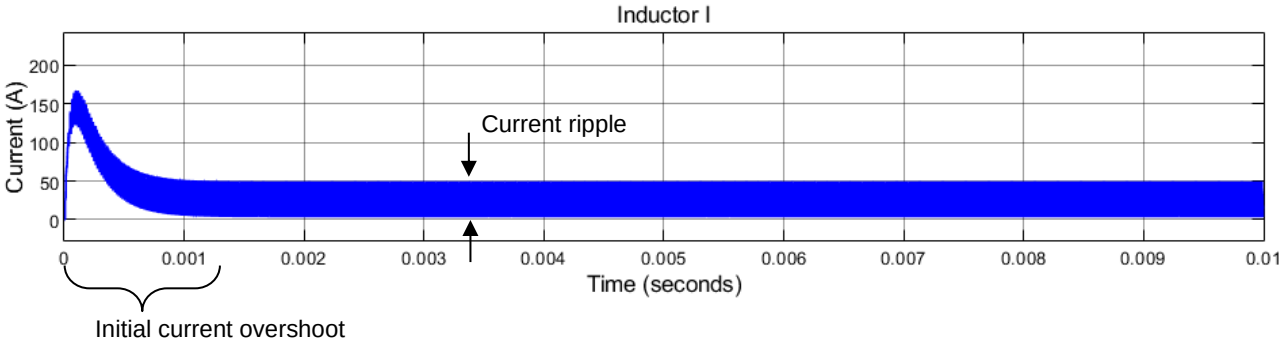


**Figure 3.28: Simulink® circuit transient analysis of the current through the inductor**

This graph has a similar form to that obtained during the LTspice® simulation with a 1.5 ms initial current ramp and overshoot. The current ripple is 0-50 A (50 A) (closer view shown in Figure 3.29, $I_L$ = 4.7 µH) which is a value significantly closer to the desired 23.5 A, when compared to the LTspice® simulations. The output current is the desired 9 A. Although the ripple is still much larger than desired

it is a better result and shows how different simulation packages can yield different results when using the same components and values.

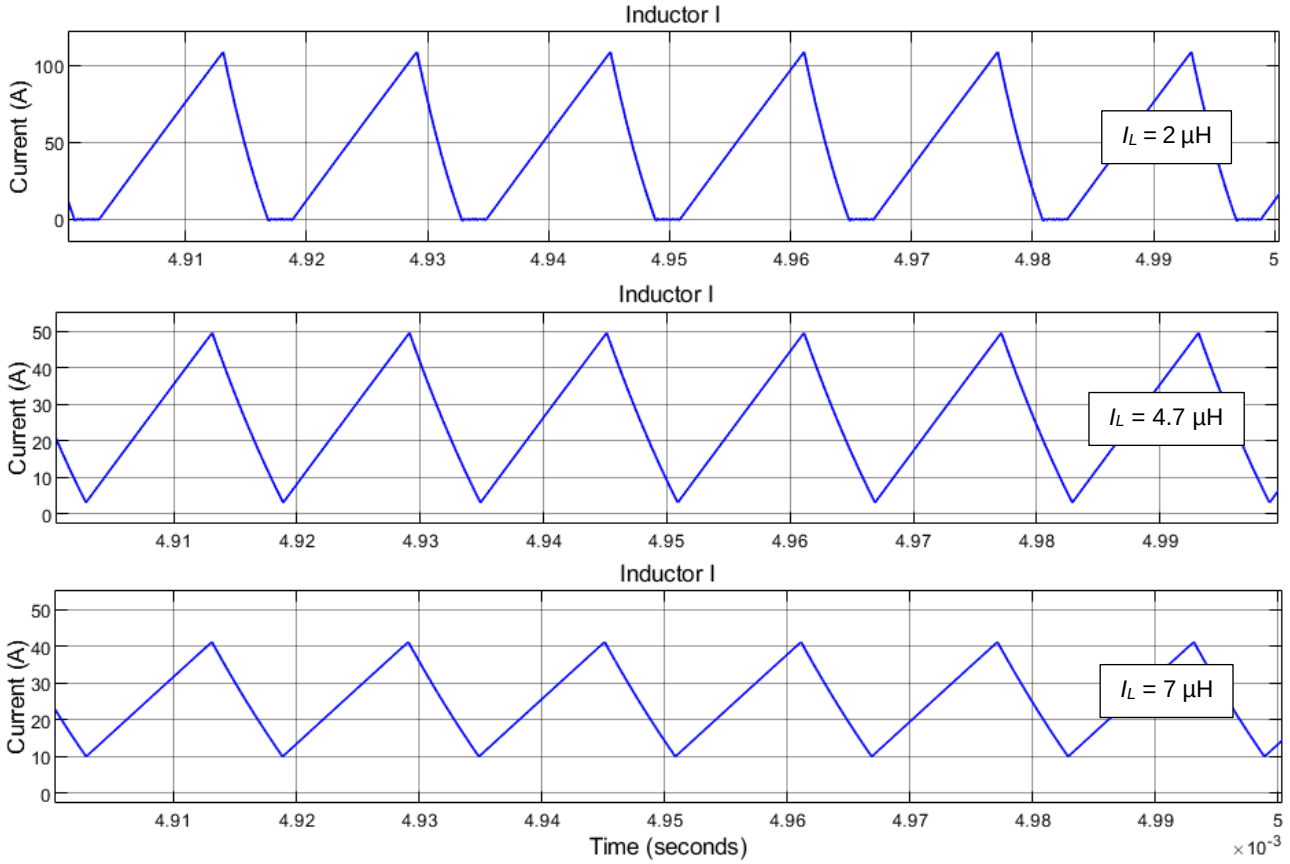


**Figure 3.29: Inductor ripple current with variation in inductor size**

The waveforms depicting the different ripple currents obtained using varying inductances are separated using the values indicated on each waveform. The calculated inductance depicts the waveform represented by the 4.7 µH inductor. It is evident from Figure 3.29 that an decrease in the inductance leads to a larger ripple current of 110 A, whereas an increase in the inductance leads to a decrease in the ripple current shown in the 7 µH waveform as 30 A.

Through these two transient analyses it is already seen that the results from the Simulink® simulation differ from the LTspice® simulation even though the values of the components (and the circuit) are the same. Where some voltage and current ripples obtained in the LTspice® simulations were above that of the desired ripples, they were within the desired ranges for the Simulink® simulation. This further justifies the use of both simulation packages for the simulation phase of this chapter. Figure 3.30 shows the waveforms of the voltages present across the inductor, output capacitor and diode. The waveforms are compared to the PWM signal switching the MOSFET.

In section 2.4.1 the operation of the inductor was explained. When the MOSFET is switched on the inductor conducts straight to ground and thus has the same voltage at its input as that at the system input ($V_{in}$); when the MOSFET is off the inductor conducts towards the output and also discharges its accumulated value.

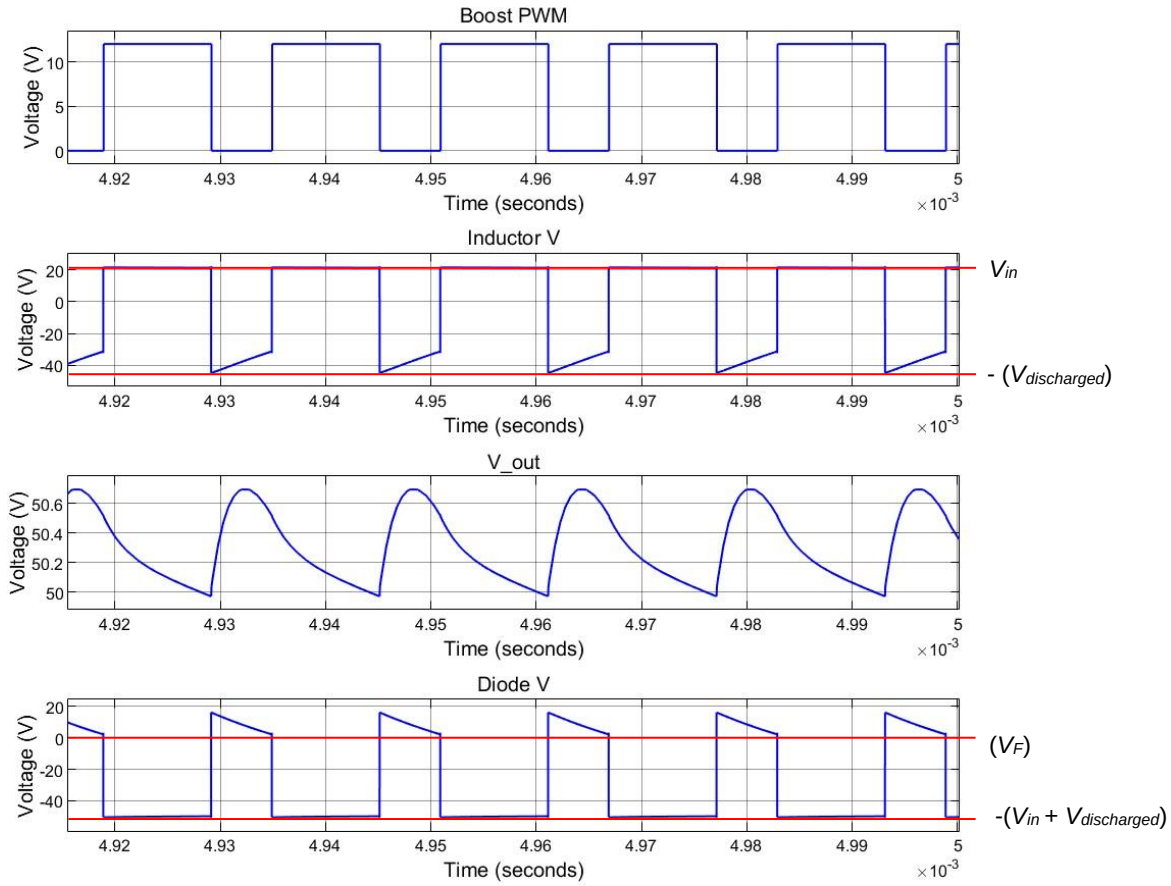


**Figure 3.30: Voltages present across inductor and output capacitor of Simulink® circuit**

This results in the output voltage of the inductor being the summation of the input voltage and the discharged voltage ($V_{discharged}$), $V_{inductor} = V_{in} + V_{discharged,}$ and thus larger than the input voltage. A larger output with respect to the input causes a negative potential difference – this is depicted in the *Inductor V* waveform; it is also seen that this negative potential difference decreases as the inductor discharges and $V_{discharged}$ decreases.

When the inductor switches from discharging to charging (MOSFET is on) its minimum voltage value at that moment is stored in the output capacitors. As soon as the MOSFET is switched off and the diode conducts the initial potential difference between the input and output of the diode is due to the difference between the voltage stored in the output capacitors and that flowing from the inductor ($V_{difference}$). The negative potential difference of this waveform is seen when the PWM signal is on and the diode does not conduct, this difference is between the voltage stored in the output capacitors ($V_{difference}$) and ground through the MOSFET. Looking at the voltage output waveform ($V_{out}$), compared to the waveform from the LTspice® simulation, this one less of a “kink” resulting in a closer resemblance to the saw tooth waveform of the inductor current.

The current waveforms are seen in Figure 3.31 below. The inductor current waveform shows no saturation at either end of the charge or discharge of the inductor, as opposed to that which is seen in the LTspice® simulation.

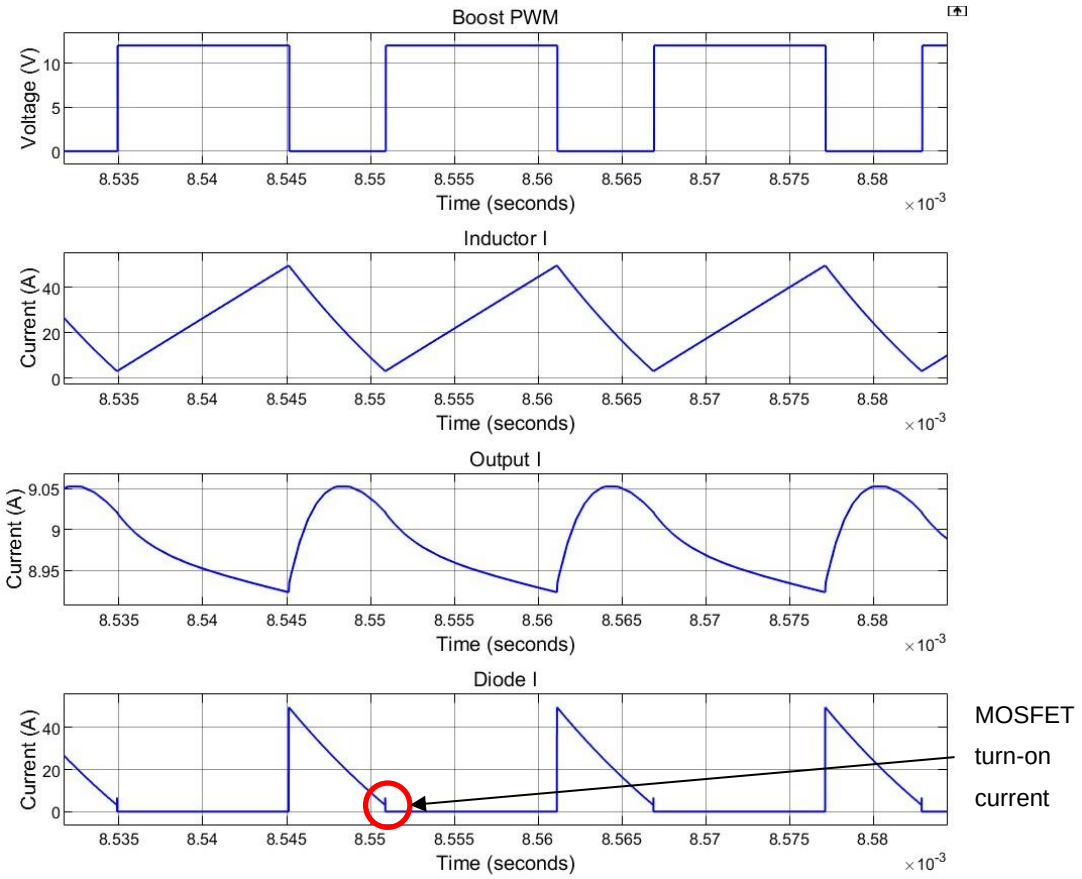


**Figure 3.31: Current flowing through inductor, output capacitor and diode of Simulink® circuit**

The waveform of the diode shows the current before it passes though the capacitors and the output current shows the diode current waveform after flowing through the capacitors. The diode current is seen to have a small spike (~5 A) when the boost PWM is turned on – this can be attributed to the turn-on current required by the MOSFET. By comparing the diode and inductor waveforms it is seen that the inductor is conducting when the PWM signal is on and the diode is rightfully off. When the PWM switches off the inductor is seen to slowly stop conducting while it discharges and the diode switches on and conducts for this duration.

For further verification and validation purposes the component values will be adjusted such that the output voltage is the desired 50 V for a 9 A load and the individual component waveforms will again be analysed for correct operation. The results for this will be shown in section 3.2.6.2.

### 3.2.3.7 Heat sink calculations

The equations for this section have been obtained from [261], [262] unless otherwise specified. The final consideration for the DC-DC converter circuit will be the necessity for heat sinks on the switching components (MOSFET and main circuit diodes). These are required due to the high switching frequencies and the large power requirements of the circuit. To calculate the size of the MOSFET's heat sink the expected power dissipation ($P_D$) of the switch needs to be calculated, this power consists of two components, the on-power dissipation and the switching power dissipation. When a transistor is switched on it behaves similar to a resistor with resistance dependent on the signal sent

to the gate. Therefore, the transistor dissipates power due to the resistive force between its input and output – in this case, the drain and source. The magnitude of this power is obtained using a general power equation for resistive power ($P = I^2R$) with $I$ – the maximum current passing through the device ($I_D$) and $R$ – the resistance that the path offers against the flow of current ($R_{DS(on)}$). The equation for this specific application is given by equation (3.33).

$$P_{D(on)} = I_D^2 R_{DS(on)} \quad \textbf{(3.33)}$$

$I$ is the maximum current that is expected to pass through the MOSFET ($I_{peak}$ from equation (3.26)) and $R_{DS(on)}$ is obtained from the datasheet of the MOSFET [248]. Using these values $P_{D(on)}$ = 6.65 W. When a MOSFET switches between its on- and off state, they move between the non-linear region of their voltage and current characteristics. Therefore, with each switch they dissipate power relative to the switching frequency. The calculation of the switching losses requires many unspecified and hard-to-quantify variables that influence the switching of the MOSFET, thus an approximation is used to determine these losses. This approximation is given in equation (3.34).

$$P = V_{DS} * I_D \quad \textbf{(3.34)}$$

For this approximation $V_{DS}$ refers to the drain-source voltage (equal to $V_{in}$) and $I_D$ is equal to $I_{Load}$. The switching losses occur at the moments when the MOSFET either switches on or off, thus for a fraction of the switching period that differs for the on and off times, this allows for the modification of the equation as shown in equation (3.35).

$$P_{sw} = (V_{in} * I_{Load})\left(\frac{t_{on}}{T_{sw}}\right) + (V_{in} * I_{Load})\left(\frac{t_{off}}{T_{sw}}\right) \quad \textbf{(3.35)}$$

Further modifications of this equation can allow for a more specific switching power that is influenced by the gate current $I_{gate}$. This equation can be rewritten to form equation (3.36).

$$P_{sw} = V_{in} I_{Load} f_{sw}(t_{on} + t_{off}) \quad \textbf{(3.36)}$$

As all the variable for equation are available the switching power losses can be determined. Further derivations can be used to obtain equation (3.37) – the suggested approximation from [261], [262], however, as $I_{gate}$ is not easily found on the datasheet and equation (3.36) can be used in its current form, these derivations seem unnecessary.

$$P_{D(sw)} = \frac{(C_{RSS} * V_{in}^2 * f_{SW} * I_{Load})}{I_{gate}} \quad \textbf{(3.37)}$$

For equation (3.37) $C_{RSS}$ refers to the reverse transfer capacitance and $I_{gate}$ refers to the current at the gate of the MOSFET at its turn-on threshold ($V_{GS(Th)}$) – both these values are obtained from the datasheet; $V_{in}$ is the input voltage to the circuit which is 17.5 – 21.5 V, $f_{sw}$ is 62.5 kHz and $I_{Load}$ is the maximum load current of 9 A. From these values $P_{D(sw)}$ is calculated using equation (3.36) as 1.8 W for 17.5 V and 2.23 W for 21.5 V.

The power dissipation of the diode is calculated using equation (3.38).

$$P_{D_{diode}} = V_F * I_F \quad \textbf{(3.38)}$$

For this equation the $I_F$ and $V_F$ refers to the forward- current and -voltage drop of the diode obtained from the datasheet [249]. $P_{D\_diode}$ is calculated as 25.5 W. The general equation used to determine the heat sink is equation (3.39),

$$\mathrm{T_j} = P_D\left(R_{jc} + R_{cs} + R_{sa}\right) + T_a \quad \textbf{(3.39)}$$

One heat sink will be used for both the diode and the MOSFET as this will reduce the area consumed by the heat sink on the circuit board and therefore this equation will be rewritten to incorporate both devices. In the equation $T_j$ refers to the junction (channel) temperature (150 °C for both) and $T_a$ refers to the ambient temperature (25 °C); $T_j$ and $R_{jc}$ are obtained from the datasheets; $R_{sa}$ is to be determined; $R_{cs}$ is a value depending on the mounting type, in this case – direct, therefore is it a value of 1.3 °C/W. This equation is rewritten into equation (3.40),

$$\mathrm{T_j} = P_{D_{diode}}\left(R_{jc} + R_{cs}\right) + P_{D_{MOSFET}}\left(R_{jc} + R_{cs}\right) + \left(P_{D_{diode}} + P_{D_{MOSFET}}\right)R_{sa} + T_a \quad \textbf{(3.40)}$$

Using this equation, where $P_{D(MOSFET)}$ refers to the summation of the on- and switching power losses of the MOSFET, and the values obtained, $R_{sa}$ is calculated as 0.99 °C/W when $T_j$ is 150 °C and 1.72 °C/W when $T_j$ is 175 °C; using equation (3.37) for the switching power losses in the MOSFET similar $R_{sa}$ values are obtained. The heat sink is desired to be any value lower than this to be suitable [261].

### 3.2.4 Circuit board design

Using Figure 3.12 and all the calculated values from section 3.2.3 the printed circuit board (PCB) can now be designed. The design process will be completed using EasyEDA® and JLCPCB®. The layout of the PCB that was designed is shown in Figure 3.32.

The individual circuit groups discussed/designed in section 3.2.3 are shown in the figure on the top layer; the bottom layer is the mirrored image of the top layer. The lighter shaded blue areas indicate larger traces in the top layer (to accommodate the large currents flowing in those specific areas) and a large copper region in the bottom layer (used as the ground for the entire circuit). These will again be indicated and shown in the final built circuit. In the SC connection area eight groups of four black dots can be seen, these dots are holes indicating where the SCs will be connected as per the recommended PCB pattern in [247]. Two terminals are indicated for their use, the other two are there for mechanical support of the SC and are isolated from the power terminals.

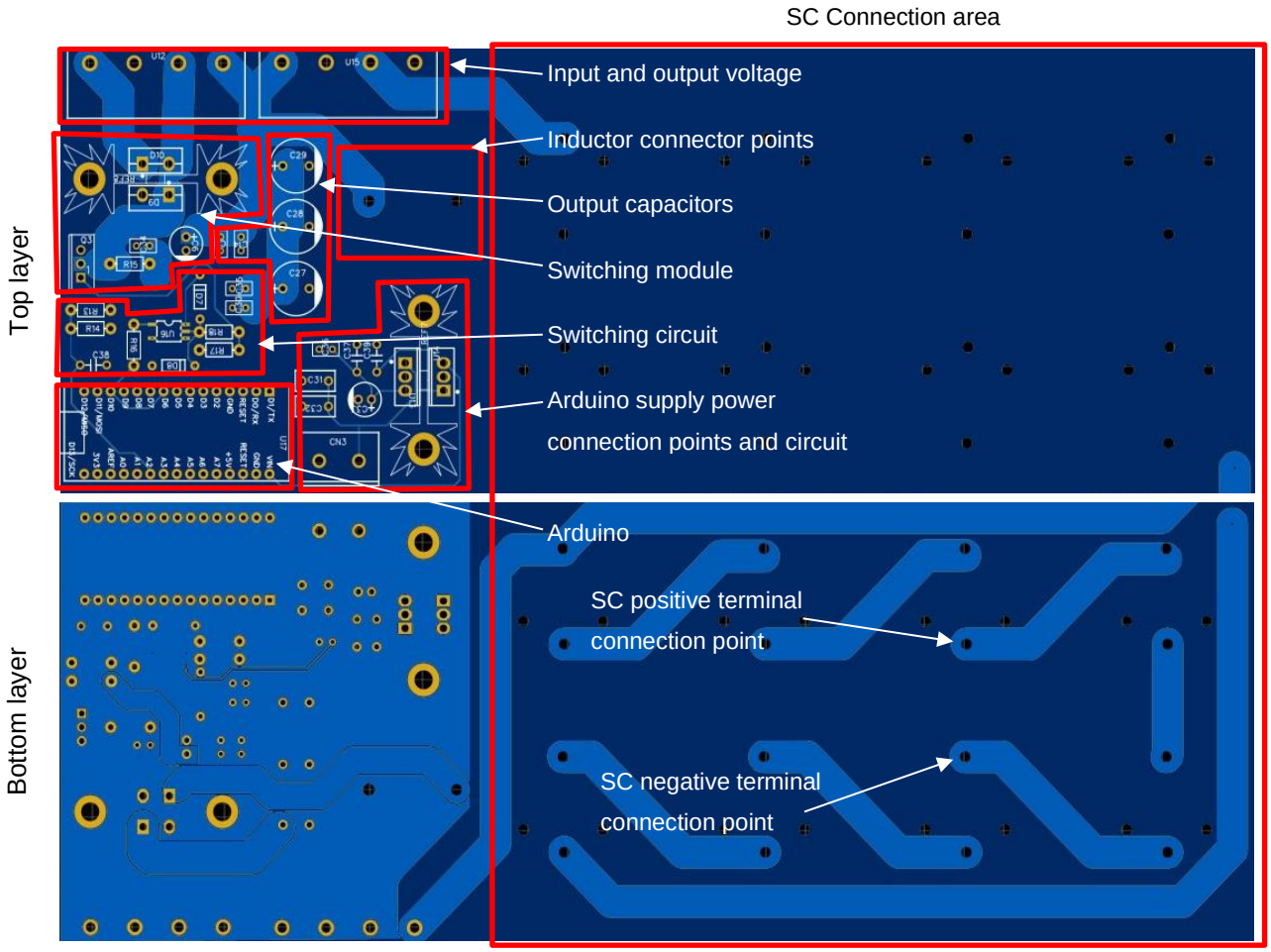


**Figure 3.32: Top and bottom layer of PCB designed**

### 3.2.5 Combined circuit

The circuit that will be used to conduct the various tests will need to be simulated to verify the connections and operation of the various components and power sources such that the built circuit can be compared to it.

From previous case studies [109], [263], [264] it has been suggested to combine the SC bank directly with the FC system, for this the maximum voltage of both sources will need to be matched and the SC bank has the lowest maximum voltage of 21.5 V – which should not be exceeded – thus the FC system will need to be equivalently reduced. This is easily achieved through setting the maximum value of the FC system to 21.5 V in the simulation circuit. The current requirement of the load profile has also been further reduced to a maximum of 3 A in order to allow for a comparison between the simulations and experimental results as the 3 A limit allows for an easier connection of the physical circuit tested in 4.2.2. This 3 A load profile is seen in Figure 3.33. This load profile will be used to simulate the various combinations discussed below.

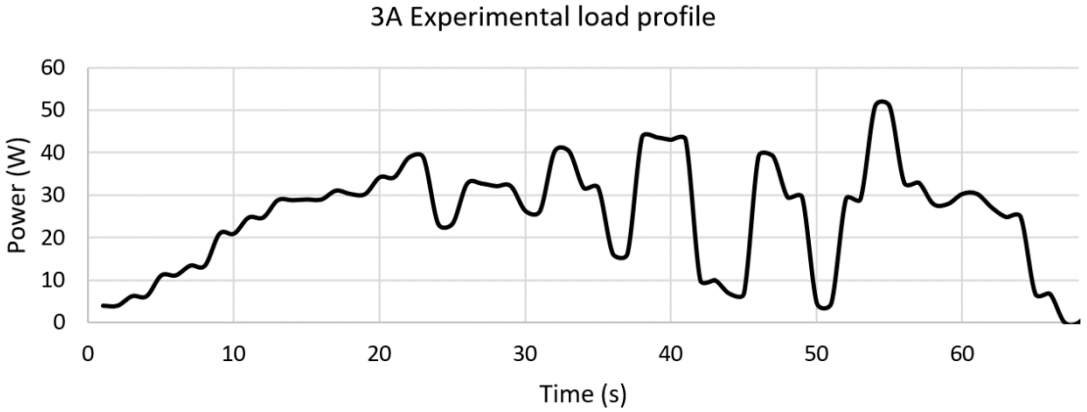


**Figure 3.33: Reduced 3 A experimental load profile**

### 3.2.5.1 Proposed circuit design

The individual components that make up the system shown in Figure 3.2 are tested to assess their response to the 3 A load profile before they are combined – this will aid in examining how the combinations affect the individual responses. These tests include the test of the FC system, the unaided SC bank and the SC bank utilizing the DC-DC converter. The FC system and the SC bank were combined in three different combinations – unaided, utilizing the DC-DC converter and utilizing both the DC-DC converter and selective switching. These final three test are conducted using two different configurations shown using switches in Figure 3.34.

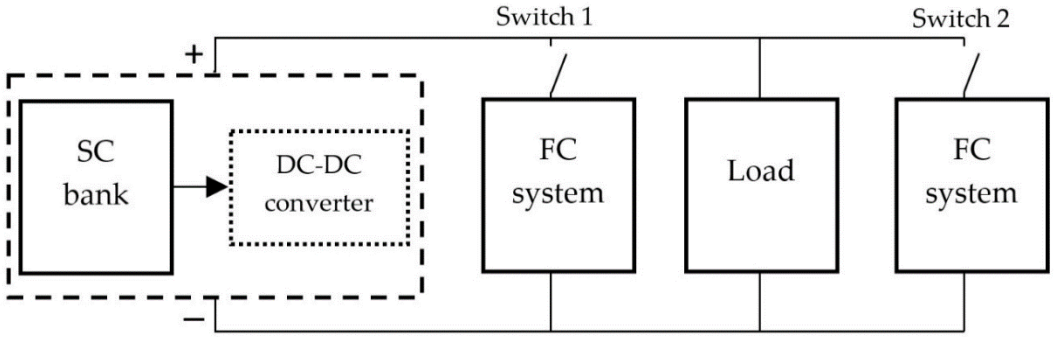


**Figure 3.34: Connection configuration setup**

Configuration 1 will consist of switch 1 being closed and switch 2 being open, with the load at the end of the parallel connection of the sources. Configuration 2 will entail an open switch 1 and closed switch 2 to allow the load to be in the middle of the power source connections. These configurations will help to verify the operation of the systems as well as evaluate any difference that occurs. The Simulink® simulations of these test are shown in the next section.

### 3.2.5.2 Simulink® Simulations

The simulation will be discussed under each respective heading showing the different combinations and circuit used for the simulations and the results of all the combinations will be summarized in section 3.2.6.3. Each Simulink circuit will have the basic form shown in Figure 3.35.

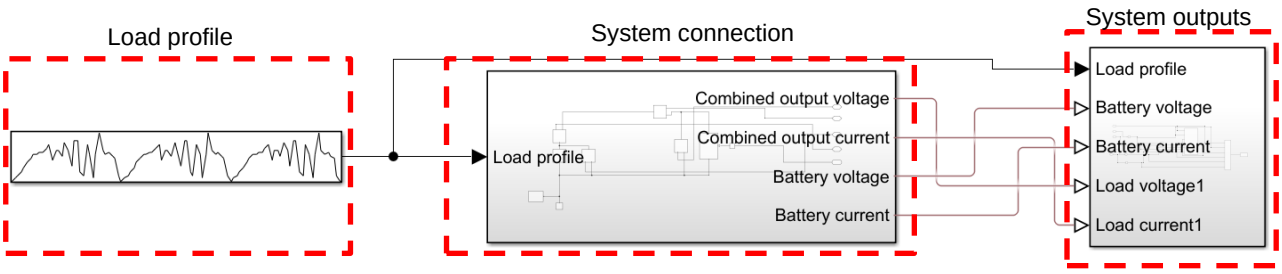


**Figure 3.35: Generic Simulink circuit**

The load profile is as shown in Figure 3.33, the system connection block contains the connections of the various components and is shown for each combination listed below and the system outputs block contains the scopes used to analyse the various values of each circuit.

#### 3.2.5.2.1 Fuel cell system

The system connection of the simulated FC circuit is given in Figure 3.36. The FC system has been simulated through the use of a Simscape® battery block with the characteristics adjusted such that it functions as the FC would.

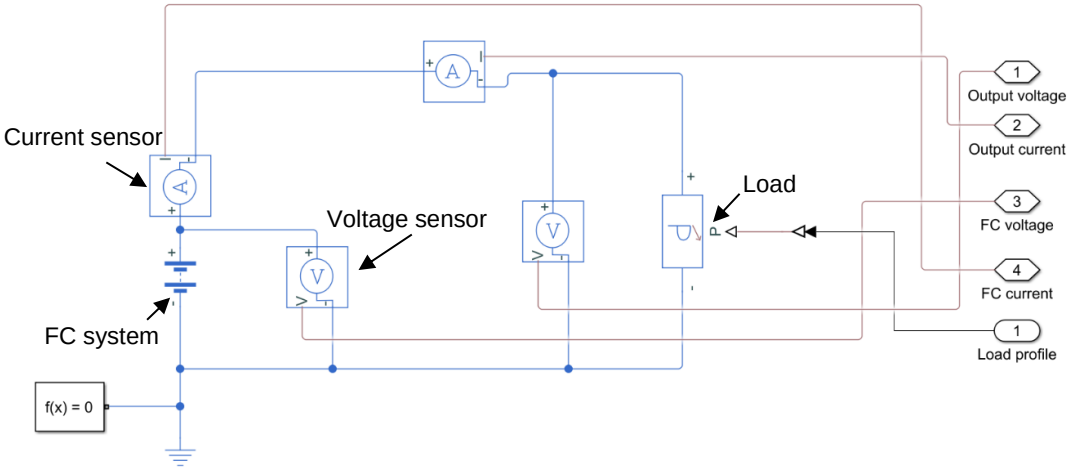


**Figure 3.36: Simulink® simulation circuit of FC system**

The response of the FC system to the load required is shown in Figure 3.37.

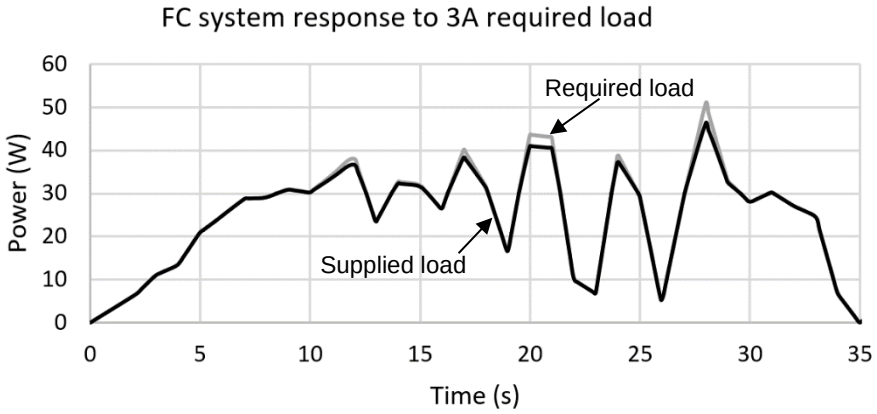


**Figure 3.37: Simulated response of FC system to 3 A load**

It is evident from the figure that the FC system did not supply the entire load but an efficiency of 99.47% was calculated. The deviation shown on the graph is where the SC bank is expected to improve the load response. This configuration allowed for a 268 s endurance time.

To examine the voltage and current waveforms of this system in response to the 3 A load Figure 3.38 is used.

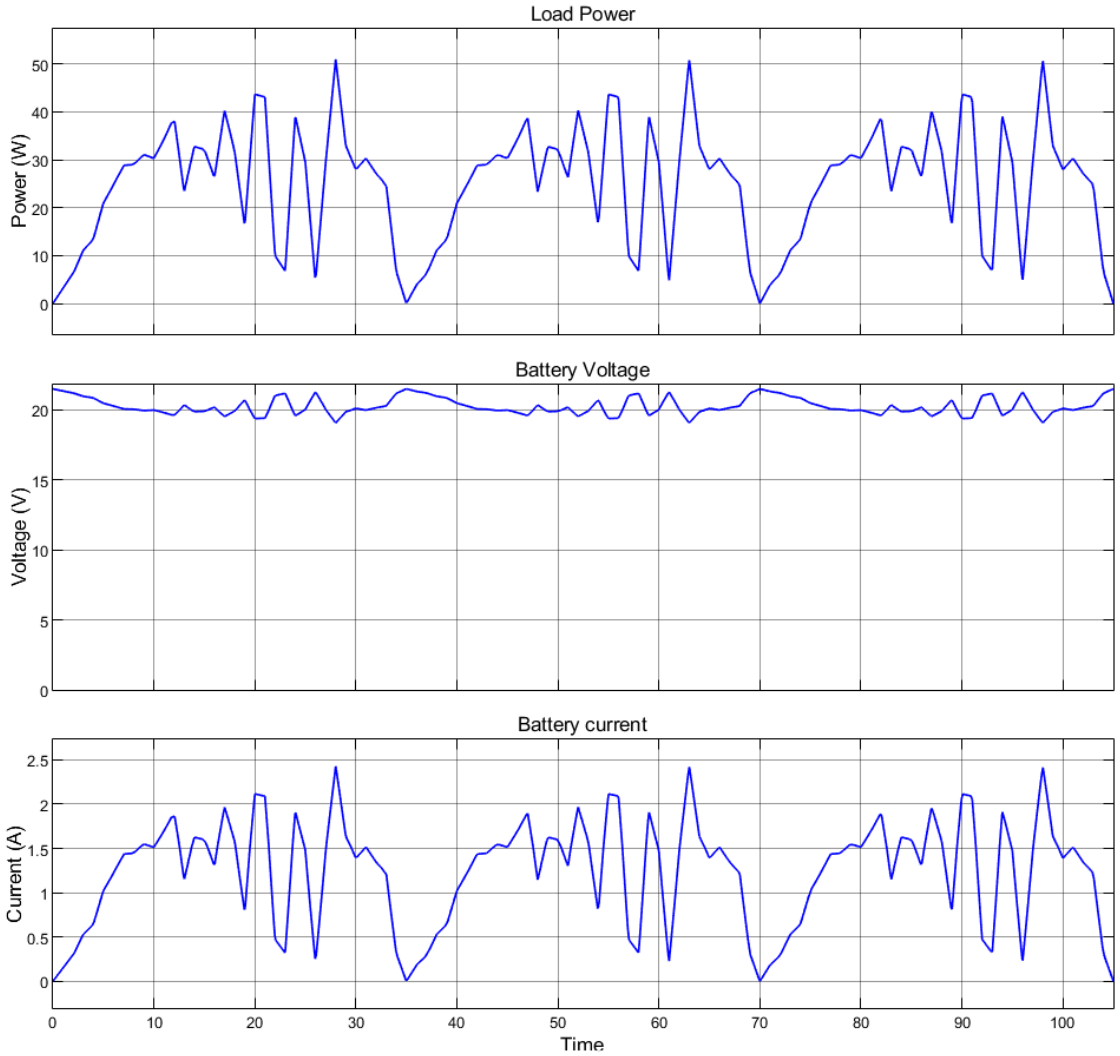


**Figure 3.38: Simulation voltage and current response of FC system to 3 A load**

As the FC system exhibits a continuous supply of voltage only three repetitions of the load are used. From this figure it is seen that the current supply increases as the load requirement increases with a drop in the supplied voltage with this current increase. Both of these observations are expected according to Ohm's law, as the voltage and current product supply the required load.

3.2.5.2.2 Super-capacitor bank – without DC-DC converter

The system connection of the simulated circuit is shown in Figure 3.39.

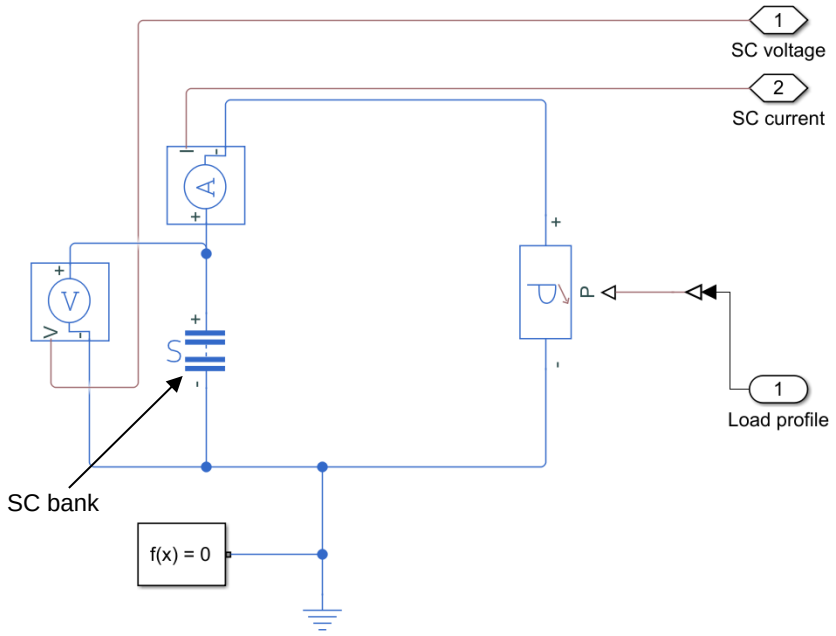


**Figure 3.39: Simulink® simulation circuit of unaided SC bank**

The SC bank was modelled using the Simscape® Supercapacitor block which represents a supercapacitor with a combination of a voltage-dependent capacitor and a network of fixed resistors and capacitors, it is in the form of a transmission line equivalent circuit model discussed in section 2.3.2.3.

For this block there are three branches whose parameters need to be specified – refer to Figure 2.8 (b). Each branch has a resistor ($R_1$, $R_3$, $R_4$) and a capacitor ($C_{1\text{-}3}$) with one branch having an additional capacitor gain value ($C_4$) to be specified. All of these values equate to a single SC cell. The resistor values were calculated using the ESR value of a signal SC, 3.4 mΩ (obtained from [247]), as the total resistance of the parallel combination. Therefore, using the equation for parallel resistors, each resistor should have a value three times that of the total – 10.2 mΩ. The capacitance of a single SC cell is 350 F; using the equation for the parallel combination of capacitors, each capacitor needs to be a third of the total capacitance – 116.67 F. The Simulink block shows that the capacitive gain is a function of the branch capacitance (116.67 F) over the cell voltage (2.7 V) – 43.21. No self-discharge value was taken into account as the system would not be utilised over an extended period of time where self-discharge is relevant.

The response of this system to the 3 A load is provided in Figure 3.40. For this system the load was repeated until the SC bank reached the recommended 80% SOC. Initially the SC bank is shown to provide the required power but as the SC bank discharges a decrease in the power supply is observed. This system achieved a 90.69% efficiency for the entire duration of the load which was found to be 190 s – this efficiency was calculated as 99.99% for the first repetition of the load and the vast decrease is due to the decrease in power supplied as the SC bank depletes.

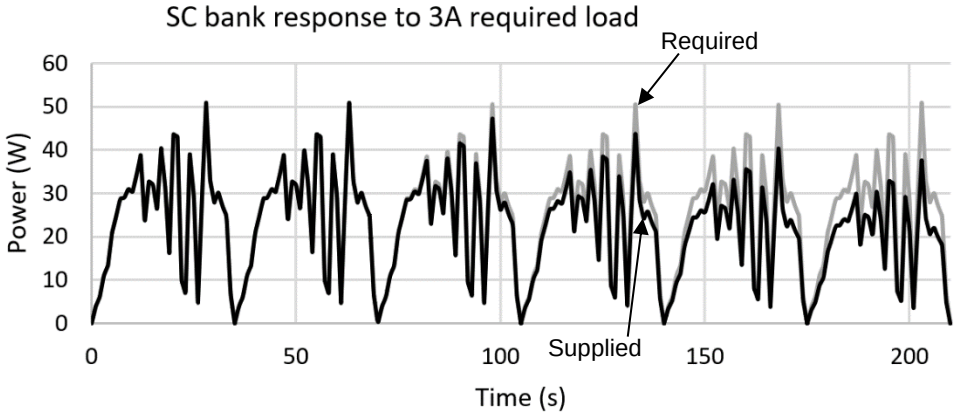


**Figure 3.40: Simulated response of SC bank to 3 A load**

To closer examine this voltage drop and current response Figure 3.41 is used.

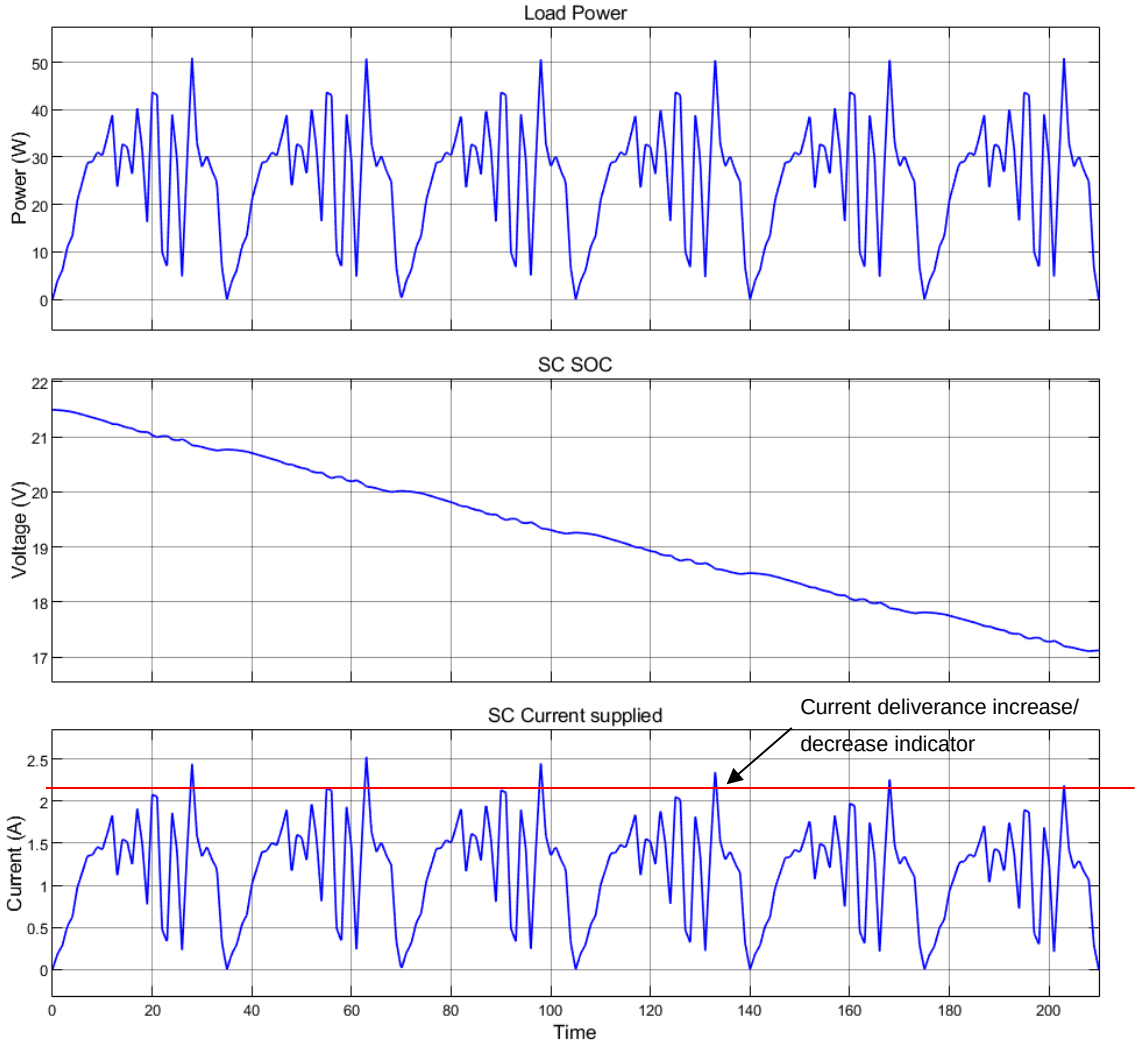


**Figure 3.41: Simulation voltage and current response of unaided SC bank to 3 A load**

Examining the SC current supplied graph, it is seen that initially the SC current deliverance increasing in response to the decreasing voltage available in order to supply the required load. This increase is seen for the first two repetitions of the load where after a clear decrease in the current deliverance is observed. This occurrence is due to an extreme decrease in the capacity of the SC bank within the first three repetitions and is indicative of the power response decrease shown in Figure 3.40.

3.2.5.2.3 Super-capacitor bank – with DC-DC converter

The system connection of the simulated circuit is given in Figure 3.42.

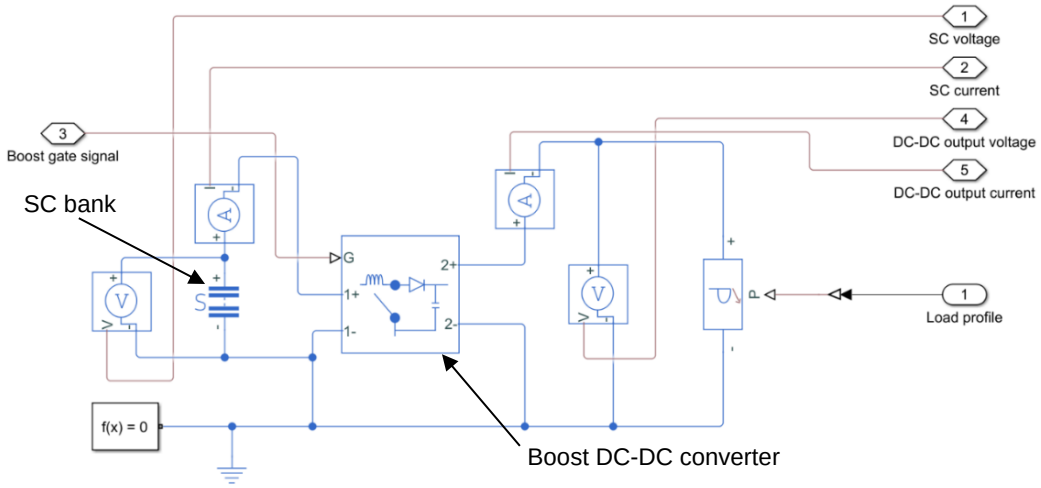


**Figure 3.42: Simulink® simulation circuit of SC bank with DC-DC converter**

The boost DC-DC converter models the operation of that designed in section 3.2.3 and receives a PWM signal containing the required duty cycle adjusted according to the SC voltage available. The response of this system to the required 3 A load is presented in Figure 3.43. The response is that of the power measured at the output of the DC-DC converter. Once again, this system was simulated with a continuous repetition of the load until the SC bank reached the recommended 80% SOC.

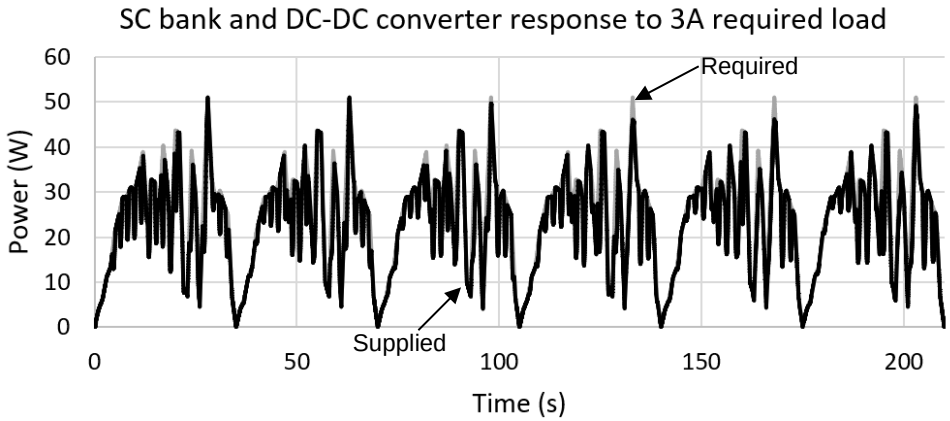


**Figure 3.43: Simulated response of aided SC bank to 3 A load**

It is clear from the figure that the system provided the required load for the majority of its repetitions, achieving a calculated efficiency of 91.58% and endurance of 186 s. In order to understand this efficiency a closer look is required into the deliverance of the system for one repetition of the load, this is shown in Figure 3.44. This figure justifies the efficiency achieved for this system as the system seems to provide the required load but shows a constant drop in the power deliverance assumed to be a result of the DC-DC converter. To further examine the effect of the DC-DC converter on this system and its response to the 3 A load Figure 3.45 is used. It is evident from the graphs that the SC bank increased the current supplied as the voltage available decreased – which in turn allowed the DC-DC converter output to maintain a relatively constant output current in response to the required load.

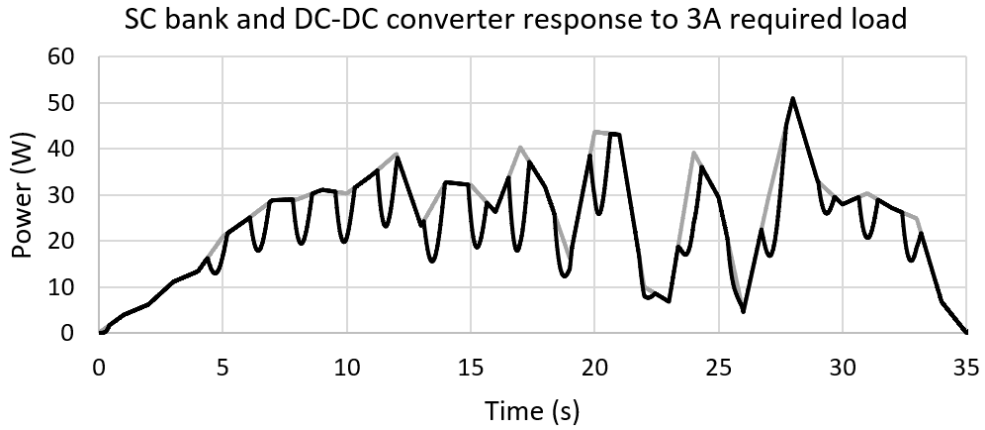


**Figure 3.44: Simulated response of aided SC bank to 1 repetition of 3 A load**

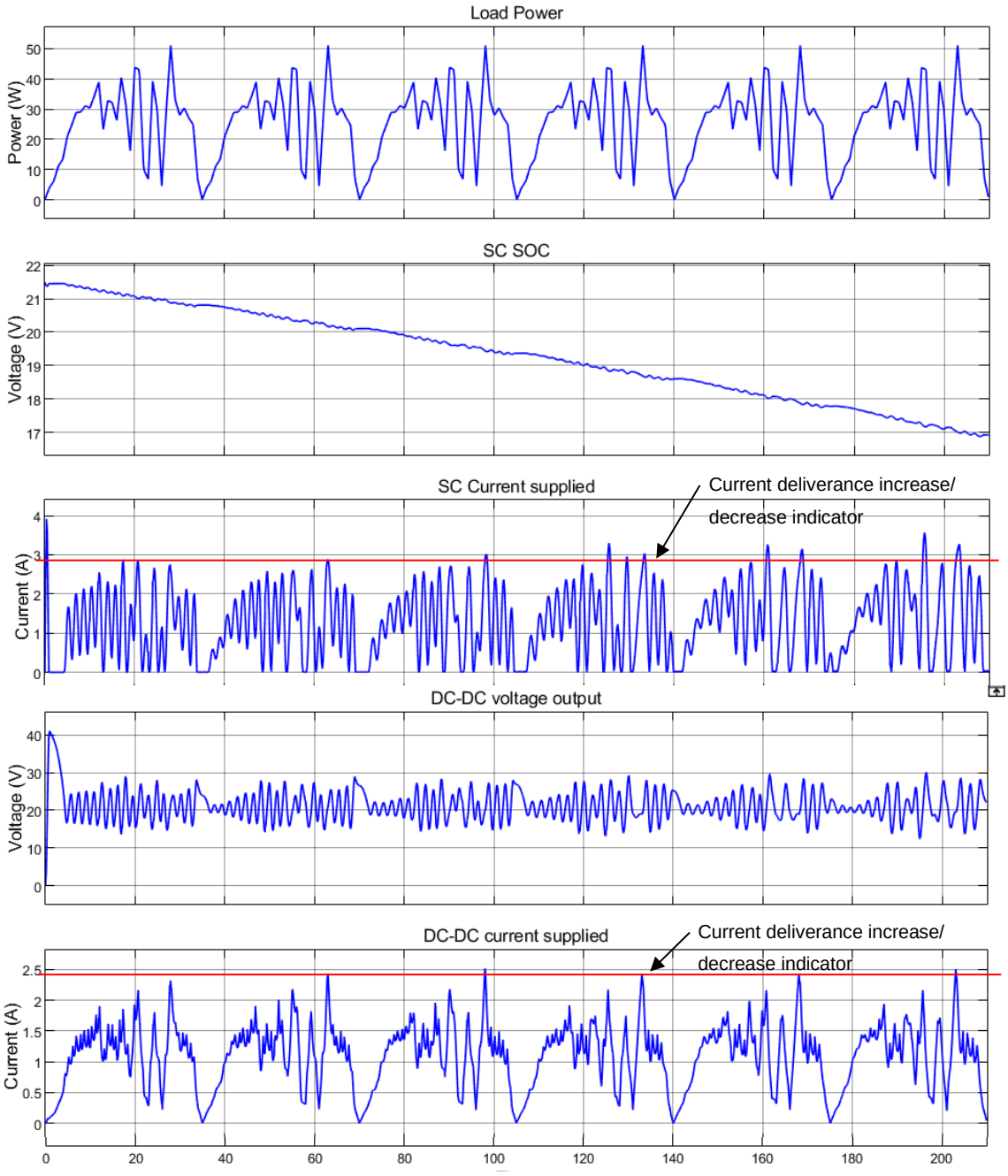


**Figure 3.45: Simulation voltage and current response of aided SC bank to 3 A load**

3.2.5.2.4 Fuel cell – super-capacitor system – unaided

The system connection of the simulated circuit is presented in Figure 3.46.

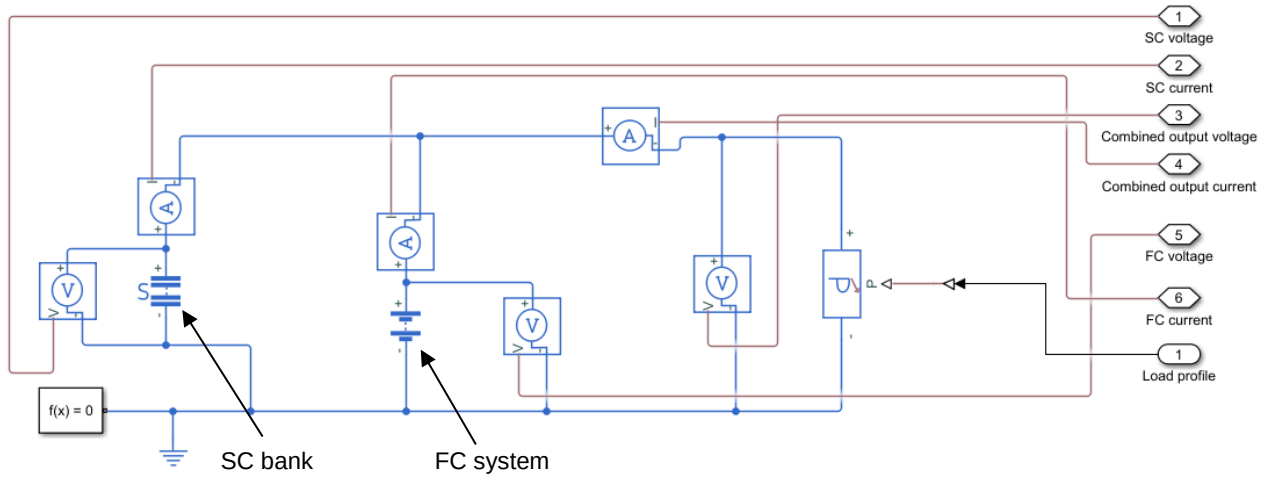


**Figure 3.46: Simulink® simulation circuit of FC-SC bank combination**

The FC system and SC bank are modelled as previously explained. The two configuration for this test involve the different placement of the FC system as shown in Figure 3.34. Both configurations achieved minimal differences in the efficiencies and power deliverances and therefore only the first configuration presented in Figure 3.46 will be discussed.

The response of this system is shown using Figure 3.47. The individual response of each power source to the load as well as the combined response is shown for the duration of the load.

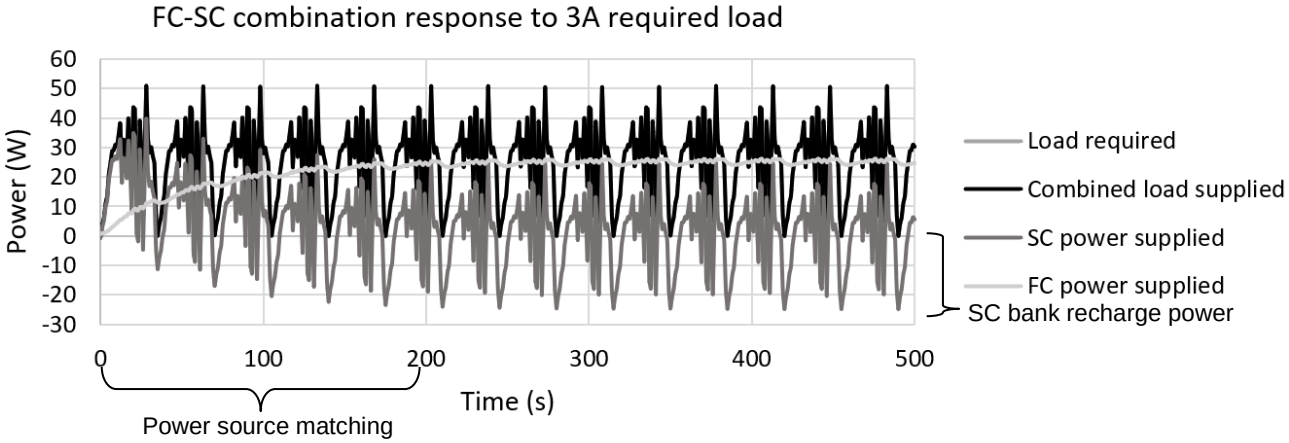


**Figure 3.47: Simulated response of combined and individual contribution to 3 A load**

The combined supply of the power sources to load follows the same pattern as that required by the load with an efficiency of 99.99% - this is why it is not clearly discernible in the Figure. It is apparent that the FC is providing the bulk of the load while the SC bank supplements the remainder. The initial decrease of the SC bank's contribution and the increase in the FC's contribution is evident of the matching of the sources. It is also observed that the SC bank experiences negative power which is due to the FC recharging the SC bank as it depletes, as there is no device blocking the flow of current towards the SC bank. To further show the separate supply of each source to the load the current contributions of each source in response to the load are shown in Figure 3.48.

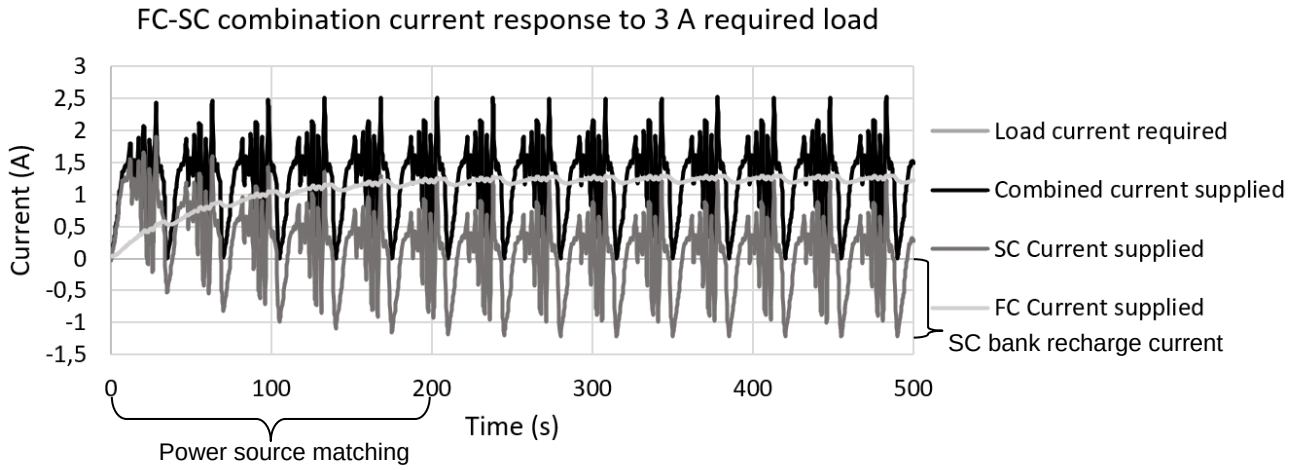


**Figure 3.48: Simulated response of combined and individual current contribution to 3 A load**

Once again it is evident that the FC is supplying the bulk of the required current with the SC bank supplementing the fluctuations and remainder of that which is required. The SC bank displays negative current showing that it is absorbing current in order for it to recharge to the point where it can once again supplement the FC as the load requirements exceed the charge current requirements of the SC bank.

As the FC system models a continuous infinite source it recharges the SC bank infinitely as well which leads to the requirement of an alternative method to determine the duration of this system. The method used is Faradays Law of Electrolysis [265]**.** This law loosely states that the hydrogen consumption is directly proportional to the current drawn by the FC. In order to have a more accurate estimation the calculations below are required, these equations are all obtained using [265]. The drone used to obtain the load profile for the experiments utilizes a 7 L hydrogen tank, equation (3.41) can be used to estimate how long this tank can last with the repetition of the load profile.

$$m = \frac{ItM}{Fz} \tag{3.41}$$

For this equation *I* refers to the average current drawn by the load, *M* refers to the moler mass of hydrogen (1.00784 g/mol), *F* refers to the faraday constant (96 485.33), *z* refers to the valence number of hydrogen (1), *m* refers to the mass of hydrogen (to be determined using equation (3.42))) and *t* refers to the time (s).

$$V = \frac{m}{\rho} \tag{3.42}$$

For this equation the Volume (*V*) is required – 7 L and the density (ρ) of hydrogen is also required – 0.08988 g/L. To determine the current rating of the FC system these equations can be combined into equation (3.43),

$$It = \frac{V\rho Fz}{M} \tag{3.43}$$

Using this equation, the capacity rating (*Ah*) can be determined by dividing the result by 3600, as the equation delivers the value in seconds. Using all the given values this capacity is determined as 60 232.5 As – which is converted to 16.73 Ah.

For an average current usage of 3.34 A, in one repetition, this allows for around 5 hours of usage from the 7 L tank – this is used to verify the calculation as this duration is provided by the company that supplied the FC system and drone load profile. Equation (3.43) uses the current measured by the simulation to determine the endurance of the system – 249.75 s; the second configuration achieved an endurance of 249.96 s. This calculation will be used for both of the remaining tests. In order to further evaluate this matching occurrence between the power sources Figure 3.49 is presented.

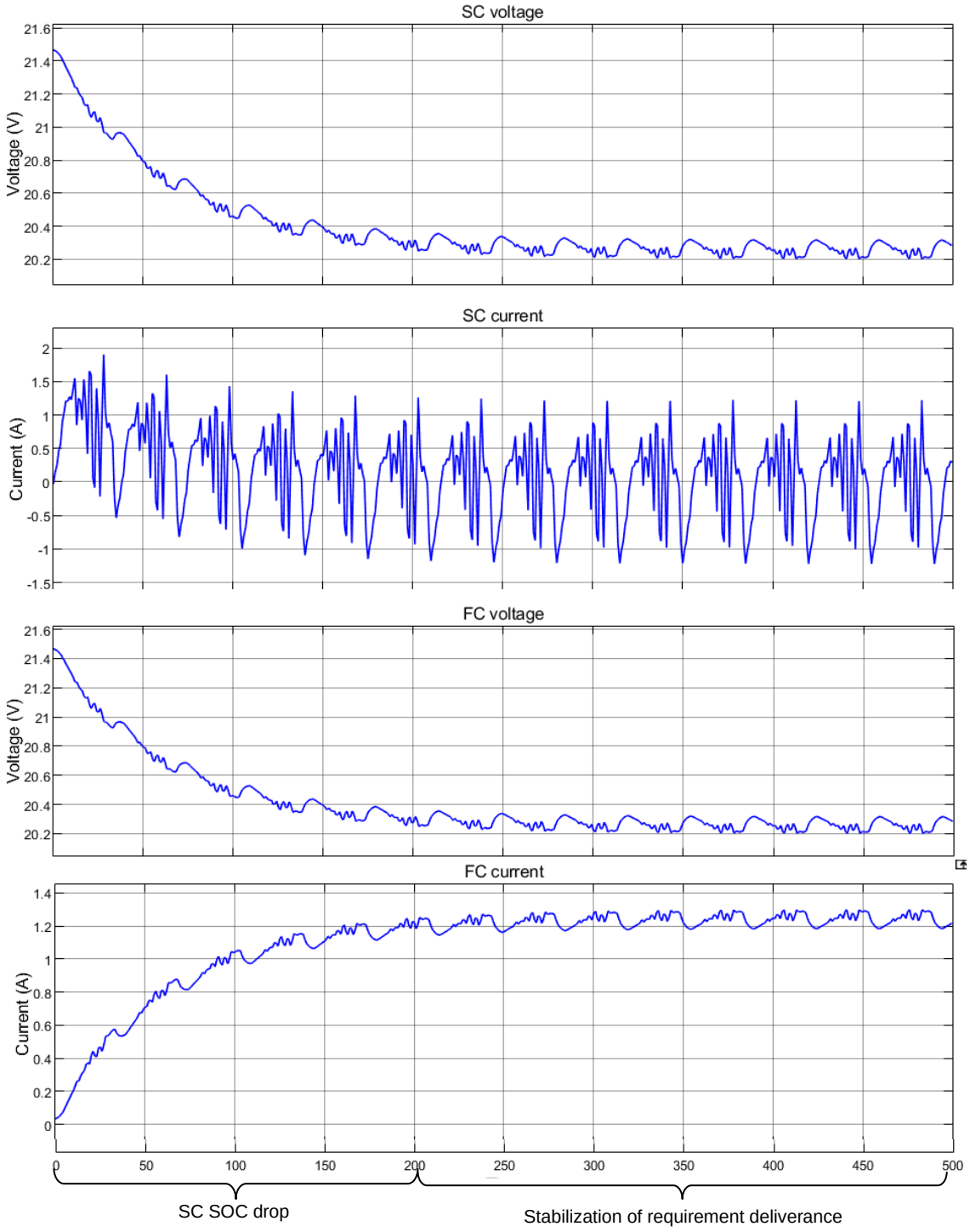


**Figure 3.49: Simulation voltage and current response of individual power sources**

From the figure it is observed that both the SC bank and FC voltage maximums decrease to a level that can be maintained by both. This initial drop is due to the SC bank discharging. When the SC bank discharges it causes an increase in the current requirement towards it. As there is no device blocking the flow of current towards the SC bank it absorbs a portion provided by the FC while the FC simultaneously supplements the remainder of the load current requirement not supplied by the SC bank. This current increase causes a voltage drop in the FC and this ascent and descent will continue until the FC reaches a current value that it can supply to both requirements within its means.

Once both sources reach this stabilization period the FC can supply both the portion of the load and the SC bank. The ripples in the various waveforms are synonymous with the supply of the power. There is no increase observed in the SC bank current supplied in response to the decreasing current as the current required form the SC bank is within its means for the duration of the load and it can therefore supply the required power with the voltage available without the necessity to increase the current supply.

3.2.5.2.5 Fuel cell – super-capacitor system – with DC-DC converter

The system connection of the simulated circuit is given in Figure 3.50.

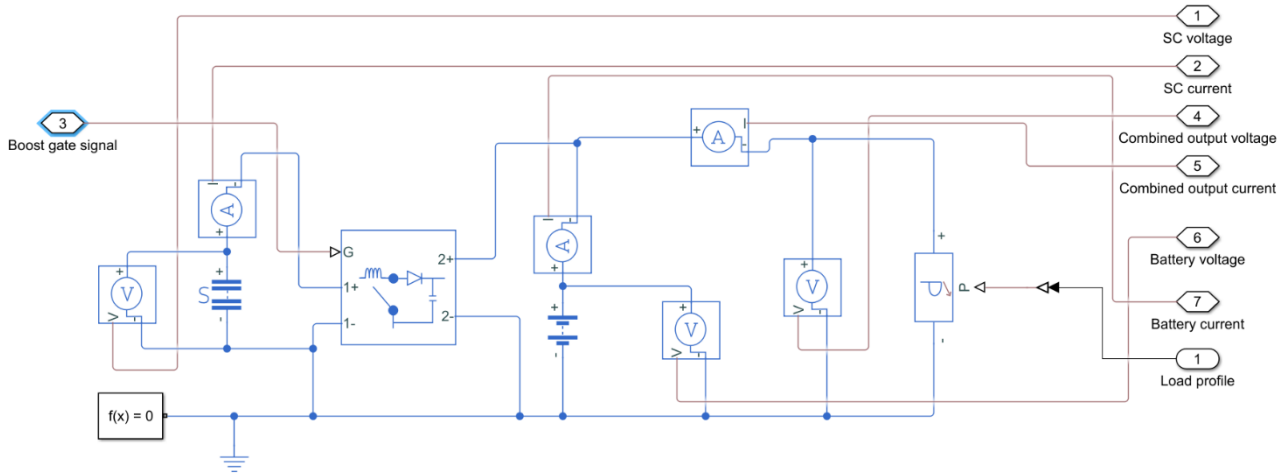


**Figure 3.50: Simulink® simulation circuit for FC-SC combination**

All the elements of this circuit have been discussed in the prior sections. The two configurations for this simulation differ in that the FC system is placed on the outer edge of the load as shown in Figure 3.34 and both configurations achieved similar efficiencies and endurances and therefore only the first configuration will be discussed.

The individual response of the power sources to the 3 A load are discussed using Figure 3.51. The DC-DC converter in this combination serves the additional purpose of blocking the flow of current towards the SC bank and therefore no recharge of the SC bank via the FC system is observed, however, a slight recharge is observed in the FC system where it draws a small current from the SC bank. The combined deliverance of the load is calculated to have an efficiency of 99.91% - this is seen as the load requirement is barely visible in the figure.

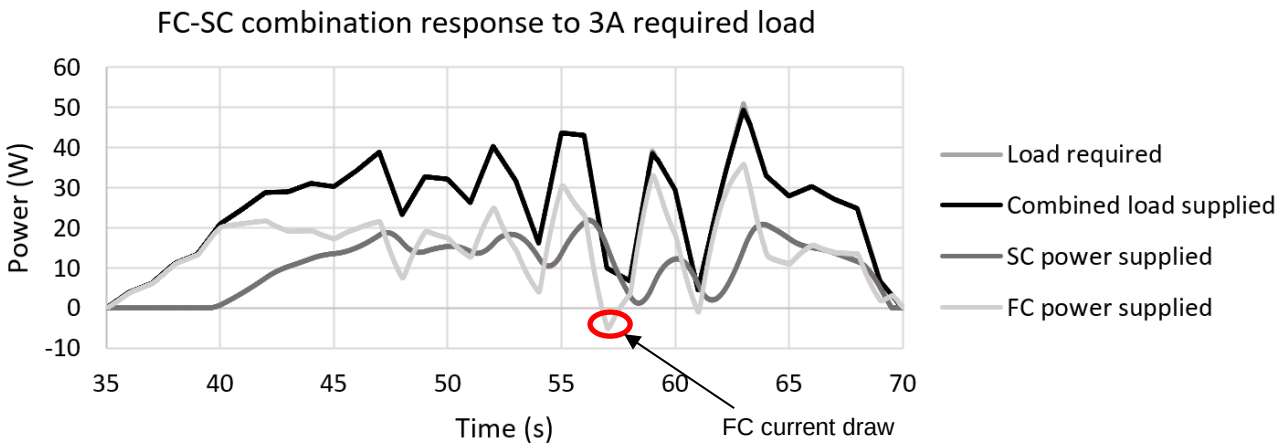


**Figure 3.51: Simulated response of combined and individual contribution to 3 A load**

For this combination the majority of the load is supplied by the FC system and only a portion is supplied by the SC bank – using equation (3.43) the FCs maximum duration is calculated as 403 s and the SC bank has a 20% SOC drop in 428.08 s, the second configuration of this system shows an endurance of 428.06 s for the SC bank. The system therefore has a maximum usable time of 403 s.

To observe the voltage and current waveforms of the individual power sources Figure 3.52 is used. As the SC voltage drops it increases the current supply to provide a constant power output to supplement the FC system with the load requirement. The figure also shows that the FC's current and voltage deliverance remains constant for the duration of the load. The SC current supplied increases as the SOC decreases due to the power requirement of the SC bank requiring a larger current for the voltage that is available.

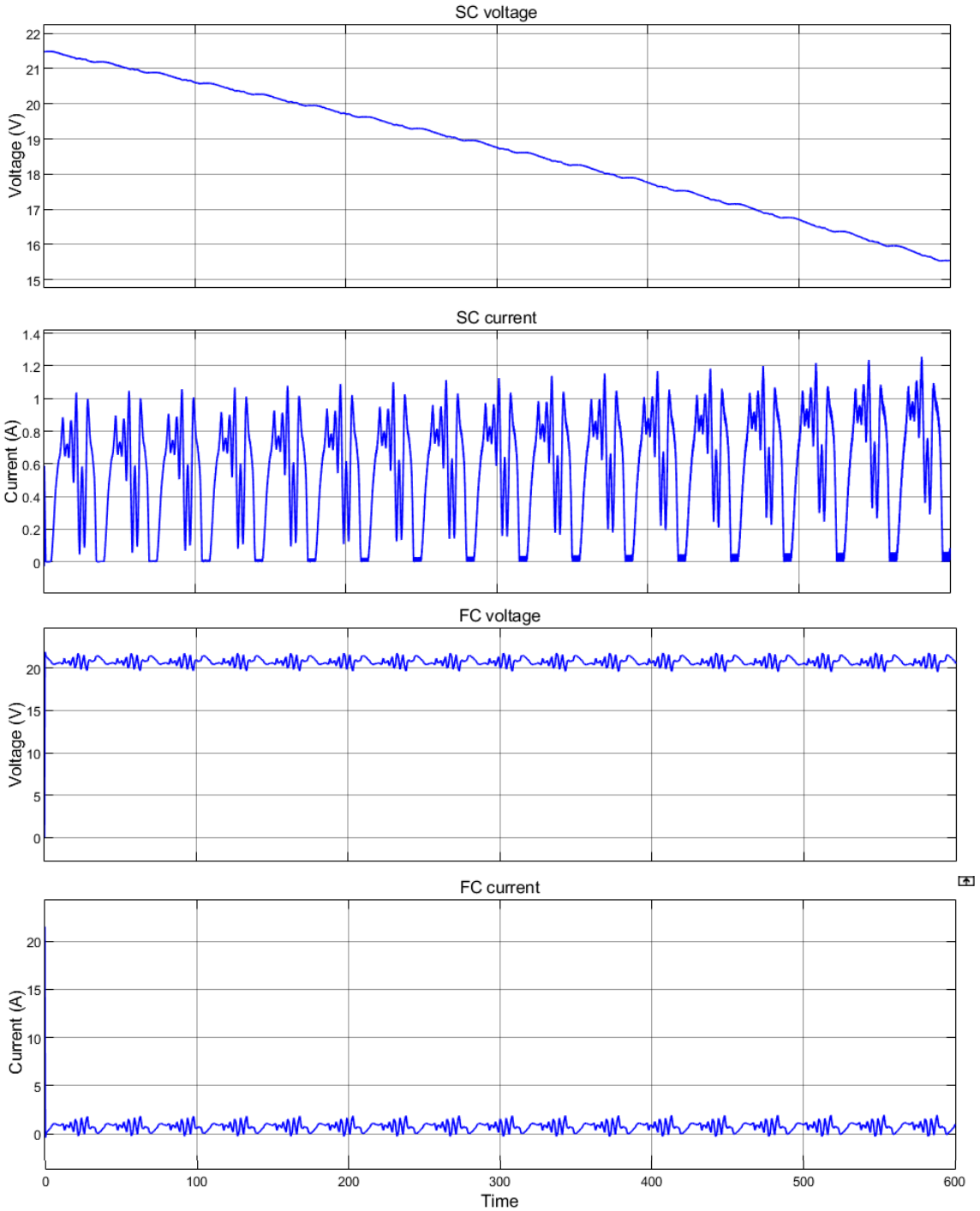


**Figure 3.52: Simulation voltage and current response of individual power sources**

3.2.5.2.6 Fuel cell – super-capacitor system – with DC-DC converter and selective switching

The system connection of the simulated circuit is presented in Figure 3.53. For this combination the SC bank and DC-DC converter combination is isolated from the FC system and load using a Simscape® Single-pole single-throw (SPST) relay block. The block is controlled using the load profile where the relay remains open while the power requirement is less than 34 W. When the power requirement exceeds 34 W the relay will close allowing the SC bank to contribute to the load requirement.

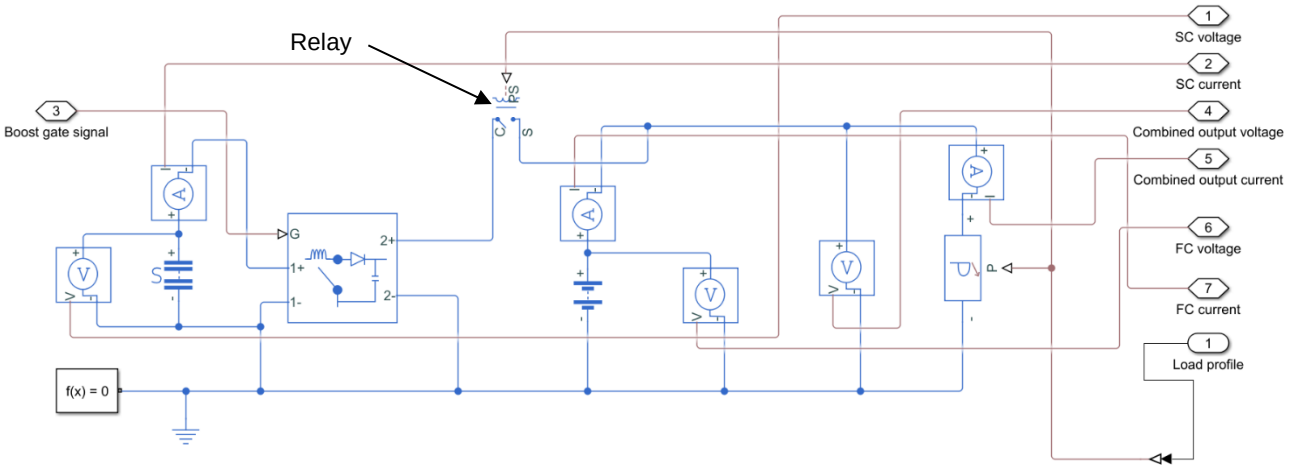


**Figure 3.53: Simulink® simulation circuit for FC-SC combination**

The second configuration of this system differs in the placement of the FC system as shown in Figure 3.34. Both configurations delivered the same efficiency and endurance and therefore only the first one shown in Figure 3.53 will be discussed. The response of this system is presented in Figure 3.54.

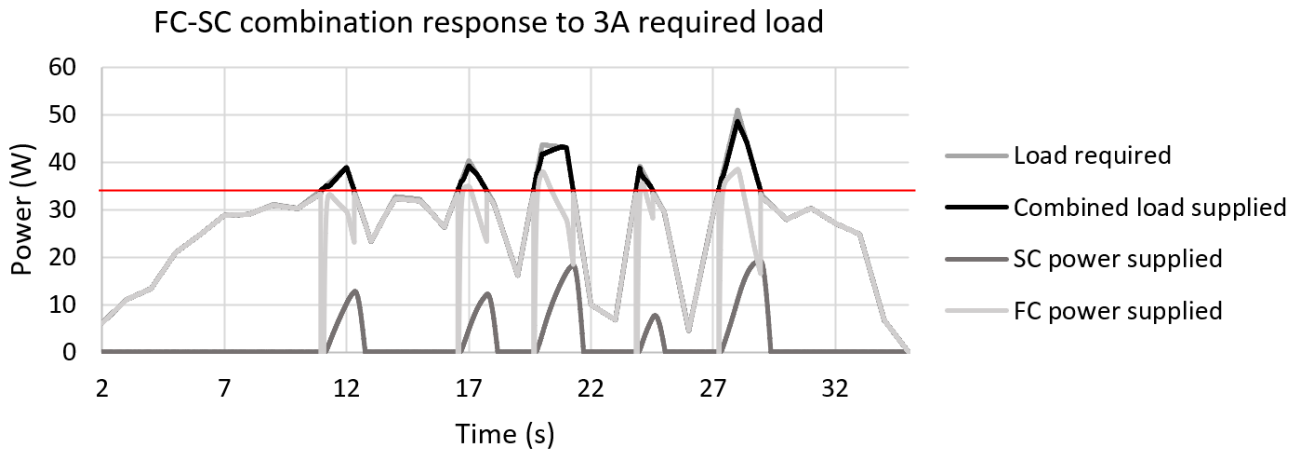


**Figure 3.54: Simulated response of combined and individual response to 3 A load**

It is evident from the figure that the combination of sources achieves in supplying the load requirement and an efficiency of 99.66% is achieved for this combination This combination achieved a 2265 s usable time for the SC bank for configuration 1 and 2200 s for configuration 2; the FC system achieved a duration of 293 s using equation (3.43). The system therefore achieved an overall duration of 293 s. The horizontal line in the figure represents the point at which the SC bank is connected to the system via the relay.

At this point (34 W) two observations can be made, firstly, it is seen that the FC initially supplies no power to the load, secondly, for the period that the SC bank is connected the FC power supply decreases in response to the increase in power supplied by the SC bank. Both of these occurrences can be attributed to the SCs willingness to supply the entire load as it has a very low internal resistance (3.4 mΩ), but the FC also has a low internal resistance (< 1 Ω) thus the deliverance contribution adjusts after this initial switch. These power dips of the FC can also be attributed to the turn-on voltage requirement of the relay. This contribution of each power source can further be

evaluated using the voltage and current waveforms of each contribution to the load shown in Figure 3.55.

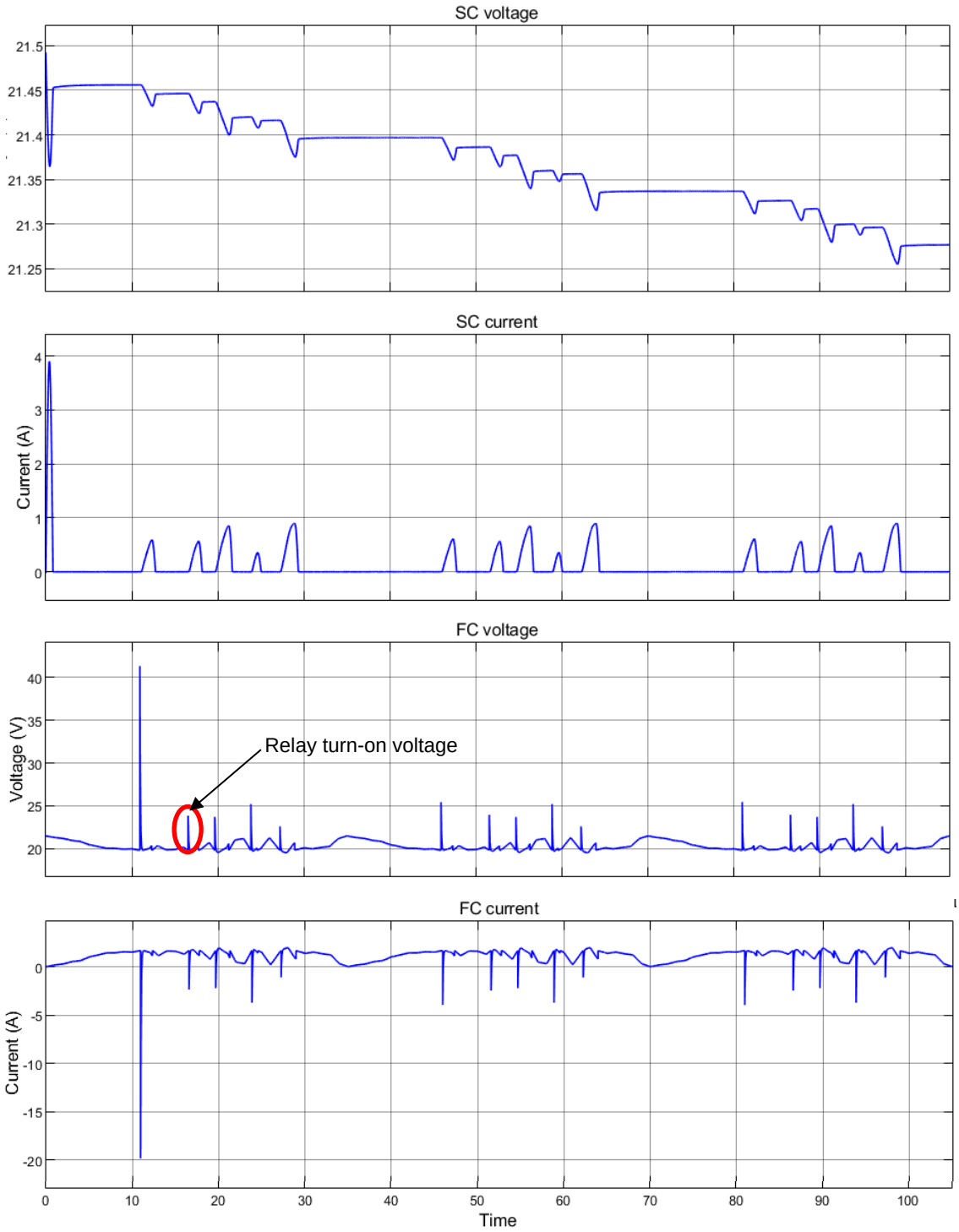


**Figure 3.55: Simulation voltage and current response of different power sources**

As this system had a long endurance the voltage and current waveforms have been reduced to only three repetitions of the load such that the pattern can be closely observed. As the SOC of the SC bank drops there is no increase in the Current supplied by the SC bank – this is due to the power required by the SC bank being within the means of the SC bank with the available voltage. The spikes observed in the FC voltage can be attributed, once again, to the turn-on voltage required by

the relay to energize the coil. This voltage spike in turn causes a dip in the current following Ohm's law.

### 3.2.6 Verification and Validation

This section of the report will discuss how the design of the main components will be verified and validated. Verification will determine whether the right component was used for the application and validation will show that although other options for the component exist, the specified one is best suited for the application. Verification will be done by ensuring the component delivers the desired output and validation will be conducted by comparing the chosen component with other options to determine its feasibility for the application. Of the five sections for the detail design the SC calculations and the DC-DC converter circuit will be verified and validated with more detail, the remainder of the sections will be verified and validated in section 4.2.2.4.

#### 3.2.6.1 Super-capacitor

The SCs need to match the characteristics of the battery in order to replace them, so to verify if the SC bank is correct, we determine whether these characteristics are given by the SC bank, these are: weight and power. The verification of these parameters was completed in the end of section 3.2.1.2. To validate that the SC bank is correct we determine if the SCs are combined correctly to give the right energy. The validation can be done through combining the SCs in different topologies and calculating the voltage, energy and weight differences of each to determine whether the chosen topology is in fact the best. 360 F SCs will be used with individual voltage of 2.7 V and weight of 71.4 g. From equation(3.7) the minimum voltage range required by the SCs to get a 20% discharge range is 15-18.75 V, the maximum allowable weight is 800 g and the required energy is 4167 J giving a minimum capacitance of 37.04 F. A few circuit configurations will be considered and a summary of the tests and their respective calculated values are given in Table 3.3.

**Table 3.3: Validation of SCs summary**

| Test | No. of SCs | Configuration | Total capacitance (F) | Total voltage range (V) | Total weight (g) |
|---|---|---|---|---|---|
| **1** | 7 | Pure series | 51.43 | 15.12-18.9 | 500 |
| **2** | 8 | Pure series | 45 | 17.5-21.6 | 571.2 |
| **3** | 21 | Parallel & series | 42.86 | 15.12-18.9 | 443.1 |

All the tests will use the starting point of the proposed configuration of eight 360 F, 2.7 V, 71.4 g SCs in series, this is done to verify that other configurations are not better than the chosen one. Test 1 involved using the minimum requirement for the voltage range (15 - 18.75 V), which requires at least 7 SCs in series to achieve. Although this results in desirable values, the voltage range is at the lower end of what is desired and results in the DC-DC converter working on the edge of its 70% duty cycle requirement, leading to increased power losses and thus a lower efficiency. Test 2 has the addition

of one more SC thus increasing the voltage range values allowing the converter to operate at a lower duty cycle allowing for a more efficient operation of the converter. The weight of the system has the requirement of being less than 800 g, but this includes the weight of the PCB. The designed PCB weighs around 300g, thus leaving 500 g for the SCs. If not for the low voltage range, test 1 would have the best configuration. From Test 1 and 2 it is thus seen that regardless of the configuration at least seven 2.7 V series connections are required to reach the voltage range minimum, but eight are preferred. A pure parallel combination of seven SCs will result in high capacitance at 2.7 V – this will not be tested as this value is unfeasibly low.

It is known that the weight of the SC decreases with a decrease in capacitance, so the next test will involve a smaller capacitance. Parallel combinations of power sources will always result in power balancing, thus the best parallel combinations are those of which the groups are of equal size. In order to utilize parallel combinations here, it will require 7 series strings of 2.7 V and 233 F each, the strings will refer to the parallel combinations. From what is available this could be eleven 22 F SCs, each one weighing 6.5 g giving a total weight of 500.5 g; five 50 F SCs, weighing 12.4 g each, thus a total of 434 g; both of these examples deliver a total capacitance on the border of what is desired and will allow the system to operate as desired but with just enough energy. With the weight allowance it is possible to obtain a configuration with a larger capacitance, thus storing more energy and giving a better functionality of the system. Test 3 includes seven series strings comprised of three 100 F, 21.1 g SCs in parallel, as shown in Figure 3.56.

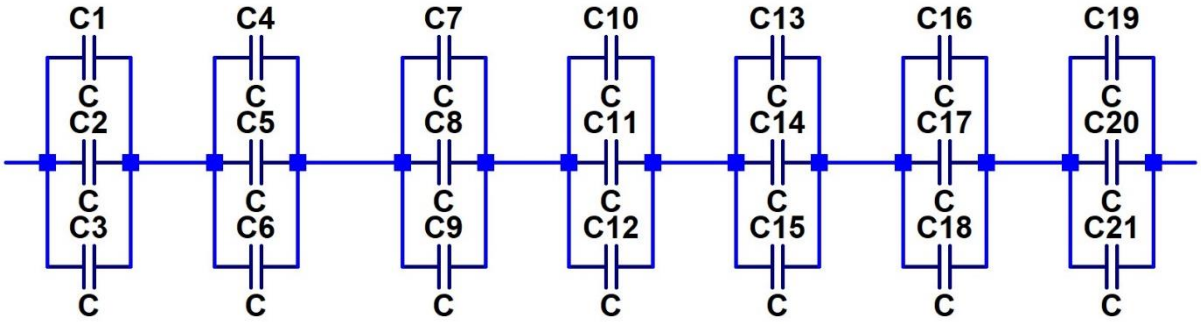


**Figure 3.56: SC verification test 3 layout**

This combination, like Test 1, results in desirable values, especially the weight (less than Test 1) and capacitance (similar to Test 2). However, 21 of these SCs will lead to a considerable initial expense and the voltage range is that of Test 1, which is smaller than the preferred range in Test 2, these two downfalls overpower the advantage of the weight decrease. The values used in these tests are those which are easily available for purchase. To decrease cost, complexity and weight it seems that the best configuration will be the simple series connection of 8 SCs. The desired values mentioned for this SC bank can essentially be obtained with this series connection and any SC above 280 F and reasonably close to 62.5 g. As the SCs will be combined with a DC-DC boost converter it is required that the SC bank be designed with a larger energy capability than what is required from the load due to the law of energy conservation through the converter. Although the chosen SC bank configuration

weighs more than what is desired, it is acceptable for this project and can be adjusted in future designs and applications of this circuit.

#### 3.2.6.2 DC-DC converter

The SC bank has a voltage of 17.5-21.5 V, the load of the circuit will require a constant 50 V and maximum 9 A output for a maximum of 450 W. The DC-DC converter will need to be able to accept the input from the SC bank and provide the required output. The verification of this operation is done through applying different voltages (in the SC range) to the input of the simulation, adjusting the duty cycle and load resistance to that which is required and examining whether the output is correct. For this the Simulink® circuit of Figure 3.25 will be used and Table 3.4 presents the results of these simulations. The output voltage and current of the simulation circuit deviates 17-18% from the required 50 V and 9 A in the first test. This deviation is unacceptable and will need to be rectified. Various adjustments (output capacitance, inductance and duty cycle) were made to the circuit to evaluate the effect and determine which would alter the output to be closer to the desired output.

**Table 3.4: Simulink® verification of simulation summary**

| $V_{in}$ (V) | Duty cycle required (%) | Duty cycle applied (%) | Duty cycle deviation (%) | $V_{out}$ (V) | Voltage ripple (%) | $I_{out}$ (A) | Current ripple (%) |
|---|---|---|---|---|---|---|---|
| 17.5 | 65 | 65 | 0 | 41.51 | 1.44 | 7.413 | 1.35 |
| 17.5 | 65 | 72 | 10.77 | 50.6 | 1.6 | 9.05 | 1.6 |
| 19.5 | 61 | 68 | 11.48 | 50.4 | 1.45 | 9 | 1.38 |
| 21.5 | 57 | 65 | 14 | 50.3 | 1.4 | 8.97 | 1.39 |

These adjustments found that an increase in the duty cycle whilst keeping the components the same as calculated, delivers the desired output. This increase in the duty cycle is shown in the table with the percent deviation from the calculated value and can be attributed to the other elements of the circuit that cause a voltage drop across them during operation. The validation of the circuit will require an in depth look at the operation of the sections of the circuit, these sections include the switching diode, the inductor and the output capacitors. Of these sections the voltage and current waveforms will be observed and compared to the switching signal of the MOSFET. The waveforms are analysed using [194], [256], [257] and the specifications detailed therein. This validation process has been completed in section 3.2.3.6 where two simulation packages were used to validate the operation of the components and the operation was compared using different values for the components to achieve the desired waveforms of the references.

#### 3.2.6.3 Combined circuit

Verification of the combined circuit involves firstly showing that the different combinations all supplied the required load and secondly showing that each power source contributed to the deliverance of the load. The former is shown through the use of Figure 3.37, Figure 3.40, Figure 3.43, Figure 3.47, Figure 3.51 and Figure 3.54 and the accompanying efficiencies. The latter is shown through the use

of Figure 3.47, Figure 3.51 and Figure 3.54. To validate the simulations of the combined circuit the various combinations are compared with each other to show variation in the results. This comparison is done using Table 3.5. The maximum usage duration is determined through comparing the usable time of the SC bank (duration for 20% SOC drop) and the usable duration of the FC system determined using equation (3.43) – the smaller of the two determines the usage duration. The efficiencies shown are calculated using equation (3.44).

$$Efficiency\ (\%) = 100 - \frac{abs(Energy\ required - Energy\ supplied)}{Energy\ required} \quad \textbf{(3.44)}$$

For equation (3.44) the *Energy required* and *Energy supplied* refers to that of the fourth and fifth column of Table 3.5, respectively. The system is designed to use the SCs mainly during two instances where the peak power exceeds that which can be provided by the FC system (illustrated in Figure 3.8 and described in section 3.2.1.2). In order to assess the efficiency of the SCs combination to the system the power provided at these instances will be expressed as a percentage of that required – this percentage is provided in the final column.

**Table 3.5: Simulation validation summary**

| | Maximum usage duration (s) | Duration for 20% SOC drop (s) | Energy required by load over 3 reps (Wh) | Energy provided to load over 3 reps (Wh) | Energy produced over 3 reps (Wh) | | Efficiency (%) | Peak power deliverance (%) |
|---|---|---|---|---|---|---|---|---|
| **Power source** | **FC/ SC** | **SC** | **Load** | **Combination** | **FC** | **SC** | **3reps** | **FC/ SC** |
| **FC and Battery (3 A load)** | 268 | - | 0.834 | 0.830 | 0.830 | - | 99.47 | 98.41 |
| **SC bank – without DC/DC converter** | 190 | 190 | 0.698 | 0.698 | - | 0.698 | 99.99 | 100.00 |
| **SC bank – with DC-DC converter** | 186 | 186 | 0.598 | 0.548 | - | 0.548 | 91.58 | 90.08 |
| **FC & SC (without DC-DC converter)** | 250 | - | 0.750 | 0.750 | 1.058 | 0.262 | 99.99 | 100.00 |
| **FC & SC (with DC-DC converter)** | 403 | 428 | 0.644 | 0.643 | 0.410 | 0.254 | 99.91 | 99.54 |
| **FC & SC (with DC-DC converter and selective switching)** | 293 | 2265 | 0.671 | 0.669 | 0.596 | 0.034 | 99.66 | 98.60 |

The different comparison will be compared using a basis of reference of the operation of the unaided SC bank – this combination has the least components and the shortest comparative endurance. Comparing this combination to the SC bank combined with the DC-DC converter an efficiency can be calculated using equation (3.9) – calculated as 87.9%. This value is on the border of acceptable

as it is less than but close to 90%, with the addition of the DC-DC converter the efficiency of the SC bank dropped by 8.41% and the endurance dropped by 4 s. The efficiency decrease is quite large keeping in mind that the SC bank's voltage range was within 20% of the required output of the converter – the efficiency of a DC-DC converter improves the closer the input is to the output. It can thus be argued that the converter will have a large decrease in efficiency if the current SC bank is to be boosted to the 50 V of the available FC system. This could lead to a significant decrease in the capacity and therefore endurance of the SC bank when implemented with the available system. This assumption will be further investigated in section 4.2.2.2.

All three FC-SC combinations exhibited similar efficiencies to that achieved by the unaided SC bank (> 99%), with the combination including the DC-DC converter but without selective switching yielding the best endurance by far. The first FC-SC combination achieved a better endurance than the SC bank but decreased the endurance of the FC system. Although the SC bank is utilized a lot less with the inclusion of the FC system due to it not having a current blocking device the FC system provides an energy above that required by the load, and above that originally supplied by the individual FC system combination, in order to recharge the SC bank – this results in a considerably faster depletion of the FC system.

With the inclusion of the DC-DC converter in the second FC-SC combination the FC system no longer charges the SC bank and a more even distribution of the individual energy provisions is observed. With the inclusion of selective switching the FC system is utilized more and provides 89% of the combined power supplied – this is seen in the much slower depletion rate of the SC bank. Both of the last two combinations show an improvement in the FC system – with the assumption that the selective switching is not necessary as it leads to less usage of the SC bank and therefore only slightly increases the usable time of the system.

From the final column it can be seen that the SC bank can alone initially provide 100% of the peak power requirement (initially – as Figure 3.40). This is an improvement on the 98.41% that the FC system provides, this is further justified where the unaided FC-SC combination also achieves 100% deliverance of the peak requirements. The negative effect of the DC-DC converter is seen, once again, where it reduces the peak power deliverance of the SC bank and the combinations. Further verification and validation will be discussed after the implementation and test of the circuit in section 4.2.2.4.

## 3.3 Conclusion

This chapter started with the conceptual design of the hybrid system focussing on the requirements, specifications and operational flow of the circuit and followed with the more in-depth detail design. The size of the SC bank was calculated pertaining to the required capacitance of each cell and the weight of the combined bank. Next was the design of the microcontroller's program used to control

the PWM signal of the MOSFET and this was demonstrated through the logic flow diagram. A large portion of this chapter was dedicated to the design of the DC-DC converter circuit. For this a circuit design was proposed and the switching element, switching circuit, inductor calculations, output capacitor calculations and snubber circuit sections of the circuit were completed. Hereafter the simulations of the circuit were conducted to verify and validate the operation of the DC-DC converter circuit. The results of the simulations were compared to those found in a few articles and the necessary adjustments were made to achieve the desired outputs. Finally, the heat sink calculations were conducted before the PCB and enclose were designed. The proposed combined circuit was simulated next to present a preliminary idea of how the system will operate as a whole. To conclude the chapter the verification and validation process was explained.

Chapter 4, below, will include the implementation, evaluation and results of the aforementioned components individually as well as in the combined system. As the simulations represent the ideal operation of these components it is understandable that a few alterations will be required to improve upon functionality and efficiency; these alterations as well as any other modifications will be presented in that chapter.

# CHAPTER 4: IMPLEMENTATION, EVALUATION AND RESULTS

In this chapter the system designed in the previous chapter is implemented and tested to verify the operation thereof. It is then compared to the simulation results and results from previous work done in similar projects to validate the results. The two main areas of focus are highlighted in Figure 4.1, the SC bank and the DC-DC converter.

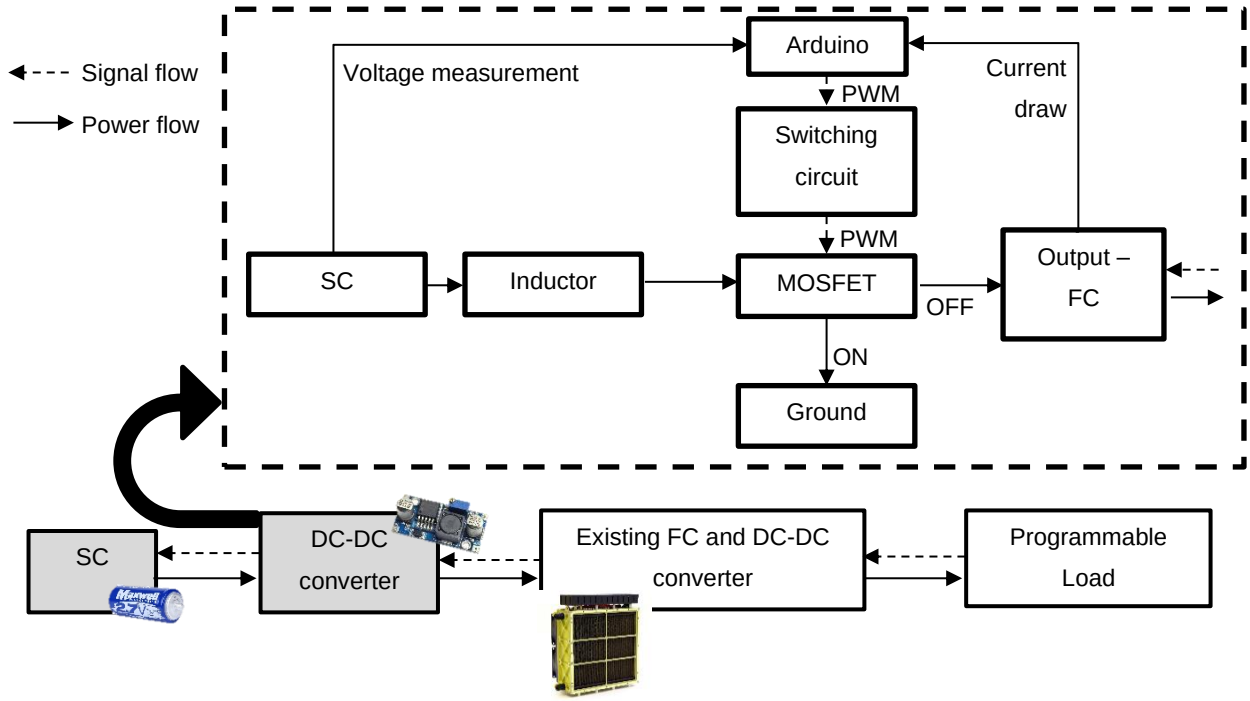


**Figure 4.1: System overview highlighting areas pertaining to the research**

The figure above also shows an outline of the concepts involved for the DC-DC converter – the inductor, the switching circuit and module, and the Arduino used for control of the converter. These elements and the other focus area will be used to conduct the various sections of this chapter. The sections of this chapter are shown in Figure 4.2 representing the layout of this chapter.

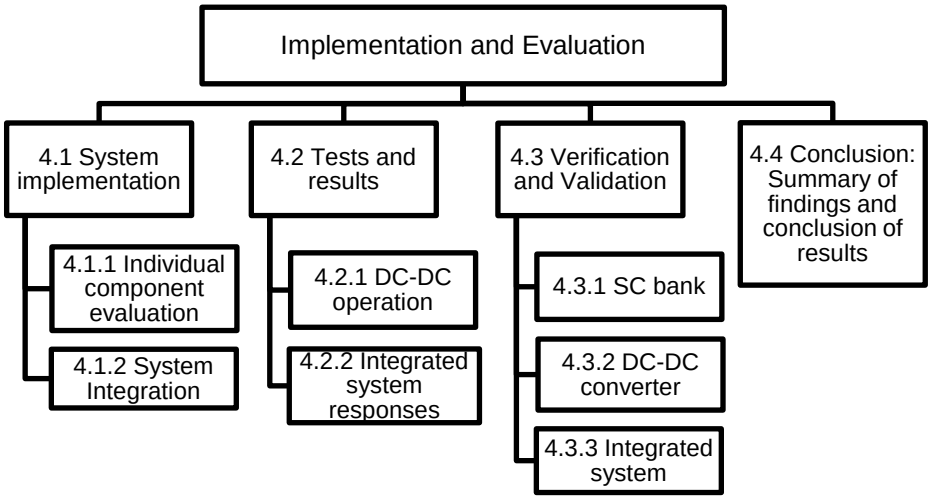


**Figure 4.2: Chapter 4 layout**

## 4.1 System Implementation

In this section each individual component of the system will be evaluated in order to obtain effective operation before the system is integrated and finally tested. All of the aforementioned will be discussed in this section.

### 4.1.1 Individual component evaluation

Before the integrated system can be tested and evaluated, each individual component needs to be validated in order to determine whether they are functioning in the correct manner for integration. Figure 4.1 shows the main components of the system, those being the SCs, the DC-DC converter, the FC and the PL. Each of these components will be evaluated under their respective headings below.

#### 4.1.1.1 Fuel cell system

The FC system that will be used for the bulk of the tests and for the integration of the system is seen in Figure 4.3 below.

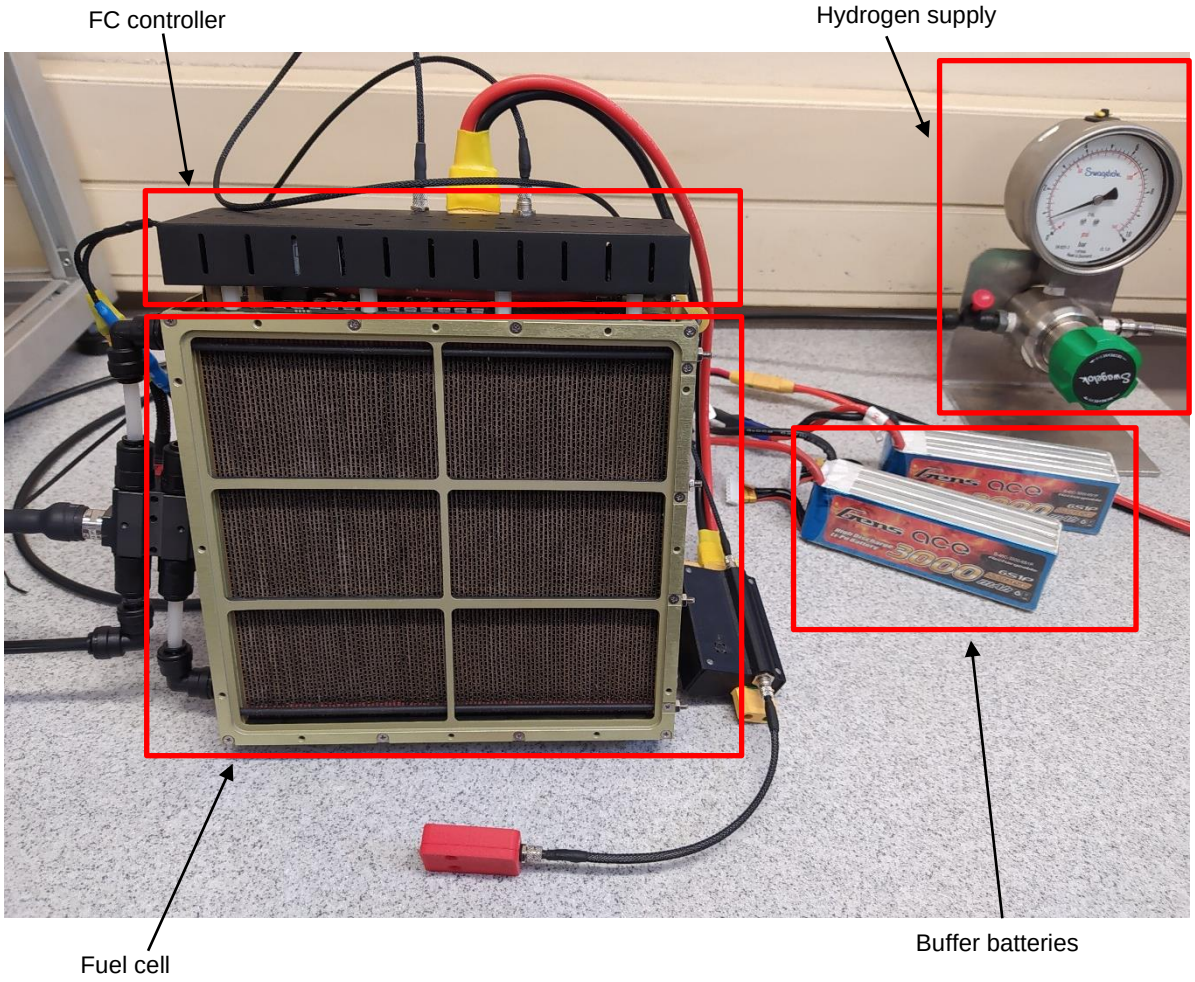


**Figure 4.3: FC system to be used for the project experiment**

The figure shows the FC, its buffer batteries and the controller as well as the hydrogen supply for it. The buffer batteries supply the initial power required for the FC to start up as well as supplying power when the power requirement is too low for the FC and when it is higher than the maximum of the FC; the FC will recharge the batteries when they decrease below 95% SOC; the controller determines these points. The buffer batteries do not contain a DC-DC converter as they have the same voltage value of the FC; the FC system will be combined with the SC bank through the use of a switching module. Table 4.1 provides a summary of the electrical characteristics of the FC system shown above. The parameters of the buffer batteries are those which will be matched by the SC bank explained in the next section.

**Table 4.1: Summary of FC system parameters (obtained from** [266]**)**

| | **Type** | **Energy density (Wh/kg)** | **Max voltage (V)** |
|---|---|---|---|
| **FC** | 1 kW BMPower | 534 | 50 |
| **Batteries** | 6s Li-Po | 160 | 50 |

#### 4.1.1.2 Super-capacitor bank

The SC bank implemented in this system is shown in Figure 4.4. This SC bank consists of eight 2.7 V, 360 F SC cells combined in a pure series configuration to give an output of 21.5 V and 45 F. This SC bank will be combined with the DC-DC converter circuit in order to match the required buffer battery values given in Table 4.1.

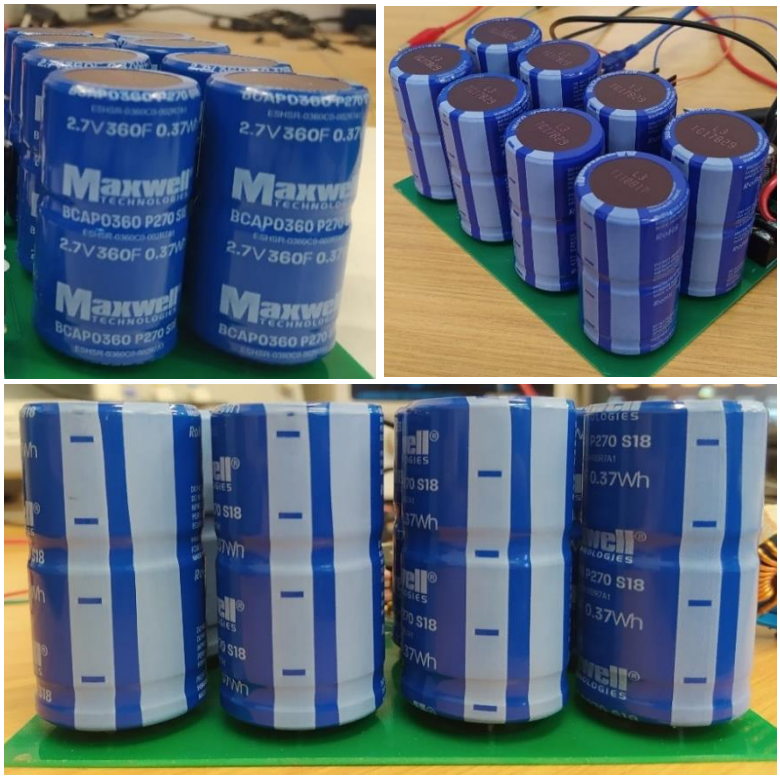


**Figure 4.4: Experimental SC bank implemented in project system**

#### 4.1.1.3 DC-DC converter

The circuit of the boost DC-DC converter is seen in Figure 4.5. This circuit is built to boost the output of the SC bank to that of the battery and what is required by the load. The load requires 50 V, 20 A maximum output to supply 1 kW. The SC bank is isolated from the DC-DC converter as it will need to be recharge independently from the converter and this is achieved through the isolation switch. The Arduino will control the MOSFET (switching module) through the switching circuit and their individual implemented operation is giving under the respective headings.

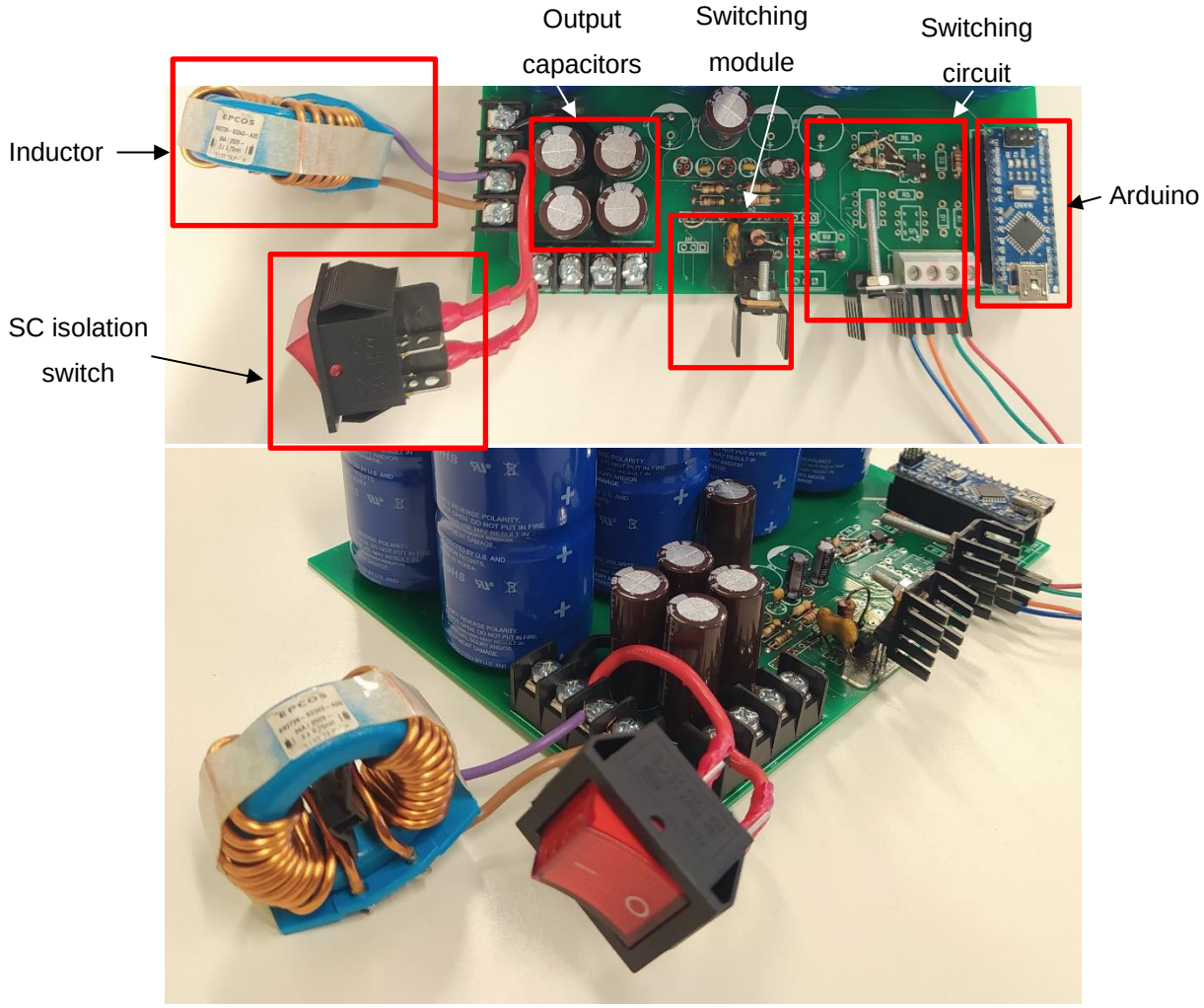


**Figure 4.5: Experimental DC-DC converter circuit built for implementation with the FC system**

The control system has been thoroughly discussed in section 3.2.2. The system consists of two main parts, the overall control and the DSP (Digital Signal Processing) control. The former entails receiving a voltage value from the power source and converting it to usable information for use in the latter system – to send DSP PWM signal to the MOSFET in order to control the switching of the gates and allow the DC-DC converter to function effectively. The main focus of this project is to examine the flow of energy and determine any inconsistencies when compared to the original system. Therefore, it is not necessary to design a complex control algorithm and also unnecessary

to use a complex controller. An Arduino Nano was chosen as the microcontroller as it has a very simple programming language and contains sufficient characteristics for its use in this system.

Once the voltage values discussed are obtained, they are used in the second aspect of control, the DSP control. This control is illustrated in Figure 4.6 below. The main system functions on high voltage and current values and it is therefore necessary to isolate each measurement from the microcontroller as well as decreasing the values to a level that is not harmful to the microcontroller itself (<5 V, 20 mA). The isolation and voltage decrease was achieved through the use of a simple voltage divider circuit.

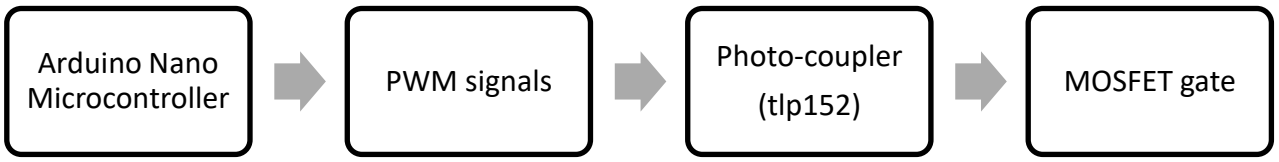


**Figure 4.6: DSP system control**

Referring to Figure 4.7, once the values are obtained and sent through the algorithm the controller can send a PWM signal to the MOSFETs. In order for this stage to be safer for the microcontroller it is, once again, isolated through the use of a photo-coupler; a photo-coupler is the combination of an opto-coupler and a MOSFET driver – thus simplifying the required circuit.

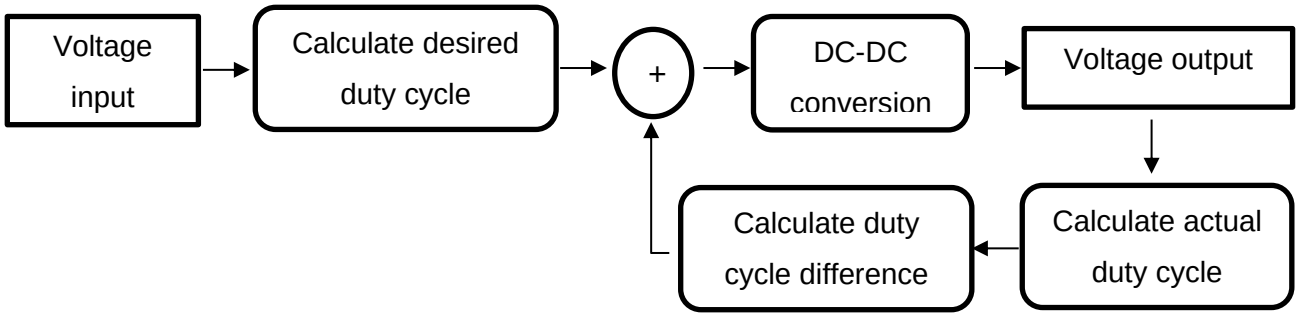


**Figure 4.7: Controller operation**

#### 4.1.1.4 Load profile

Due to power limitations of the available FC system the load profile will be reduced to a third of its size, this is shown in Figure 4.8. The available FC system is slightly degraded and can supply a maximum of 350 W, therefore when the power needs exceed that value a supplementation is required to allow the system to still operate efficiently. This is the point where the SCs will be utilised. This point is estimated and shown in the figure using the red line. The actual response of the FC system to the load will be provided in the next section of this chapter.

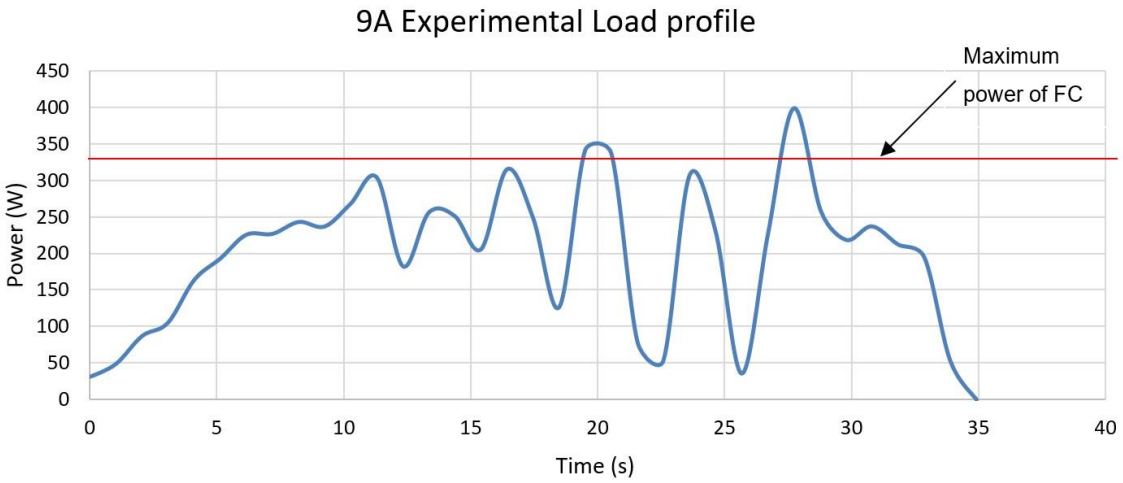


**Figure 4.8: 9 A Experimental load profile**

### 4.1.2 System integration and operation

The final experimental circuit to replace the buffer batteries is given in Figure 4.9 below.

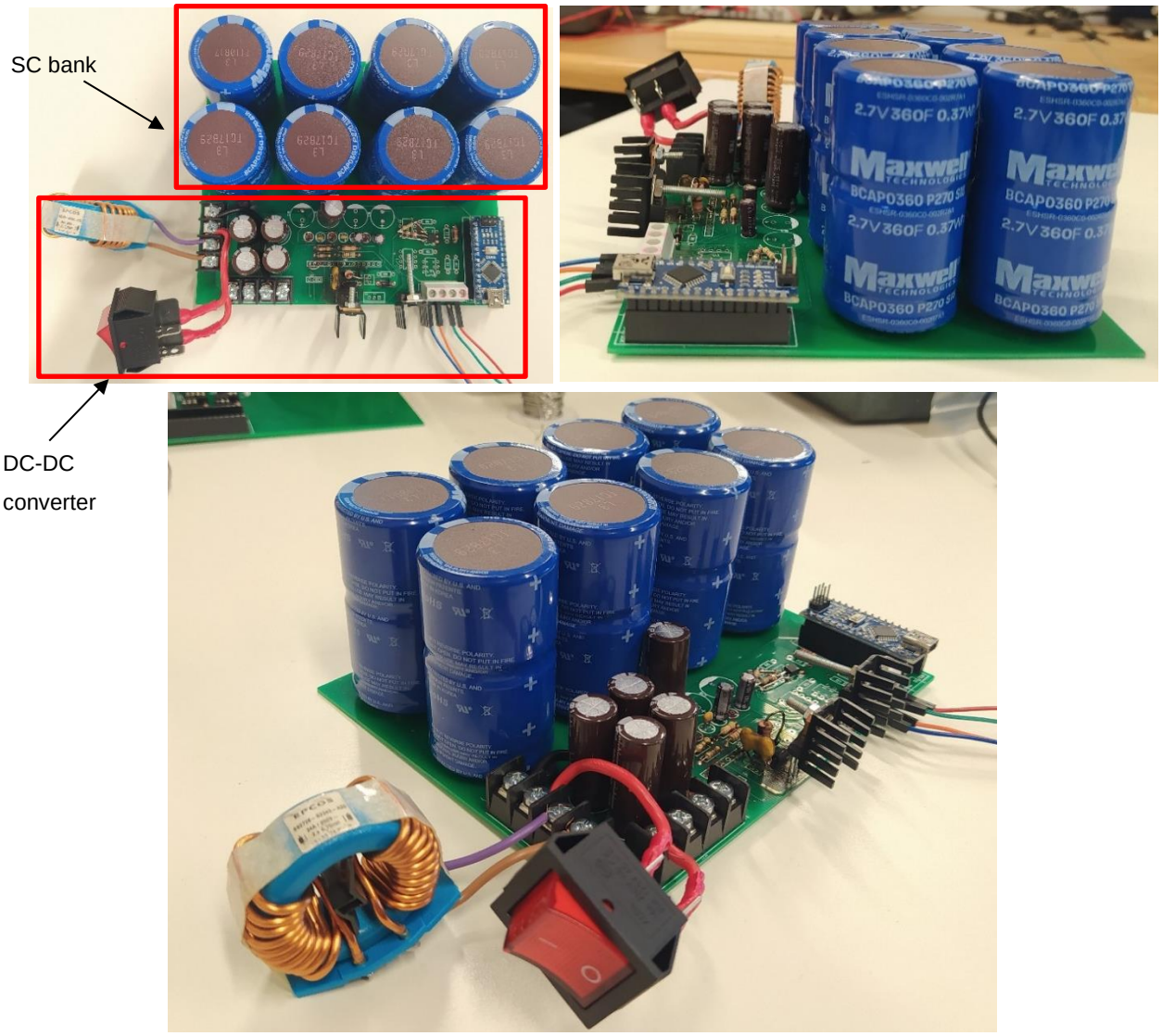


**Figure 4.9: Experiment SC & DC-DC converter circuit**

With the system integrated it should function better than the original system at the peak power requirements this will be tested and the results shown later in this chapter. The DC-DC converter circuit has five main components specifically chosen for this experiment. The MOSFET used is a TK72E12N1 with datasheet [248]; the MOSFET is driven using the switching circuit designed in section 3.2.3.2 and utilizes a photo-coupler with code TLP152 and datasheet [267]; for the microcontroller an Arduino Nano is used with datasheet [220]; eight 350 F, 2.7 V SCs with ESR of 3.4 mΩ each and datasheet [247] will be used in a pure series connection; the inductor used has inductance of 4.7 µH, saturation current of 52 A and DCR of 1.43 mΩ with datasheet [176].

## 4.2 Tests and Experimental results

Now that the system has been built and integrated it can be tested to see if it operates as expected and also to see if it operates differently to that of the original system. The system was tested through the use of a few different tests, testing the operation of the DC-DC converter itself, testing each source on their own and in the different combination configurations. These different tests and their respective results are given below.

### 4.2.1 DC-DC converter

The DC-DC converter circuit will be tested as two parts, the switching circuit and the switching module. This will be done in order to verify the operation of the controller and switching circuit as well as the DC-DC converter as a whole. The experimental setup for this first test is shown in Figure 4.10.

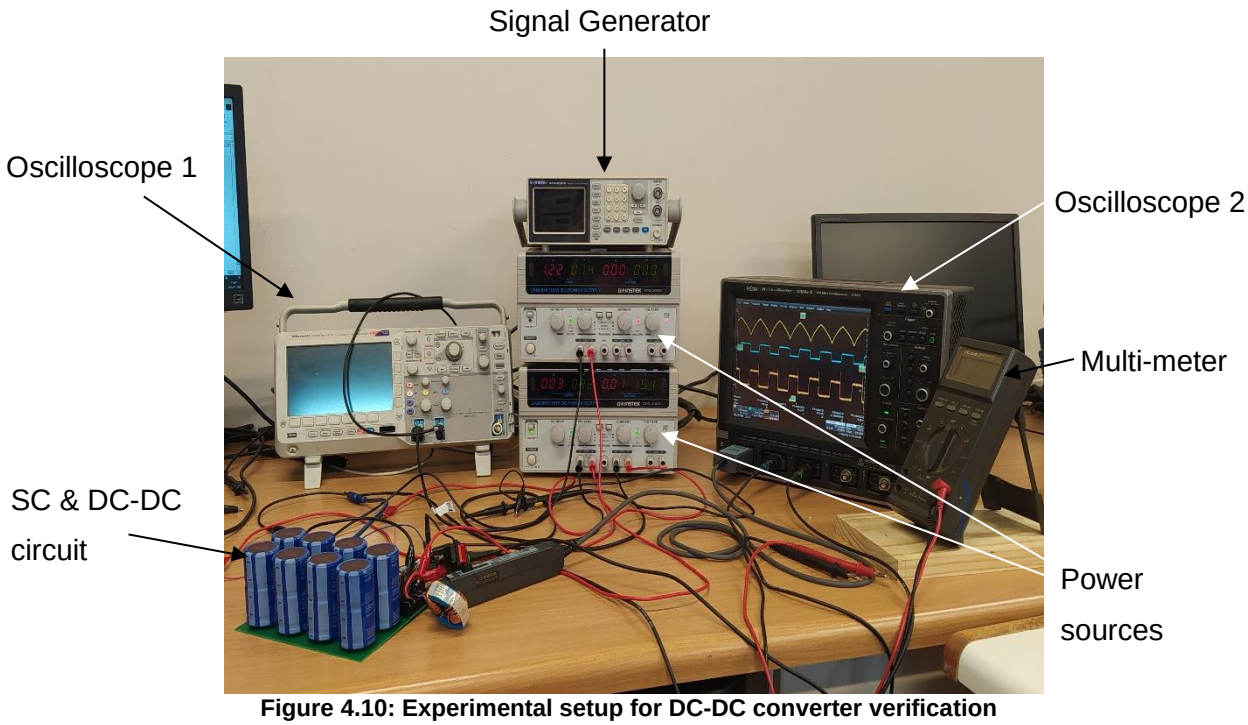


**Figure 4.10: Experimental setup for DC-DC converter verification**

For the experimentation two types of oscilloscopes were used as only one contains a current probe, which was very useful during the design phase of this experiment.

#### 4.2.1.1 Switching circuit

The first verification test is that of the operation of the switching circuit and will involve a hardcoded program uploaded to the Arduino that will send out a specific PWM signal. An oscilloscope will be used to measure the PWM signal at the Arduino and at the MOSFET gate. The measurements will include the frequency, the duty cycle and the maximum voltage. These values will be compared with each other and with the desired values. Figure 4.11 gives a comparison of the two experimental measurements.

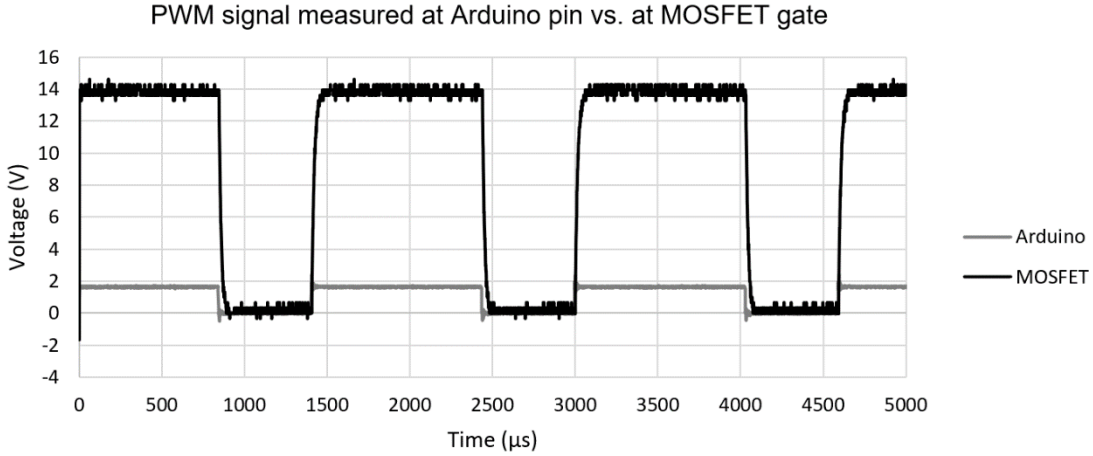


**Figure 4.11: Experimental test 1 of switching circuit**

The Arduino has been programmed to produce a PWM signal with 65% duty cycle. The desired frequency and minimum voltage at the gate are 62.5 kHz and 12 V, respectively. From examining the measured outputs, the Arduino gave a 62.5 kHz signal with a duty cycle of 66.3% and amplitude of 1.5 V. The values measured at the gate are 62.5 kHz, 64.93% and 13.5 V, respectively. The frequency measured at the gate is as desired whereas, the duty cycle has a 0.11% deviation from the desired value and the amplitude is 3.5% larger than the minimum required value, these deviations are acceptable. It is also seen that the duty cycle from the Arduino isn't exactly as desired, however, as it delivers a more precise duty cycle at the MOSFET gate this value is acceptable.

The second verification test will require the full Arduino code that calculates the duty cycle from the measured input voltage. For this test the code will be uploaded, an input voltage will be supplied and the Arduino will determine the required duty cycle. The required duty cycle will be calculated and compared to that of the Arduino output and that supplied at the MOSFET gate. Figure 4.12 provides the oscilloscope outputs at the Arduino pin and MOSFET gate.

The input supplied is 30 V, using equation (2.3) and a desired $V_{out}$ of 50 V the duty cycle is calculated as 40%. Using the oscilloscope, the frequency is measured as 62.5 kHz at both ends and the duty cycle is measured as 41.5% at the MOSFET gate and as 41.46% at the Arduino output. This gives a deviation of 0.1% between the MOSFET gate and Arduino output and a 3.75% deviation between the MOSFET gate and the desired duty cycle. Again, this deviation is used to account for the power losses present in the circuit.

The third test will involve the validation of the switching circuit, which will be conducted by varying the input voltage and analysing the adjustments made by the Arduino and measured at the MOSFET gate.

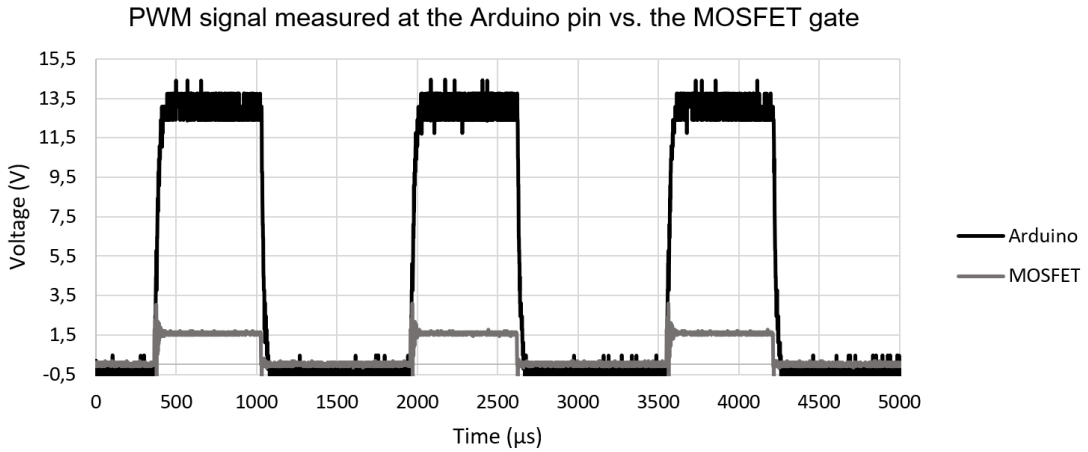


**Figure 4.12: Experimental test 2 of switching circuit**

Table 4.2 provides a summary of the measured values for the varying input voltages and their deviations to that of the calculated/desired values.

**Table 4.2: Summary of output of experimental test 3 of the switching circuit**

| $V_{in}$ | Calculated duty cycle (%) | Measured duty cycle at the MOSFET gate (%) | % deviation |
|---|---|---|---|
| 17.3 | 65.4 | 67 | 2.44 |
| 30.7 | 38.7 | 40 | 3.18 |
| 34.6 | 30.7 | 32 | 3.95 |

This test was conducted on the preliminary circuit using a desired output voltage of 50 V. It is seen that the duty cycle deviation increases as the input voltage grows closer to the 50 V, this is however still acceptable as it is less than a 5% deviation and the increased duty cycle can account for the power losses that occur in the circuit.

#### 4.2.1.2 DC-DC converter operation

To verify the operation of the converter a constant voltage will be supplied to the input of the circuit and various measurements will be taken to be compared to the simulated values in section 3.2.3.6. These measurements include the MOSFET switching signal and the current and voltage waveforms of the output, inductor and switching diode. Figure 4.13 provides the oscilloscope readings obtained from the current measurements. Comparing the switching signal of the MOSFET to the current through the inductor it is evident that the inductor is charging and discharging with the pulse of the MOSFET. The curve is similar to that of a saw tooth waveform, however, the ascent has an increasing gradient which is evident of the inductor operating just under saturation. This area of

operation is acceptable as it does not saturate yet and it can be attributed to the inductor operating at its higher current bounds.

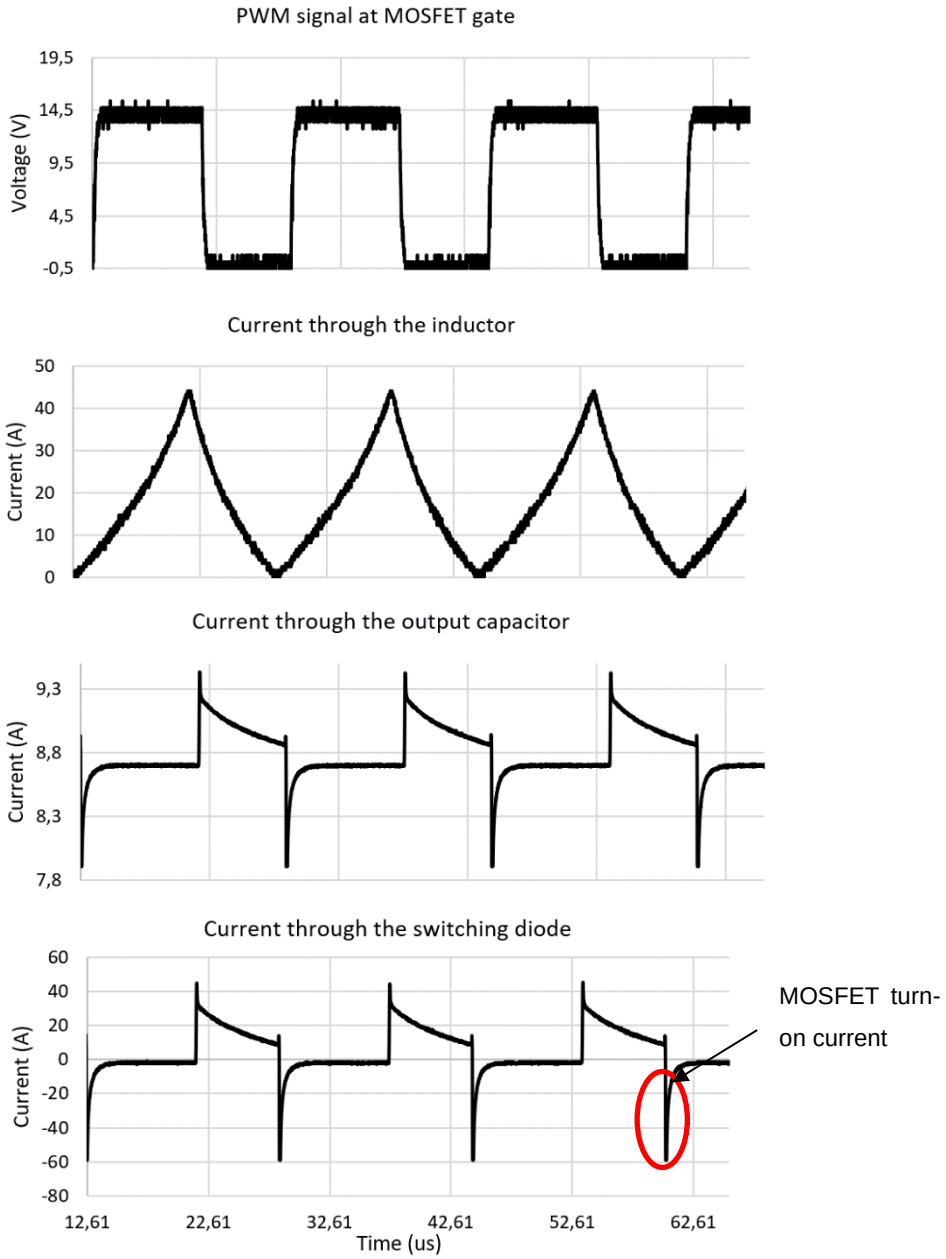


**Figure 4.13: Experimental results for verification of current waveforms of DC-DC converter**

The current peaks at 45 A which is similar to that calculated ($I_{peak}$) in section 3.2.3.3. The current through the output follows a similar waveform to that of the diode which is expected as the output current is that which flows out of the diode. The current ripples from 7.9-9.5 A (1.6 A) which gives a 17.8% ripple compared to the output current of 9 A; this value is closer to the desired 20-40% although still below and is also similar to that obtained in the simulations. Seen in both the current of the output and that through the diode are inverted spikes representing the MOSFET turn-on current required when the MOSFET switches on. The voltage waveforms of the experimental circuit are given in Figure 4.14.

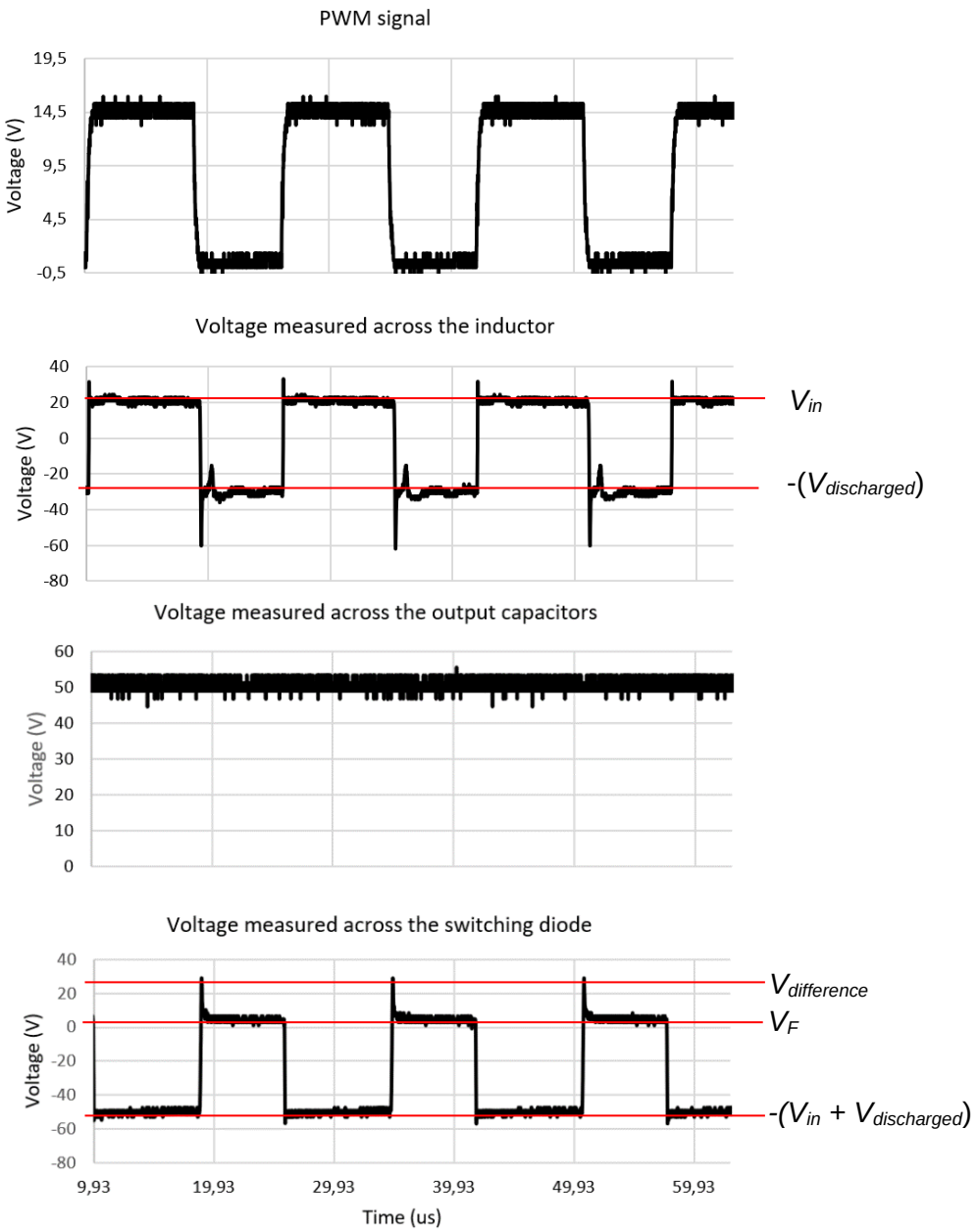


**Figure 4.14: Experimental results for the verification of the voltage waveforms of the DC-DC converter**

As with the simulations the maximum of the inductor voltage represents potential difference between the input and output of the inductor and is equivalent to the input voltage of the system as the MOSFET is on allowing current to flow to ground. The minimum voltage of this waveform represents the maximum voltage stored in the inductor during the charge phase and is seen to increase as this discharge voltage decreases (as the inductor discharges). The voltage waveform across the output gives a relatively continuous output of 52 V, which is the desired value.

The output voltage ripples between 50 and 54 V resulting in a 7.69% ripple. Although this is larger than the desired ripple it is still within an acceptable range. The maximum voltage measured across the diode shows the difference between the voltage stored in the output capacitors and the voltage sent from the inductor initially when the MOSFET switches on – this voltage decreases, as the values start to balance, to the voltage drop across the diode ($V_F$). The minimum voltage is that of the voltage

stored in the output capacitors with respect to ground (the MOSFET is on – input of diode is ground). These waveforms and values are similar to those obtained in the simulations.

To validate the operation of the converter various voltages will be applied to the input and the output will be measured to determine the deviation from the desired output (50 V).Table 4.3 provides a summary of the results obtained for the various input voltages.

**Table 4.3: Summary of experimental results for the validation process of the DC-DC converter**

| $V_{in}$ (V) | $V_{out\ desired}$ (V) | $V_{out\ measured}$ (V) | $V_{out\ deviation}$ (%) |
|---|---|---|---|
| 17.33 | 50 | 49.62 | 0.74 |
| 30.66 | 50 | 49.76 | 0.48 |
| 34.66 | 50 | 49.49 | 1.01 |

From the table it is evident that the deviation is close to 1% for all tested values and thus the output is close to that which is desired and this deviation is acceptable.

### 4.2.2 Combination responses

As this system is designed around the functionality of the available FC (&battery combination), the response of the FC to the 9 A load profile (Figure 3.9) will be used to determine when the FC requires the capacitor banks. The FCs response will be reduced to obtain values that can be provided by the capacitor banks without the need of a DC-DC converter – the case studies from section 2.2 suggest the use of SCs without a DC-DC converter, as explained in section 3.2.1 this would require a capacitor bank with weight in excess of 8 kg. As this project is investigating the use of SCs with an existing FC drone, the weight of the system needs to be minimal. With this in mind, the SC bank has been designed to provide the energy requirements of the full load but it cannot provide the necessary voltage, hence the boost DC-DC converter.

The effect of the DC-DC converter on the SC bank capabilities and therefore the system will need to be investigated – it needs to be determined whether the DC-DC converter will benefit the system. For this, some reference values, that do not vary, will be required allowing for a basis of comparison across the different experiments – this basis will be the characteristics of the SC bank. Therefore, the load profile has been reduced such that the current requirements will not exceed 3 A and the voltage requirements will not exceed the capabilities of the SC bank – providing a maximum load of 51 W. This new load profile is shown in Figure 4.15.

The load profile from Figure 3.9 will be used to examine the operation of the FC system, where after the 3 A load profile will be used for the remainder of the tests. The individual operation and responses of each source is discussed in detail below where after a summary will be provided to compare the different results.

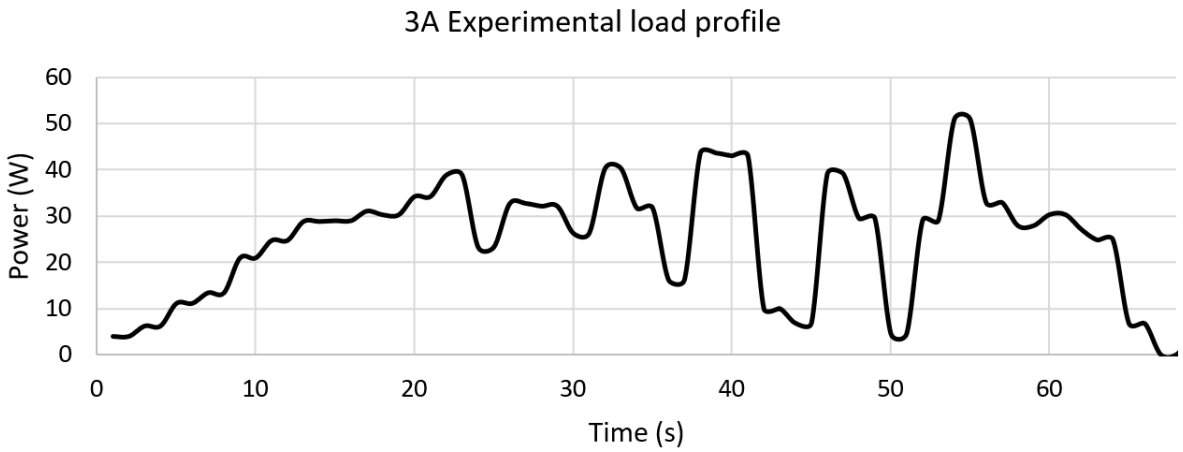


**Figure 4.15: Adjusted experimental 3 A load profile**

#### 4.2.2.1 Fuel cell and battery

The FC-battery combination was first tested with the 9 A load profile to assess its response to the load as well as determine when the SC bank will be required. Figure 4.16 shows the response of the FC and battery combination to the 3 repetitions of the load.

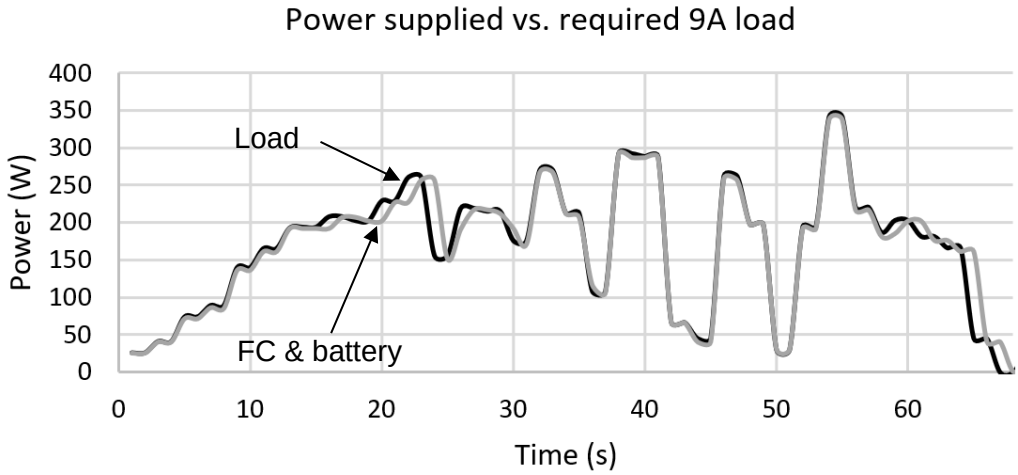


**Figure 4.16: Experimental response of FC and battery combination to load power**

The figure shows that the FC and battery combination provide the required load with a calculated efficiency of 99.62%. This system achieves an endurance of 16800 s. In order to examine the response of the FC current to the required load one repetition of the load and the FCs response to it will be analysed closer, this single repetition is shown in Figure 4.17.

It is seen that the current supplied by the FC is, for the majority of the profile, smaller than required. This shows that the FC adjusts the supplied current according to the available voltage to maintain the required power output.

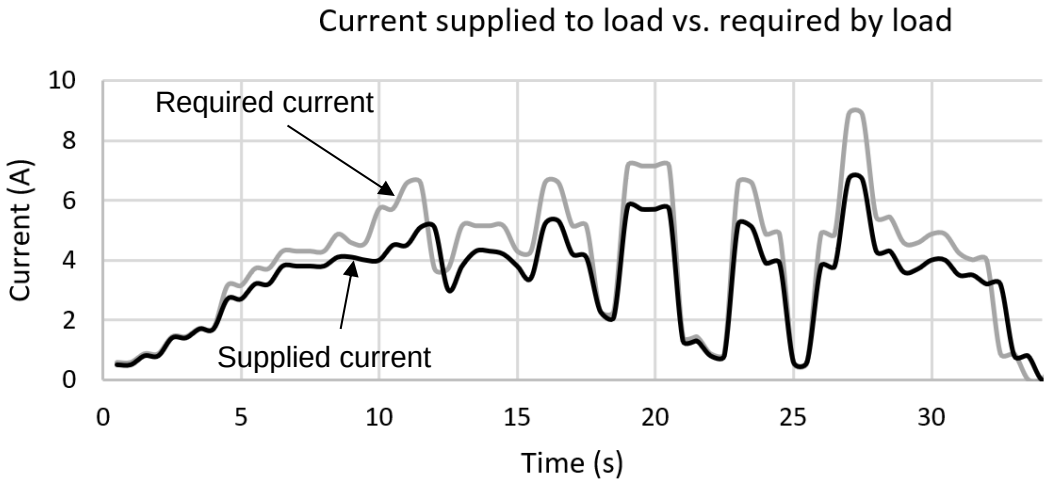


**Figure 4.17: Experimental response of FC system to load profile**

In order to verify where the battery supplements the FC such that the requirement of the SC bank can be determined Figure 4.18 is used. All the red circles enclose fluctuations seen in the voltage supplied which indicate the inclusion or removal of the battery as the combined voltage will initially increase or decrease before balancing of the sources occurs.

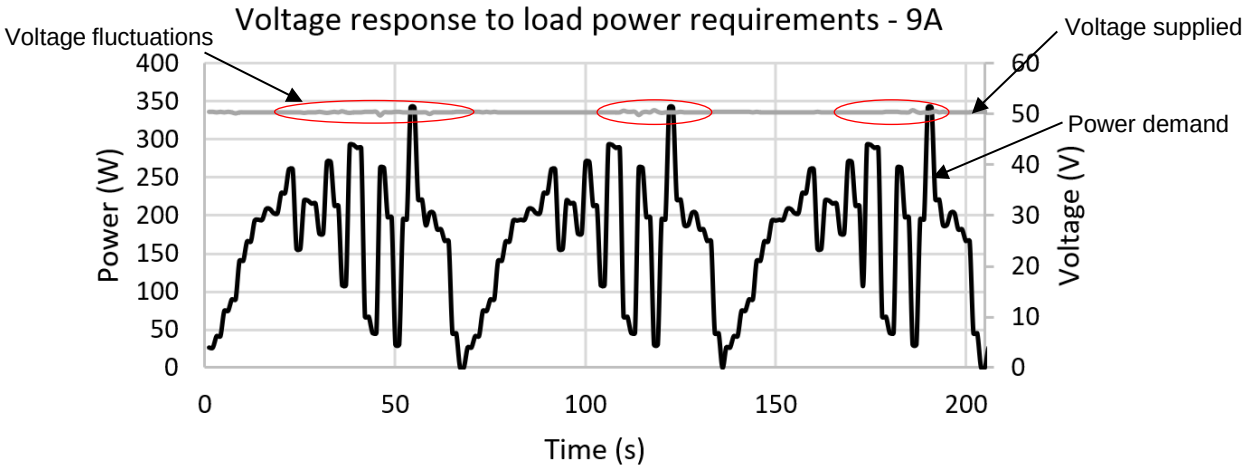


**Figure 4.18: Experimental results of FC-battery combination Voltage supplying the load**

It is clear from the figure that the voltage supplied by the FC and battery combination does not decrease for the duration of the load, it remains an average of 50 V – this justifies that a laboratory power source can be implemented to provide the power of the FC system. The reason for this replacement is due to the available FC having a high power capability (500-1000 W) with its 50 V output – therefore the FC cannot be used with the smaller load in combination with the SCs as it will either supply the entire load, or if a larger load is used the SC bank will need to supply a current in excess of 23 A. This level of current is too large for the other components of the circuit.

Another reason is that the FC system contains a controller that controls the functionality of the FC itself as well as the buffer battery usage – a combination with the SC bank would require an entirely new controller which is not within the scope of this project. As the laboratory power supply can only provide 30 V at 3 A it will be set to provide the maximum voltage of the SC bank at a reduced current of 1.6 A – this value is chosen such that a better representation can be obtained of how the SC bank

affects the functionality with utilized. The laboratory power source will replace the FC system for the remainder of the tests so that the SC bank can match the FC voltage without a DC-DC converter.

As the FC and battery system function in a way that the battery is constantly recharged when it dips below a 95% SOC value and the hydrogen is supplied by a source much larger than that of the typical size of a tank on the drone used in this report, another method was required to determine the run time of this combination. The method used is Faradays Law of Electrolysis [265] explained in section 3.2.5.2.4. As the FC system has been replaced with the laboratory power source its repsonse to the 3 A load will need to be exmained, this is shown in Figure 4.19.

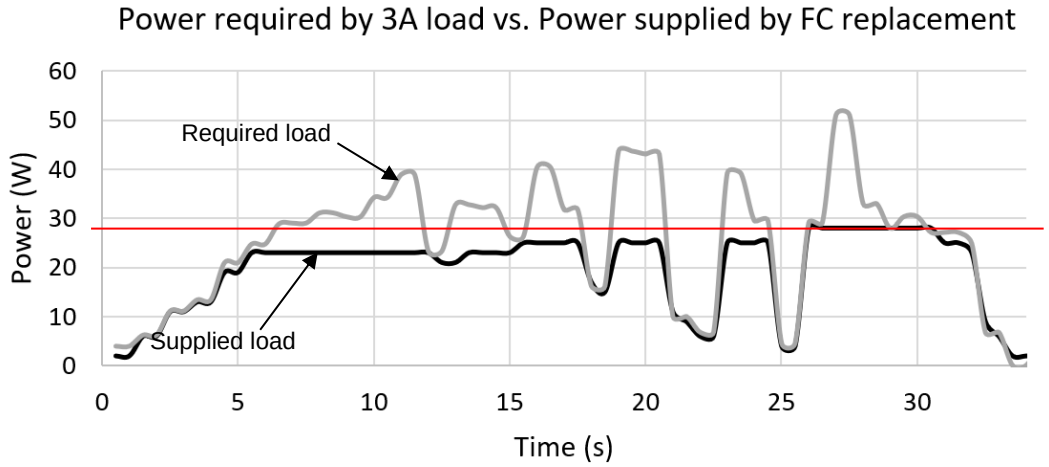


**Figure 4.19: Experimental response of laboratory power source to required 3 A load**

From the figure it is evident that the power supply can provide a maximum of 28 W (indicated by the red line). This plateau is expected as a point is desired above which a supplementation of power will be required. This is the point where the SCs will be utilized. This combination achieved a usable time of 168 s and efficiency of 76.27% -it will be attempted to improve both of these values through the use of the SC bank. The current and voltage waveforms of the power supply in Figure 4.20 will be used to further examine where the SC bank will thus be required.

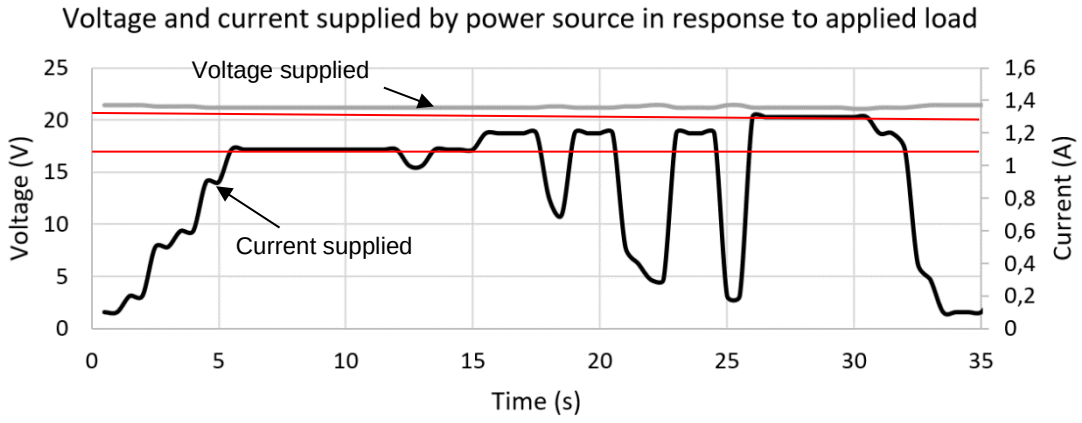


**Figure 4.20: Voltage and current waveforms of power supply in response to required load**

In the figure there are six points between 1.1 A-1.3 A, shown between the red lines, where the power source plateaus – this is evident of a power requirement above the limits of the source. This plateau region is where the SC bank supplementation is desired.

#### 4.2.2.2 Super-capacitor

As the SCs will be combined with the FC it is necessary to initially know how the SCs respond to the load on their own. This test is done in two parts – with and without the DC-DC converter, this extra test will give an indication of how the DC-DC converter affects the functionality of the SCs. These two tests will also serve to determine the efficiency of the DC-DC converter. The SCs have a suggested voltage decrease of 20% as this allows them to operate optimally for the full lifetime, therefore the SCs were used with a maximum voltage of 21.5 V and a minimum of 17 V. the response of these two systems to the 3 A load have been tested and the results are given and discussed below.

##### 4.2.2.2.1 Without DC-DC converter

The SC bank was first tested without the DC-DC converter to examine how it responds to the applied load. Figure 4.21 shows the operation of the SCs in response to the load required without the use of a DC-DC converter.

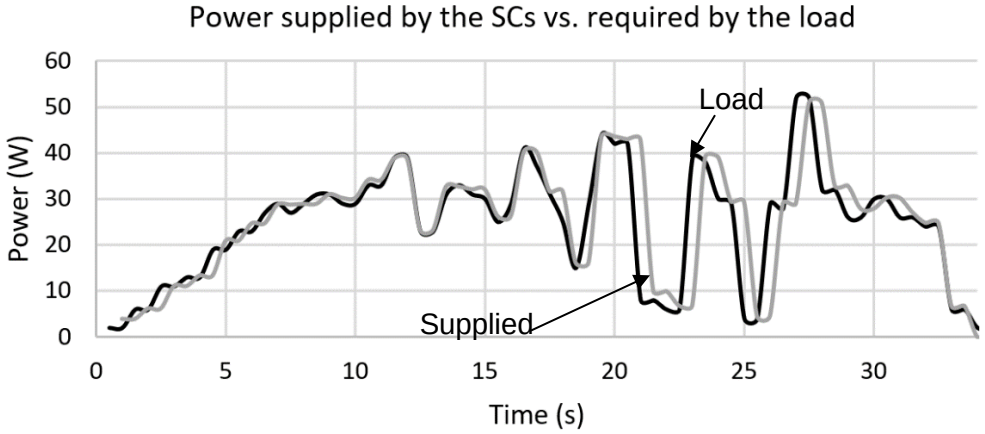


**Figure 4.21: Experimental operation of SCs in response to load - without DC-DC converter**

It is seen that the SCs provide the required load with a slight delay and the efficiency is calculated as 97.21%. The noticeable time delay between the supplied and required load can be attributed to a delay caused by the length of the conductors between the load and SCs. Figure 4.22 will be used to analyse the voltage drop of the SC bank for the duration of the load.

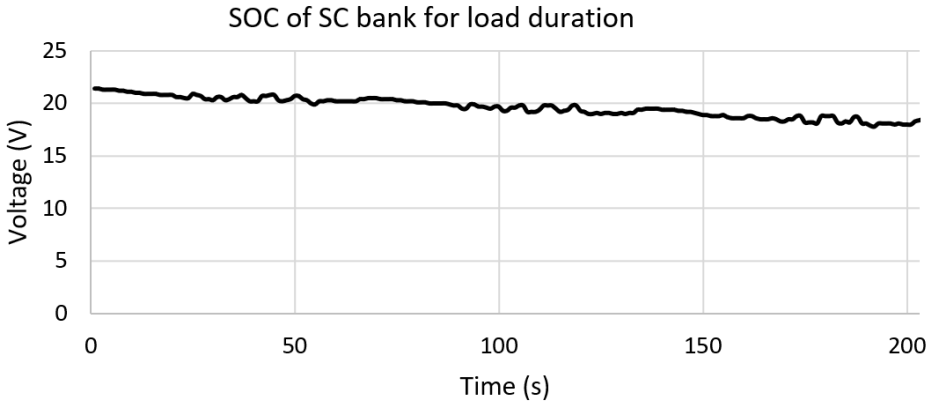


**Figure 4.22: SC without DC-DC converter SOC depletion curve for duration of load**

The load was repeated until the SC bank dropped to 80% SOC as recommended. From the figure it can be seen that the voltage dropped 20% of full charge in 130 s. Figure 4.23 will be used to show the adjustment of the current supplied by the SC bank in response to load required and the decreasing SOC.

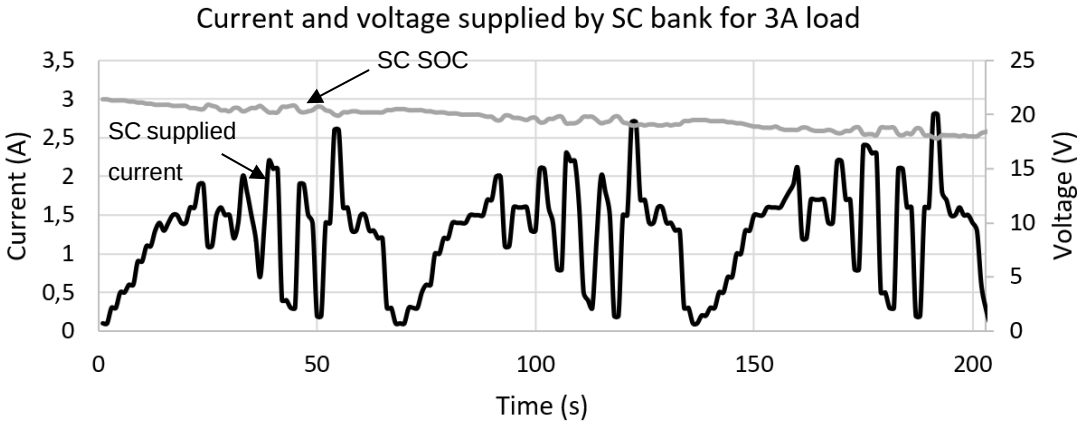


**Figure 4.23: DC-DC SOC and current deliverance in response to 3 repetitions of load**

It is seen in the figure that as the SOC of the SC bank decreases the current supplied increases – this is due to the SC bank adjusting the current according to the voltage capabilities to meet the power demands of the load.

#### 4.2.2.2.2 With DC-DC converter

Next, the DC-DC converter will be combined with the SC bank to assess the effects thereof whilst supplying the required load. The response of this system to the load is given in Figure 4.24.

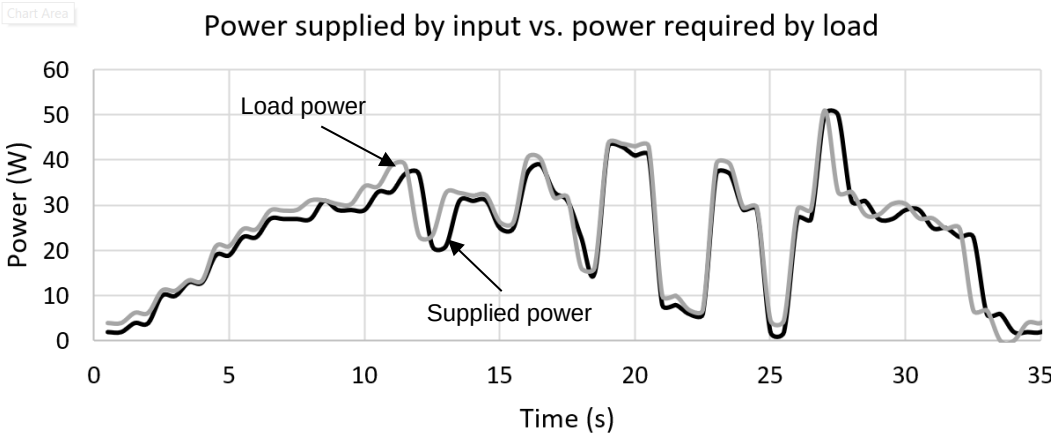


**Figure 4.24: Experimental operation of SC bank in response to load – with DC-DC converter**

It is clear that the supplied power follows the same pattern as that of the load power with a calculated efficiency of 96.66%. This can be attributed to the SC bank experiencing power losses through the DC-DC converter which is synonymous with its efficiency. The figure also shows a noticeable time delay between the load required and supplied – this is attributed to a delay caused by the length of the conductors between the load and the SC supply. In order to determine the usable time of this combination the SOC curve of the SC bank at the input of the DC-DC converter (SC SOC) and at the input to the system (output of the DC-DC converter) will be examined, shown in Figure 4.25.

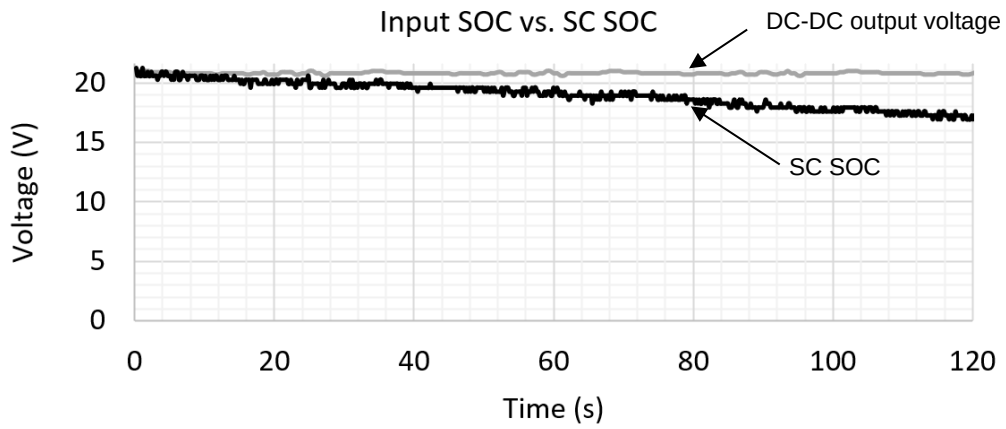


**Figure 4.25: SC SOC curve at both input and output of the DC-DC converter in response to the load**

It is evident from the figure that the DC-DC converter supplies a constant voltage output in response to the decreasing SOC of the SC bank at its input. To show the use of the SC bank the current and voltage waveforms at the input of the DC-DC converter will be discussed, using Figure 4.26.

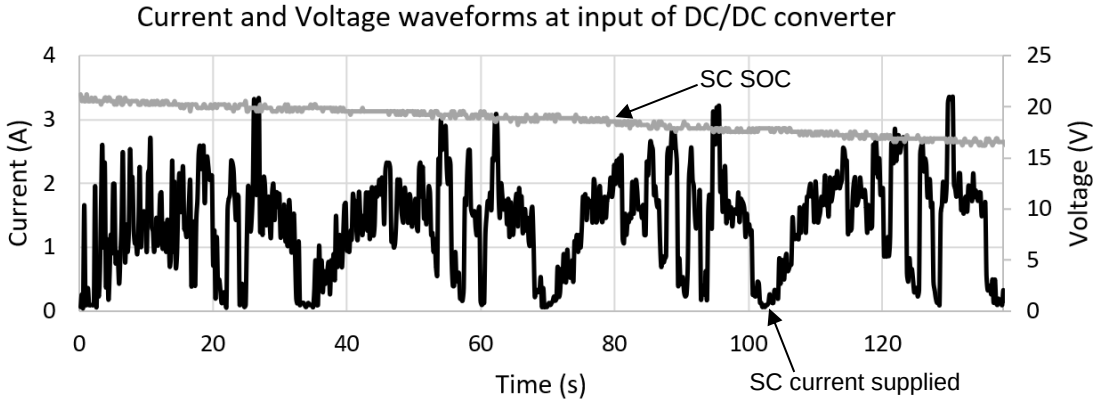


**Figure 4.26: Voltage and current waveforms of input and output of DC-DC converter**

It is evident from the Figures that the input to the converter has a decreasing SOC and an increasing supplied current – this is to maintain the delivery of the required load at the output of the converter, which is seen to hold a constant current and voltage level.

#### 4.2.2.3 Fuel cell and Super-capacitor

This combination will comprise of three tests and two rounds of each test – these tests and the configurations are discussed in section 3.2.5.1 using Figure 3.34. The setup for the six tests and two rounds of the specified tests is shown using Figure 4.27.

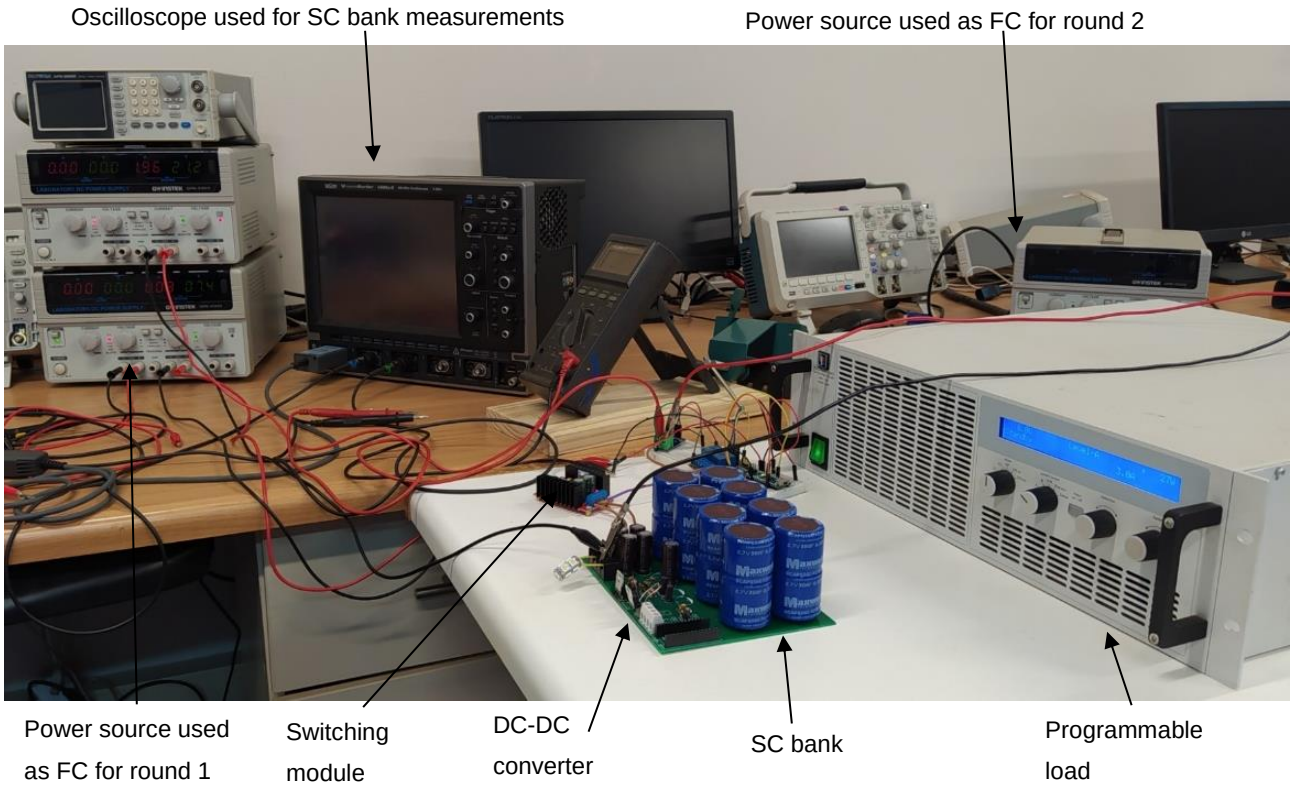


**Figure 4.27: Setup for final circuit experimentation**

For these tests the FC system has been replaced by a laboratory power supply and the remainder of the components are shown in the Figure. In the figure two different power sources are presented and used to replace the FC system, one for each connection round. Using this setup, the mentioned tests will be conducted and the results are provided below. The results from round 2 will be presented and the differences between the rounds will be discussed in the comparison section of this chapter. In these tests the oscilloscope is connected to the input of the DC-DC converter, to obtain the current and voltage waveforms of the SC bank, and to the output to be used to examine the effect of the DC-DC converter on the system.

##### 4.2.2.3.1 FC and SCs without DC-DC converter

The case studies from Chapter 2 of this report suggest the use of SCs without a DC-DC converter, as such, this will be the first test of the SC and FC combination. The operation of the combination in response to the required load is given in Figure 4.28.

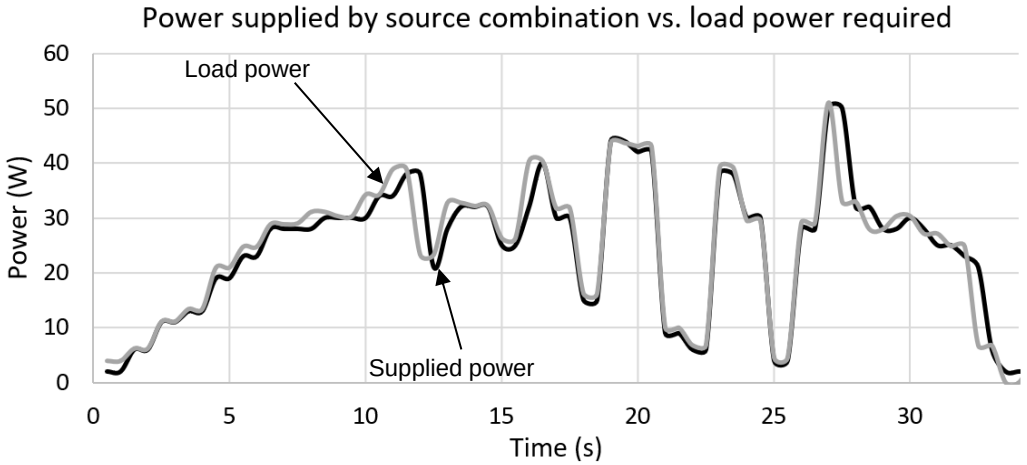


**Figure 4.28: Experimental results of combination in response to applied load**

It is seen in the figure that the load is supplied by the power source combination with a slight deviation and calculated efficiency of 97.09%. This deviation can be attributed to the power losses that occur in the conductors between all the components of the system. There is a time shift observed at the intervals of 10-15 s and again at 25-30 s – this shift can be attributed to a delay in the power supplied by the SCs caused by the length of the conductors between the power sources and the load. The separate use of the SC bank and the FC system are shown in Figure 4.29.

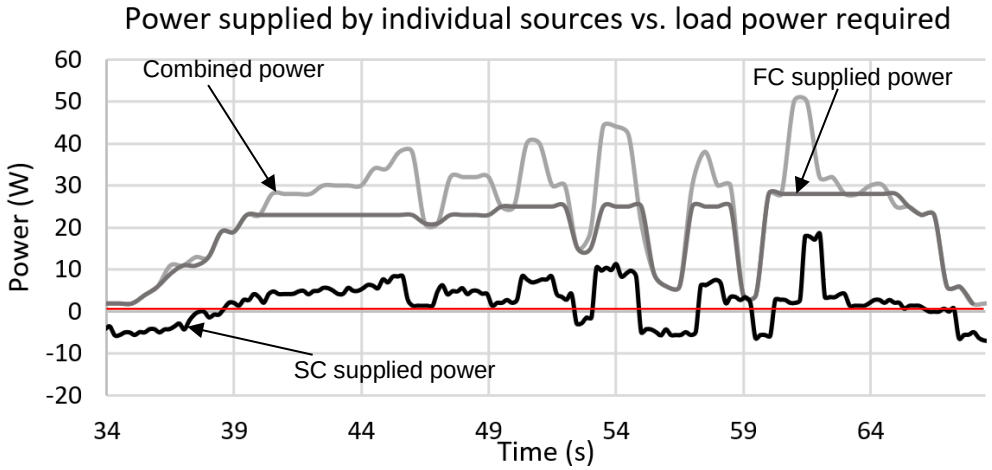


**Figure 4.29: Separate power supply from FC and SC systems**

It is seen that the SC bank provides a low amount of power smaller than that of the FC, however, the power observed above the red line seems to be able to fill the gaps of the power not provided by the FC system to supply the load requirement. This is justified through Figure 4.28 where the power has sufficiently been provided. Under the red line the SC bank exhibits negative energy which is evident of it receiving energy from the FC in order to recharge. To further investigate this occurrence the voltage provided to the load and by the SC bank will be presented. To examine the voltage of this system Figure 4.30 will be used.

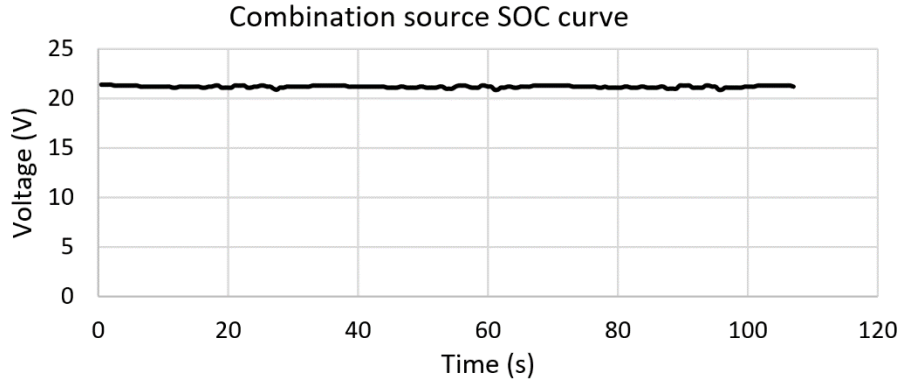


**Figure 4.30: Experimental results of SOC of combination in response to load**

This figure shows the response of the voltage provided by the combination to the applied load. For this combination it is seen that the voltage does not decrease and remains at an average of 21 V for the duration of the applied load – as the voltage does not fluctuate the load was repeated 3 times. This combination connects the FC supply and the SC bank in parallel with each other and the load; there is no device blocking the flow of current towards the SC when required. The voltage of both the SC bank and FC system are matched with each other and thus both can supply the required load continuously.

When the SC drops below the voltage level of the FC system, the FC will supply both the load and the SC bank. Figure 4.31 will be used to examine this voltage and current supply from the SC bank.

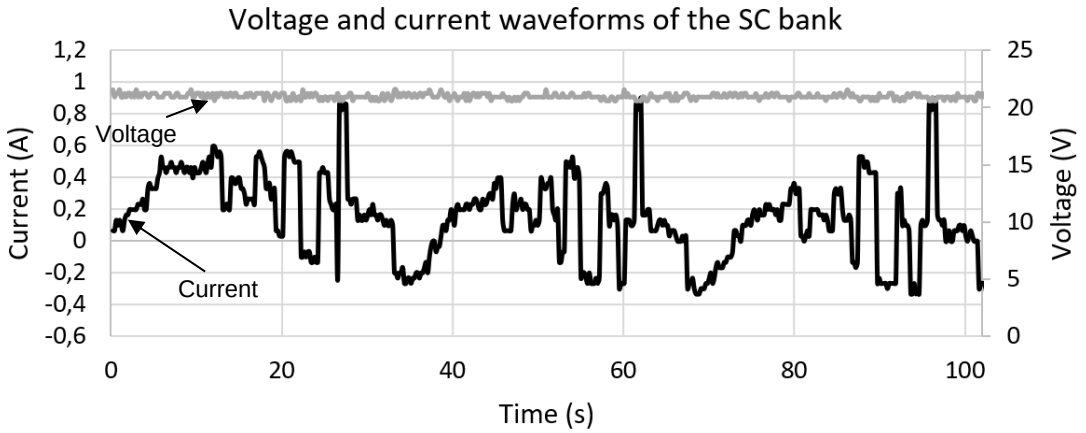


**Figure 4.31: System voltage level and current supplied in response to 3 repetitions of load**

The voltage waveform is seen to have various fluctuations but is kept at an average of 21 V and the current waveform exhibits negative currents, once again showing that the FC system is recharging the SCs when they drop below the voltage level of the FC system. It is however evident that the system is using the SCs to supplement the FC system when the load increases above its capabilities. This combination achieves an overall endurance of 160 s calculated using equation (3.43).

#### 4.2.2.3.2 FC and SCs with DC-DC converter

It is evident from the previous test that the combination between the FC system and SC bank requires a method of blocking the flow of current towards the SCs – this will help to extend the usable time of the FC system. This extension will be examined with the use of a DC-DC converter in this section of the tests. Figure 4.32 presents the response of the combination to the required load.

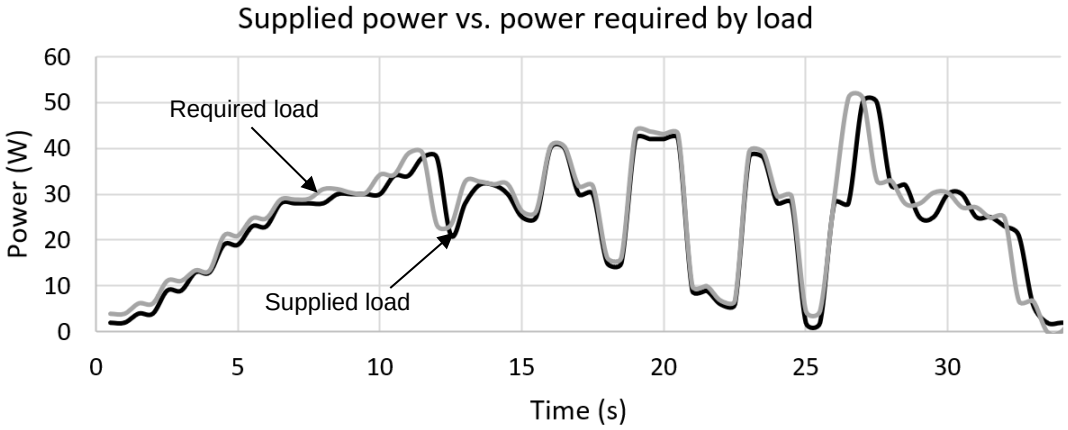


**Figure 4.32: Experimental results of combination in response to applied load**

Once again it is seen that the power supplied by the combination of the sources has a slight deviation and the efficiency is calculated as 96.25%. As with the previous combination a delay is observed between the power supplied and the power required specifically in the same intervals – this is attributed to the time loss caused by the length of the conducting wires between the sources and the load. This time delay is also slightly larger than that of the previous combination, which is attributed an additional delay caused by the DC-DC converter. The separate use of each individual source is shown in Figure 4.33.

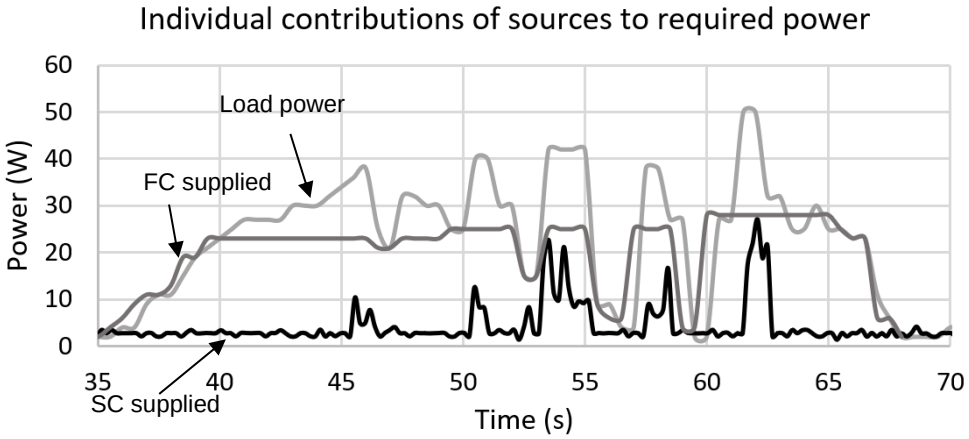


**Figure 4.33: Separate supply of power from individual sources to supply load**

It is evident from the figure that once again the SC bank is being used to supplement the FC system to provide the required power. Another justification showing the use of the SC bank is provided through the use of Figure 4.34.

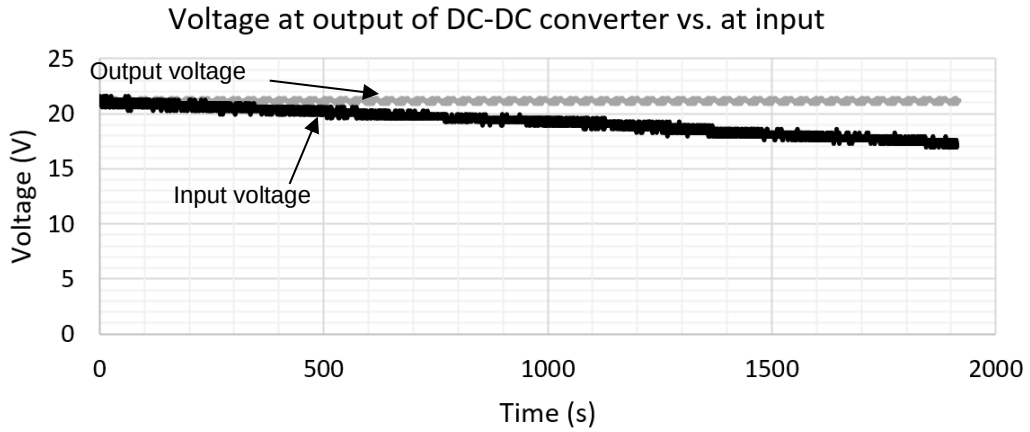


**Figure 4.34: Experimental results of SOC at input and output of DC-DC converter**

This figure presents the SOC curve of the SC bank at the input of the DC-DC converter compared to the output of the DC-DC converter. It is evident that the SC bank is discharging for the duration of the applied load and drops to 80% SOC level in 1906.74 s. To examine how the parallel connection of the sources affects the current and voltage waveforms of the SC bank Figure 4.35 will be used with a continuous repetition of the load.

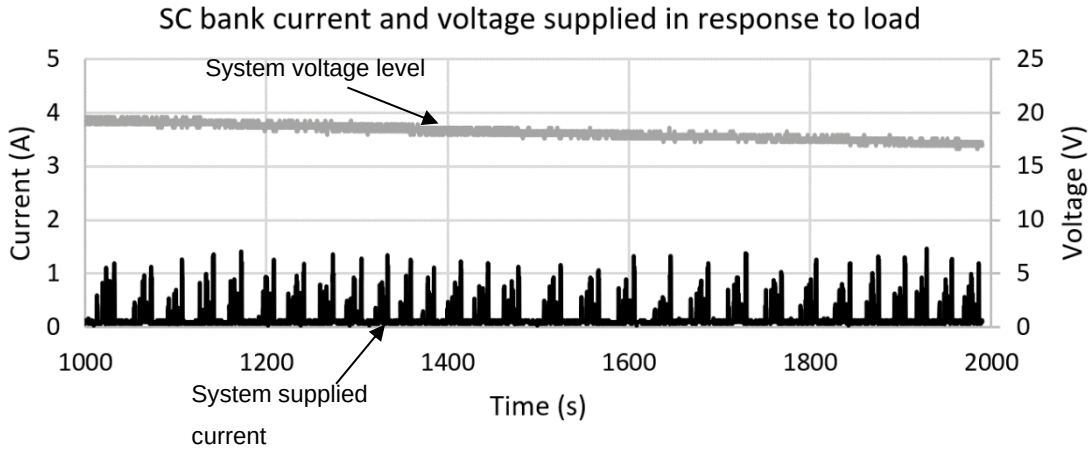


**Figure 4.35: System voltage and current supplied in response to 3 repetitions of load**

As the SOC of the SC bank drops current supplied peaks remain relatively constant. As the FC system is carrying the bulk of the load only a small portion is provided by the SC bank. The SC bank saw a larger increase in the current peaks, as the system depleted, in the unaided tests – this is due to the SC bank supplying the entire load and thus needing to adjust the current levels according to the voltage available.

The maximum power requirement of the load (50 W) is designed for the minimum voltage level of the SC bank (17 V) – 3 A are only required at 17 V to meet the 50 W requirement; when fully charged (21 V) the current requirement was low (2.38 A) to accommodate the power requirement and as the SC bank depleted this current level needed to increase. In this case, the SC bank is only supplying a small quantity of the power and can therefore comfortably supply a relatively constant peak current (1.5 A) in response to the decreasing voltage. Using Ohm's law, only once the voltage level of the

SC bank drops to a level that can no longer supply the required power will the current increase to accommodate this. This combination allows for a 1918 s usable time of the SC bank, however as the FC system depletes in 214 s (calculated using equation (3.43)) the overall endurance of this combination is 214 s.

#### 4.2.2.3.3 FC and SCs with DC-DC converter and controlled switching

For this combination the FC system and SC bank have been combined using a switching module that selects when the SC bank is required (current levels > 1.5 A). It is only at these instances that the SC bank will be in use, for the remainder of the load the SC bank will be off. Figure 4.36 shows the response of the combination to the required power of the load.

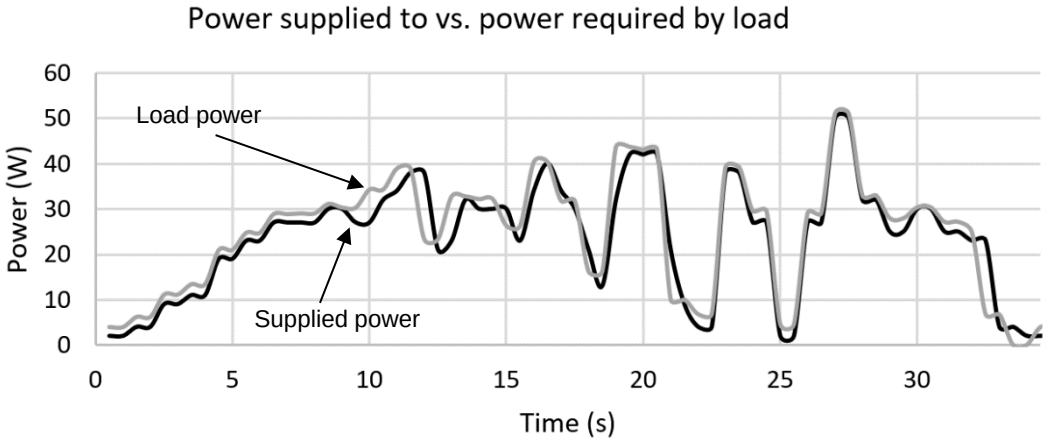


**Figure 4.36: Experimental results of combination in response to load**

The Required power is seen to be supplied by the combination of the load with a slight deviation and a calculated efficiency of 94.29%. As with the prior two combinations a time delay is observed between the power required and power delivered, but it is a smaller delay than the previous two. Due to the controlled switching the SC bank (and resultantly, the DC-DC converter) is utilized less than in both the previous combinations and therefore the time delay caused by the DC-DC converter circuit and the conductors between the SC bank and the load is of a smaller extent. The individual contribution of each source to the load supplied is given in Figure 4.37.

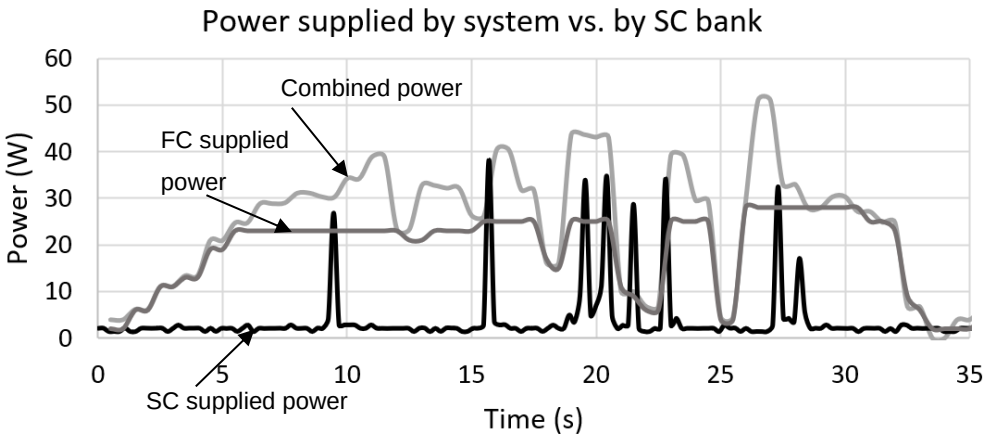


**Figure 4.37: Individual contribution of sources to required load**

It is evident that the SC bank is supplementing the FC system at the peak requirements. This is justified through the observation of the SOC curve of the SC bank at the input of the DC-DC converter shown in Figure 4.38.

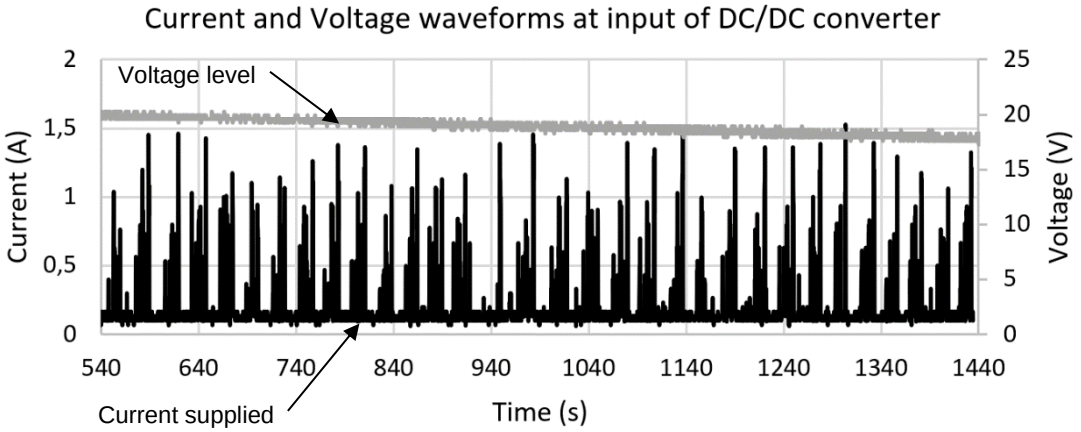


**Figure 4.38: Experimental results of voltage level at input and output of DC-DC converter**

The SC bank SOC drops by 20% in 1916 s, but the voltage drop is regulated to 21 V for the entire duration of the load at the output of the DC-DC converter. To examine the effect of the selective switching on the use of the SC bank the voltage and current waveforms measured at the input of the DC-DC converter in response to the load are given in Figure 4.39.

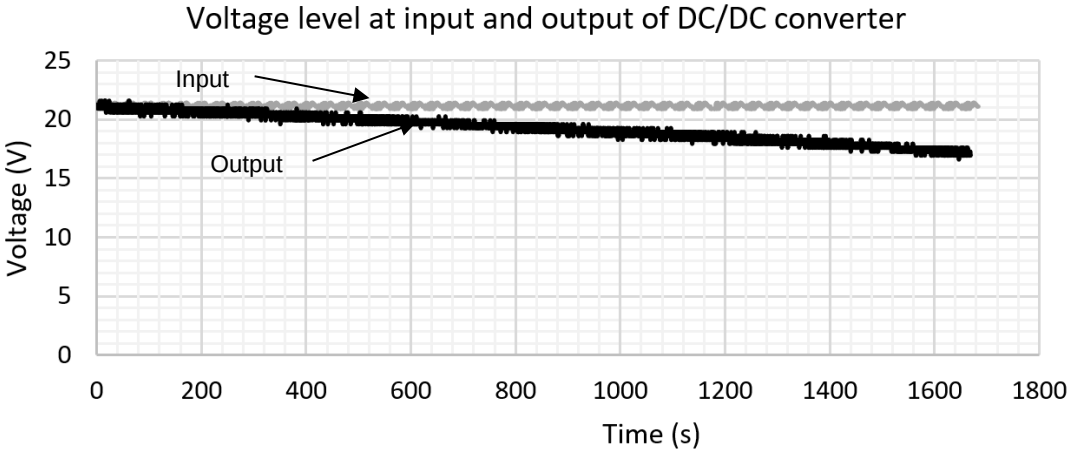


**Figure 4.39: SC SOC and current in response to load**

As before the peak current values are seen to remain at a constant value smaller than 1.5 A even though the SOC is decreasing. The reason for this is the same as for the previous test with the FC-SC combination. This system allows the SC bank to have an endurance of 1916 s but the FC system still provides the bulk of the load and therefore the overall endurance is calculated, using equation (3.43), as 223 s.

#### 4.2.2.4 Comparison of results

The results obtained from the respective combinations have been processed and combined into Table 4.4. This table will be used to compare the different combinations.

As the unaided SC bank is used as the reference point for the comparisons its duration will be used as in equation (3.43) to determine the duration of the FC system used for the 3 A load. For this equation the maximum current chosen to be the limit of the FC replacement (1.6 A) will be used to determine the volume of hydrogen required for the specified duration of 130 s. This delivers a FC system that can provide for a load within its limits. This calculated volume and the average current that the 1.6 A FC system can deliver in response to the 3 A load is then used to determine the duration of the FC system. The FC-SC combinations are reliant on the capacity of the FC system to determine its duration. The duration refers to the maximum usable time obtained from each combination when used with the load profile. The FC-battery combination refers to the power source replacement's response to the load; the SOC drop duration refers to the time it took each combination involving a SC bank to drop 20% in SOC.

The last column of the table provides the peak power supplied by the system for the two instances (described in section 3.2.1.2) as a percentage of the power required for these instances.

**Table 4.4: Individual source response**

| | Weight (kg) | Duration (s) | Duration for 20% SOC drop (s) | Energy required by load over 3 reps | Energy provided to load over 3 reps | Energy components over 3 reps (Wh) | | Efficiency (%) | Peak power deliverance (%) |
|---|---|---|---|---|---|---|---|---|---|
| **Power source** | **Full system** | **FC/ SC** | **SC** | **(Wh)** | **Wh** | **FC** | **SC** | **3reps** | **FC/ SC** |
| **FC and Battery (3A load)** | 1.4 | 168 | - | 0.714 | 0.545 | 0.545 | 0 | 76.27 | 67.99 |
| **SC bank – without DC-DC converter** | 0.5 | 130 | 130 | | 0.694 | 0 | 0.694 | 97.21 | 97.79 |
| **SC bank – with DC-DC converter** | 0.7 | 125 | 125 | | 0.685 | 0 | 0.685 | 96.66 | 97.36 |
| **FC & SC (without DC-DC converter)** | 1.9 | 160 | - | | 0.691 | 0.665 | 0.157 | 97.09 | 95.30 |
| **FC & SC (with DC-DC converter)** | 2.1 | 365 | 574 | | 0.688 | 0.597 | 0.097 | 96.25 | 95.93 |
| **FC & SC (with DC-DC converter and selective switching)** | 2.2 | 223 | 1916 | | 0.677 | 0.566 | 0.117 | 94.29 | 96.92 |

In order to compare the different combinations a point of reference is required which was chosen as three repetitions of the load – this is due to the SC bank without a DC-DC converter having a maximum SOC drop over three repetitions. The percentage in SOC drop for the other combinations is presented in the appropriate column; the amount of energy provided by each source in the different combinations is provided to be compared to the energy required by the load over three repetitions to determine the efficiency of each combination.

To determine the total energy component provided by the combinations that include the DC-DC converter, the efficiency of said converter is required. As measurements of the SC banks operation had been recorded, the energy is known at the input of the converter; thus, multiplying the latter values with the efficiency of the converter gives their contribution to the total energy.

The efficiency of the converter is calculated as 94.96%. The values of the SC bank in the 'energy provided' column refer to the energy at the output of the DC-DC converter, where applicable. The SC bank with converter test shows that the DC-DC converter reduced the efficiency and usable time of the SC bank; furthermore, there was an 8% increase in the rate of SOC drop. Hence, deducing that although the converter can reduce the weight of the system it is questionable whether the increase in SOC drop will nullify this benefit. This assumption is justified through the similar difference in efficiencies noted between the FC-SC combinations with and without the DC-DC converter. It is also noted through the last three tests that each addition of a component to the system leads to a decrease in efficiency, attributed to power losses of each component resulting in a higher requirement from the FC system.

A further observation was the selective switching element was not necessarily required – no significant improvement to the system was evident. As the endurance is highly dependent on the usage of the FC system to increase endurance the FC system would need to be used less and the SC bank used more. Therefore, the switching value/point can be adjusted to allow the use of the SC bank at an earlier stage. However, due to the internal resistances of each power source the system decides when each power source is utilized – it is assumed that this endurance is the best that can be achieved with the available power sources.

The first FC-SC combination shows an improvement in the endurance of the SC bank but a decrease in that of the FC system – this is attributed to the lack of a current blocking device prohibiting the FC system from charging the SC bank. When the SC bank is recharged by the FC system, the FC system supplies a significantly larger amount of energy in a shorter period of time depleting its capacity faster. It is also seen that all the FC combinations with the SC increased the energy supplied in response to the load, not only in the combination but also in the FC systems' component. Thus, the FC system (when combined with the SC bank) responds more efficiently to the required load.

It was mentioned that two rounds of each test were conducted for the FC- SC combinations and for both rounds all the combinations obtained similar efficiencies and it is thus not necessary to present both results. However, the FC-SC combination containing the DC-DC converter (without selective switching) obtained a significant variance in the durations between the rounds – round 1 achieved 365 s of operation (with 574 s usable time for the SC bank) whereas round 2 achieved 214 s. This leads to the assumption that the self-regulation of the sources is highly dependent on the order of

connection of the sources and can thus be as efficient (if not better) than a method using selective switching.

In the final column the SC bank was able to deliver a better peak power performance compared to the FC system which led to an improvement of the peak deliverance when the two systems were combined – this is mirrored in the results of Table 3.5. Opposite to Table 3.5, however, was the effect that the DC-DC converter had on the combined systems – the inclusion of the converter caused a slight improvement in the peak power deliverance.

## 4.3 Verification and validation

In order to verify that the experiments and results of the system built are an actual solution to the problem statement made in section 1.2, the output delivered by the system must be compared to the required input of the load. In order to validate this solution, it will be compared to alternative solutions examined in the experiments as well as those provided in previous published documents. The details of the verification and validation of the two individual sections of the system and the integrated system are discussed below.

### 4.3.1 Super-capacitor bank

The SC bank was designed for a specific power requirement and used for its rapid charge and discharge capabilities. These two aspects will be used to verify and validate the use of the SC bank in this experiment. The SC bank was designed to provide power mainly during the peak power surges required by the load, for this the energy required at those moments was obtained from the load profile Figure 3.8 and the SCs' size was then calculated in section 3.2.1.

Using the experimental load profile, the total energy for one repetition of the load is calculated and compared to the total energy stored in the SC bank. From the load only the instances when the graph is ascending will be used as the descending sections have negative energy and if accounted for the SC would in fact be storing this energy, however, this is not how the system was designed and thus those descending sections will be omitted. Through the summation of the ascending sections the total energy required for one repetition of the load profile is 4167 J. The SC bank stores 10 498 J, this verifies that the SC bank has sufficient energy to provide the load. To verify the response of the SC bank to different applied and requested loads the charge/discharge curves have been obtained through the use of different supply/load currents, these curves are shown in Figure 4.40 below.

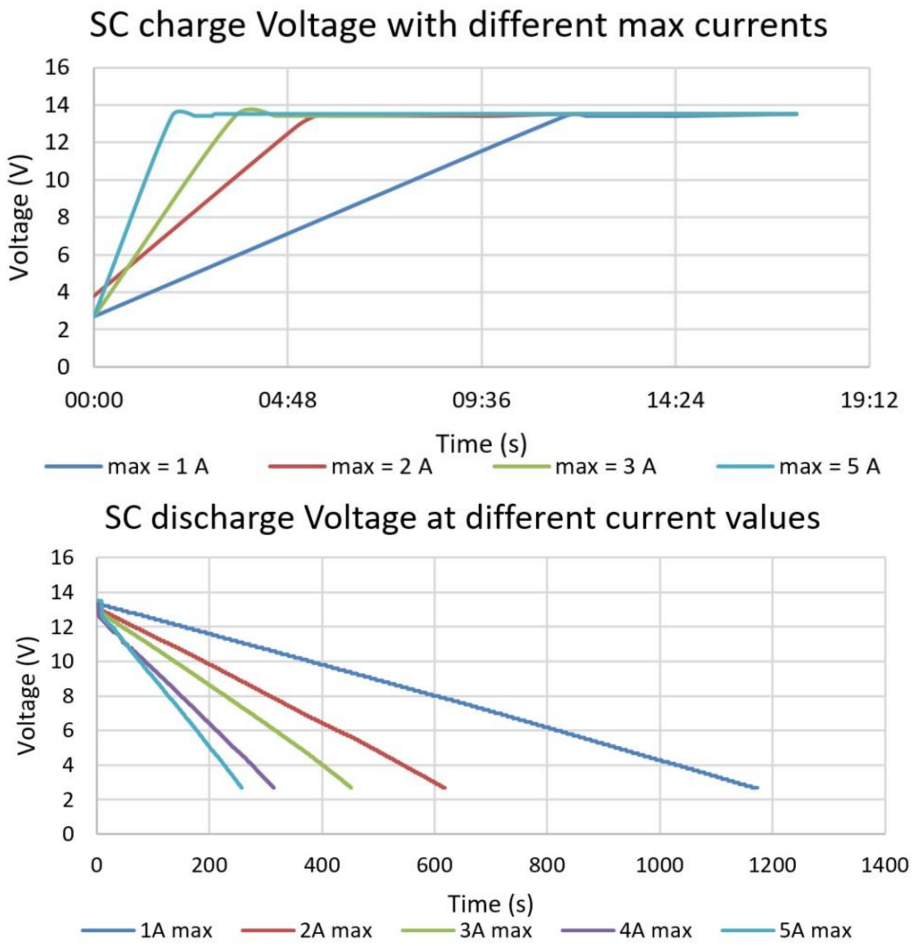


**Figure 4.40: Experimental charge/ discharge curve of the SC bank**

For experimental purposes the SC bank was only charged to 13.5 V and discharged to 2.7 V. From the curves it can be seen that with an increase in current the SCs charge and discharge increasingly faster. To validate the use of the SC bank with the Li-Po battery the discharge waveforms of both will be compared using Figure 4.41.

By comparing the two graphs it is seen that the correlation coefficient ($R^2$) of the SC bank is much closer to 1 than that of the battery – this indicates that the SC has a more linear response to the current and therefore that it's voltage decreases more linearly and does not fluctuate as it depletes.

It is also seen that the SC bank discharges a larger percentage of its voltage (80%) significantly faster (600 s or 10 min) than the battery (20% in 145.5 min) with a 2 A load. This difference in discharge speed shows that the SC does not function well when supplying a constant load although it has a very linear discharge curve. The battery functions significantly better but the voltage does fluctuate as it discharges.

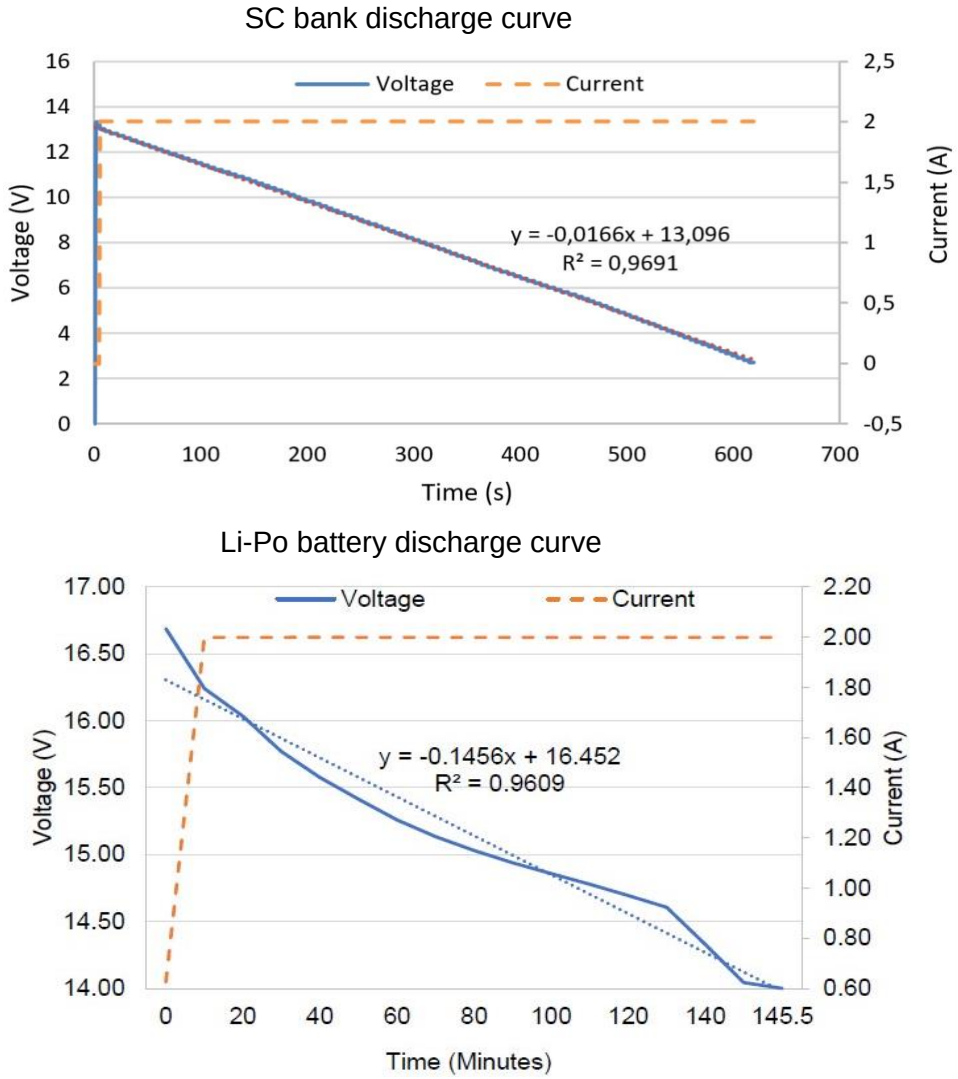


**Figure 4.41: Discharge curve of SC bank and Li-Po battery with a constant 2 A load.**

### 4.3.2 DC-DC Converter

The DC-DC converter was verified and validated in two sections, the switching circuit and the converters operation as a whole. To verify the switching circuit the switching frequency, voltage and PWM duty cycle was compared at the output of the Arduino to that of the input at the MOSFET gate. Initially this was done with a specified PWM signal where after an input voltage was supplied and the response of the Arduino was measured. To validate the switching circuit the input voltage was varied and the response of the Arduino was compared to that which was desired to assess the level of deviation. To verify the operation of the converter as a whole an input was supplied and the output was measured to determine the deviation from the desired 50 V. To validate this operation the waveforms of the inductor and output capacitor were compared to those of the simulations and previously published works. This was all completed in section 4.2.1.

### 4.3.3 Integrated system

For this section the SC bank with DC-DC converter will first need to be verified – this is done through showing that the energy supplied at the output of the converter meets the requirements of the load.

To validate its operation the SC bank and DC-DC converter need to provide the required energy for each combination and also show that the SC bank is in fact being used – this is done through the use of the SOC curves for each test. These verification and validation methods mentioned have been completed and shown in section 4.2.2.

To verify the operation of the proposed SC and FC hybridizations it is necessary to show that the systems actually function to provide the power required by the load and also to show that each power source is in fact contributing to the power supplied to the load. This is shown in section 4.2.2.3, this was also achieved through the use of two rounds of each test. To validate the results the operation of each combination needs to be compared to each other to show that there is a variance in the results obtained. This is done in section 4.2.2.4 using Table 4.4 and its explanation. Finally, the results from the tests will be used to obtain specific variables that can be used to compare the different combinations and determine the effect of each. The comparison of these variables is presented in Figure 4.42.

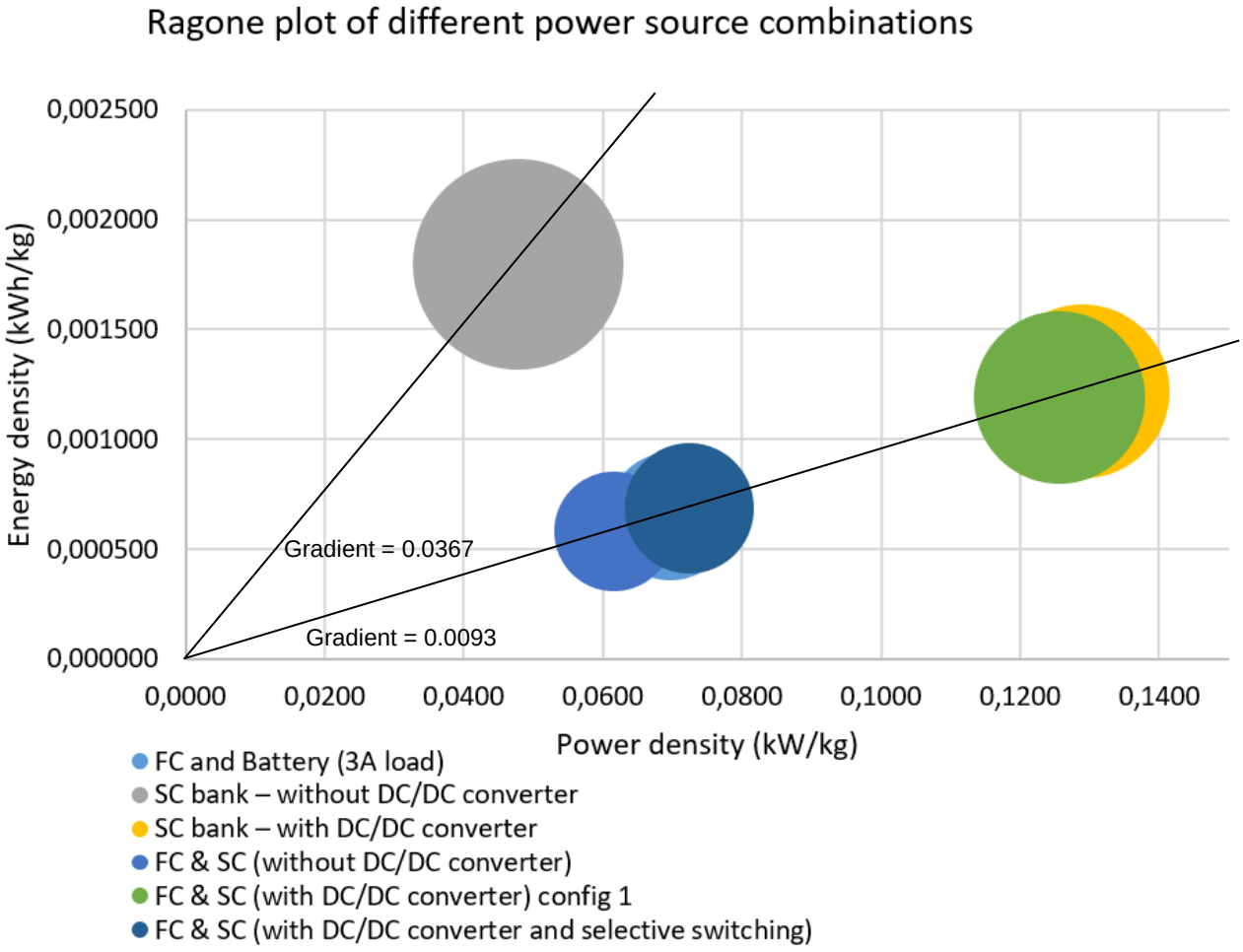


**Figure 4.42: Ragone plot containing experimental results of different power source combinations**

Comparing this achieved Ragone plot to that of Figure 1.1 it is observed that the experimental FC system utilizes a buffer battery thus affording it a larger power density and lower energy density – therefore lying in a more central position on the experimental Ragone plot as compared to the

referenced Ragone plot. A further observation is that the SC banks (with- and without the DC-DC converter) have a larger energy density than the FC system in both Ragone plots – this is firstly due to the FC system replacement chosen to have a smaller capacity such that the effect of the SC bank can better be observed and secondly due to the capacity of the SC bank being designed for the available FC system and full 1 kW load profile.

The DC-DC converter is seen to significantly improve the power density of the system with a larger factor than the decrease caused in the energy density. The graph contains two diagonal lines whose gradient is determined by dividing the y-axis by the x-axis – this delivers the endurance of each combination. It is noteworthy to bear in mind that these densities are calculated using the weight of each system and therefore the endurance is affected by this weight, with the unaided SC bank having the lowest weight of 0.5 kg.

The three FC-SC combinations fall on the same gradient thus delivering a similar endurance with respect to the weight variance of each (seen in Table 4.4). By simply adding the unaided SC bank to the FC system, the energy- and power densities of the FC system experience a considerable decrease. When the DC-DC converter is included in the FC-SC combinations a noteworthy improvement in the densities of the FC system is observed. As mentioned the weight of the system plays a significant role in the calculation of these densities, it is thus understandable that the addition of the SC bank caused a decrease in the densities of the FC system, however, as the DC-DC converter and switching module add an additional weight to the unaided FC-SC system, the increase in the densities is of much more interest and is considerably more significant than observed on the graph.

Another noteworthy observation is that of the difference between the densities achieved between the FC-SC (with DC-DC converter) with and without selective switching. Without selective switching the addition of the DC-DC converter no longer required the utilization of the FC to recharge the SC bank, resultantly leading to an increase in the duration of the FC system and both the densities.

The addition of the selective switching element increased the use of the FC as the SC bank was only utilized at specified instances of the load – thus leading to a large reduction in the usable time of the combination. As the power and energy density are reliant on the usable duration of the system – these too where reduced.

From the Ragone plot it is evident that the addition of a SC bank does lead to an overall improvement to the FC system, but only if the FC system is prohibited from recharging the SC bank.

### 4.3.4 Comparison

In order to complete the verification and validation process the results obtained from simulations and the experiments will be compared using Table 4.5, for this comparison the methods discussed in section 3.2.6 and section 4.3.

The verification process involves determining whether the operation of the system is correct – for this the experimental and simulated values are compared to each other and the desired values. Starting with the SC bank it is seen that it delivers a power closer to that of the desired value during experiments and an energy less than but still within acceptable limits compared to that desired. The DC-DC converter delivered an energy from the SC bank in response to the load verifying its operation.

**Table 4.5: Validation and verification comparison and deviation of simulations and experiments**

| **Verification** | | | | |
|---|---|---|---|---|
| | | **Desired** | **Simulated** | **Experimental** |
| **SC** | **Weight (g)** | 800 | 571.2 | 600 |
| | **Power (W)** | 25.08 | 23.93 | 24.68 |
| | **Energy (J)** | 840.27 | 837.65 | 828 |
| **DC-DC ($V_{in}$ =17.5 V)** | **Duty cycle (%)** | 65 | 72 | 67 |
| | **$f_{SW}$ (kHz)** | 62.5 | 62.5 | 62.5 |
| | **$V_{out}$ (V)** | 50 | 50.6 | 49.62 |
| | **Voltage ripple (%)** | 5 | 1.6 | 7.69 |
| | **Current ripple (%)** | 20-40 | 1.6 | 17.8 |
| **SC-DC-DC** | **Energy at DC-DC input (J)** | 933.64 | 657.39 | 850.24 |
| | **Energy at DC-DC output (J)** | 840.27 | 577.97 | 808.43 |
| **SC-FC** | **Combined Energy (J)** | 829.54 | 900.18 | 820.26 |
| | **SC contribution (J)** | 663.63 | 314.70 | 188.39 |
| | **FC contribution (J)** | 331.82 | 864.55 | 798.45 |
| **SC-FC with DC-DC** | **Combined Energy (J)** | 840.34 | 771.81 | 811.39 |
| | **SC contribution (J)** | 504.20 | 304.85 | 115.80 |
| | **FC contribution (J)** | 336.13 | 492.46 | 715.76 |
| **SC-FC with DC-DC & selective switching** | **Combined Energy (J)** | 841.41 | 802.40 | 800.55 |
| | **SC contribution (J)** | 504.84 | 40.28 | 139.97 |
| | **FC contribution (J)** | 201.94 | 714.81 | 679.04 |
| **Validation** | | | | |
| | | **Desired** | **Simulated** | **Experimental** |
| **SC** | **Energy - configuration 1 (J)** | 4167 | 5878.82 | - |
| | **Energy - configuration 2 (J)** | 4167 | 6890.63 | - |
| | **Energy - configuration 3 (J)** | 4167 | 4899.21 | - |
| **DC-DC $V_{in}$ = 17.5 V** | **Voltage ripple (%)** | 5 | 9.05 | 7.69 |
| | **Current ripple (%)** | 20-40 | 1.6 | 17.8 |
| | **$V_{out}$ (V)** | 50 | 50.6 | 49.62 |
| **DC-DC $V_{in}$ = 19.5 V** | **Voltage ripple (%)** | 5 | 1.45 | 7.69 |
| | **Current ripple (%)** | 20-40 | 1.38 | 17.8 |
| | **$V_{out}$ (V)** | 50 | 50.4 | 49.5 |

**Table 4.5: Validation and verification comparison and deviation of simulations and experiments (continued)**

| Validation | | | | |
|---|---|---|---|---|
| | | **Desired** | **Simulated** | **Experimental** |
| **DC-DC $V_{in}$ = 21.5 V** | **Voltage ripple (%)** | 5 | 1.4 | 7.69 |
| | **Current ripple (%)** | 20-40 | 1.39 | 17.8 |
| | **$V_{out}$ (V)** | 50 | 50.3 | 49.76 |
| **SC-DC-DC** | **Efficiency (%)** | > 90 | 87.92 | 95.08 |
| **SC-FC** | **Efficiency (%)** | > 90 | 99.99 | 97.09 |
| | **Duration (s)** | | 250.00 | 160 |
| | **FC power contribution (%)** | 40 | 65.04 | 77.03 |
| | **SC power contribution (%)** | 60 | 34.96 | 22.97 |
| **SC-FC with DC-DC** | **Efficiency (%)** | > 90 | 99.91 | 96.25 |
| | **Duration (s)** | | 403.00 | 213.56 |
| | **FC power contribution (%)** | 40 | 63.81 | 88.21 |
| | **SC power contribution (%)** | 60 | 39.50 | 14.27 |
| **SC-FC with DC-DC & selective switching** | **Efficiency (%)** | > 90 | 99.66 | 94.29 |
| | **Duration (s)** | | 293.00 | 223.43 |
| | **FC power contribution (%)** | 40 | 89.08 | 84.82 |
| | **SC power contribution (%)** | 60 | 5.02 | 17.48 |

The final tests for verification of the system involved determining whether each power source (in the FC-SC combinations) contributed to the energy supplied by the system in response to the load as well as determining whether the energy supplied was sufficient compared to that required. It is assumed that eh SC bank will supply 60% of the energy while the FC system supply the remaining 40% - these values of the combined energy have been calculated for the verification categories. For both the experimental and simulated results the reverse is observed, where the FC system supplies over 60% of the energy for all the contributions.

The validation process involves comparing the different combinations to each other in order to validate that the did yield some differences. The SC bank was validated through comparing the different energy levels obtained from the various configurations discussed in section 3.2.6.1, showing that the chosen configuration (configuration 2) indeed delivers the highest amount of energy from the SC bank. The DC-DC converter is validated through comparing the voltage-and current ripples and the output voltage deliverance with various voltage inputs. It is observed that the current ripples achieved through experimentation are closer to the desired values than those achieved through simulation. No noteworthy deviations were observed in the output voltages achieved in the experiments and simulations, with both achieving the desired output voltage.

The DC-DC converter is validated through comparing the efficiencies of the simulated and experimental results to each other and that required. The converter achieved a better efficiency and within the desired range during experimentation compared to simulations (94% vs 87%). The final validation process involves the validation of the SC-FC combinations – this is achieved through comparing the results obtained for each combination to each other in simulation and experimental results. For the simulations it was found that the combination including only the DC-DC converter

achieved the best endurance, the combination including the selective switching achieved the best endurance during the experimental results. However, not shown in the table but discussed in section 4.2.2.4, the SC-FC combination including only the DC-DC converter achieved a duration of 365 s using configuration 1 during experimentation thus allowing it to yield the best endurance. For both the experimentation and simulation results a decrease in efficiency is observed as each component is added to the system.

## 4.4 Conclusion

In this chapter the implementation of the system was discussed, the results were obtained through various tests and these were analysed. Two different storage devices were discussed and used for the experiments in this chapter – a FC and SC bank. Six different combinations of these sources were implemented and assessed for viability. The best combination was found to be the FC-SC combination with the DC-DC converter and without the use of selective switching – when connected with the after the two sources.

The FC-SC combination with both the DC-DC converter and selective switching was also found to deliver desirable results however, it is found to be questionable as to whether the selective switching method is redundant. It is also found that the DC-DC converter has a negative effect on the efficiency of the SC bank – it reduces the usable time by increasing the energy usage of the SC bank at the converter input whilst decreasing the deliverance of said energy to the required load at its output. The inclusion of the SC bank increased the total efficiency of the power source as a whole and also allowed the FC system to function more optimally to provide energy to the system.

The proposed solution implemented a uni-directional boost converter with the SC bank in order to be able to use a smaller quantity of cells to match the battery it was in place of. This is to reduce costs and also the weight of the overall system as it is designed for application on a drone. The DC-DC converter exhibited an efficiency above 94% and the optimal hybridized storage system obtained an energy density of 0.696 Wh/kg and a power density of 73.5 W/kg. The results obtained from this experiment show that,

1. The FC system response to the load requirements is improved with the addition of the SC bank.
2. The use of a DC-DC converter reduced the efficiency of the SC bank although improving the efficiency of the FC-SC combinations – this is mainly due to its unidirectional flow characteristics.
3. The applied selective switching does not offer any significant improvement to the system.
4. The usable duration of the system is highly dependent on the order of connection of the power sources.

All the results were verified and validated with those from the literature study and the design simulations of the project. The results obtained in this section have been processed and submitted as an article provided in Appendix C. The next chapter presents the conclusion of this dissertation providing a brief summary of the project and also any recommendations for future improvements.

# CHAPTER 5: CONCLUSION

The final chapter of this dissertation discusses the project as a whole, giving special attention to the key research questions from Chapter 1 as well as detailing the verification and validation process of the project. A summary of the project is supplied giving recommendations of future improvements to the project and finally a conclusion is provided.

## 5.1 Key Research Questions

In section 1.5.4 key research questions were presented that would serve as a basis on whether the project was completed successfully or not. These questions are listed below and will be answered in this section to determine completion of the project.

1. How does the SC bank affect the operation of the FC?

   With the FC system replaced by a laboratory power source it is able to provide 0.545 Wh for three repetitions of the load in response to the 0.714 Wh required, shown in Figure 4.19. With the addition of the SC bank it provides 0.665 Wh without the DC-DC converter (Figure 4.29), 0.597 Wh with the DC-DC converter (Figure 4.33) and 0.566 Wh when using selective switching (Figure 4.37) in response to the load – with the remainder of the requirement supplied by the SC bank. The first combination contains two components – that supplied to the load (0.534 Wh) and that supplied to the SC bank for recharge (0.131 Wh) – thus leading to an actual decrease of 2.01% in energy deliverance by the FC. The last two combinations improve this FC energy deliverance by 9.54% and 3.85%, respectively. Although the FC system still does not supply the entire load its functionality is improved with the addition of the SC bank.

2. Was the SC able to improve the provision of the peak power requirements of the system?
   When the SC bank was used to supply the load unaided, the bank was able to supply 97.79% of the peak power requirements for the two instances mentioned in section 3.2.1.2. This deliverance is illustrated in Figure 4.21. When the SC bank was combined with the FC system it was able to increase the individual FC system peak deliverance of 67.99% to 95.30% as a combined system. This combined deliverance is illustrated in Figure 4.28 and the peak power deliverances for each combination are provided Table 4.4. The system was initially designed such that the SC bank would aid the FC system when peak power demands exceeded that of its capabilities and the experiment set out to investigate the effect of the SC on these instances mentioned in section 3.2.1.2. Through the experimental tests it has been confirmed that the SC bank can improve the peak power performance of the FC system.

3. Which combination of SCs and FC provided the longest flight time?

   Due to the unavailability of a smaller FC system for experimental purposes, the original FC system still has the longest flight time of 16800 s, however when replaced with the laboratory power source the flight time was decreased to 168 s. The FC-SC combination without a DC-DC converter or selective switching delivered 160 s of use; the FC-SC combination with a DC-DC converter and without selective switching delivered 365 s of use; and the FC-SC combination utilizing both a DC-DC converter and selective switching delivered 223 s of use. The combination with the DC-DC converter sans selective switching was only able to deliver this large endurance when combined with the load after the two sources as shown in Figure 3.34 for configuration 1. When connected as in configuration 2 the system could only provide 214 s of use. Thus, the best combination of the power sources is one utilizing a DC-DC converter and having the power sources first connected to each other with the load at the end.

4. Which combination of SCs and FC had the best power- and energy density?

   With reference to the Ragone plot of Figure 4.42, the FC replacement provided 69.7 W/kg and 0.65 Wh/kg, the unaided SC bank provided 47.9 W/kg and 1.80 Wh/kg, the SC-DC-DC converter combination provided 128.9 W/kg and 1.22 Wh/kg, the unaided FC-SC combination provided 61.5 W/kg and 0.58 Wh/kg, the FC-SC with DC-DC converter combination provided 73.5 W/kg and 0.70 Wh/kg and finally the FC-SC with DC-DC converter and selective switching provided 72.4 W/kg and 0.68 Wh/kg, all in response to the load for the full duration of each combination. This shows that the SC bank with DC-DC converter achieved the best power- and energy density. However, of the FC-SC combinations the combination with DC-DC converter has the best power- and energy density. The inclusion of selective switching also provided superior densities compared to the other combinations with only a slight deviation from the combination sans selective switching.

5. Is the system better or worse than the current system?

   If all the results are compared to the original FC system and its response to the full 9 A load, section 4.2.2.1 – these systems achieve no improvement to the current system as the best combination provided 365 s of use whereas the current system can provide 16800 s of use, a staggering 2.17% of what is currently available. However, as the current system has no basis for comparison between the other sources the FC system replacement must be used. Using Table 4.4 and comparing all the results to the FC system replacement, the addition of the SC bank does provide a significant improvement in the endurance of the system, from 168 s to 365 s. It not only increases the energy output of the system as a whole (from 0.54 Wh to 0.69 Wh), but it also improves the response of the FC system to the applied load (from 0.54Wh to 0.6 Wh). The

best system provided an efficiency of 96.25% compared to the 76.27% provided by the FC system replacement.

## 5.2 Verification and Validation

The verification and validation process that was followed throughout this project will be discussed in detail in this section, using Figure 5.1 as reference.

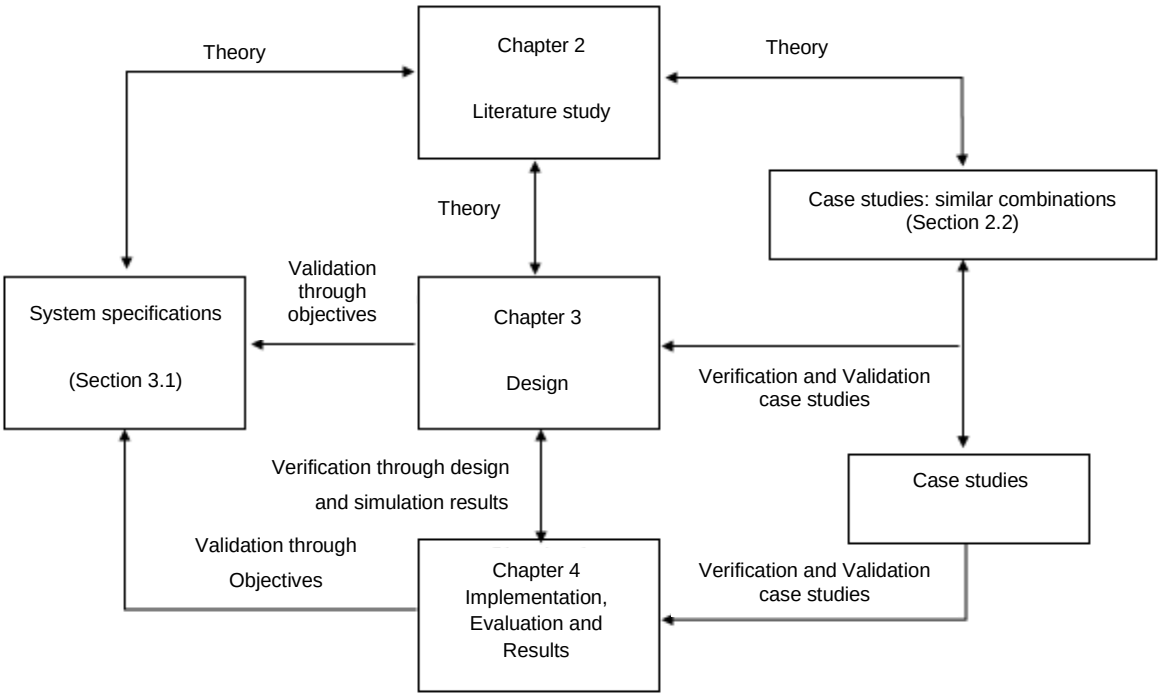


**Figure 5.1: Verification and Validation process**

The literature study of section 2.2 was used to identify case studies of similar projects that have already been completed to use as a basis of reference for the objectives listed in section 1.3, the system requirements listed in section 3.1.1 and also to design the operation and testing methods of the system.

The references used in the literature study of the DC-DC converter in section 2.4 were consulted to design the converter in section 3.2.3, verifying the correct operation of the simulations. The simulations were then validated using these references once again. Two simulation software packages were applied to further verify and validate the results obtained from each and with the references articles. These designs were obtained through the combination of various previous case studies.

The verification and validation of the experimental system in section 4.1 was conducted in sections to ensure that each section functioned correctly, as determined by the previous articles, before integration of the sections occurred. These results were first compared to those obtained in the simulations for verification and validation purposes – the operation of the DC-DC converter was seen

to closely resemble that which was expected and obtained through the simulations. The combined system was then verified and validated through the use of previous case studies and the simulated results of section 3.2.5. The implemented system was finally compared to the system requirements and objectives to further verify and validate that the correct system was built.

## 5.3 Summary

In finalizing the completion of this dissertation and project a summary is required of the respective chapter – this will be provided in this section.

Chapter 1 starts with a brief background to this study; the problem of sufficient energy supply to UAVs pertaining to the specific necessity of minimal weight considerations whilst maintaining an extended flight endurance is presented with the suggested objectives of utilizing a hybrid system containing a FC and SC bank. The primary objective is to assess how the addition of SCs to an existing FC system can affect the functionality thereof and the secondary objectives include the steps required to achieve this eventual result. The scope and research methodology of this study were discussed and the citations of publications achieved and/ under review as a result of this study were listed.

Chapter 2 pertained to the literature study of the major topics relevant to this research. These include: Alternative solutions to the problem, Case studies of similar hybridization topologies, Energy sources mainly used in drones and DC-DC converters and their respective elements. The review of these topics is imperative for this study as they bring light to gaps in the understanding of these topics and also assist in determining methods of verification and validation of the dissertation. The literature review helps understand how the problem statement presented in Chapter 1 needs to be addressed.

The design and simulation of the proposed solution is presented in Chapter 3. First the system requirements were laid out to understand how the solution can address the problem. The design of the system had two major components – the SC bank and the DC-DC converter. The SC bank needed to be designed for a specific purpose and thus required specific characteristics, these characteristics where listed and the calculations required for their acquisition were presented. The SCs needed to match the capacity of the existing Li-Po battery and it was found that this is achieved if a DC-DC converter is utilized.

A single input uni-directional boost DC-DC converter reviewed in Chapter 2 was selected and designed for the use with the SC bank. As it is desired that the SC bank match the voltage of the Li-Po battery whilst maintaining minimal weight a boost converter is required. SCs are suggested for use with regenerative breaking as these are large bursts of energy that can sufficiently recharge the SCs within a short period of time. It is required that the SCs not be able to accept energy from other components in the system – hence the uni-directionality. The calculations of this converter and the

other requirements were presented and discussed. As this system is designed for drone use it is heavily dependent on size and weight, therefore a PCB was designed to reduce the size of the system – this design is presented in the chapter.

Chapter 3 also included the design and simulation of the proposed circuit for the combined system – it presented the proposed switching circuit and the simulations thereof providing the results for comparison. The separate components of the circuit as well as the switching circuit were verified and validated in the last section of this chapter.

Chapter 4 contains the implementation, evaluation and results for the suggested hybrid combinations of the power sources. The DC-DC converter was tested for operation with the available FC system and was seen to function as desired – this was verified and validated in this section against the simulations and previous case studies. A load profile was obtained from an existing hydrogen drone to be used for the experimentations – this load profile was used to obtain the functionality of the available FC system and the Li-Po battery pack.

Due to the suggestions of previous case studies it was desired to observe the response of the SC bank, without the DC-DC converter, to the load when used individually as well as in combination with the FC system. For this it was necessary to replace the FC system with one of a lower voltage rating similar to that of the maximum of the SC bank. It was noted that the available FC system delivers a constant voltage and current output regardless of the load and as such it was decided to be replaced with a laboratory power source for the remainder of the experiments. The laboratory power source has a maximum current rating of 3 A and therefore it was decided to reduce the load profile to a maximum of 21.1 V and 3 A and utilize the laboratory power source at a maximum of 1.6 A, as the FC system, for a better observation of the effect of the SC bank.

The SC bank was tested with and without the DC-DC converter to determine the efficiencies in both cases as well as determine the effect of the converter on the SC banks operation. It was seen that the DC-DC converter decreased the efficiency of the SC bank and reduced the usable time thereof and it was thus concluded that the DC-DC converter had a negative effect on the DC-DC converter. This was further justified through the tests conducted on the FC-SC combinations where the only benefit observed was the decrease in size and weight of the SC bank. The FC system and SC bank were combined in three configurations – purely parallel, separated through a DC-DC converter and finally using selective switching. Each combination was also tested using two different connection topologies – with the load in parallel after the power source connections and with the load parallel between the power sources. It was found that the addition of the SC bank to the FC system improved the systems response to the load as well as the FCs response individually. The best combination was found to be the FC-SC combination with a DC-DC converter and the load after the two power

sources. It was found that the order of connections played a vital role in the overall duration of the hybrid system – such that the selective switching module is found infeasible.

The verification and validation of the system as a whole was conducted through the comparison of the different test results with each other, the simulated values and the previous case studies. The converter efficiency was found to be greater than 90% for all applicable tests and the results concluded that the hybrid system functioned appropriately delivering the desired power in response to the load with deviations around 5%. At the end of Chapter 4 it was concluded that selective switching need not be applied to the hybrid system if sufficient time is taken to determine the best connection of the power sources to the load. It was also concluded that the SC bank does in fact improve the efficacy of the FC system.

In this, the final chapter of the dissertation, the key research questions are revisited and appropriately answered, the verification and validation of the entire project is discussed, a summary of the dissertation is presented and recommendations for future research and adjustments are offered. This chapter will close with the conclusion.

### 5.4 Adjustments and Recommendations

Through the research completed in this dissertation opportunities for additional research and room for improvement to the project arouse, which are as follows:

- As the DC-DC converter is seen to decrease the efficacy of the SC bank it is suggested to examine these results at a higher power demand to assess whether the efficiency drop increases and the benefit of the reduced weight of the system justifies this increase.

- These experiments were conducted using a FC system that already contains and utilizes a battery for supplementation, thus it was not possible to adjust the use of the battery. For future research it is recommended that a FC system be used where the use of all three sources can be controlled to further improve/ assess the effects thereof.

- This system has only been tested in a theoretical and simulated environment using the load profile of a drone and should therefore in future be implemented on a drone in order to test the actual operation in a real environment.

- SCs are great at storing reverse/negative energy such as that which is present during breaking or when a drone decreases altitude – this is also seen in the hybrid test without the DC-DC converter. As this current system was not applied to an actual drone, it is recommended that if the system is integrated with a drone this concept be applied which would lead to a further increase in the usable time.

## 5.5 Conclusion

This research was conducted to determine whether SCs can improve the efficacy of FCs such that duration and operation of hydrogen FC drones can further be improved. All of the objectives set out in Chapter 1 have been met and fulfilled and the key research questions answered. The hybridization of a FC system with SCs has been proposed, the system has been designed and implemented and the results have been analysed. The results obtained suggest a new method of utilizing the SC bank – with a DC-DC converter to adhere to strict weight considerations in drone applications.

# REFERENCES


[1] Q. Zhai, K. Meng, Z. Y. Dong, and J. Ma, “Modeling and Analysis of Lithium Battery Operations in Spot and Frequency Regulation Service Markets in Australia Electricity Market,” *IEEE Trans. Ind. Informatics*, vol. 13, no. 5, pp. 2576–2586, Oct. 2017, doi: 10.1109/TII.2017.2677969.

[2] Z. F. Pan, L. An, and C. Y. Wen, “Recent advances in fuel cells based propulsion systems for unmanned aerial vehicles,” *Appl. Energy*, vol. 240, no. February, pp. 473–485, Apr. 2019, doi: 10.1016/j.apenergy.2019.02.079.

[3] A. M. Jawad, H. M. Jawad, R. Nordin, S. K. Gharghan, N. F. Abdullah, and M. J. Abu-Alshaeer, “Wireless Power Transfer With Magnetic Resonator Coupling and Sleep/Active Strategy for a Drone Charging Station in Smart Agriculture,” *IEEE Access*, vol. 7, pp. 139839–139851, 2019, doi: 10.1109/ACCESS.2019.2943120.

[4] D. Lee, J. Zhou, and W. T. Lin, “Autonomous battery swapping system for quadcopter,” in *2015 International Conference on Unmanned Aircraft Systems (ICUAS)*, 2015, pp. 118–124, doi: 10.1109/ICUAS.2015.7152282.

[5] E. Schmitt, “U.S. Drones Crowd Iraq’s Skies to Fight Insurgents,” *The New York Times*, 2005. [Online]. Available: https://www.nytimes.com/2005/04/05/world/middleeast/us-drones-crowd-iraqs-skies-to-fight-insurgents.html. [Accessed: 07-Dec-2020].

[6] R. Kellermann, T. Biehle, and L. Fischer, “Drones for parcel and passenger transportation: A literature review,” *Transp. Res. Interdiscip. Perspect.*, vol. 4, p. 100088, Mar. 2020, doi: 10.1016/j.trip.2019.100088.

[7] T. F. Shmelova and D. I. Bondarev, “Graph theory applaying for Quantitative estimation of UAVs group flight into Aerial photography,” *Electron. Control Syst.*, vol. 4, no. 46, Dec. 2015, doi: 10.18372/1990-5548.46.9982.

[8] M. Alwateer, S. W. Loke, and N. Fernando, “Enabling Drone Services: Drone Crowdsourcing and Drone Scripting,” *IEEE Access*, vol. 7, pp. 110035–110049, 2019, doi: 10.1109/ACCESS.2019.2933234.

[9] A. Butler and D. A. Fulghum, “U.S. Air Force wants to be Pentagon’s UAV manager, but the plan has Army and Navy officials worried,” *Aviat. Week Sp. Technol.*, vol. 162, no. 10, p. 22, 2005.

[10] L. Tang and G. Shao, “Drone remote sensing for forestry research and practices,” *J. For. Res.*, vol. 26, no. 4, pp. 791–797, 2015, doi: 10.1007/s11676-015-0088-y.

[11] V. Aravindan, J. Gnanaraj, Y.-S. Lee, and S. Madhavi, “Insertion-Type Electrodes for Nonaqueous Li-Ion Capacitors,” *Chem. Rev.*, vol. 114, no. 23, pp. 11619–11635, Dec. 2014, doi: 10.1021/cr5000915.

[12] M. Alwateer, S. W. Loke, and A. M. Zuchowicz, “Drone services: issues in drones for location-based services from human-drone interaction to information processing,” *J. Locat. Based Serv.*, vol. 13, no. 2, pp. 94–127, Apr. 2019, doi: 10.1080/17489725.2018.1564845.

[13] L. Ruan *et al.*, “Energy-efficient multi-UAV coverage deployment in UAV networks: A game-theoretic framework,” *China Commun.*, vol. 15, no. 10, pp. 194–209, Oct. 2018, doi: 10.1109/CC.2018.8485481.

[14] A. Claesson *et al.*, “Drones may be used to save lives in out of hospital cardiac arrest due to drowning,” *Resuscitation*, vol. 114, pp. 152–156, May 2017, doi: 10.1016/j.resuscitation.2017.01.003.

[15] S. W. Loke, M. Alwateer, and V. S. A. Abeysinghe Achchige Don, “Virtual Space Boxes and Drone-as-Reference-Station Localisation for Drone Services,” in *Proceedings of the 2nd Workshop on Micro Aerial Vehicle Networks, Systems, and Applications for Civilian Use - DroNet ’16*, 2016, pp. 45–48, doi: 10.1145/2935620.2935627.

[16] A. Shukla, H. Xiaoqian, and H. Karki, “Autonomous tracking and navigation controller for an unmanned aerial vehicle based on visual data for inspection of oil and gas pipelines,” in *2016 16th International Conference on Control, Automation and Systems (ICCAS)*, 2016, pp. 194–200, doi: 10.1109/ICCAS.2016.7832320.

[17] M. Bacco *et al.*, “Smart farming: Opportunities, challenges and technology enablers,” in *2018 IoT Vertical and Topical Summit on Agriculture - Tuscany (IOT Tuscany)*, 2018, pp. 1–6, doi: 10.1109/IOT-TUSCANY.2018.8373043.

[18] G. Ding, Q. Wu, L. Zhang, Y. Lin, T. A. Tsiftsis, and Y.-D. Yao, “An Amateur Drone Surveillance System Based on the Cognitive Internet of Things,” *IEEE Commun. Mag.*, vol. 56, no. 1, pp. 29–35, Jan. 2018, doi: 10.1109/MCOM.2017.1700452.

[19] Ministry of Defence, “Unmanned Aircraft Systems,” *Joint Doctrine Publication*, 2017. [Online]. Available: https://assets.publishing.service.gov.uk/government/uploads/system/uploads/attachment_data/file/673940/doctrine_uk_uas_jdp_0_30_2.pdf. [Accessed: 07-Dec-2020].

[20] F. Schroth, “Drone Energy Sources – Pushing the Boundaries of Electric Flight,” *Drone Industry Insights*, 2017. [Online]. Available: https://droneii.com/drone-energy-sources. [Accessed: 27-Nov-2020].

[21] G. Warwick, “Record-Breaking Zephyr’s Battery Holds eVTOL Potential,” *Aviation Week Network*, 2018. [Online]. Available: https://aviationweek.com/future-aerospace/record-breaking-zephyr-s-battery-holds-evtol-potential.

[22] A. Gong, R. MacNeill, D. Verstraete, and J. L. Palmer, “Analysis of a Fuel-Cell/Battery/Supercapacitor Hybrid Propulsion System for a UAV using a Hardware-in-the-Loop Flight Simulator,” in *2018 AIAA/IEEE Electric Aircraft Technologies Symposium*, 2018, doi: 10.2514/6.2018-5017.

[23] J. Lee *et al.*, “Constructing a reliable and fast recoverable network for drones,” in *2016 IEEE International Conference on Communications (ICC)*, 2016, pp. 1–6, doi: 10.1109/ICC.2016.7511317.

[24] S. Yoo *et al.*, “A Multi-Drone Platform for Empowering Drones’ Teamwork,” in *Proceedings of the 21st Annual International Conference on Mobile Computing and Networking - MobiCom ’15*, 2015, pp. 275–277, doi: 10.1145/2789168.2795180.

[25] J. Zhou, B. Zhang, W. Xiao, D. Qiu, and Y. Chen, “Nonlinear Parity-Time-Symmetric Model for Constant Efficiency Wireless Power Transfer: Application to a Drone-in-Flight Wireless Charging Platform,” *IEEE Trans. Ind. Electron.*, vol. 66, no. 5, pp. 4097–4107, May 2019, doi: 10.1109/TIE.2018.2864515.

[26] M. Lu, M. Bagheri, A. P. James, and T. Phung, “Wireless Charging Techniques for UAVs: A Review, Reconceptualization, and Extension,” *IEEE Access*, vol. 6, pp. 29865–29884, May 2018, doi: 10.1109/ACCESS.2018.2841376.

[27] T. Das and S. Snyder, “Adaptive Control of a Solid Oxide Fuel Cell Ultra-Capacitor Hybrid System,” *IEEE Trans. Control Syst. Technol.*, vol. 21, no. 2, pp. 372–383, Mar. 2013, doi:

10.1109/TCST.2011.2181514.

[28] J. R. Meacham, F. Jabbari, J. Brouwer, J. L. Mauzey, and G. S. Samuelsen, “Analysis of stationary fuel cell dynamic ramping capabilities and ultra capacitor energy storage using high resolution demand data,” *J. Power Sources*, vol. 156, no. 2, pp. 472–479, Jun. 2006, doi: 10.1016/j.jpowsour.2005.05.094.

[29] T. Campi, S. Cruciani, M. Feliziani, and F. Maradei, “High efficiency and lightweight wireless charging system for drone batteries,” in *2017 AEIT International Annual Conference*, 2017, vol. 2017-Janua, pp. 1–6, doi: 10.23919/AEIT.2017.8240539.

[30] S. Aldhaher, P. D. Mitcheson, J. M. Arteaga, G. Kkelis, and D. C. Yates, “Light-weight wireless power transfer for mid-air charging of drones,” in *2017 11th European Conference on Antennas and Propagation (EUCAP)*, 2017, pp. 336–340, doi: 10.23919/EuCAP.2017.7928799.

[31] X. He, J. Bito, and M. M. Tentzeris, “A drone-based wireless power transfer anc communications platform,” in *2017 IEEE Wireless Power Transfer Conference (WPTC)*, 2017, pp. 1–4, doi: 10.1109/WPT.2017.7953846.

[32] T. Campi, F. Dionisi, S. Cruciani, V. De Santis, M. Feliziani, and F. Maradei, “Magnetic field levels in drones equipped with Wireless Power Transfer technology,” in *2016 Asia-Pacific International Symposium on Electromagnetic Compatibility (APEMC)*, 2016, pp. 544–547, doi: 10.1109/APEMC.2016.7522793.

[33] M. Simic, C. Bil, and V. Vojisavljevic, “Investigation in Wireless Power Transmission for UAV Charging,” *Procedia Comput. Sci.*, vol. 60, pp. 1846–1855, Dec. 2015, doi: 10.1016/j.procs.2015.08.295.

[34] S. Das Barman, A. W. Reza, N. Kumar, M. E. Karim, and A. B. Munir, “Wireless powering by magnetic resonant coupling: Recent trends in wireless power transfer system and its applications,” *Renew. Sustain. Energy Rev.*, vol. 51, pp. 1525–1552, Nov. 2015, doi: 10.1016/j.rser.2015.07.031.

[35] N. Zhao, S. Zhang, F. R. Yu, Y. Chen, A. Nallanathan, and V. C. M. Leung, “Exploiting Interference for Energy Harvesting: A Survey, Research Issues, and Challenges,” *IEEE Access*, vol. 5, pp. 10403–10421, May 2017, doi: 10.1109/ACCESS.2017.2705638.

[36] T. Campi, S. Cruciani, G. Rodriguez, and M. Feliziani, “Coil design of a wireless power transfer charging system for a drone,” in *2016 IEEE Conference on Electromagnetic Field Computation (CEFC)*, 2016, vol. 51, no. 1, pp. 1–1, doi: 10.1109/CEFC.2016.7816070.

[37] A. Costanzo *et al.*, “Electromagnetic Energy Harvesting and Wireless Power Transmission: A Unified Approach,” *Proc. IEEE*, vol. 102, no. 11, pp. 1692–1711, Nov. 2014, doi: 10.1109/JPROC.2014.2355261.

[38] J. Garnica, R. A. Chinga, and J. Lin, “Wireless Power Transmission: From Far Field to Near Field,” *Proc. IEEE*, vol. 101, no. 6, pp. 1321–1331, Jun. 2013, doi: 10.1109/JPROC.2013.2251411.

[39] Liguang Xie, Yi Shi, Y. T. Hou, and A. Lou, “Wireless power transfer and applications to sensor networks,” *IEEE Wirel. Commun.*, vol. 20, no. 4, pp. 140–145, Aug. 2013, doi: 10.1109/MWC.2013.6590061.

[40] X. Lu, P. Wang, D. Niyato, D. I. Kim, and Z. Han, “Wireless Charging Technologies: Fundamentals, Standards, and Network Applications,” *IEEE Commun. Surv. Tutorials*, vol. 18, no. 2, pp. 1413–1452,

2016, doi: 10.1109/COMST.2015.2499783.

[41] K. Sang-Won, C. In-Kui, and H. Sung-Yong, “Comparison of charging region differences according to receiver structure in drone wireless charging system,” in *2017 International Conference on Information and Communication Technology Convergence (ICTC)*, 2017, pp. 1058–1060, doi: 10.1109/ICTC.2017.8190853.

[42] C. H. Choi, H. J. Jang, S. G. Lim, H. C. Lim, S. H. Cho, and I. Gaponov, “Automatic wireless drone charging station creating essential environment for continuous drone operation,” in *2016 International Conference on Control, Automation and Information Sciences (ICCAIS)*, 2016, pp. 132–136, doi: 10.1109/ICCAIS.2016.7822448.

[43] T. M. Mostafa, A. Muharam, and R. Hattori, “Wireless battery charging system for drones via capacitive power transfer,” in *2017 IEEE PELS Workshop on Emerging Technologies: Wireless Power Transfer (WoW)*, 2017, pp. 1–6, doi: 10.1109/WoW.2017.7959357.

[44] G. SACHS, “Minimum shear wind strength required for dynamic soaring of albatrosses,” *Ibis (Lond. 1859).*, vol. 147, no. 1, pp. 1–10, Dec. 2004, doi: 10.1111/j.1474-919x.2004.00295.x.

[45] Y. J. Zhao and Y. C. Qi, “Minimum fuel powered dynamic soaring of unmanned aerial vehicles utilizing wind gradients,” *Optim. Control Appl. Methods*, vol. 25, no. 5, pp. 211–233, Sep. 2004, doi: 10.1002/oca.744.

[46] P. Lissaman, “Wind Energy Extraction by Birds and Flight Vehicles,” in *43rd AIAA Aerospace Sciences Meeting and Exhibit*, 2005, doi: 10.2514/6.2005-241.

[47] Syama M, Dineshkumar M, and Arun Kishore W. C., “Trajectory optimization of an autonomous dynamic soaring UAV,” in *2015 International Conference on Control Communication & Computing India (ICCC)*, 2015, pp. 95–100, doi: 10.1109/ICCC.2015.7432875.

[48] P. L. Richardson, “Upwind dynamic soaring of albatrosses and UAVs,” *Prog. Oceanogr.*, vol. 130, pp. 146–156, Jan. 2015, doi: 10.1016/j.pocean.2014.11.002.

[49] V. Bonnin, C. Toomer, J.-M. Moschetta, and E. Benard, “Energy Harvesting Mechanisms for UAV Flight by Dynamic Soaring,” in *AIAA Atmospheric Flight Mechanics (AFM) Conference*, 2013, doi: 10.2514/6.2013-4841.

[50] N. Akhtar, J. Whidborne, and A. Cooke, “Wind Shear Energy Extraction using Dynamic Soaring Techniques,” in *47th AIAA Aerospace Sciences Meeting including The New Horizons Forum and Aerospace Exposition*, 2009, doi: 10.2514/6.2009-734.

[51] M. Boslough, “Autonomous dynamic soaring,” in *2017 IEEE Aerospace Conference*, 2017, pp. 1–20, doi: 10.1109/AERO.2017.7943967.

[52] N. R. J. Lawrance and S. Sukkarieh, “A guidance and control strategy for dynamic soaring with a gliding UAV,” in *2009 IEEE International Conference on Robotics and Automation*, 2009, pp. 3632–3637, doi: 10.1109/ROBOT.2009.5152441.

[53] T. Zhang, X. Zhu, Z. Zhou, R. Wang, and R. Chen, “Energy Management of Solar UAV Level Flight,” in *2018 IEEE International Conference on Prognostics and Health Management (ICPHM)*, 2018, pp. 1–6, doi: 10.1109/ICPHM.2018.8448508.

[54] H. B. Park, J. S. Lee, and K. H. Yu, “Experiment and evaluation of solar powered UAV by virtual flight system,” in *2015 54th Annual Conference of the Society of Instrument and Control Engineers of Japan (SICE)*, 2015, pp. 1052–1057, doi: 10.1109/SICE.2015.7285519.

[55] T. S. Chandrasekar Rao and K. Geetha, “Categories, Standards and Recent Trends in Wireless Power Transfer: A Survey,” *Indian J. Sci. Technol.*, vol. 9, no. 20, May 2016, doi: 10.17485/ijst/2016/v9i20/91041.

[56] C. H. Tie, C. K. Gan, and K. A. Ibrahim, “Probabilistic Impact Assessment of Electric Vehicle Charging on Malaysia Low-Voltage Distribution Networks,” *Indian J. Sci. Technol.*, vol. 8, no. 3, p. 199, Feb. 2015, doi: 10.17485/ijst/2015/v8i3/59576.

[57] Siqi Li and C. C. Mi, “Wireless Power Transfer for Electric Vehicle Applications,” *IEEE J. Emerg. Sel. Top. Power Electron.*, vol. 3, no. 1, pp. 4–17, Mar. 2015, doi: 10.1109/JESTPE.2014.2319453.

[58] B. Sushil Kumar, S. Krithiga, and P. Sarathi Subudhi, “Wireless Electric Vehicle Battery Charging System using PV Array,” *Indian J. Sci. Technol.*, vol. 9, no. 36, Sep. 2016, doi: 10.17485/ijst/2016/v9i36/98147.

[59] S. Jashnani, T. R. Nada, M. Ishfaq, A. Khamker, and P. Shaholia, “Sizing and preliminary hardware testing of solar powered UAV,” *Egypt. J. Remote Sens. Sp. Sci.*, vol. 16, no. 2, pp. 189–198, Dec. 2013, doi: 10.1016/j.ejrs.2013.05.002.

[60] S. Morton, R. D’Sa, and N. Papanikolopoulos, “Solar powered UAV: Design and experiments,” in *2015 IEEE/RSJ International Conference on Intelligent Robots and Systems (IROS)*, 2015, pp. 2460–2466, doi: 10.1109/IROS.2015.7353711.

[61] Z. Guo, X. Chen, Z. Hou, and J. Guo, “Development of a Solar Electric Powered UAV for Long Endurance Flight,” in *11th AIAA Aviation Technology, Integration, and Operations (ATIO) Conference*, 2011, doi: 10.2514/6.2011-6966.

[62] Jaw-Kuen Shiau, Der-Ming Ma, Pin-Ying Yang, Geng-Feng Wang, and Jhij Hua Gong, “Design of a Solar Power Management System for an Experimental UAV,” *IEEE Trans. Aerosp. Electron. Syst.*, vol. 45, no. 4, pp. 1350–1360, Oct. 2009, doi: 10.1109/TAES.2009.5310303.

[63] M. N. Boukoberine, Z. Zhou, and M. Benbouzid, “Power Supply Architectures for Drones - A Review,” in *IECON 2019 - 45th Annual Conference of the IEEE Industrial Electronics Society*, 2019, pp. 5826–5831, doi: 10.1109/IECON.2019.8927702.

[64] T. J. Nugent, Jr. and J. T. Kare, “Laser power beaming for defense and security applications,” in *Proc SPIE*, 2011, p. 804514, doi: 10.1117/12.886169.

[65] Q. Chen, D. Zhang, D. Zhu, Q. Shi, J. Gu, and Y. Ai, “Design and experiment for realization of laser wireless power transmission for small unmanned aerial vehicles,” in *Advances in Laser Technology and Applications*, 2015, p. 96710N, doi: 10.1117/12.2199235.

[66] M. C. Achtelik, J. Stumpf, D. Gurdan, and K.-M. Doth, “Design of a flexible high performance quadcopter platform breaking the MAV endurance record with laser power beaming,” in *2011 IEEE/RSJ International Conference on Intelligent Robots and Systems*, 2011, pp. 5166–5172, doi: 10.1109/IROS.2011.6048336.

[67] Y. Du, K. Wang, K. Yang, and G. Zhang, “Trajectory Design of Laser-Powered Multi-Drone Enabled Data Collection System for Smart Cities,” in *2019 IEEE Global Communications Conference (GLOBECOM)*, 2019, pp. 1–6, doi: 10.1109/GLOBECOM38437.2019.9013552.

[68] T. Chang and H. Yu, “Improving Electric Powered UAVs’ Endurance by Incorporating Battery Dumping Concept,” *Procedia Eng.*, vol. 99, pp. 168–179, Dec. 2015, doi: 10.1016/j.proeng.2014.12.522.

[69] B. Michini *et al.*, “Automated Battery Swap and Recharge to Enable Persistent UAV Missions,” in *Infotech@Aerospace 2011*, 2011, doi: 10.2514/6.2011-1405.

[70] K. A. Swieringa *et al.*, “Autonomous battery swapping system for small-scale helicopters,” in *2010 IEEE International Conference on Robotics and Automation*, 2010, pp. 3335–3340, doi: 10.1109/ROBOT.2010.5509165.

[71] N. K. Ure, G. Chowdhary, T. Toksoz, J. P. How, M. A. Vavrina, and J. Vian, “An Automated Battery Management System to Enable Persistent Missions With Multiple Aerial Vehicles,” *IEEE/ASME Trans. Mechatronics*, vol. 20, no. 1, pp. 275–286, Feb. 2015, doi: 10.1109/TMECH.2013.2294805.

[72] Y. Wang, K. S. Chen, J. Mishler, S. C. Cho, and X. C. Adroher, “A review of polymer electrolyte membrane fuel cells: Technology, applications, and needs on fundamental research,” *Appl. Energy*, vol. 88, no. 4, pp. 981–1007, Apr. 2011, doi: 10.1016/j.apenergy.2010.09.030.

[73] N. Lapeña-Rey, J. A. Blanco, E. Ferreyra, J. L. Lemus, S. Pereira, and E. Serrot, “A fuel cell powered unmanned aerial vehicle for low altitude surveillance missions,” *Int. J. Hydrogen Energy*, vol. 42, no. 10, pp. 6926–6940, Mar. 2017, doi: 10.1016/j.ijhydene.2017.01.137.

[74] J. Katrasnik, F. Pernus, and B. Likar, “A Survey of Mobile Robots for Distribution Power Line Inspection,” *IEEE Trans. Power Deliv.*, vol. 25, no. 1, pp. 485–493, Jan. 2010, doi: 10.1109/TPWRD.2009.2035427.

[75] J. Katrasnik, F. Pernus, and B. Likar, “New Robot for Power Line Inspection,” in *2008 IEEE Conference on Robotics, Automation and Mechatronics*, 2008, pp. 1195–1200, doi: 10.1109/RAMECH.2008.4681335.

[76] F. Morbidi, R. Cano, and D. Lara, “Minimum-energy path generation for a quadrotor UAV,” in *2016 IEEE International Conference on Robotics and Automation (ICRA)*, 2016, pp. 1492–1498, doi: 10.1109/ICRA.2016.7487285.

[77] M. Lu, A. James, and M. Bagheri, “Unmanned Aerial Vehicle (UAV) charging from powerlines,” in *2017 IEEE PES Asia-Pacific Power and Energy Engineering Conference (APPEEC)*, 2017, vol. 2017-Novem, pp. 1–6, doi: 10.1109/APPEEC.2017.8308912.

[78] P. T. Marshall, “Power line sentry charging,” US7318564B1, 2005.

[79] E. . Silberg and J. . Milgram, “Battery charging arrangement for unmanned aerial vehicle utilizing the electromagnetic field associated with utility power lines to generate power to inductively charge energy supplies,” US7714536B1, 2007.

[80] V. Gupta, A. Kandhalu, and R. (Raj) Rajkumar, “Energy harvesting from electromagnetic energy radiating from AC power lines,” in *Proceedings of the 6th Workshop on Hot Topics in Embedded Networked Sensors - HotEmNets ’10*, 2010, p. 1, doi: 10.1145/1978642.1978664.

[81] B. Griffin and C. Detweiler, “Resonant wireless power transfer to ground sensors from a UAV,” in *2012 IEEE International Conference on Robotics and Automation*, 2012, pp. 2660–2665, doi: 10.1109/ICRA.2012.6225205.

[82] M. Soma, D. C. Galbraith, and R. L. White, “Radio-Frequency Coils in Implantable Devices: Misalignment Analysis and Design Procedure,” *IEEE Trans. Biomed. Eng.*, vol. BME-34, no. 4, pp. 276–282, Apr. 1987, doi: 10.1109/TBME.1987.326088.

[83] A. Kurs, A. Karalis, R. Moffatt, J. D. Joannopoulos, P. Fisher, and M. Soljacic, “Wireless Power Transfer via Strongly Coupled Magnetic Resonances,” *Science (80-. ).*, vol. 317, no. 5834, pp. 83–86, Jul. 2007, doi: 10.1126/science.1143254.

[84] J. M. Miller *et al.*, “Demonstrating Dynamic Wireless Charging of an Electric Vehicle: The Benefit of Electrochemical Capacitor Smoothing,” *IEEE Power Electron. Mag.*, vol. 1, no. 1, pp. 12–24, Mar. 2014, doi: 10.1109/MPEL.2014.2300978.

[85] S. Y. Choi, B. W. Gu, S. Y. Jeong, and C. T. Rim, “Advances in Wireless Power Transfer Systems for Roadway-Powered Electric Vehicles,” *IEEE J. Emerg. Sel. Top. Power Electron.*, vol. 3, no. 1, pp. 18–36, Mar. 2015, doi: 10.1109/JESTPE.2014.2343674.

[86] C. Cai *et al.*, “Resonant Wireless Charging System Design for 110-kV High-Voltage Transmission Line Monitoring Equipment,” *IEEE Trans. Ind. Electron.*, vol. 66, no. 5, pp. 4118–4129, May 2019, doi: 10.1109/TIE.2018.2808904.

[87] J. Fabian, M. Hirz, and K. Krischan, “State of the Art and Future Trends of Electric Drives and Power Electronics for Automotive Engineering,” *SAE Int. J. Passeng. Cars - Electron. Electr. Syst.*, vol. 7, no. 1, pp. 2014-01–1888, Apr. 2014, doi: 10.4271/2014-01-1888.

[88] A. Emadi, K. Rajashekara, S. S. Williamson, and S. M. Lukic, “Topological Overview of Hybrid Electric and Fuel Cell Vehicular Power System Architectures and Configurations,” *IEEE Trans. Veh. Technol.*, vol. 54, no. 3, pp. 763–770, May 2005, doi: 10.1109/TVT.2005.847445.

[89] J. Walters, H. Husted, and K. Rajashekara, “Comparative Study of Hybrid Powertrain Strategies,” in *14th International Symposium on Advanced Vehicle Control*, 2001, doi: 10.4271/2001-01-2501.

[90] M. Yilmaz and P. T. Krein, “Review of Battery Charger Topologies, Charging Power Levels, and Infrastructure for Plug-In Electric and Hybrid Vehicles,” *IEEE Trans. Power Electron.*, vol. 28, no. 5, pp. 2151–2169, May 2013, doi: 10.1109/TPEL.2012.2212917.

[91] A. Emadi, Young Joo Lee, and K. Rajashekara, “Power Electronics and Motor Drives in Electric, Hybrid Electric, and Plug-In Hybrid Electric Vehicles,” *IEEE Trans. Ind. Electron.*, vol. 55, no. 6, pp. 2237–2245, Jun. 2008, doi: 10.1109/TIE.2008.922768.

[92] P. Bajec, D. Voncina, D. Miljavec, and J. Nastran, “Bi-directional power converter for wide speed range integrated starter-generator,” in *2004 IEEE International Symposium on Industrial Electronics*, 2004, vol. 2, pp. 1117–1122 vol. 2, doi: 10.1109/ISIE.2004.1571970.

[93] L. Chedot, G. Friedrich, J.-M. Biedinger, and P. Macret, “Integrated Starter Generator: The Need for an Optimal Design and Control Approach. Application to a Permanent Magnet Machine,” *IEEE Trans. Ind. Appl.*, vol. 43, no. 2, pp. 551–559, Apr. 2007, doi: 10.1109/TIA.2006.889900.

[94] A. K. Jain, S. Mathapati, V. T. Ranganathan, and V. Narayanan, “Integrated starter generator for 42-V powernet using induction machine and direct torque control technique,” *IEEE Trans. Power Electron.*, vol. 21, no. 3, pp. 701–710, May 2006, doi: 10.1109/TPEL.2006.872364.

[95] M. Chen, L. Huang, J. Yang, and Y. Lyu, “Design and simulation of multi-energy hybrid power system based on wave and wind energy,” in *2017 20th International Conference on Electrical Machines and Systems (ICEMS)*, 2017, pp. 1–6, doi: 10.1109/ICEMS.2017.8056368.

[96] D. Kraemer, L. Hu, A. Muto, X. Chen, G. Chen, and M. Chiesa, “Photovoltaic-thermoelectric hybrid systems: A general optimization methodology,” *Appl. Phys. Lett.*, vol. 92, no. 24, p. 243503, Jun. 2008, doi: 10.1063/1.2947591.

[97] J. M. Miller, “Hybrid electric vehicle propulsion system architectures of the e-CVT type,” *IEEE Trans. Power Electron.*, vol. 21, no. 3, pp. 756–767, May 2006, doi: 10.1109/TPEL.2006.872372.

[98] H. Fathabadi, “Plug-In Hybrid Electric Vehicles: Replacing Internal Combustion Engine With Clean and Renewable Energy Based Auxiliary Power Sources,” *IEEE Trans. Power Electron.*, vol. 33, no. 11, pp. 9611–9618, Nov. 2018, doi: 10.1109/TPEL.2018.2797250.

[99] Y. Zhang, Y. Mou, and Z. Yang, “An Energy Management Study on Hybrid Power of Electric Vehicle Based on Aluminum Air Fuel Cell,” *IEEE Trans. Appl. Supercond.*, vol. 26, no. 7, pp. 1–6, Oct. 2016, doi: 10.1109/TASC.2016.2610719.

[100] T. Mesbahi, F. Khenfri, N. Rizoug, P. Bartholomeus, and P. Le Moigne, “Combined Optimal Sizing and Control of Li-Ion Battery/Supercapacitor Embedded Power Supply Using Hybrid Particle Swarm–Nelder–Mead Algorithm,” *IEEE Trans. Sustain. Energy*, vol. 8, no. 1, pp. 59–73, Jan. 2017, doi: 10.1109/TSTE.2016.2582927.

[101] A. Townsend, I. N. Jiya, C. Martinson, D. Bessarabov, and R. Gouws, “A comprehensive review of energy sources for unmanned aerial vehicles, their shortfalls and opportunities for improvements,” *Heliyon*, vol. 6, no. 11, pp. 1–22, Nov. 2020, doi: 10.1016/j.heliyon.2020.e05285.

[102] J. I. Vasquez Gomez, M. M. Melchor, and J. C. Herrera Lozada, “Optimal Coverage Path Planning Based on the Rotating Calipers Algorithm,” in *2017 International Conference on Mechatronics, Electronics and Automotive Engineering (ICMEAE)*, 2017, pp. 140–144, doi: 10.1109/ICMEAE.2017.11.

[103] J. Modares, F. Ghanei, N. Mastronarde, and K. Dantu, “UB-ANC planner: Energy efficient coverage path planning with multiple drones,” in *2017 IEEE International Conference on Robotics and Automation (ICRA)*, 2017, pp. 6182–6189, doi: 10.1109/ICRA.2017.7989732.

[104] T. Glick and S. Arogeti, “Control of Tethered Drones with state and input Constraints - a Unified Model Approach,” in *2018 International Conference on Unmanned Aircraft Systems (ICUAS)*, 2018, pp. 995–1002, doi: 10.1109/ICUAS.2018.8453452.

[105] J. Montanya, J. A. Lopez, P. Fontanes, M. Urbani, O. van der Velde, and D. Romero, “Using tethered drones to investigate ESD in wind turbine blades during fair and thunderstorm weather,” in *2018 34th International Conference on Lightning Protection (ICLP)*, 2018, pp. 1–4, doi: 10.1109/ICLP.2018.8503283.

[106] D. Trends, “Digital Trends,” *Designtechnica corporation*, 2020. [Online]. Available:

https://www.digitaltrends.com/cool-tech/9-awesomely-weird-drone-projects/. [Accessed: 14-Jan-2020].

[107] A. Boggio-Dandry and T. Soyata, “Perpetual Flight for UAV Drone Swarms Using Continuous Energy Replenishment,” in *2018 9th IEEE Annual Ubiquitous Computing, Electronics & Mobile Communication Conference (UEMCON)*, 2018, pp. 478–484, doi: 10.1109/UEMCON.2018.8796684.

[108] J. Bauman and M. Kazerani, “A Comparative Study of Fuel-Cell–Battery, Fuel-Cell–Ultracapacitor, and Fuel-Cell–Battery–Ultracapacitor Vehicles,” *IEEE Trans. Veh. Technol.*, vol. 57, no. 2, pp. 760–769, Mar. 2008, doi: 10.1109/TVT.2007.906379.

[109] P. Thounthong, V. Chunkag, P. Sethakul, B. Davat, and M. Hinaje, “Comparative Study of Fuel-Cell Vehicle Hybridization with Battery or Supercapacitor Storage Device,” *IEEE Trans. Veh. Technol.*, vol. 58, no. 8, pp. 3892–3904, Oct. 2009, doi: 10.1109/TVT.2009.2028571.

[110] J. Otto, “Lead Acid type Storage Battery,” US3257237A, 1965.

[111] D. H. McClelland and J. L. Devitt, “Maintenance-free type Lead acid,” US3862861A, 1972.

[112] S. Ci, N. Lin, and D. Wu, “Reconfigurable Battery Techniques and Systems: A Survey,” *IEEE Access*, vol. 4, pp. 1175–1189, Jan. 2016, doi: 10.1109/ACCESS.2016.2545338.

[113] K. Rajashekara, “Present Status and Future Trends in Electric Vehicle Propulsion Technologies,” *IEEE J. Emerg. Sel. Top. Power Electron.*, vol. 1, no. 1, pp. 3–10, Mar. 2013, doi: 10.1109/JESTPE.2013.2259614.

[114] C. Vidal, O. Gross, R. Gu, P. Kollmeyer, and A. Emadi, “xEV Li-Ion Battery Low-Temperature Effects—Review,” *IEEE Trans. Veh. Technol.*, vol. 68, no. 5, pp. 4560–4572, May 2019, doi: 10.1109/TVT.2019.2906487.

[115] F. T. Wagner, B. Lakshmanan, and M. F. Mathias, “Electrochemistry and the Future of the Automobile,” *J. Phys. Chem. Lett.*, vol. 1, no. 14, pp. 2204–2219, Jul. 2010, doi: 10.1021/jz100553m.

[116] E. Karden, S. Ploumen, B. Fricke, T. Miller, and K. Snyder, “Energy storage devices for future hybrid electric vehicles,” *J. Power Sources*, vol. 168, no. 1, pp. 2–11, May 2007, doi: 10.1016/j.jpowsour.2006.10.090.

[117] Taesic Kim, Wei Qiao, and Liyan Qu, “Power Electronics-Enabled Self-X Multicell Batteries: A Design Toward Smart Batteries,” *IEEE Trans. Power Electron.*, vol. 27, no. 11, pp. 4723–4733, Nov. 2012, doi: 10.1109/TPEL.2012.2183618.

[118] J. Meng, G. Luo, and F. Gao, “Lithium Polymer Battery State-of-Charge Estimation Based on Adaptive Unscented Kalman Filter and Support Vector Machine,” *IEEE Trans. Power Electron.*, vol. 31, no. 3, pp. 2226–2238, Mar. 2016, doi: 10.1109/TPEL.2015.2439578.

[119] R. Components, “FG20201 Lead Acid Battery - 12V, 2Ah.” [Online]. Available: https://za.rs-online.com/web/p/lead-acid-batteries/8431308/. [Accessed: 18-May-2020].

[120] R. Components, “RS PRO 12V NiMH AA Rechargeable Battery Pack, 2000mAh.” [Online]. Available: https://za.rs-online.com/web/p/rechargeable-battery-packs/7770400/. [Accessed: 18-May-2020].

[121] R. Components, “Samsung 3.6V 18650 Lithium-ion Battery, 2000mAh.” [Online]. Available: https://za.rs-online.com/web/p/speciality-size-rechargeable-batteries/8182992/. [Accessed: 18-May-

2020].

[122] R. Components, “RS PRO 12V CS NiCd Rechargeable Battery, 1800mAh.” [Online]. Available: https://za.rs-online.com/web/p/rechargeable-battery-packs/1253427/. [Accessed: 18-May-2020].

[123] R. Components, “RS PRO 1.5V Alkaline AA Battery.” [Online]. Available: https://za.rs-online.com/web/p/aa-batteries/7442199/. [Accessed: 18-May-2020].

[124] R. Components, “RS PRO 3.7V Wire Lead Terminal Lithium Rechargeable Battery, 2000mAh.” [Online]. Available: https://za.rs-online.com/web/p/speciality-size-rechargeable-batteries/1251266/. [Accessed: 18-May-2020].

[125] R. Components, “RS Button Battery, PR44, 1.4V, 11.6mm Diameter.” [Online]. Available: https://za.rs-online.com/web/p/button-batteries/8010730/. [Accessed: 18-May-2020].

[126] Mantech, “Lithium cell/ battery AA 3V6 2.2Ah 14x50.” [Online]. Available: https://www.mantech.co.za/ProductInfo.aspx?Item=310M0007. [Accessed: 18-May-2020].

[127] NASA, “Technology Readiness Level Definitions,” *NASA*, 1989. [Online]. Available: https://www.nasa.gov/pdf/458490main_TRL_Definitions.pdf. [Accessed: 07-Dec-2020].

[128] Ji-Yan Zou, Li Zhang, and Jin-Yan Song, “Development of the 40 V hybrid super-capacitor unit,” *IEEE Trans. Magn.*, vol. 41, no. 1, pp. 294–298, Jan. 2005, doi: 10.1109/TMAG.2004.839290.

[129] M. K. Andreev, “An Overview of Supercapacitors as New Power Sources in Hybrid Energy Storage Systems for Electric Vehicles,” in *2020 XI National Conference with International Participation (ELECTRONICA)*, 2020, pp. 1–4, doi: 10.1109/ELECTRONICA50406.2020.9305104.

[130] K. Zhuge and M. Kazerani, “Development of a hybrid energy storage system (HESS) for electric and hybrid electric vehicles,” in *2014 IEEE Transportation Electrification Conference and Expo (ITEC)*, 2014, pp. 1–5, doi: 10.1109/ITEC.2014.6861868.

[131] M. Ortuzar, J. Moreno, and J. Dixon, “Ultracapacitor-Based Auxiliary Energy System for an Electric Vehicle: Implementation and Evaluation,” *IEEE Trans. Ind. Electron.*, vol. 54, no. 4, pp. 2147–2156, Aug. 2007, doi: 10.1109/TIE.2007.894713.

[132] E. Frackowiak and F. Béguin, “Carbon materials for the electrochemical storage of energy in capacitors,” *Carbon N. Y.*, vol. 39, no. 6, pp. 937–950, May 2001, doi: 10.1016/S0008-6223(00)00183-4.

[133] A. F. Burke, J. E. Hardin, and E. J. Dowgiallo, “Application of ultracapacitors in electric vehicle propulsion systems,” in *Proceedings of the 34th International Power Sources Symposium*, pp. 328–333, doi: 10.1109/IPSS.1990.145857.

[134] L. Gao, R. A. Dougal, and S. Liu, “Power Enhancement of an Actively Controlled Battery/Ultracapacitor Hybrid,” *IEEE Trans. Power Electron.*, vol. 20, no. 1, pp. 236–243, Jan. 2005, doi: 10.1109/TPEL.2004.839784.

[135] R. L. Spyker and R. M. Nelms, “Classical equivalent circuit parameters for a double-layer capacitor,” *IEEE Trans. Aerosp. Electron. Syst.*, vol. 36, no. 3, pp. 829–836, Jul. 2000, doi: 10.1109/7.869502.

[136] L. Zubieta and R. Bonert, “Characterization of double-layer capacitors for power electronics applications,” *IEEE Trans. Ind. Appl.*, vol. 36, no. 1, pp. 199–205, 2000, doi: 10.1109/28.821816.

[137] A. Rufer and P. Barrade, “A supercapacitor-based energy-storage system for elevators with soft commutated interface,” *IEEE Trans. Ind. Appl.*, vol. 38, no. 5, pp. 1151–1159, Sep. 2002, doi: 10.1109/TIA.2002.803021.

[138] R. A. Dougal, L. Gao, and S. Liu, “Ultracapacitor model with automatic order selection and capacity scaling for dynamic system simulation,” *J. Power Sources*, vol. 126, no. 1–2, pp. 250–257, Feb. 2004, doi: 10.1016/j.jpowsour.2003.08.031.

[139] Lingling Du, “Study on supercapacitor equivalent circuit model for power electronics applications,” in *2009 2nd International Conference on Power Electronics and Intelligent Transportation System (PEITS)*, 2009, pp. 51–54, doi: 10.1109/PEITS.2009.5406744.

[140] F. I. Simjee and P. H. Chou, “Efficient Charging of Supercapacitors for Extended Lifetime of Wireless Sensor Nodes,” *IEEE Trans. Power Electron.*, vol. 23, no. 3, pp. 1526–1536, May 2008, doi: 10.1109/TPEL.2008.921078.

[141] S. Rai, R. Bhujel, and B. P. Swain, “Electrochemical Analysis of Graphene Oxide and Reduced Graphene Oxide for Super Capacitor Applications,” in *2018 IEEE Electron Devices Kolkata Conference (EDKCON)*, 2018, pp. 489–492, doi: 10.1109/EDKCON.2018.8770433.

[142] C. Lee, X. Wei, J. W. Kysar, and J. Hone, “Measurement of the Elastic Properties and Intrinsic Strength of Monolayer Graphene,” *Science (80-. ).*, vol. 321, no. 5887, pp. 385–388, Jul. 2008, doi: 10.1126/science.1157996.

[143] S. Pei and H.-M. Cheng, “The reduction of graphene oxide,” *Carbon N. Y.*, vol. 50, no. 9, pp. 3210–3228, Aug. 2012, doi: 10.1016/j.carbon.2011.11.010.

[144] Y. Zhu *et al.*, “Graphene and Graphene Oxide: Synthesis, Properties, and Applications,” *Adv. Mater.*, vol. 22, no. 46, pp. 5226–5226, Dec. 2010, doi: 10.1002/adma.201090156.

[145] A. Rose, K. Guru Prasad, T. Sakthivel, V. Gunasekaran, T. Maiyalagan, and T. Vijayakumar, “Electrochemical analysis of Graphene Oxide/Polyaniline/Polyvinyl alcohol composite nanofibers for supercapacitor applications,” *Appl. Surf. Sci.*, vol. 449, pp. 551–557, Aug. 2018, doi: 10.1016/j.apsusc.2018.02.224.

[146] M. F. El-kady and R. B. Kaner, “Introducing the micro-super-capacitor laser-etched graphene brings Moore’s law to energy storage,” *IEEE Spectr.*, vol. 52, no. 10, pp. 40–45, Oct. 2015, doi: 10.1109/MSPEC.2015.7274194.

[147] S. S. Roy, “A novel approach of high durable super battery (super battery using capacitor tray),” in *2015 International Conference on Applied and Theoretical Computing and Communication Technology (iCATccT)*, 2015, pp. 811–814, doi: 10.1109/ICATCCT.2015.7456994.

[148] C. Atwell, “Supercapacitors: Past, Present, and Future,” *Power Electronics*, 2018. [Online]. Available: https://www.powerelectronics.com/technologies/alternative-energy/article/21864122/supercapacitors-past-present-and-future#:~:text=The most promising future of,with existing energy-storage technologies.&text=The closest future application for,energy storage and rapid charging. [Accessed: 10-Feb-2021].

[149] K. Schmidt-Rohr, “Why Combustions Are Always Exothermic, Yielding About 418 kJ per Mole of O 2,” *J. Chem. Educ.*, vol. 92, no. 12, pp. 2094–2099, Dec. 2015, doi: 10.1021/acs.jchemed.5b00333.

[150] S. A. Kalogirou, “Industrial Process Heat, Chemistry Applications, and Solar Dryers,” in *Solar Energy Engineering*, 2nd ed., Elsevier, 2014, pp. 397–429.

[151] Y. Liu and X. Ning, “Influence of α-Al2O3 (0001) surface reconstruction on wettability of Al/Al2O3 interface: A first-principle study,” *Comput. Mater. Sci.*, vol. 85, no. April, pp. 193–199, Apr. 2014, doi: 10.1016/j.commatsci.2013.12.059.

[152] D. M. du Plooy and J. Meyer, “PEM fuel cells: Failure, mitigation and dormancy recovery: Understanding the factors affecting the efficient control of PEMFC,” in *2017 IEEE AFRICON*, 2017, pp. 1119–1124, doi: 10.1109/AFRCON.2017.8095639.

[153] S. Ganguly, S. Das, K. Kargupta, and D. Bannerjee, *Optimization of Performance of Phosphoric Acid Fuel Cell (PAFC) Stack using Reduced Order Model with Integrated Space Marching and Electrolyte Concentration Inferencing*, vol. 31. Elsevier, 2012.

[154] V. Kumar, R. Rudra, S. Hait, P. Kumar, and P. P. Kundu, “Performance Trends and Status of Microbial Fuel Cells,” in *Progress and Recent Trends in Microbial Fuel Cells*, 1st ed., Elsevier, 2018, pp. 7–24.

[155] S. M. Haile, D. A. Boysen, C. R. I. Chisholm, and R. B. Merle, “Solid acids as fuel cell electrolytes,” *Nature*, vol. 410, no. 6831, pp. 910–913, Apr. 2001, doi: 10.1038/35073536.

[156] S. M. Haile, C. R. I. Chisholm, K. Sasaki, D. A. Boysen, and T. Uda, “Solid acid proton conductors: from laboratory curiosities to fuel cell electrolytes,” *Faraday Discuss.*, vol. 134, pp. 17–39, Feb. 2007, doi: 10.1039/B604311A.

[157] M. Uzunoglu and M. S. Alam, “Fuel-Cell Systems for Transportations,” in *Power Electronics Handbook*, 4th ed., Elsevier, 2018, pp. 1091–1112.

[158] B. Abderezzak, “Introduction to Hydrogen Technology,” in *Introduction to Transfer Phenomena in PEM Fuel Cell*, 1st ed., Elsevier, 2018, pp. 1–51.

[159] S. Dharmalingam, V. Kugarajah, and M. Sugumar, “Membranes for Microbial Fuel Cells,” in *Microbial Electrochemical Technology*, 1st ed., Elsevier, 2019, pp. 143–194.

[160] C. Thanomjit, Y. Patcharavorachot, and A. Arpornwichanop, “Design and Thermal Analysis of a Solid Oxide Fuel Cell System Integrated with Ethanol Steam Reforming,” *Comput. Aided Chem. Eng.*, vol. 30, pp. 287–291, 2012, doi: 10.1016/B978-0-444-59519-5.50058-7.

[161] M. Steilen and L. Jörissen, “Hydrogen Conversion into Electricity and Thermal Energy by Fuel Cells,” in *Electrochemical Energy Storage for Renewable Sources and Grid Balancing*, 1st ed., Elsevier, 2015, pp. 143–158.

[162] I. Dincer and M. A. Rosen, “Exergy Analysis of Fuel Cell Systems,” in *Exergy*, 2nd ed., Elsevier, 2013, pp. 363–382.

[163] V. Mehta and J. S. Cooper, “Review and analysis of PEM fuel cell design and manufacturing,” *J. Power Sources*, vol. 114, no. 1, pp. 32–53, Feb. 2003, doi: 10.1016/S0378-7753(02)00542-6.

[164] O. A. Mohammed, D. Lowther, M. H. Lean, and B. Alhalabi, “On the creation of a generalized design optimization environment for electromagnetic devices,” *IEEE Trans. Magn.*, vol. 37, no. 5, pp. 3562–3565, Oct. 2001, doi: 10.1109/20.952662.

[165] F. Barreras, A. Lozano, L. Valiño, C. Marín, and A. Pascau, “Flow distribution in a bipolar plate of a

proton exchange membrane fuel cell: experiments and numerical simulation studies," *J. Power Sources*, vol. 144, no. 1, pp. 54–66, Jun. 2005, doi: 10.1016/j.jpowsour.2004.11.066.

[166] T. Hodgkinson, "Long Live the Senses," *Cult. Crit.*, vol. 104, no. 1, pp. 192–201, 2019, doi: 10.1353/cul.2019.0031.

[167] K. Reif, *Dieselmotor-Management im Überblick*, 2nd ed. Springer, 2014.

[168] B. Lojek, *History of Semiconductor Engineering*, 1st ed. Berlin, Heidelberg: Springer, Berlin, Heidelberg, 2007.

[169] L. Fraas and L. Partain, "Summary, Conclusions, and Recommendations," in *Solar Cells and their Applications*, 2nd ed., Hoboken, NJ, USA: John Wiley & Sons, Inc., 2010, pp. 581–611.

[170] J. Chu, "MIT engineers fly first-ever plane with no moving parts," *MIT News*, 21-Nov-2018. [Online]. Available: http://news.mit.edu/2018/first-ionic-wind-plane-no-moving-parts-1121. [Accessed: 07-Dec-2020].

[171] I. Jiya, N. Gurusinghe, and R. Gouws, "Electrical Circuit Modelling of Double Layer Capacitors for Power Electronics and Energy Storage Applications: A Review," *Electronics*, vol. 7, no. 11, p. 268, Oct. 2018, doi: 10.3390/electronics7110268.

[172] A. P. Dancy, R. Amirtharajah, and A. P. Chandrakasan, "High-efficiency multiple-output DC-DC conversion for low-voltage systems," *IEEE Trans. Very Large Scale Integr. Syst.*, vol. 8, no. 3, pp. 252–263, Jun. 2000, doi: 10.1109/92.845892.

[173] K. Chomsuwan, P. Prisuwanna, and V. Monyakul, "Photovoltaic grid-connected inverter using two-switch buck-boost converter," in *Conference Record of the Twenty-Ninth IEEE Photovoltaic Specialists Conference, 2002.*, 2002, pp. 1527–1530, doi: 10.1109/PVSC.2002.1190902.

[174] P. P. Urone, *College Physics*, 2nd ed. Sacramento, California: Brooks/Cole, 2001.

[175] S. C. Chung, R. Huang, and C. I. Lin, "Applications of describing functions to estimate the continuous and discontinuous conduction mode for a DC-to-DC buck converter," *IEE Proc. - Electr. Power Appl.*, vol. 147, no. 6, p. 513, 2000, doi: 10.1049/ip-epa:20000589.

[176] Vishay, "Vishay, High Current Through Hole Inductor, High Temperature Series datasheet," *Vishay*, 2020. [Online]. Available: http://www.vishay.com/docs/34349/ihth-1125kz-5a.pdf. [Accessed: 07-Feb-2020].

[177] J. C. Rosas-Caro, F. Mancilla-David, J. C. Mayo-Maldonado, J. M. Gonzalez-Lopez, H. L. Torres-Espinosa, and J. E. Valdez-Resendiz, "A Transformer-less High-Gain Boost Converter With Input Current Ripple Cancelation at a Selectable Duty Cycle," *IEEE Trans. Ind. Electron.*, vol. 60, no. 10, pp. 4492–4499, Oct. 2013, doi: 10.1109/TIE.2012.2211314.

[178] S. Palanidoss and T. V. S. Vishnu, "Experimental analysis of conventional buck and boost converter with integrated dual output converter," in *2017 International Conference on Electrical, Electronics, Communication, Computer, and Optimization Techniques (ICEECCOT)*, 2017, pp. 323–329, doi: 10.1109/ICEECCOT.2017.8284521.

[179] MIT-COE, "IEEE MIT College of Engineering SB, Pune," *mitcoe.ac.in*. [Online]. Available: http://mitcoe.ac.in/ieee/. [Accessed: 15-Apr-2019].

[180] K. Yao, Y. Qiu, M. Xu, and F. C. Lee, “A Novel Winding-Coupled Buck Converter for High-Frequency, High-Step-Down DC–DC Conversion,” *IEEE Trans. Power Electron.*, vol. 20, no. 5, pp. 1017–1024, Sep. 2005, doi: 10.1109/TPEL.2005.854022.

[181] Y. V. Kolokolov and A. V. Monovskaya, “Experimental Identification of Uncertainties in Dynamics of PWM Buck Converter,” *IFAC-PapersOnLine*, vol. 48, no. 11, pp. 366–371, 2015, doi: 10.1016/j.ifacol.2015.09.213.

[182] S. N. Soheli, G. Sarowar, M. A. Hoque, and M. S. Hasan, “Design and Analysis of a DC -DC Buck Boost Converter to Achieve High Efficiency and Low Voltage Gain by using Buck Boost Topology into Buck Topology,” in *2018 International Conference on Advancement in Electrical and Electronic Engineering (ICAEEE)*, 2018, vol. 7, no. 4, pp. 1–4, doi: 10.1109/ICAEEE.2018.8643001.

[183] G. Litichever, O. Gutentag, E. Zvuluny, and A. Hershler, “System and method for securely connecting to a peripheral device,” EP3531321A1, 2016.

[184] J. Ejury, “Buck Converter Design,” *Infineon Technologies North America*, 2013. [Online]. Available: https://www.mouser.de/pdfdocs/BuckConverterDesignNote.pdf. [Accessed: 07-Dec-2020].

[185] S. Cuk and R. D. Middlebrook, “Advances in Switched-Mode Power Conversion Part I,” *IEEE Trans. Ind. Electron.*, vol. IE-30, no. 1, pp. 10–19, Feb. 1983, doi: 10.1109/TIE.1983.356697.

[186] L. Dinca, J. I. Corcau, and E. Ureche, “Mathematical modeling for buck converter in continuous conduction mode,” in *2016 International Conference on Applied and Theoretical Electricity (ICATE)*, 2016, pp. 1–6, doi: 10.1109/ICATE.2016.7754687.

[187] Y. Lee, A. Khaligh, A. Chakraborty, and A. Emadi, “Digital Combination of Buck and Boost Converters to Control a Positive Buck–Boost Converter and Improve the Output Transients,” *IEEE Trans. Power Electron.*, vol. 24, no. 5, pp. 1267–1279, May 2009, doi: 10.1109/TPEL.2009.2014066.

[188] C. M. C. Duarte and I. Barbi, “An improved family of ZVS-PWM active-clamping DC-to-DC converters,” *IEEE Trans. Power Electron.*, vol. 17, no. 1, pp. 1–7, Jan. 2002, doi: 10.1109/63.988661.

[189] H. Mao, O. Abdel Rahman, and I. Batarseh, “Zero-Voltage-Switching DC–DC Converters With Synchronous Rectifiers,” *IEEE Trans. Power Electron.*, vol. 23, no. 1, pp. 369–378, Jan. 2008, doi: 10.1109/TPEL.2007.911768.

[190] P. Das, B. Laan, S. A. Mousavi, and G. Moschopoulos, “A Nonisolated Bidirectional ZVS-PWM Active Clamped DC–DC Converter,” *IEEE Trans. Power Electron.*, vol. 24, no. 2, pp. 553–558, Feb. 2009, doi: 10.1109/TPEL.2008.2006897.

[191] D. B. Costa and C. M. C. Duarte, “The ZVS-PWM Active-Clamping CUK Converter,” *IEEE Trans. Ind. Electron.*, vol. 51, no. 1, pp. 54–60, Feb. 2004, doi: 10.1109/TIE.2003.819697.

[192] H.-L. Do, “Zero-Voltage-Switching Synchronous Buck Converter With a Coupled Inductor,” *IEEE Trans. Ind. Electron.*, vol. 58, no. 8, pp. 3440–3447, Aug. 2011, doi: 10.1109/TIE.2010.2084973.

[193] S. Parui and S. Banerjee, “Bifurcations due to transition from continuous conduction mode to discontinuous conduction mode in the boost converter,” *IEEE Trans. Circuits Syst. I Fundam. Theory Appl.*, vol. 50, no. 11, pp. 1464–1469, Nov. 2003, doi: 10.1109/TCSI.2003.818618.

[194] M. S. Rahman, “Buck converter design issues,” *Division of Electronic Devices Linkopings University*,

2007. [Online]. Available: http://www.diva-portal.org/smash/record.jsf?pid=diva2:24104. [Accessed: 07-Dec-2020].

[195] F. Caricchi, F. Crescimbini, G. Noia, and D. Pirolo, “Experimental study of a bidirectional DC-DC converter for the DC link voltage control and the regenerative braking in PM motor drives devoted to electrical vehicles,” in *Proceedings of 1994 IEEE Applied Power Electronics Conference and Exposition - ASPEC’94*, 1994, pp. 381–386, doi: 10.1109/APEC.1994.316373.

[196] S. Tank, K. Manavar, and N. Adroja, “Non-Isolated Bi-directional DC-DC Converters for Plug-In Hybrid Electric Vehicle Charge Station Application,” in *National Conference on Emerging Trends in Computer, Electrical & Electronics*, 2015, pp. 2348–4470.

[197] Dimna Denny C and Shahin M, “Analysis of bidirectional SEPIC/Zeta converter with coupled inductor,” in *2015 International Conference on Technological Advancements in Power and Energy (TAP Energy)*, 2015, pp. 103–108, doi: 10.1109/TAPENERGY.2015.7229600.

[198] Lung-Sheng Yang and Tsorng-Juu Liang, “Analysis and Implementation of a Novel Bidirectional DC–DC Converter,” *IEEE Trans. Ind. Electron.*, vol. 59, no. 1, pp. 422–434, Jan. 2012, doi: 10.1109/TIE.2011.2134060.

[199] Y. Ye, K. W. E. Cheng, J. Liu, and C. Xu, “Bidirectional tapped-inductor-based buck-boost convertor and its circuit application,” in *2013 5th International Conference on Power Electronics Systems and Applications(PESA)*, 2013, pp. 1–7, doi: 10.1109/PESA.2013.6828226.

[200] Henry Shu-hung Chung, A. Ioinovici, and Wai-Leung Cheung, “Generalized structure of Bi-directional switched-capacitor DC/DC converters,” *IEEE Trans. Circuits Syst. I Fundam. Theory Appl.*, vol. 50, no. 6, pp. 743–753, Jun. 2003, doi: 10.1109/TCSI.2003.812615.

[201] H. Wu, J. Lu, W. Shi, and Y. Xing, “Nonisolated Bidirectional DC–DC Converters With Negative-Coupled Inductor,” *IEEE Trans. Power Electron.*, vol. 27, no. 5, pp. 2231–2235, May 2012, doi: 10.1109/TPEL.2011.2180540.

[202] A. Lavanya, J. D. Navamani, K. Vijayakumar, and R. Rakesh, “Multi-input DC-DC converter topologies-a review,” in *2016 International Conference on Electrical, Electronics, and Optimization Techniques (ICEEOT)*, 2016, pp. 2230–2233, doi: 10.1109/ICEEOT.2016.7755089.

[203] K. Tytelmaier, O. Husev, O. Veligorskyi, and R. Yershov, “A review of non-isolated bidirectional dc-dc converters for energy storage systems,” in *2016 II International Young Scientists Forum on Applied Physics and Engineering (YSF)*, 2016, no. November 2017, pp. 22–28, doi: 10.1109/YSF.2016.7753752.

[204] C. E. Sheridan, M. M. C. Merlin, and T. C. Green, “Assessment of DC/DC converters for use in DC nodes for offshore grids,” in *10th IET International Conference on AC and DC Power Transmission (ACDC 2012)*, 2012, vol. 2012, pp. 31–31, doi: 10.1049/cp.2012.1966.

[205] C. Yao, X. Ruan, X. Wang, and C. K. Tse, “Isolated Buck–Boost DC/DC Converters Suitable for Wide Input-Voltage Range,” *IEEE Trans. Power Electron.*, vol. 26, no. 9, pp. 2599–2613, Sep. 2011, doi: 10.1109/TPEL.2011.2112672.

[206] L. Dobrescu, R. Smeu, and D. Dobrescu, “Load switch power MOSFET SPICE model,” in *2016 International Conference and Exposition on Electrical and Power Engineering (EPE)*, 2016, pp. 644–

647, doi: 10.1109/ICEPE.2016.7781418.

[207] S. Castagno, R. D. Curry, and E. Loree, “Analysis and Comparison of a Fast Turn-On Series IGBT Stack and High-Voltage-Rated Commercial IGBTS,” *IEEE Trans. Plasma Sci.*, vol. 34, no. 5, pp. 1692–1696, Oct. 2006, doi: 10.1109/TPS.2006.879551.

[208] M. D. Singh and K. B. Khanchandani, *Power Electronics*, 2nd ed. New Delhi: McGraw Hill, 2007.

[209] RS Components, “MOSFETs.” [Online]. Available: https://za.rs-online.com/web/c/semiconductors/discrete-semiconductors/mosfets/?sra=p. [Accessed: 10-Feb-2021].

[210] RS Components, “Bipolar Transistors.” [Online]. Available: https://za.rs-online.com/web/c/semiconductors/discrete-semiconductors/bipolar-transistors/?sra=p. [Accessed: 10-Feb-2021].

[211] RS Components, “IGBT’s.” [Online]. Available: https://za.rs-online.com/web/c/semiconductors/discrete-semiconductors/igbts/?searchTerm=igbt&sort-by=Maximum Collector Emitter Voltage&sort-order=desc&pn=1. [Accessed: 10-Feb-2021].

[212] J. Konjevod, H. Hegedus, R. Malaric, and I. Kunst, “Switch based on relays with low operation and release time for AC-DC transfer difference measurements,” in *2018 First International Colloquium on Smart Grid Metrology (SmaGriMet)*, 2018, pp. 1–3, doi: 10.23919/SMAGRIMET.2018.8369837.

[213] A. Damjanovic, “Protection of Medium Voltage SCR Driven Soft-Starter From High-Frequency Switching Transients,” *IEEE Trans. Ind. Appl.*, vol. 52, no. 6, pp. 4652–4655, Nov. 2016, doi: 10.1109/TIA.2016.2594220.

[214] A. Smeti, W. Chagra, and M. Ksouri, “Implementation of a Predictive controller on the STM32 board,” in *2013 International Conference on Control, Decision and Information Technologies (CoDIT)*, 2013, pp. 250–253, doi: 10.1109/CoDIT.2013.6689552.

[215] J. Schmidhuber, “Deep learning in neural networks: An overview,” *Neural Networks*, vol. 61, pp. 85–117, Jan. 2015, doi: 10.1016/j.neunet.2014.09.003.

[216] R. Bellman, *Adaptive Control Processes: A Guided Tour*, 1st ed. Londen: Princeton Legacy Library, 2015.

[217] B. C. Arabacioglu, “Using fuzzy inference system for architectural space analysis,” *Appl. Soft Comput.*, vol. 10, no. 3, pp. 926–937, Jun. 2010, doi: 10.1016/j.asoc.2009.10.011.

[218] M. J. Walker, “The programmable logic controller : its prehistory, emergence and application,” The Open University, 2012.

[219] A. Nayyar and V. Puri, “A review of Arduino board’s, Lilypad’s & Arduino shields,” in *2016 3rd International Conference on Computing for Sustainable Global Development (INDIACom)*, 2016, pp. 1485–1492.

[220] Farnell, “Arduino Nano.” [Online]. Available: https://za.rs-online.com/web/p/arduino/6961667/. [Accessed: 07-Dec-2020].

[221] STMicroeletronics, “STM32F103x8,” 2015. [Online]. Available: https://www.st.com/resource/en/datasheet/stm32f103c8.pdf. [Accessed: 07-Dec-2020].

[222] ST.com, “STM32 32-bit Arm Cortex MCUs,” *ST life.augmented*. [Online]. Available: https://www.st.com/en/microcontrollers-microprocessors/stm32-32-bit-arm-cortex-mcus.html. [Accessed: 10-Apr-2019].

[223] Broadcom, “BCM2835 ARM Peripherals,” *Broadcom Corporation Datasheets*, 2012. [Online]. Available: https://www.raspberrypi.org/documentation/hardware/raspberrypi/bcm2835/BCM2835-ARM-Peripherals.pdf. [Accessed: 07-Dec-2020].

[224] R. Barnes, “Raspberry Pi 3: Specs, Benchmarks and Testing,” *The MagPi Magazine*, 2016. [Online]. Available: https://magpi.raspberrypi.org/articles/raspberry-pi-3-specs-benchmarks. [Accessed: 07-Dec-2020].

[225] L. Chang, M. Knox, and T. Li, “Pros and Cons of Raspberry Pi,” *MIS 237 Group Project Raspberry Pi*. [Online]. Available: https://sites.google.com/site/mis237groupprojectraspberrypi/home/what-is-raspberry-pi/pros-and-cons-of-the-raspberry-pi. [Accessed: 10-Apr-2019].

[226] R. Wiśniewski, “Synthesis of compositional microprogram control units for programmable devices,” University of Zielona Gora, 2009.

[227] L. Cloer, “FPGA vs Microcontroller – Advantages of Using An FPGA,” *Duotech*, 2017. [Online]. Available: https://duotechservices.com/fpga-vs-microcontroller-advantages-of-using-fpga. [Accessed: 10-Apr-2019].

[228] Lattice Semiconductor, “DS1040 - iCE40 LP/HX Family Data Sheet,” *Lattice Semiconductor Datasheet*, 2017. [Online]. Available: http://www.latticesemi.com/~/media/LatticeSemi/Documents/DataSheets/iCE/iCE40LPHXFamilyDataSheet.pdf. [Accessed: 07-Dec-2020].

[229] RF Wireless World, “Advantages of FPGA | disadvantages of FPGA,” *RF Wireless World*. [Online]. Available: https://www.rfwireless-world.com/Terminology/Advantages-and-Disadvantages-of-FPGA.html#:~:text=Benefits or advantages of FPGA&text=➡FPGAs can be programmed,software level at any time. [Accessed: 10-Apr-2019].

[230] ieee.org, “History of IEEE,” *History of IEEE*. [Online]. Available: https://www.ieee.org/about/ieee-history.html. [Accessed: 15-Apr-2019].

[231] J. Geier, “Overview of the IEEE 802.11 Standard,” *informIT*, 2001. [Online]. Available: http://www.informit.com/articles/article.aspx?p=24411. [Accessed: 15-Apr-2019].

[232] J. Van Heerden, “Transmission and Distribution: Medium voltage fixed electrical installations: SANS 10142 – Part 2,” *Energize*, 2014. [Online]. Available: https://www.ee.co.za/wp-content/uploads/legacy/energize_2012/07_TT_03_Medium-V.pdf. [Accessed: 07-Dec-2020].

[233] SABS, “About the SABS,” *SABS.co.za*, 2019. [Online]. Available: https://www.sabs.co.za/. [Accessed: 15-Apr-2019].

[234] IEEE Standards Association, “IEEE Recommended Practice for the Design and Application of Power Electronics in Electrical Power Systems IEEE Industry Applications Society IEEE Recommended Practice for the Design and Application of Power Electronics in Electrical Power Systems,” 2017.

[235] D. Petterson, “SABS, SANS or SATAS? Clearing up the confusion,” *infrastructurenews*, 2016. [Online].

Available: http://infrastructurenews.co.za/2016/06/14/sabs-sans-or-satas-clearing-up-the-confusion/. [Accessed: 15-Apr-2019].

[236] IEC, “About the IEC,” *IEC.ch*, 2019. [Online]. Available: https://www.iec.ch/about-us. [Accessed: 15-Apr-2019].

[237] IEC, “IEC 62477-2:2018,” 2018.

[238] G. Brocard, *Application handbook for LTspice*, 1st ed. Swiridoff Verla, 2013.

[239] M. H. Rashid, *SPICE for Power Electronics and Electric Power*, 3rd ed. CRC Press, 2017.

[240] S. Nagar, *Introduction to MATLAB for Engineers and Scientists*. Berkeley, CA: Apress, 2017.

[241] S. L. Eshkabilov, *MATLAB/Simulink Essentials: MATLAB/Simulink for Engineering Problem Solving and Numerical Analysis*. Lulu Publishing Services, 2017.

[242] JLCPCB, “JLCPCB,” *JLCPCB*. [Online]. Available: https://jlcpcb.com/about. [Accessed: 16-Apr-2019].

[243] F. Zhang, L. Wang, S. Coskun, H. Pang, Y. Cui, and J. Xi, “Energy Management Strategies for Hybrid Electric Vehicles: Review, Classification, Comparison, and Outlook,” *Energies*, vol. 13, no. 13, p. 3352, Jun. 2020, doi: 10.3390/en13133352.

[244] H. Marzougui, A. Kadri, M. Amari, and F. Bacha, “Frequency separation based energy management strategy for fuel cell electrical vehicle with super-capacitor storage system,” in *2018 9th International Renewable Energy Congress (IREC)*, 2018, pp. 1–6, doi: 10.1109/IREC.2018.8362521.

[245] J. W. Nilsson and S. A. Riedel, *Electric circuits*, 9th ed. New Jersey: Pearson, 2011.

[246] Maxwell Technologies, “3.0V 3400F Ultracapacitor Cell,” *Maxwell Technologies, Inc.*, 2020. [Online]. Available: https://www.maxwell.com/products/ultracapacitors/.

[247] Maxwell Technologies, “2.7V 360F Ultracapacitor Cell,” *Maxwell Technologies*, 2020. [Online]. Available: https://www.maxwell.com/images/documents/2_7_360F_ds_3001963_datasheet.pdf. [Accessed: 27-Nov-2020].

[248] Toshiba, “TK72E12N1,” *Toshiba datasheet*, 2014. [Online]. Available: https://www.mouser.com/datasheet/2/408/TK72E12N1_datasheet_en_20140630-1140063.pdf. [Accessed: 07-Dec-2020].

[249] Infineon, “IDP08E65D1 Data sheet Industrial Power Control,” *Infineon datasheet*, 2020. [Online]. Available: https://www.infineon.com/dgdl/Infineon-IDP15E65D1-DS-v02_02-en.pdf?fileId=db3a30433d68e984013d691402dd0153. [Accessed: 07-Dec-2020].

[250] IXYS, “Thyristor,” *IXYS datasheet*, 2015. [Online]. Available: https://ixapps.ixys.com/DataSheet/CS60-16io1.pdf. [Accessed: 07-Dec-2020].

[251] ST, “Low voltage transistor,” *ST Datasheet*, 2008. [Online]. Available: https://www.soemtron.org/downloads/disposals/bd135.pdf. [Accessed: 07-Dec-2020].

[252] Philips, “N-channel FET,” *Discrete semiconductors datasheet*, 2012. [Online]. Available: http://www.papersearch.net/view/detail.asp?detail_key=10000715. [Accessed: 07-Dec-2020].

[253] International Rectifier, “IRLB3034PbF,” *IR Datasheet*, 2009. [Online]. Available: https://www.mouser.com/datasheet/2/196/irlb3034pbf-1732822.pdf. [Accessed: 07-Dec-2020].

[254] IXYS, “IGBT,” *IXYS Datasheet*, 2016. [Online]. Available: https://m.littelfuse.com/~/media/electronics/datasheets/discrete_igbts/littelfuse_discrete_igbts_xpt_ixx_110n65b4h1_datasheet.pdf.pdf. [Accessed: 07-Dec-2020].

[255] OMRON, “G2RL Power Relay,” *Omron Datasheet*, 2005. [Online]. Available: https://omronfs.omron.com/en_US/ecb/products/pdf/en-g2rl.pdf. [Accessed: 07-Dec-2020].

[256] H. Fan, “Design tips for an efficient non-inverting buck-boost converter,” *Analog Applications Journal*, 2015. [Online]. Available: https://www.ti.com/lit/an/slyt584/slyt584.pdf?ts=1607342904526&ref_url=https%253A%252F%252Fwww.google.com%252F. [Accessed: 07-Dec-2020].

[257] W. Elektronik, “Power Inductors & Design Tips: A practical guide for the selection of power inductors for DC / DC converters,” *WE-online*, 2020. [Online]. Available: https://www.we-online.com/web/en/electronic_components/produkte_pb/application_notes/8designtipps.php. [Accessed: 07-Dec-2020].

[258] B. Hauke, “Basic Calculation of a Boost Converter’s Power Stage,” *Texas Instruments, Application Report November*, 2009. [Online]. Available: http://scholar.google.com/scholar?hl=en&btnG=Search&q=intitle:Basic+Calculation+of+a+Boost+Converter’s+Power+Stage#0. [Accessed: 07-Dec-2020].

[259] A. Garcia-Caraveo, A. Soto, R. Gonzalez, and P. Banuelos-Sanchez, “Brief review on snubber circuits,” in *2010 20th International Conference on Electronics Communications and Computers (CONIELECOMP)*, 2010, pp. 271–275, doi: 10.1109/CONIELECOMP.2010.5440754.

[260] CDE Cornell Dubilier, “Application Guide: Snubber Capacitors.” [Online]. Available: https://www.cde.com/resources/catalogs/igbtAPPguide.pdf. [Accessed: 04-Feb-2021].

[261] Toshiba, “Power MOSFET Thermal Design and Attachment of a Thermal Fin,” *Toshiba Application Notes*, 2016. [Online]. Available: https://toshiba.semicon-storage.com/info/docget.jsp?did=13417. [Accessed: 07-Dec-2020].

[262] N. Seshasayee, “Understanding Thermal Dissipation and Design of a Heatsink,” *TI, Texas Instruments*, 2011. [Online]. Available: http://www.ti.com/lit/an/slva462/slva462.pdf. [Accessed: 30-Nov-2020].

[263] N. S. Mubenga and T. Stuart, “A case study on the hybridization of an electric vehicle into a fuel cell hybrid vehicle and the development of a solar powered hydrogen generating station,” in *2011 IEEE Power and Energy Society General Meeting*, 2011, pp. 1–8, doi: 10.1109/PES.2011.6039198.

[264] G. Pede, A. Iacobazzi, S. Passerini, A. Bobbio, and G. Botto, “FC vehicle hybridisation: an affordable solution for an energy-efficient FC powered drive train,” *J. Power Sources*, vol. 125, no. 2, pp. 280–291, Jan. 2004, doi: 10.1016/j.jpowsour.2003.07.018.

[265] D. Barker and F. C. Walsh, “Applications of Faraday’s Laws of Electrolysis in Metal Finishing,” *Trans. IMF*, vol. 69, no. 4, pp. 158–162, Jan. 1991, doi: 10.1080/00202967.1991.11870915.

[266] BMPower, “Hydrogen Fuel Cell Power System for drones and robots,” *BMPower*, 2020. [Online]. Available: https://bmpower.us/. [Accessed: 27-Nov-2020].

[267] Toshiba, “TLP152 Datasheet.” [Online]. Available: http://www.farnell.com/datasheets/2017786.pdf.

[Accessed: 05-Feb-2021].

[268] L. Solero, A. Lidozzi, and J. A. Pomilio, “Design of Multiple-Input Power Converter for Hybrid Vehicles,” *IEEE Trans. Power Electron.*, vol. 20, no. 5, pp. 1007–1016, Sep. 2005, doi: 10.1109/TPEL.2005.854020.

[269] K. Salah-ddine, “Implementation of Fuzzy Logic Controller (FLC) for DC-DC Boost Converter Using Matlab/Simulink,” *Int. J. Sensors Sens. Networks*, vol. 5, pp. 1–5, 2017, doi: 10.11648/j.ijssn.s.2017050501.11.

[270] A. Townsend, C. Martinson, D. Bessarabov, and R. Gouws, “Effect of super-capacitors on air cooled hydrogen fuel cell,” *Int. J. Hydrogen Energy*, pp. 1–14, 2021.

[271] B. Landoni, “Let’s code with STM32 NUCLEO,” *OpenElectronics*, 2015. [Online]. Available: https://www.open-electronics.org/lets-code-with-stm32-nucleo/. [Accessed: 30-Nov-2020].

[272] MathWorks, “Third-Party Products and Services,” 2020. [Online]. Available: https://www.mathworks.com/products/connections/search-products.html?q=&fq=connections-product-type:dataacq&page=1. [Accessed: 30-Nov-2020].

[273] M. Marchesoni and C. Vacca, “New DC–DC Converter for Energy Storage System Interfacing in Fuel Cell Hybrid Electric Vehicles,” *IEEE Trans. Power Electron.*, vol. 22, no. 1, pp. 301–308, Jan. 2007, doi: 10.1109/TPEL.2006.886650.

[274] A. R. Nikhar, S. M. Apte, and R. Somalwar, “Review of various control techniques for DC-DC interleaved boost converters,” in *2016 International Conference on Global Trends in Signal Processing, Information Computing and Communication (ICGTSPICC)*, 2016, pp. 432–437, doi: 10.1109/ICGTSPICC.2016.7955340.

[275] T. L. Floyd, *Electronic Devices (Electron Flow Version) Value Package (Includes Laboratory Exercises for Electronic Devices)*, 9th ed. Prentice Hall, 2008.

[276] R. Faranda, M. Gallina, and D. T. Son, “A new simplified model of Double-Layer Capacitors,” in *2007 International Conference on Clean Electrical Power*, 2007, pp. 706–710, doi: 10.1109/ICCEP.2007.384288.

# APPENDIX A – PUBLICATIONS

An effort was made to receive feedback on the relevance of the topic of this dissertation in the field of power electronics and energy. Two articles were submitted of which one has been published and the other is under review. Citations of the publications are given below with the full texts available in Appendix A.

- A. Townsend, I. N. Jiya, C. Martinson, D. Bessarabov and R. Gouws, “A comprehensive review of energy sources for unmanned aerial vehicles, their shortfalls and opportunities for improvements.” in *Heliyon 6 (2020) Elsevier*, pp. 1-22, doi.org/10.1016/j.heliyon.2020.e05285, [published].

- A. Townsend, C. Martinson, D. Bessarabov and R. Gouws, “Effect of super-capacitors on an air-cooled hydrogen fuel cell.” In *Heliyon (2021) Elsevier*, pp. 1-27, ISSN: 0360-3199, [submitted].

Heliyon 6 (2020) e05285

Contents lists available at ScienceDirect

Heliyon

journal homepage: www.cell.com/heliyon

Review article

# A comprehensive review of energy sources for unmanned aerial vehicles, their shortfalls and opportunities for improvements

Ashleigh Townsend [a,*], Immanuel N. Jiya [b], Christiaan Martinson [c], Dmitri Bessarabov [c], Rupert Gouws [a]

[a] School of Electrical, Electronic and Computer Engineering, North West University, Potchefstroom 2520, South Africa
[b] Department of Engineering and Science, University of Agder, 4879 Grimstad, Norway
[c] HySA Infrastructure Center of Competence, Faculty of Engineering, North West University, Potchefstroom 2520, South Africa

ARTICLE INFO

*Keywords:*
Aerospace engineering
Electrical engineering
Energy
Electric power transmission
Fuel cell
Energy storage technology
Hydrogen energy
Fuel technology(FC)
Lithium-polymer (Li-Po)
Super-capacitor (SC)
Unmanned aerial vehicle (UAV)

ABSTRACT

Unmanned Aerial Vehicles were first introduced almost 40 years ago and their applications have increased and diversified substantially since then, in both commercial and private use. One of the UAVs main issues when it comes to mobility is that the power sources available are inadequate, this highlights an area for improvement as the interest in drones is on the increase. There exist many different types of power supplies applied to UAVs, however each has their own limitations and strengths that pertain to weight contributions, charging and discharging times, size, payload capabilities, energy density and power density. The aim of this paper is to review the main power sources available for UAVs, determine their shortfalls, compare the power sources with each other and offer suggestions as to how they can be improved – hence identifying where the gap lies for developing better alternative power sources.

## 1. Introduction

As the world becomes more reliant on technology, the requirement for autonomous and more mechanized operations, that remove the possibility of human error, is also increasing [1]. Operations involving visual condition inspections, in areas inaccessible by humans, necessitate stealth, safety considerations and viability, which in turn requires that the object used for such a purpose be quiet and small [2]. Autonomous motorized vehicles offer these characteristics, however, they are limited with regard to mobility as they require a surface to operate on and such surfaces are often unavailable. This brings in the added requirement of a vehicle that does not require an operating surface, one that is aloft, shifting the focus to unmanned aerial vehicles (UAVs).

UAVs can be relatively small, very mobile and quiet, with the top of the line ranges tending to be less affected by external influences such as wind direction or speed changes. On top of all these benefits they also have a wide range of applications; however, the smaller UAVs do not solve the mechanization issue fully as they have one predominant flaw, the power supply is inadequate [3]. The larger drones, such as those predominantly used in military applications, offer the advantage of adequate (and in many cases more than adequate) power supplies, however this advantage makes them much larger, less mobile and quite noisy. The aspect of an adequate power supply is imperative as it leads to a long flight endurance, it is also important that the drone be very mobile and minimally affected by the surrounding environment [4].

In recent years the requirement for UAVs in different areas of application, whether commercial, recreational or public, has increased tenfold, currently this demand is mainly consumed by military use but it is expected to exponentially shift to more of the recreational and public use [5, 6]. One major application is in the use of criminal, theft and poaching surveillance [7]. There is also a very big market for the use thereof for scientific monitoring purposes (water sampling, landslides and volcanic activity) as well as for transmission line surveillance [8, 9, 10, 11].

Combustion engines currently remain one of the favored power supplies for most military and commercial UAVs, however, electrical systems offer a higher efficacy and tend to be more reliable, with the added benefit of having low to no greenhouse gas emissions and low noise [2]. This is why electrical systems for UAV applications are becoming more prevalent. The field of electrical systems extends to

* Corresponding author.
*E-mail address:* ashleighktownsend2@gmail.com (A. Townsend).

https://doi.org/10.1016/j.heliyon.2020.e05285
Received 14 February 2020; Received in revised form 8 June 2020; Accepted 14 October 2020

batteries, fuel cells (FCs) and solar power, amongst others, these systems will be further discussed in the paper. All of the mentioned electrical systems utilize a battery (generally to increase the energy density of the system during peak energy requirements), however, batteries do not offer an energy density much higher than that of the main power source, as they have high power densities but low energy densities. Therefore, the addition of the battery can increase the endurance of the system and its peak power capabilities, but it does not increase them to the desired point and therefore still drains both of the power supplies during these instances considerably, still limiting the flight pattern of the system.

Ever since drones have come into the picture many creators have been assessing and re-evaluating the efficiency thereof and more specifically the options to increase the flight time [12, 13]. Two main options exist, change the power source in a way that increases the capacity thereof or refuel the power source sporadically [14]. The latter option requires an external refueling station. This in itself presents more limitations: the drone will be required to land periodically and refuel – decreasing actual usable flight time; the stations will be required along the flight path – limiting the path, decreasing mobility and increasing complexity; finally, this method increases overall costs unnecessarily.

The first mentioned option has many more possibilities that can be much simpler and more cost effective than the last, such as: increasing the capacity of the power source by replacing it with a larger one (or a different type of power source) or combining the existing power source with another to exploit the benefits of the combination. All of the options [15] have their advantages and disadvantages and these will further be discussed in this paper. This paper will briefly discuss the three main types of drones, giving more detail about their main power sources and the shortcomings thereof, focusing on possible solutions in the form of hybrid systems and how they can affect each drone type.

## 2. Types of UAVs

Before the different power sources are discussed, the two main types of UAVs (shown in Figure 1) will be briefly discussed. There are two main types of UAVs, rotary-wing types and fixed-wing types. The former consists of a body that travels using multiple rotors and the latter has the look of a general aircraft having a fixed wing on either side of the body.

The rotor-craft types tend to be more popular since they can take-off and land vertically, thus not requiring a launcher or runway, they can hover and are very agile making them best suited for more precision maneuverability applications. However, these types of UAVs require more mechanical and electronic complexity leading to more complicated maintenance, decreasing operational time and increasing costs. Rotary-wing types also have the disadvantage of smaller load capabilities, increasing power requirements, decreasing operational duration and increasing costs even further.

Fixed-wing types have the advantage of a much simpler structure, compared to rotary types, allowing for simpler maintenance and more efficient aerodynamics, decreasing operational costs and increasing flight time. The fixed wings also give the craft a natural gliding ability, decreasing power consumption, while the aircraft itself can carry larger loads for longer distances using less power, once again decreasing costs and increasing efficiency. The disadvantages of this type include the necessity of a runway or launching device for takeoff and landing, they need to be in a constant forward motion and can thus not hover as a rotary type can and they tend to be much larger and bulkier in comparison. These all decrease the maneuverability of the UAV [16].

Amongst all the rotary- and fixed-wing drones exists a unique type of drone that combines both drone types. As a combination it provides the stability and maneuverability of a rotary-wing drone with the long flight range of a fixed-wing drone. Furthermore, no runway or additional equipment is required for take-off, [17]. An example of the combination drone can be seen in Figure 2. All three types have respective applications suited to their advantages and disadvantages and there also exists many different power sources used in these drones.

## 3. UAV power sources

There are many different power sources available on the market, such as batteries, solar power, FCs, combustion engines, etc., most of which can be applied to drones. Over the years some of these power sources have been disregarded as they have more disadvantages than advantages regarding the specific application, some of these include having a too large weight or size, being restricted to specific movements or simply not having a large enough energy density. Most power sources are defined using their respective energy- and power densities.

The power density refers to the amount of power the source can provide at a specific instance, whereas the energy density refers to the energy that can be stored within the source, therefore how long that amount of power can be delivered. With reference to the Ragone plot from [18] super capacitors (SCs) have a large power density (80–75 000 W/kg) but a small energy density (0.09–0.10 Wh/kg), allowing them to be able to provide a large amount of power but for a short period of time. FCs have a large energy density (200–3 000 Wh/kg) but a low power density (1.5–20 W/kg), thus allowing them to provide an average (low) amount of power for an extended period of time. Li-ion capacitors fall in the middle providing a comparably large amount of power (power density, 1 000–55 000 W/kg) over an arguably long period of time (energy density, 18–350 Wh/kg) [18].

In order to determine the shortcomings of the different UAVs available on the market some more in-depth research into the different power sources is required. This section will mainly focus on the main types of power sources used in drone applications.

### 3.1. Batteries

There are many different types of batteries used onboard UAVs, each of which has its respective advantages and disadvantages. The types include: Lead acid (Pb-acid), Nickel cadmium (NiCad), Nickel Metal Hydride (NiMH), Alkaline, Lithium Polymer (Li-Po), Lithium Ion (Li-ion), Zinc Oxide (Zn-$O_2$), Lithium-air (Li-air) and Lithium-Thionyl-chloride (Li-$SOCl_2$) [19]. The most common batteries for drones are Li-Po and Li-Ion. Li-$SOCl_2$ – batteries have two times higher energy density per kg

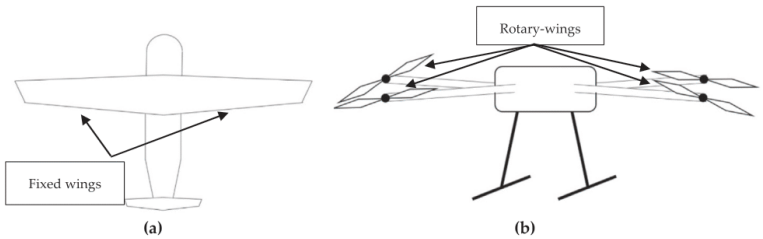


**Figure 1.** Drone types. Above (a), fixed wing drone, and above (b), rotary-wing drone.

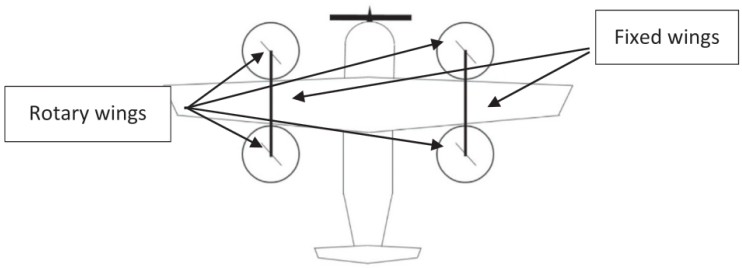


**Figure 2.** Transition type drone.

compared to the aforementioned and Li-air batteries can be up to seven times higher, however, they are unfortunately not so widely available and are much more expensive than Li-Po and Li-ion. Another variation of Li-batteries, Lithium sulphur (Li-S), also offer a higher density compared to Li-ion at a reduced cost making them the obvious choice to replace Li-ion batteries in the near future.

The most suitable type of battery is determined by comparing the power density, energy density, weight, volume, cycle life, cost, safety and maintenance (to name a few criteria) of the different options. Each of the criteria affect different aspects of the drone, power density affects the acceleration capabilities, energy density determines the range, cycle life determines how often the battery will need to be replaced, weight and volume affect the range of the system and cost affects availability [20]. Pb-acid, NiMH and Li-ion batteries are the most popular for electric vehicles (EV) applications as they are capable of meeting the requirements of EVs.

Li-ion batteries are able to deliver high energy and power per unit of battery mass; they are also lighter and more compact than the other rechargeable batteries. Other advantages include high energy efficiency, no memory effects and a comparably long cycle life. The one major shortcoming of these batteries is the cost which is significantly more than the other two [21].

Li-air batteries could cause a significant increase in the range of EVs as they have a very high energy density, almost comparable to that of gasoline. They can hold 5–10 times the energy of a Li-ion battery, with the same weight, or twice the energy for the same volume. For comparison they have an estimated energy density of around 2000–3500 Wh/kg, which is much higher than any other known battery. A small lithium-air battery has already been designed with a 600 mAh/g density compared to the 100–150 mAh/g density of a Li-ion battery of the same size [22, 23]. Amongst all of these advantages lie a few disadvantages, a rechargeable version of this battery presents a challenge as they have a very limited number of recharge/discharge cycles, they have a very slow recharge rate and they are extremely dangerous if water vapor is present in the oxygen, as lithium reacts violently with this.

Table 1, below, compares the energy-/power -densities and usable life of the mentioned battery types. For cost comparisons between the different types to be relevant it is necessary to choose a reference point, chosen as the capacity of the battery, namely: 2 Ah. Due to availability the closest values to this chosen value were used and in the case of the Zn-$O_2$ battery, the largest value was used. The sites where the respective battery-ratings where obtained are referenced below the table.

Li-Po batteries are preferred over most other batteries in portable devices and electric transportation (EV and their hybrid counterparts) due to their superior energy density, power-to-energy balance and long cycle life [20, 24, 25].

The main advantages of battery powered drones relate to being capable of charging almost anywhere, transported generally without limitations and easily recharged by simply replacing the battery pack. The disadvantages include small amounts of recharge cycles and comparably low energy densities.

### 3.2. Hydrogen FCs

As renewable fuel vehicles become more popular, alternative power sources to batteries are being investigated, one of which has to do with FCs. FCs can be divided into different categories, i.e., Proton Exchange Membrane (PEM) FC (also known as *Polymer electrolyte fuel cell* [36]), Phosphoric Acid FC (PAFC), Solid Acid FC (SAFC), Alkaline FC (AFC), High temperature FC (HTFC) and Electric storage FC (ESFC).

A PEMFC operates in a similar manner to that of a battery, there are two electrodes, an anode and a cathode, separated via a membrane and

**Table 1.** Comparison of different characteristics of different battery types (combined from [20, 22, 23, 24, 25, 26]).

| | Battery Type | | | | | | | | |
|---|---|---|---|---|---|---|---|---|---|
| | Pb-acid | NiMH | Li-ion | NiCad | Alkaline | Li-Po | Zn-$O_2$ | Li-air | Li-$SOCl_2$ |
| Nominal cell voltage (V) | 2.1 | 1.2 | 3.6–3.85 | 1.2 | 1.3–1.5 | 2.7–3 | 1.45–1.65 | 2.91 | 3.5 |
| Energy density (Wh/kg) | 30–40 | 60–120 | 100–265 | 40–60 | 85–190 | 100–265 | 442 | 11 140 | 500–700 |
| Power density (W/kg) | 180 | 250–1000 | 250–340 | 150 | 50 | 245–430 | 100 | 11 400 | 18 |
| Cycle life | <350 | 180–2000 | 400–1200 | 2000 | NA, non-rechargeable | 500 | 100 | 700 | NA |
| Charge/Discharge efficiency (%) | 50–95 | 66–92 | 80–90 | 70–90 | 45–85 | 90 | 60–70 | 93 | 6–94 |
| Self-discharge rate (%) | 3–20 | 13.9–70.6 | 0.35–2.5 | 10 | <0.30 | 0.3 | 0.17 | 1–2 | 0.08 |
| Rating | 12 V | 12 V | 3.6 V | 12 V | 1.5 V | 3.7 V | 1.4 V | N/A | 3.6 V |
| | 2 Ah | 2 Ah | 2 Ah | 1.8 Ah | 2.2 Ah | 2 Ah | 300 mAh | | 2.2 Ah |
| Costs (US$/Wh)* | 0.6975 | 0.8546 | 0.9361 | 2.6778 | 1.6727 | 2.3095 | 0.3095 | N/A | 0.5492 |
| TRL** | 9 | 9 | 9 | 9 | 9 | 9 | 9 | 6 | 9 |

* Available for purchase on 18/05/2020 [27, 28, 29, 30, 31, 32, 33, 34], relative for comparison.
** Technology Readiness Level, [35].

connected using an electrolyte. A fuel is supplied to the anode and an oxidant to the cathode, which then reacts with the electrolyte as well as with each other causing electrons to flow in the external circuit from the one electrode to the other inducing a voltage. This chemical process produces two types of byproducts, one from the fuel and one from the oxidant. A hydrogen FC has a fuel of hydrogen and oxidant of air, thus producing water and air as byproducts. These FCs have an energy density of up to 150 times that of a Li-Po battery. In recent advancements a hand-launchable fixed-wing UAV has been developed that is capable of a 10 h flight with a distance of 500 km. Another drone design uses the hollow structure of its body to store hydrogen instead of air allowing the elimination of the weight contributed by the usual storage of the hydrogen [37]. For the implementation of hydrogen FCs in vehicles the FCs are required to have a high power density, rapid response to loads and a hydrogen supply infrastructure. PAFCs use hydrogen as the fuel and liquid phosphoric acid is the electrolyte [38]. This FC has a few drawbacks including: the phosphate ion being absorbed at the catalyst surface hindering the electrochemical reaction, an acid loss when operated at high temperatures for extended periods of time, the platinum catalyst particles migrating and forming larger particles on the electrode reducing the active surface thereof and at high voltages a gradual carbon corrosion becomes present [39].

SAFCs utilize a solid acidic material as the electrolyte. Solid acids are chemical intermediates between salts and acids, at low temperatures they act like salts, while at higher temperatures they undergo a phase transition to act like acids. This increases conductivity and allows for increased efficacy of the FC. The electrolyte of the PEMFC is a water-based acidic polymer membrane (constantly in the liquid state) whereas the SAFC has an acid that transitions from solid to liquid when required. This type of FC can function using hydrogen gas obtained from a variety of different fuels, increasing their areas of application [40, 41].

AFCs are one of the first developed FC technologies and have a liquid potassium hydroxide (KOH) solution as electrolyte [42]. This FC is advantageous as it has a high efficiency, lower costs and a simple structure, however their shortfalls include quite a short operating life due to the KOH eroding the FC parts and purified oxygen is required in the system as it is very intolerant to carbon dioxide [42].

HTFCs have two main types, Solid oxide FCs (SOFC) and Molten carbonate FCs (MCFC). The former uses a solid ceramic inorganic oxide as the electrolyte [43]. The latter uses a mixture of molten potassium and lithium carbonate as the electrolyte [44], but is irrelevant to the use in UAVs and will not be further discussed. SOFCs are not limited to the more common flat shape and are often in the shape of a rolled tube, they only operate at high temperatures allowing for the use of more inexpensive catalysts and can be run on a variety of fuels, without the need of purification [45]. The final FC is the ESFC which is a conventional battery that includes the use of hydrogen and oxygen as alternative inputs for charging the battery.

PEMFCs require relatively low operating temperatures while maintaining high efficiency, power density and rapid response to load changes, which makes them the preferred variation for EVs or other applications requiring a light weight power source that is small in size [46, 47, 48, 49]. FCs used onboard drones contain a buffer (Li-Po) battery that is used to supplement the power when peak power is required. This allows the FC to have a longer usage time per flight as it isn't drained during the peak power instances. However, these batteries cause the system to be heavier and decrease the life of the aircraft as batteries have a limited cycle life. This cycle life is less than that of the FC. Another issue is that the FC constantly recharges the battery once it is depleted below its optimal voltage, which then decreases the overall range of the FC.

Advantages of FCs on drones include no direct pollution, no sound, large energy density and an almost instant recharge. Disadvantages are related to the size being significantly larger than conventional battery-powered drones, operating costs are dependent on the availability of hydrogen gas [50] and the size of the hydrogen gas tank limits the build of the drone. The hydrogen tank needs to be taken into consideration when balancing the drone keeping in mind that the weight decreases as the tank empties.

### 3.3. Combustion engine

Both petrol and diesel engines fall under the term combustion engines and consist of relatively the same components, an engine block containing (amongst others) a combustion chamber, pistons, fuel injectors, and an intake and exhaust valve. A two stroke engine, the most commonly used combustion engine, consists of two strokes and four stages, intake, compression, power and exhaust. One of the main differences between petrol and diesel engines is that the former have spark plugs, whereas the latter do not require this due to diesel self-igniting when under extreme pressure. Diesel engines sometimes require a glow plug to heat up the diesel before it enters the chamber as diesel engines can have complications when starting in cold weather. Other differences include petrol engines having a faster rotational speed compared to diesel as they have lighter pistons, connecting rods and crankshaft (lower compression ratios) and due to petrol igniting easier than diesel. However, petrol engines have lower efficiency than diesel engines; this includes thermal efficiency [51].

Kerosene, Methanol, Ethanol and LPG Propane are all variations of the petrol-powered solutions available and some of them have a remarkable performance, one performance of a gasoline-powered fixed wing UAV being more than 20-hours with one full tank of gasoline [51]. The weight of the drone is continuously decreased in flight due to the weight of the fuel decreasing, therefore increasing the range. Diesel engines have the highest effective efficiency of all the combustion engines, they can also operate on a variety of fuels, some of which have higher energy densities and are safer for the environment and the external system requires lower voltages allowing for better environmental adaptability [52, 53]. Diesel engines are in general more robust than petrol engines but this also leads them to be heavier and bulkier which is counterproductive when used onboard a drone.

The advantages of combustion engine drones comprise of longer flight times, robustness, small, light-weight and having a good specific fuel consumption. The disadvantages comprise of being heavier compared to battery-powered drones and require more complex maintenance [54].

### 3.4. Solar power

The conversion of sunlight into electricity is most commonly done by converting light into electric current through the photovoltaic (PV) effect. This current is then either directly used or stored in a battery and the battery provides power to the system. There are two main technologies used for solar power, PV systems or concentrated solar power (CSP). The former being a direct conversion of sunlight into electricity and the latter being used to make steam that allows a turbine to generate electricity [55, 56, 57]. Solar panels are generally used onboard fixed-wing drones as they require a large surface for the panels, but they can also be used to extend the range of a rotor-type drone (used to assist the main power of the rotor-type). Solar powered drones are quiet, have low operational costs, low maintenance costs and an excellent carbon footprint, however, in order for them to be efficient a large area is required for the panels, therefore increasing the size of the drone tremendously and the panels also require sunlight to operate.

### 3.5. Summary of power source shortfalls

Under each of the respective power sources mentioned above a description was given with some of the main advantages and disadvantages thereof. In this section the shortfalls of each power source will be elaborated on in order to highlight where there is room for improvement, this is summarized in Table 2, below.

### 3.6. Comparison of main power sources

Each of the power sources in the previous section have their advantages and disadvantages, these will be discussed in this section with specific emphasis on the following aspects, specific energy, flight time, weight, payload capability, recharge/discharge time and cost. For this comparison the most common power sources used in drones will be assessed. The Li-Po battery drone will be assessed for the battery variation as they tend to give the best results [64] and are the most common battery used in drones at present.

In order to compare the sources sufficiently a reference point of the payload capability of around 5 kg for each drone has been chosen, this allows for a more sensible comparison between the sources. It is worthy to be noted that the flight time of the combustion engine- and FC-powered drone is dependent on the size of fuel tank. The above-mentioned aspects are summarized in Table 3 below.

In order to compare the different drones a basis of reference will be required. In this paper that basis will be the ratios of flight time to weight, payload to flight timr, payload to weight, flight time to cost and flight time to recharge time. These values are laid out in Table 4. For the first ratio a value larger than 1 is preferred and the larger the better as this indicates that the UAVs flight time is less affected by the weight thereof, therefore, fewer losses. The second ratio prefers values smaller but closer to 1 as this reflects a good flight time while still including a payload capability, which is beneficial as it can have a wider field of application. Values above 0 for the third ratio show that the UAV is capable of carrying a weight above its own, again increasing the field of application thereof, the larger – the better. For the fourth ratio it is desired that the drone have a large flight time and a smaller comparable cost as this indicates good value for money, therefore a value closer or larger than one is desired. And for the final ratio it is preferred that the flight time be much larger than the recharge time as this indicates very good efficiency and once again allows the UAV to be applied into many more fields, thus a value larger than 1 is desired.

The bold formatted values indicate where the best value was obtained for each ratio, thus from examining the results it seems that the combustion drones are the best option. Batteries have the best payload to flight time ratio while the other ratios lag far behind the other power sources. Hydrogen FCs come in second compared to Combustion as they have the best flight time to weight ratio and were either second or third best for all the other ratios. This allows FCs to lean towards being the better option for use onboard drones as FCs only fall behind when it comes to cost. They are quite light, have a great flight time, can carry a large payload to weight ratio and recharge very quickly, this allows them to have many more applications than most of the other options. Hydrogen FC powered drones are mainly limited when it comes to cost, size of the fuel tank and acquisition of the hydrogen fuel. Table 5 summarizes the content of section 3.1 of this paper.

Some of the advantages and disadvantages of each power source have been listed as well as the possible combinations for each source. The main criteria to determine the efficacy of each source pertain to flight time, peak power, size, noise, charge/discharge rate and the amount of combinations each source can be a part of. Each source was given a rating out of 4, 4 being the worst and 1 being the best, just to compare the sources against each other. These values were estimated from either the literature of each power source or from Table 3. From the table, batteries are the best when only considering size as they lack in all other categories, hydrogen FCs seem to be a good option as they are top 3 in all categories, combustion engines are a good option if size and noise are not a problem and solar panels are the largest option and have the lowest peak power.

Hydrogen FC drones function with the use of a buffer battery essentially making them a hybrid system. This battery is usually a Li-Po battery and solves, to a degree, the problem of bad peak power performance. However, as mentioned in this paper, Li-Po batteries take long to recharge, have a short cycle life and a low power density. Although this increases the efficiency of the FC, it, to an extent, also decreases the overall life time of the FC and does not offer such a large increase in the overall power density of the system. This opens a window for further investigation into solving the power density problem, to be discussed in the next section.

### 3.7. Possible solutions to improving flight time

There are some possible solutions to improve the flight time of drones powered by these different power sources, i.e.

1. Wireless charging techniques, which include, Gust- soaring, PV arrays, Laser and Battery dumping
2. Electro-magnetic field (EMF) -based techniques
3. Wireless charging techniques, which include, Gust- soaring, PV arrays, Laser and Battery dumping
4. Hybridization

The first three techniques pertain to battery powered drones or drones containing batteries. The fourth technique can be applied to all the mentioned power sources and will therefore be the only solution discussed further.

#### 3.7.1. Hybridization

Hybrid systems contain two or more types of power sources, generally one is used to generate the other or one is preferred and the other is used at specific times to improve efficacy. The principle behind this is that one of the power sources has more advantages than the other in normal conditions, whereas the other provides specialized advantages which are beneficial at certain times during operation. This helps improve the energy and fuel efficiency of the system [69, 70, 71]. From section 3.1 it is evident that some of the power sources have advantages over the others and vice versa. There are disadvantages of some of the sources that can be resolved or improved by using alternate sources. This is where the concept of hybridization comes into consideration. By combining two or more power sources their advantages can be combined and their disadvantages can be minimized. However, special attention needs to be given to the method of hybridization.

There are generally five categories of hybrid vehicles, parallel (PH), mild parallel (MPH), power split or series parallel (SPH), series (SH) and plug in hybrid (PIH). PH can function using either of the sources used in the hybrid or one individually; when both are used the use is split equally. MPH prefers the use of one and uses the other when assistance is

**Table 2.** Summary of the shortfalls of each power source.

| Power source | Shortfall |
|---|---|
| Batteries | Low recharge cycles; low energy density; low flight time in comparison; recharge period significantly longer than others; dangerous to the environment and/or operators; limited flight time thus limited applications [58, 59, 60]. |
| Hydrogen FCs | Larger size; limited by availability of hydrogen gas and gas tank size; quite expensive; lower energy efficiency compared to batteries due to complex power management requirements [61]; hydrogen extraction process increases refuel time [62]; |
| Combustion engine | Heavier; larger size; noisy; complex maintenance; |
| Solar power | Large surface required for solar panels; requires sunlight; much heavier than others; significantly larger cost than others; maximum power point tracking (MPPT) algorithm is required [63]. |

**Table 3.** Comparison of the different characteristics of various power sources.

| Product name* | Li-Po Battery | Hydrogen FC | Gasoline | Solar |
|---|---|---|---|---|
| | DJI Matrice 600 | BMPower 1 kW | Yeair! | Airbus Zephyr 8 |
| Specific energy (Wh/kg) | 9.99 | 646 | 2600 | 435 |
| Flight time (min) | 20 | 250 | 120** | 20 160 |
| Weight (kg) | 10 | 6.5 | 4.9 | 60 |
| Payload (kg) | 5 | 5 | 5 | 5 |
| Recharge/discharge time (min) | 92 | Refuel time | Refuel time | Constant recharge via panels |
| Cost (USD from 2019 figures) | 5699 | 13 410 | 1 550 | 3 000 000 |

* obtained from online sources on 18/05/2020 [65, 66, 67, 68].
** For comparison 1.5 L tank is chosen, which yields 5 kg payload.

**Table 4.** Comparison of power source ratios.

| | Ratios | | | | |
|---|---|---|---|---|---|
| | $\frac{Flight\ time\ (min)}{Weight\ (kg)}$ | $\frac{Payload\ (kg)}{Flight\ time\ (min)}$ | $\frac{Payload\ (kg)}{Weight\ (kg)}$ | $\frac{Flight\ time\ (min)}{Cost\ (USD)}$ | $\frac{Flight\ time\ (min)}{Recharge\ time\ (min)}$ |
| Battery | 2 | **0.25** | 0.5 | 0.003509 | 0.217391 |
| Hydrogen FC | **38.46154** | 0.02 | 0.769231 | 0.018643 | <250 |
| Combustion | 24.4898 | 0.041667 | **1.020408** | **0.077419** | <120 |
| Solar | 5.6 | 0.014881 | 0.083333 | 0.000112 | **<336** |

The bold formatted values indicate the best value obtained for each ratio.

required. SPH can utilize both in varying ratios, i.e. 100% of both or 60% one and 40% the other; therefore one can regulate the efficiency. Generally SPH also only uses the one power source, either when assistance is required or when the power requirements are really low in order to decrease fuel usage. SH uses the one power source (electric power) as its main power source and utilizes the other (petrol/diesel generator) to recharge the main source, thus the second power source is not connected to the main power system. PIH uses the main power source permanently and uses grid power via a plug to recharge, thus avoiding the use of the combustion engine for this purpose. The use of the combustion engine is then up to the discretion of the driver, making this option the more pure of the five [72, 73, 74, 75, 76].

The type of hybrid method used depends on many aspects including, cost, availability, user preference and application. Some areas in the world are far from a reliable source of energy, therefore utilizing renewable energy sources becomes imperative, but these sources tend to have low energy density and poor stability. To combat this, the renewable source is combined with something of a less renewable nature or another renewable source [77]. Another advantage of hybrid systems can be the reduction in one's carbon footprint. In order to meet the needs of both energy and power, hybrid power supplies are becoming more popular. A couple of these hybrid power supplies, solar hybrids, gasoline-electric hybrids, plug-in hybrid electric (PHE) and hybrids containing SCs, are explained further below.

Solar Hybrid systems include the combination of PV and CSP systems with each other or other forms of power generation such as diesel, wind or biogas. This hybridization allows the system to modulate power output depending on the demand or to reduce fluctuations caused by the solar power [78]. Solar power-hybrid drones deliver astonishing endurances. Tethered systems also fall under these types of drones. These are systems that allow an unlimited flight time within the small radius. These types of UAVs are used more for military or industrial application and are therefore not of interest for this paper.

Gasoline-Electric Hybrids are mainly used for regenerative breaking, dual power or less idling. As the vehicle slows down for breaking the energy is used to recharge the batteries, depending on the driving circumstances the power can be divided between the dual sources or the vehicle can be shut off and restarted easier using an electric motor when the vehicle comes to a stop [79]. For UAV applications these types combine the quick reactions of an electric motor with the advantages of gasoline powered flight. Plug in Hybrid Electric (PHE) systems use a combustion engine to supplement the electric engine when the battery levels are too low. The electric motor is powered mainly using PV-arrays. The main shortcoming to this hybrid system is the necessity of the combustion engine [80].

**Table 5.** Summary of information presented regarding power sources.

| Power source | Advantages vs. Disadvantages | Possible Combinations | Flight time | Peak power | Size | Noise | Charge/ discharge rate |
|---|---|---|---|---|---|---|---|
| Batteries | Smaller, light weight.<br>Cannot supply peak power demands. | Hydrogen FC<br>Solar panel<br>S/HCs | 4 | 2 | 1 | 3 | 4 |
| Hydrogen FC | No pollution, quieter, fast recharge.<br>Larger size, cannot supply peak power demands, operating costs subject to hydrogen availability. | Batteries<br>S/HCs | 2 | 3 | 2 | 1 | 1 |
| Combustion engine | Robust.<br>Heavy, bulky, limited to fixed wing type drone. | Solar<br>Electric | 3 | 1 | 3 | 4 | 2 |
| Solar panels | Quiet, low operational and maintenance costs.<br>Larger size due to panel space requirements, limited to fixed wing type drone. | Batteries<br>Laser | 1 | 4 | 4 | 2 | 3 |

**Table 6.** Comparison of different hybrid solutions.

| Method | Advantages | Disadvantages |
|---|---|---|
| Solar hybrid | Reduces fluctuations present in pure solar power, high flight time. | Limited flight range and application. |
| Gasoline electric hybrid | Quick reaction of electric motor, long endurance of combustion engine. | Complex circuitry, bulky, pollution. |
| Plug in hybrid | Relies mainly on solar thus more efficient. | Pollution, bulky, complex circuitry. |
| FC and SC hybrid | Eco-friendly, high energy and power density. | Bulky, reliant on hydrogen availability, initially expensive. |
| Li-ion and SC hybrid | High energy and power density, longer endurance. | Limited by recharge rate and cycles of batteries. |

A capacitor consists of electrodes (anode and cathode) separated by an electrolyte [81]. The variations of capacitors are differentiated through the type of electrodes and electrolyte used. Electrostatic capacitors store charges through dielectric polarization, their energy density is not very high, however the power density is, making them good for applications requiring short duration, high efficiency and high output power. SCs can be classified into two categories, double layer capacitors (DLC) and electrochemical capacitors (EC). The former involves a separation of charges at the interface of the electrodes and the electrolytes; the capacitance is proportional to the area of the electrode material. The latter functions on the principle of fast Faraday redox reactions, therefore relying on high reversible redox reactions occurring on the electrodes surface or inside the electrodes to produce the specific capacitance. The breakdown potential of the electrolyte limits the voltage of the capacitors to a maximum of 3 V; therefore a series connection is required to increase the working voltage, which simultaneously reduces the effective capacitance.

The SC is based on the high working voltage of an electrolytic capacitor and combines the electrolytic and ECs to have the best features with a high working voltage, specific capacitance and energy density [81]. SCs have the advantage of fast charging, large power density and a long cycle life with the main disadvantage being their low energy density. Their advantages make them the best suited option for supplementing another power source requiring an increase in peak power. SCs have the capability to deliver quick bursts of energy during peak power demands and store energy and excess power that would otherwise be lost. They have a much lower energy density than batteries but are great at supplementing these power shortages [82, 83, 84, 85].

The uses of SCs on drones are still in the initial stages of implementation and as such there are very limited resources detailing the efficiency thereof. The charge and discharge of SCs occurs very quickly compared to batteries, they have high power density, and almost unlimited recharge cycles. On the other hand they can be large and bulky, must be used to supplement main power supply and cannot efficiently function as the main power source. The use of SCs on drones is usually in the supplementation capacity, they are used as a secondary source to supplement the primary source when peak power is required and as such there are many different hybrid systems containing SCs.

An aluminum air FC (AAFC) can be combined with super capacitors to form a power source. AAFCs have a higher energy density than most other batteries, but have a lower power density, therefore on its own, the AAFC is not a viable driving source of power. As mentioned above, SCs have a high power density, fast charge and discharge, but a poor energy density. This makes them ideal for supplementing the AAFC. There are three stages in power supply of this system, stage 1 involves only the use of the AAFC when there is a low power demand, stage 2 uses both AAFC and SC for larger power demands and stage 3 is one that occurs continuously, known as regenerative breaking, where the SC is charged through the use of energy that is usually lost when the system idles [86].

The Li-ion battery has many advantages over other batteries including, high voltage, light weight, low self-discharging and long cycle life. The shortcoming of Li-ion batteries is that if they are used in a high power demand application, their performance in terms of weight, cost and lifetime degrades tremendously. By adding the SCs, the battery can satisfy the average power demands while the SCs satisfy the peak power demands during acceleration or breaking [87].

#### 3.7.2. Comparison of hybrid solutions

By comparing the different hybrid methods laid out in this section it will be possible to determine how relevant and also how efficient they are. This comparison of the advantages and disadvantages of each is done in Table 6, below. According to Table 6, FC and SC hybrids have the best advantages and have more desirable disadvantages when compared to the other hybrid methods, Li-ion and SC hybrids come in close second as they have the difference of the disadvantage of a limited cycle life when compared to the FC and SC hybrid. The other hybrid methods are also very advantageous however they have the downfall of being quite a bit larger and more complex than the last two.

## 4. Conclusion

UAVs are fast becoming a ubiquitous resource for industrial and commercial use as they offer many technological and safety advantages. However, in order for the areas of application to expand, the power supply system needs to be upgraded to increase its endurance. There are many different power sources for drones, each with their own advantages and disadvantages, some more than others, depending on the application. Presently the most popular power sources are combustion engines, FCs and batteries.

The aim of this paper was to review the different power sources currently available for UAVs, to determine their shortfalls and what solutions currently exist to address these shortfalls. The review has been done to help highlight the shortcomings pertained to the specific sources. From this the following conclusions can be made:

### 4.1. Power sources

- Combustion engine powered drones offer the best characteristics across the board, their biggest downfall being their pollution aspect.
- Solar systems, although extremely eco-friendly with a preferable flight time, are much more expensive than the other options.
- If the cost could be justified by the advantages, hydrogen fuel cells offer a great alternative to combustion engines as they have a large flight time, low weight and considerably quick refuel time. They are also very eco-friendly.
- SCs have inverse advantages and disadvantages as compared to the other power sources.

### 4.2. Possible solutions

- Most of the solutions increase complexity of the system.
- The top solutions are FC and SC hybrids and Li-ion and SC hybrids.
- Hybrid systems allow for the reduction of a power source's shortfalls by combining it with another power source that has those aspects as advantages. This allows the user or designer to decide which disadvantages can be tolerated.

Combustion engines are robust but much heavier and have a limited application due to them being mainly applied to fixed-wing types. FCs and batteries offer a large flight time and a larger range since they are more maneuverable but both struggle to supply peak current when required and the supply thereof drains the source at a drastic rate.

Hybrid systems tend to offer a very good advantage over all other systems. They can utilize more than one power source in order to acquire the specific advantages that each power source has to offer. These systems also tend to eliminate small issues such as prolonged charging time, short flight times, poor peak power supply, etc. The most common power source used in hybrid systems is SCs, as they tend to have advantages that overcome the disadvantages of the other power sources.

It was found that the flight time of drones can be improved by implementing a hybrid system. This system however would need to be comparable in weight and size, to an existing drone, while increasing the efficiency in order to be an improvement on the current systems. Hydrogen FC are effectively a hybrid system as they contain Li-Po batteries, but Li-Po batteries have many disadvantages when it comes to their use in drones, they have low energy density, short flight time, comparably long recharge time, they can be hazardous to the environment and have a limited life span compared to the other power sources. As SCs have a high energy density, short recharge period and almost infinite cycle life, they seem to be the obvious replacement for the Li-Po battery in this system but further research is required into how they affect the efficacy of the FC system in drone applications.

## Declarations

### *Author contribution statement*

All authors listed have significantly contributed to the development and the writing of this article.

### *Funding statement*

This work was supported by Hydrogen South Africa (HySA).

### *Competing interest statement*

The authors declare no conflict of interest.

### *Additional information*

No additional information is available for this paper.

## References

[1] Q. Zhai, K. Meng, Z.Y. Dong, J. Ma, Modeling and analysis of lithium battery operations in spot and frequency regulation service markets in Australia electricity market, IEEE Trans. Ind. Informat. 13 (5) (Oct. 2017) 2576–2586.
[2] Z.F. Pan, L. An, C.Y. Wen, Recent advances in fuel cells based propulsion systems for unmanned aerial vehicles, Appl. Energy 240 (February) (2019) 473–485.
[3] M. Alwateer, S.W. Loke, N. Fernando, Enabling drone services: drone crowdsourcing and drone scripting, IEEE Access 7 (2019) 110035–110049.
[4] L. Tang, G. Shao, Drone remote sensing for forestry research and practices, J. For. Res. 26 (4) (2015) 791–797.
[5] M. Alwateer, S.W. Loke, A.M. Zuchowicz, Drone services: issues in drones for location-based services from human-drone interaction to information processing, J. Locat. Based Serv. 13 (2) (2019) 94–127.
[6] L. Ruan, et al., Energy-efficient multi-UAV coverage deployment in UAV Networks : a game-theoretic framework 15 (October) (2018) 194–209.
[7] A. Claesson, et al., Drones may be used to save lives in out of hospital cardiac arrest due to drowning, Resuscitation 114 (2017) 152–156.
[8] S. Loke, M. Alwateer, V. Abeysinghe, Virtual space boxes and drone-as-reference-station localisation for drone services: an approach based on signal strengths, 2016.
[9] A. Shukla, X. Huang, H. Karki, Autonomous Tracking and Navigation Controller for an Unmanned Aerial Vehicle Based on Visual Data for Inspection of Oil and Gas Pipelines, 2016.
[10] M. Bacco, et al., Smart Farming: Opportunities, Challenges and Technology Enablers, 2018, pp. 1–6.
[11] G. Ding, Q. Wu, L. Zhang, Y. Lin, T. Tsiftsis, Y.-D. Yao, An amateur drone surveillance system based on cognitive internet of things, IEEE Commun. Mag. 56 (2017).
[12] J. Lee, et al., Constructing a Reliable and Fast Recoverable Network for Drones, 2016, pp. 1–6.
[13] S. Yoo, et al., Poster, 2015, pp. 275–277.
[14] J. Zhou, B. Zhang, W. Xiao, D. Qiu, Y. Chen, Nonlinear parity-time-symmetric model for constant efficiency wireless power transfer: application to a drone-in-flight wireless charging platform, IEEE Trans. Ind. Electron. (2018) 1.
[15] M. Lu, M. Bagheri, A. James, T. Phung, UAV wireless charging: a review, reconceptualization, and extension, IEEE Access (May 2018).
[16] A. Sato, H. Naknishi, Observation and measurement in disaster areas using industrial use unmanned helicopters, in: 12th IEEE Int. Symp. Safety, Secur. Rescue Robot. SSRR 2014 - Symp. Proc., 2014, pp. 1–5.
[17] A. A. Cc., Afridrones, Afridrones.com, 2019 [Online]. Available: https://afridrones.com/.
[18] V. Aravindan, J. Gnanaraj, Y. Lee, S. Madhavi, Insertion-type electrodes for nonaqueous Li-ion capacitors, Chem. Rev. 114 (Jul) (2014).
[19] S. Ci, N. Lin, D. Wu, Reconfigurable battery techniques and systems: a survey, IEEE Access 4 (Jan) (2016) 1.
[20] K. Rajashekara, Present status and future trends in electric vehicle propulsion technologies, Emerg. Sel. Top. Power Electron. IEEE J. 1 (Mar. 2013) 3–10.
[21] C. Vidal, S. Member, O. Gross, R. Gu, P. Kollmeyer, A. Emadi, xEV Li-ion battery low-temperature effects — review 68 (5) (2019) 4560–4572.
[22] F. Wagner, B. Lakshmanan, M. Mathias, Electrons to go: electrochemistry and the future of the automobile, J. Phys. Chem. Lett. - J PHYS CHEM LETT 1 (Jul. 2010).
[23] E. Karden, S. Ploumen, B. Fricke, T. Miller, K. Snyder, Energy storage devices for future hybrid electric vehicles, J. Power Sources 168 (May 2007) 2–11.
[24] T. Kim, W. Qiao, L. Qu, Power electronics-enabled self-X multicell batteries: a design toward smart batteries, IEEE Trans. Power Electron. 27 (11) (2012) 4723–4733.
[25] J. Meng, G. Luo, F. Gao, Lithium polymer battery state-of-charge estimation based on adaptive unscented Kalman filter and support vector machine, IEEE Trans. Power Electron. 31 (Jan. 2015) 1.
[26] M. Song, et al., Improved charging performances of Li2O2 cathodes in non-aqueous electrolyte lithium-air batteries at high test temperatures, ICMREE 2013 - Proc. 2013 Int. Conf. Mater. Renew. Energy Environ. 2 (82604132222) (2013) 513–515.
[27] R. Components, FG20201 lead acid battery - 12V, 2Ah [Online]. Available: https://za.rs-online.com/web/p/lead-acid-batteries/8431308/. (Accessed 18 May 2020).
[28] R. Components, RS PRO 12V NiMH AA rechargeable battery pack, 2000 mAh [Online]. Available: https://za.rs-online.com/web/p/rechargeable-battery-packs/7770400/. (Accessed 18 May 2020).
[29] R. Components, Samsung 3.6V 18650 lithium-ion battery, 2000mAh [Online]. Available: https://za.rs-online.com/web/p/speciality-size-rechargeable-batteries/8182992/. (Accessed 18 May 2020).
[30] R. Components, RS PRO 12V CS NiCd rechargeable battery, 1800mAh [Online]. Available: https://za.rs-online.com/web/p/rechargeable-battery-packs/1253427/. (Accessed 18 May 2020).
[31] R. Components, RS PRO 1.5V alkaline AA battery [Online]. Available: https://za.rs-online.com/web/p/aa-batteries/7442199/. (Accessed 18 May 2020).
[32] R. Components, RS PRO 3.7V Wire Lead Terminal Lithium Rechargeable Battery, 2000mAh." .
[33] R. Components, "RS Button Battery, PR44, 1.4V, 11.6mm Diameter." .
[34] Mantech, "LITHIUM CELL/BATTERY AA 3V6 2.2AH 14x50." .
[35] NASA, Technology Readiness Level Definitions, 1989, p. 1.
[36] S.A. Kalogirou, Industrial process heat, chemistry applications, and solar dryers, in: Solar Energy Engineering, Elsevier, 2014, pp. 397–429.
[37] DroneII, Drone energy sources [Online]. Available: https://www.droneii.com/drone-energy-sources. (Accessed 30 July 2020).
[38] S. Ganguly, S. Das, K. Kargupta, D. Bannerjee, Optimization of performance of phosphoric acid fuel cell (PAFC) stack using reduced order model with integrated space marching and electrolyte concentration inferencing, Computer Aided Chem. Eng. 31 (2012) 1010–1014.
[39] V. Kumar, R. Rudra, S. Hait, P. Kumar, P.P. Kundu, Performance trends and status of microbial fuel cells, in: Progress and Recent Trends in Microbial Fuel Cells, Elsevier, 2018, pp. 7–24.
[40] S. Haile, D. Boysen, C. Chisholm, R. Merle, Solid acids as fuel cell electrolytes, Nature 410 (May 2001) 910–913.
[41] S. Haile, C. Chisholm, K. Sasaki, D. Boysen, T. Uda, Solid acid proton conductors: from laboratory curiosities to fuel cell electrolytes, Faraday Discuss 134 (Feb. 2007) 17–39, discussion 103.
[42] M. Uzunoglu, M.S. Alam, Fuel-cell systems for transportations, in: Power Electronics Handbook, Elsevier, 2018, pp. 1091–1112.
[43] S. Dharmalingam, V. Kugarajah, M. Sugumar, Membranes for microbial fuel cells, in: Microbial Electrochemical Technology, Elsevier, 2019, pp. 143–194.
[44] M. Steilen, L. Jörissen, Hydrogen conversion into electricity and thermal energy by fuel cells, in: Electrochemical Energy Storage for Renewable Sources and Grid Balancing, Elsevier, 2015, pp. 143–158.
[45] C. Thanomjit, Y. Patcharavorachot, A. Arpornwichanop, Design and Thermal Analysis of a Solid Oxide Fuel Cell System Integrated with Ethanol Steam Reforming, 2012, pp. 287–291.
[46] V. Mehta, J. Cooper, Review and analysis of PEM fuel cell design and manufacturing, J. Power Sources 114 (Feb. 2003) 32–53.

[47] O. Mohammed, D. Lowther, M. Lean, B. Alhalabi, On the creation of a generalized design optimization environment for electromagnetic devices, Magn. IEEE Trans. 37 (Oct. 2001) 3562–3565.
[48] F. Barreras, A. Lozano, L. Valiño, C. Marin, A. Pascau, Flow distribution in a bipolar plate of a proton exchange membrane fuel cell: experiments and numerical simulation studies, J. Power Sources 144 (Jun. 2005) 54–66.
[49] G.Y. Jeon, et al., PEM (proton exchange membrane) fuel cell bipolar plates, in: Proceeding Int. Conf. Electr. Mach. Syst. ICEMS 2007, 2007, pp. 1891–1893.
[50] A. Gong, R. Macneill, D. Verstraete, J. Palmer, Analysis of a Fuel-Cell/Battery/Supercapacitor Hybrid Propulsion System for a UAV Using a Hardware-In-The-Loop Flight Simulator, 2018.
[51] T. Hodgkinson, Long live the senses, Cult. Critiq. 104 (1) (2019) 192–201.
[52] K. Grote, B. Bender, D. Göhlich, Dubbel – Taschenbuch für den Maschinenbau, 25th ed., Springer, 2018.
[53] K. Reif, Dieselmotor-Management im Überblick, second ed., Springer, 2014.
[54] A. Jammer, C. Support, and C. Relay, "Non Sensitive Information – Releasable to the Public ANNEX B NATO Unmanned Aircraft Systems - Operational as Determined via Open-Source ( Public ) Documents ( HALE and MALE Systems Are Presented in Bold ) Non Sensitive Information – Releasable to the Publ," Nation, pp. 1–9.
[55] Y. Liu, X. Ning, Al/Al 2 O 3 interface : a first-principle study, Comput. Mater. Sci. 85 (April) (2014) 193–199.
[56] B. Lojek, History of semiconductor engineering, Hist. Semicond. Eng. (2007) 1–387.
[57] L. Fraas, L. Partain, Solar Cells and Their Applications, second ed., 2010, pp. 581–611.
[58] D. Verstraete, K. Lehmkuehler, K.C. Wong, Design of a fuel cell powered blended wing body UAV, Adv. Aerosp. Technol. 1 (2012) 621–629.
[59] T. Donateo, A. Ficarella, L. Spedicato, A. Arista, M. Ferraro, A new approach to calculating endurance in electric flight and comparing fuel cells and batteries, Appl. Energy 187 (Feb. 2017) 807–819.
[60] L.W. Traub, Range and endurance estimates for battery-powered aircraft, J. Aircraft 48 (2) (Mar. 2011) 703–707.
[61] Y. Wang, K.S. Chen, J. Mishler, S.C. Cho, X.C. Adroher, A review of polymer electrolyte membrane fuel cells: technology, applications, and needs on fundamental research, Appl. Energy 88 (4) (Apr. 2011) 981–1007.
[62] G. Rhoads, T. Bradley, N. Wagner, B. Taylor, D. Keen, Design and flight test results for a 24 hour fuel cell unmanned aerial vehicle, in: 8th Annual International Energy Conversion Engineering Conference, 2010.
[63] L. Peng, S. Zheng, X. Chai, L. Li, A novel tangent error maximum power point tracking algorithm for photovoltaic system under fast multi-changing solar irradiances, Appl. Energy 210 (Jan. 2018) 303–316.
[64] Y. Chen, D. Baek, A. Bocca, A. Macii, E. Macii, M. Poncino, A Case for a Battery-Aware Model of Drone Energy Consumption, 2018.
[65] D. Store, Matrice 600 pro. [Online]. Available: https://store.dji.com. (Accessed 18 May 2020).
[66] BMPower, BMPower Range of products [Online]. Available: https://bmpower.us/. (Accessed 18 May 2020).
[67] Yeair!, Yeair! Is the next generation quadcopter solution [Online]. Available: https://yeair.de/features/. (Accessed 18 May 2020).
[68] Sinovoltaics, Top 8 solar powered drone (UAV) developing companies [Online]. Available: https://sinovoltaics.com. (Accessed 18 May 2020).
[69] K. Rajashekara, Power Electronics for the Future of Automotive Industry, in: PCIM, 2002.
[70] A. Emadi, K. Rajashekara, S. Williamson, S.M. Lukic, Topological overview of hybrid electric and fuel cell vehicular power system Architectures and configurations, Veh. Technol. IEEE Trans. 54 (Jun. 2005) 763–770.
[71] B. Chen, X. Li, S. Evangelou, Comparative Study of Hybrid Powertrain Architectures from a Fuel Economy Perspective, 2018.
[72] M. Yilmaz, P. Krein, Review of battery charger topologies, charging power levels, and infrastructure for plug-in electric and hybrid vehicles, Power Electron. IEEE Trans. 28 (May 2013) 2151–2169.
[73] A. Emadi, Y. Lee, K. Rajashekara, Power electronics and motor drives in electric, hybrid electric, and plug-in hybrid electric vehicles, Ind. Electron. IEEE Trans. 55 (Jul. 2008) 2237–2245.
[74] P. Bajec, D. Voncina, D. Miljavec, J. Nastran, Bi-directional power converter for wide speed range Integrated Starter-Generator 2 (2004).
[75] L. Chedot, G. Friedrich, J.-M. Biedinger, P. Macret, Integrated starter generator: the need for an optimal design and control approach. Application to a permanent magnet machine, Ind. Appl. IEEE Trans. 43 (Apr. 2007) 551–559.
[76] A. Jain, S. Mathapati, V.T. Ranganathan, V. Narayanan, Integrated starter generator for 42-V powernet using induction machine and direct torque control technique, Power Electron. IEEE Trans. 21 (Jun. 2006) 701–710.
[77] M. Chen, L. Huang, J. Yang, Y. Lyu, Design and Simulation of Multi-Energy Hybrid Power System Based on Wave and Wind Energy, 2017.
[78] D. Kraemer, L. Hu, A. Muto, X. Chen, G. Chen, M. Chiesa, Photovoltaic-thermoelectric hybrid systems: a general optimization methodology, Appl. Phys. Lett. 92 (Jun. 2008) 243503.
[79] S.D. Shah, Electrification of Transport and Oil Displacement: How Plug-Ins Could lead to a 50 Percent Reduction in US. Demand for Oil, Jan. 2009, pp. 22–44.
[80] H. Fathabadi, Plug-in hybrid electric vehicles (PHEVs): replacing internal combustion engine with clean and renewable energy based auxiliary power sources, IEEE Trans. Power Electron. 1 (Jan. 2018).
[81] J.-Y. Zou, L. Zhang, J.-Y. Song, Development of the 40 V hybrid super-capacitor unit, Magn. IEEE Trans. 41 (Feb. 2005) 294–298.
[82] R. Lu, C. Zhu, L. Tian, Q. Wang, Super-capacitor stacks management system with dynamic equalization techniques, IEEE Trans. Magn. 43 (1) (2007) 254–258.
[83] A. Burke, M. Miller, Comparisons ultracapacitors and advanced batteries for pulse power in vehicle applications: Performance, Life Cost EVS 19 (Jan. 2002) 855–866.
[84] L.J. Deal, Department of energy 3 (April 2013) (1982) 203–204.
[85] A. Burke, The Present and Projected Performance and Cost of Double-Layer Pseudo-capacitive Ultracapacitors for Hybrid Vehicle Applications, 2005.
[86] Y. Zhang, Y. Mo, Z. Yang, An energy management study on hybrid power of electric vehicle based on aluminum air fuel cell, IEEE Trans. Appl. Supercond. (Sep. 2016) 1.
[87] T. Mesbahi, F. Khenfri, P. Bartholomeus, P. moigne, Combined optimal sizing and control of Li-ion battery/supercapacitor embedded power supply using hybrid particle swarm-Nelder-Mead algorithm, IEEE Trans. Sustain. Energy 8 (Jan. 2016) 1.

# Effect of supercapacitors on the operation of an air-cooled hydrogen fuel cell

**Ashleigh Townsend [a,*], Christiaan Martinson [b], Rupert Gouws [a], Dmitri Bessarabov [b]**

[a] School of Electrical, Electronic and Computer Engineering, North West University, Potchefstroom 2520, South Africa;

[b] DST HySA Infrastructure Center of Competence, Faculty of Engineering, North West University, Potchefstroom 2520, South Africa;

**Abstract** One of the greatest challenges associated with efficient energy use in unmanned aerial vehicles (drones) is that of the energy storage systems – more specifically it's weight and capacity. Current hydrogen fuel cell drones have very promising flight durations, but have a low power density thus performing poorly at peak power demands. Supercapacitors are known to have high power densities and respond significantly well to peak power demands. For this research it is desired to evaluate how supercapacitors can affect the operation of an existing hydrogen fuel cell system, when combined. This study will include the evaluation of the viability of a DC-DC converter used to reduce the size (and subsequently, weight) of a supercapacitor bank. It also evaluates whether specified switching of the sources has an effect. Using data generated from the experiment it was determined that the DC-DC converter (with efficiency >94%) reduced the efficiency (by 0.5%) and duration (by 3.8%) of the supercapacitor bank whilst increasing the weight (by 16.7%). It was also seen that the method of selective switching offered no benefit over that of a self-selecting system, where the former obtained 223 s of usability and the latter 365 s. However, comparing all the results it was observed that the addition of a supercapacitor bank allowed for an improvement in energy- and power density, of the hydrogen fuel cell system, from 0.65 Wh/kg to 1.19 Wh/kg and from 69.7 W/kg to 125.7 W/kg, respectively.

**Nomenclature**

| | |
|---|---|
| DC | Direct current |
| HFC | Hydrogen fuel cell |
| Li-ion | Lithium ion |
| LiPo | Lithium polymer |
| LPS | Laboratory power supply |
| PEMFC | Proton-exchange membrane fuel cell |
| PWM | Pulse width modulation |
| SC | Supercapacitor |
| SOC | State of charge |
| UAV | Unmanned aerial vehicle |

**Highlights**

The effect of a DC-DC converter on a supercapacitor bank is examined.
A DC-DC converter reduces the energy efficiency of a supercapacitor bank.
Supercapacitors improve the response of a fuel cell system.
The energy efficiency of the system is highly dependent on the connection order of components.
Self-selective switching can be achieved through considering the connection order.

**Keywords:** fuel cell; supercapacitor; unmanned aerial vehicle; fuel cell hybrid; supercapacitor hybrid

* Corresponding author:
Email address: ashleighktownsend2@gmail.com (A.Townsend)

## 1 Introduction

Since drones have become more prevalent, many researchers have been evaluating the efficiency of drones and methods to increase the flight times thereof [1,2]. There are mainly two options in achieving this goal: replace the power source with one of a greater capacity, or refuel the power source sporadically [3,4]. The latter requires the use of refueling stations, which, in itself, presents more problems—the unmanned aerial vehicle (UAV) will be required to land periodically and refuel throughout its flight, decreasing the actual usable flight time [5]; stations will be required along the flight path, limiting the range and path, subsequently decreasing the mobility and increasing complexity [6]. These aspects all contribute to increasing the overall costs, unnecessarily. The former option in increasing the flight time offers more possibilities that could be simpler to implement and ultimately more cost effective. Some such possibilities include the following: increasing the capacity by replacing the original power source with one of a greater capacity or combining the existing power source with another to exploit the benefits of both (i.e., hybridization). However, all these options do have their respective advantages and disadvantages [7].

The Ragone plot reported by Aravindan et al. [8] depicts the energy and power densities of selected energy sources. This Ragone plot assists in providing a better understanding of why some sources are preferred over others. The power density refers to the amount of power contained within the volume capacity of a source that it can provide at a specific instance, whereas the energy density refers to the energy (Wh) contained within the volume capacity of a source, therefore, how long it can provide a specific amount of power. From this figure [8], the following are evident: supercapacitors (SCs) can provide a large amount of power (80–75 000 W/kg) but for a short period of time (energy density 0.9–0.1 Wh/kg), while hydrogen fuel cells (HFCs) can provide a small amount of power (1.5–20 W/kg) for a longer period of time (energy density 200–3000 Wh/kg). Furthermore, lithium ion (Li-ion) batteries are similar to HFCs as they too can provide a small amount of power (15–400 W/kg) for relatively long periods of time (energy density 20–150 Wh/kg) [8].

Currently, the demand for UAVs is mainly consumed by military applications, however, in recent years the demand in commercial, recreational and public applications has increased tenfold, and it is expected to exponentially shift further in this direction [9,10]. The use of UAVs in criminal, theft and poaching surveillance is one of the major applications [11], with other applications including scientific monitoring (water sampling, landslides, volcanic activity) and transmission line surveillance [12–15]. At present, combustion engines remain the most popular power supply for UAVs. Yet electrical systems offer a higher efficiency, can be more reliable, they have low to no greenhouse gas emissions and minimal noise [16]—clearly indicating why these systems are becoming more prevalent.

There are many different power sources available on the market such as, batteries, solar power, HFCs, combustion engines, amongst others [17], most of which can be applied to UAVs. Over the years, some of these power sources have been disregarded because, regarding this specific application, they have more disadvantages than advantages, for example, having a weight/size that is too large, being restricted to specific movements, or simply not having sufficient energy density.

Fuel cells offer several advantages, including the following: no direct pollution and no sound, with the refuel/recharge time of a HFC only limited to the availability of hydrogen in the environment and the speed of the acquisition of the hydrogen [18]. According to Schroth et al. [19], a HFC, compared to an equivalent lithium polymer (LiPo) battery, can have an energy density increase by a factor of 150 which is also superior to a gasoline-

powered UAV. However, a HFC has the disadvantage of a lower power density in comparison to a gasoline-powered UAV, meaning that peak power requirements drain the HFC significantly, hence limiting applications and flight times [18,20].

HFCs are often combined with LiPo batteries to improve the power density; however, batteries can have a similarly low power density [19]. Thus, although the addition of a battery can increase the endurance of the system and improve peak power performance, the increase is not to the desired point. Furthermore, both power supplies are still significantly drained during these peak power instances—thus still limiting the flight time of the system.

SCs have a very large energy capability, with a fast release aspect. This means that they can provide very large amounts of current over very short periods of time. However, SCs are very large in size (and weight) when compared to LiPo batteries of equivalent capabilities, thus making drones quite large in size. Although SCs have low energy densities, in comparison to batteries, they offer quick bursts of energy during peak power demands and can store energy quickly that would otherwise be lost [20]. Thus, the addition of SCs to any of the energy sources mentioned should lead to much better efficiencies of UAVs, especially during peak power requirements. SCs are relatively new, therefore they are still quite expensive and little research has been carried out into their application in combination with HFCs.

The HFC available to this project is currently being used in combination with a LiPo battery of similar power- and energy density. It was thus seen as beneficial to examine how the use of SCs can affect the functionality of this HFC system. The aim was to investigate this hybrid combination, with the future desire to replace the power source of a HFC UAV. Specific aspects focused on: determining the effect of the use of a DC-DC converter in conjunction with the SC bank, determining the effect of SCs on the operation of a HFC and determining the effect of selective switching and power source connection order on the operation of the hybrid combination.

## 2 Materials, methods and calculations

This project entails the design and build of an experimental setup to be used to test a proposed solution to a highlighted problem – combining multiple sources with various energy- and power densities to improve the characteristics of the energy source for eventual use in and improvement of a drone flight. For this it is necessary to discuss the setup of the experiment, the power sources to be used and the configuration of their use. These will be discussed below.

### 2.1 Hydrogen fuel cell hybridization case studies

To combine the power sources it is necessary to first determine how previous combinations were made and what the results and recommendations from those previous experiments were. This is done using case studies discussed below.

#### 2.1.1 Hydrogen fuel cell and battery combination

Many studies have been done using this particular type of combination, these case studies will be used to assess the specific energy management of each as well as the outcomes and suggested improvements. Bauman et al. [21] utilizes a 35 kW HFC is combined with a Li-ion battery of 346.5 V, where the HFC utilizes a DC-DC converter in order to boost the voltage to (250 – 400 V) in order to use a smaller HFC to reduce costs and

vehicle mass; the battery, however, does not use a converter as it delivers the required voltage. In this study the battery stores regenerative braking energy (when battery is less than 98% charged), supplements the HFC during extra power requirements as well as very low power requirements (the HFC is inefficient below a certain power level – 7.55% of the total) and is only charged via the HFC when the state of charge (SOC) is less than 50%.

Charging the battery through regenerative braking instead of the HFC increases fuel economy. From this study it is seen that the HFC & battery combination has a slightly lower efficiency when compared to the HFC, SC & battery combination, even though the weight of the former system is significantly less. An advantage of the HFC & battery combination is that it is more cost effective due to the absence of the SCs and the bidirectional DC-DC converter. A major disadvantage is that the battery life is much shorter than that of the HFC, SC & battery combination as the battery is continuously charged/discharged throughout the operation of the vehicle.

Thoungthong et al. [22] utilizes a proton-exchange membrane fuel cell (PEMFC) of 500 W, 40 A, 13 V is combined with a lead-acid battery of 33 Ah, 48 V to supply a HFC vehicle. The HFC will utilize a boost converter to optimize the characteristics and boost the output voltage to that of the battery. The battery will not use a converter in order to minimize costs and improve efficiency of the system. The HFC will be the main energy source and when the power demands are large, decrease below the specified level of the HFC or regenerative breaking energy is present in the system the battery will be utilized. This configuration leads to a significant degradation in the battery lifetime, as the battery is constantly supplementing the HFC there is no method to improve this issue without altering the setup (i.e. the use of an additional SC bank to rather supply the peak power demands). The HFC is also used to recharge the battery throughout the operation. This system does improve the efficiency and fuel consumption of the HFC however it leads to an additional consideration in lifetime of the battery as this is significantly reduced due to the charge/discharge of the battery throughout the operation of the system.

The combination suggested by Bauman et al. [21] consisted of a battery pack used in conjunction with an HFC; the former used when there is a high-power demand and the latter as the main source of power. It can also be seen from this configuration that the battery will receive the surplus energy that is not absorbed by the load during low load power. The system worked well with the exception of equipment having lower precision than desired causing a higher error rate and, on occasion, the incorrect operation of the hybrid power system. The system had an overall high efficiency (>90%) with lower hydrogen fuel consumptions.

### 2.1.2 Hydrogen fuel cell and supercapacitor combination

The combination of the HFC & SC has had a few previous studies and experimental combinations, but all had some form of a limitation, these limitations will be of importance in this experiment. Bauman et al. [21] utilizes a 35 kW HFC combined with a SC bank to supply a HFC vehicle. The HFC utilizes a boost DC-DC converter to increase its voltage to that required by the motor (250 – 400 V) such that a smaller HFC can be used to reduce vehicle mass and overall costs. The SC bank consists of 27 SC-packs are used in series comprising of six 2.5 V, 350 F cells in series, thus 405 V, 2 F capacity. The SCs do not use a DC-DC converter in order to reduce costs and weight of the system and improve efficiency. The SCs store the regenerative braking energy and only provide extra power when it is required (during accelerations). Best fuel economy is achieved when the sum of kinetic energy in the vehicle and the potential energy of the SCs is kept constant. This study shows

that the HFC & SC combination cannot compete with the HFC & battery combination as the SC bank does not have enough energy storage to provide for the peak power requirements. It is suggested that a few SC banks be combined in parallel to increase the energy storage capabilities, however, this increases the weight of the system tremendously decreasing fuel consumption to an infeasible point lower than the HFC & battery combination.

Thoungthong et al. [22] utilizes a PEMFC of 500 W, 40 A, 13 V combined with a SC bank of 292 F, 500 A, 30 V to theoretically power a HFC vehicle. The HFC will utilize a uni-directional boost converter while the SCs will utilize a bi-directional converter to facilitate the power requirements and the storage of the regenerative breaking energy. For this setup, the HFC will be the main supply of power and when peak power demands are observed or regenerative breaking energy is increased above 0, the SC bank will be utilized. The HFC will also be used to recharge the SCs throughout the operation. This setup does allow for HFC downsizing, increased efficiency characteristics as compared to only HFC use and energy recovery through regenerative breaking. The downside of using only SCs as the auxiliary power source is that the system could malfunction during start-up as the HFC requires 5-10 minutes of constant power. For both of these case studies the future adjustments would be to either increase the SCs energy characteristics or to look into a hybrid system that includes the use of a battery to absorb the bulk of these constant power requirements.

### 2.1.3 Hydrogen fuel cell, battery and supercapacitor combination

Fewer studies have been done into the use of the power sources in this combination than in the prior two combinations. These case studies will be used to assess the viability of the combinations as well as defining some limitations observed leading to room for improvement.

Bauman et al. [21] utilizes a 35 kW HFC combined with a SC bank (405 V, 2 F) and a Li-ion battery (346.5 V) to supply a HFC vehicle. The HFC utilizes a boost converter such that the HFC required can be smaller and thus more cost effective and the battery will use a bi-directional converter in order to be recharged while the system is in use. In order to minimize mass of the system it is determined that only one of the additional power sources (batteries or SC) will use a converter. The SC will be used to supply power only during peak power requirements and will accept regenerative braking energy only if the SCs are below 400 V; the batteries will continuously supplement the HFC during normal operation, will also be used to store regenerative braking energy (when the SCs don't) and will also be used when the power requirements are too low for the HFC (< 7. 55%), thus, the bi-directional converter is chosen to be used in conjunction with the batteries for its charge/discharge.

The SCs are used to lengthen the lifetime of the batteries and are therefore monitored to remain within the required 250 – 400 V of the load motor. One major advantage of this setup is that the degradation of the battery is delayed due to it not undergoing high current charge/discharges. The battery in this setup is only used for peak power when the SC is discharged, whereas it is used for all peak power requirements in the HFC & battery combination. This setup does have the downside of being much heavier (due to the SC pack addition) and also more expensive (due to the addition of the SCs and the bidirectional converter), however, it still has a lower fuel consumption compared to that of the HFC & battery setup.

Thoungthong et al. [22] utilizes a combination of a HFC – used as the main source of power, batteries – used to provide boost power over moderate durations and SCs – providing a fast acting source to smooth rapid transients and reduce the degradation of the

HFC and battery. This system was tested using a flight simulator in order to get a desired flight profile and performed adequately during all stages of the simulation. These sources are used in conjunction to supplement each other. The battery removes a significant load off of the HFC allowing the HFC to have a much lower voltage drop throughout the simulation. The SC allows for a much smoother power curve providing significant energy absorption to the system. Thus, it provides considerable load smoothing to the HFC and has the expected benefit of increasing the lifetime and durability of not only the HFC but also the battery.

## 2.2 Experimental setup

The general concept for the proposed experiment will be explained using the conceptual flow diagram shown in Fig. 1. The shaded blocks represent the main focus of this experiment – the SCs, controller, DC-DC converter and load switch. The HFC system to be used contains its own DC-DC converter and controller – this existing controller controls when the HFC requires a power supplementation as well as controlling the operation of the HFC, therefore, this controller will not be altered and an additional controller will be used to control the auxiliary circuit (shaded blocks). The solid lines represent the flow of power within the circuit while the striped lines represent the flow of control (either measurements or signals).

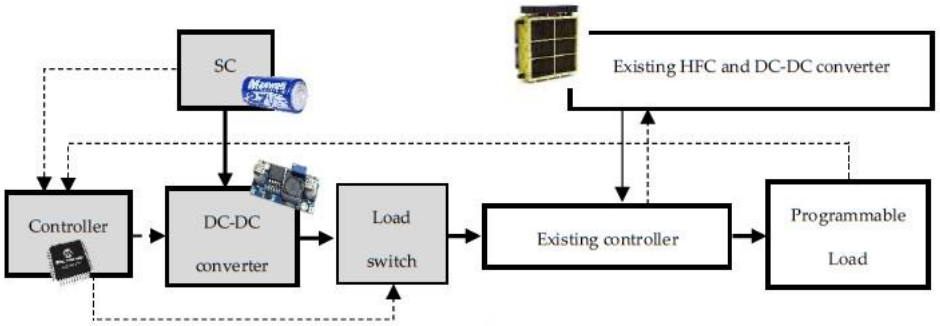


**Fig. 1 – Conceptual flow diagram**

The controller receives the power requirements from the programmable load which is used to control the load switch (ON or OFF) – this switch remains closed (ON) for the majority of the tests as it is only desired to remotely control when the SCs are available for certain tests (further explained in section 2.3.4). The SCs send a signal of SOC to the controller which is used to calculate the duty cycle required for the desired output of the DC-DC converter, this duty cycle is sent as pulse width modulation (PWM) signals to control the converter.

The existing HFC system has a constant voltage rating and it is desired to match the SCs voltage with this rating; as the SCs deplete their voltage decreases to a level below this required voltage; to avoid this, a DC-DC converter will be used to boost the voltage of the SCs, to that of the HFC system. The DC-DC converter will also be used to limit the current provided by the SCs to the converter's capabilities. The DC-DC converter will be uni-directional such that the SCs can only provide power and not use it. The HFC system will be used to supply the load and when the load has a power requirement above that which the HFC system can provide, the SCs will be utilized. For the initial tests there will be no control over the use of the SCs (the load switch will be closed), thus allowing them to continuously contribute to the load when required. For a more detailed discussion of the

operation Fig. 2 will be used. The solid lines indicate power transmission and the striped lines represent signal transmission.

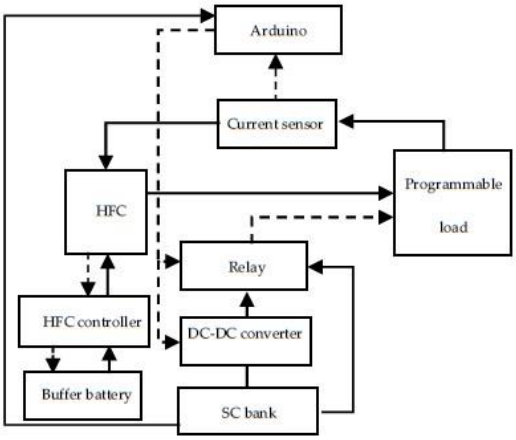


**Fig. 2 – Operational flow diagram.**

The programmable load was programmed to repeat a specified load (see subsection 1.1 for a detailed discussion). The current requirements of the load were measured using a current sensor placed between the HFC and the load and sent to the microcontroller (Arduino); the HFC controller determined the use of the buffer battery to supplement the HFC. The current measurement sent to the microcontroller was used to determine the switching of the relay (further discussed using Fig. 3 and section 2.3.4). The SOC of the SC bank was sent to the microcontroller to be used to determine the PWM signal of the DC-DC converter. Dependent on the configuration, the SC bank was used either with or without the inclusion of the DC-DC converter, these configurations are discussed in section 2.3.4.

Fig. 3 shows a functional flow diagram. Here, a relay was used to select when the SC bank was required to supplement the HFC system in supplying the load. This relay was switched using an Arduino, which simply read the value measured by the current sensor and, if determined to be >7 A, the Arduino would send a signal to the relay to engage the coil and allow current to flow from the SC bank to the load. This selection was only used for a specific configuration discussed in section 2.3.4, for all other configurations the relay remained engaged.

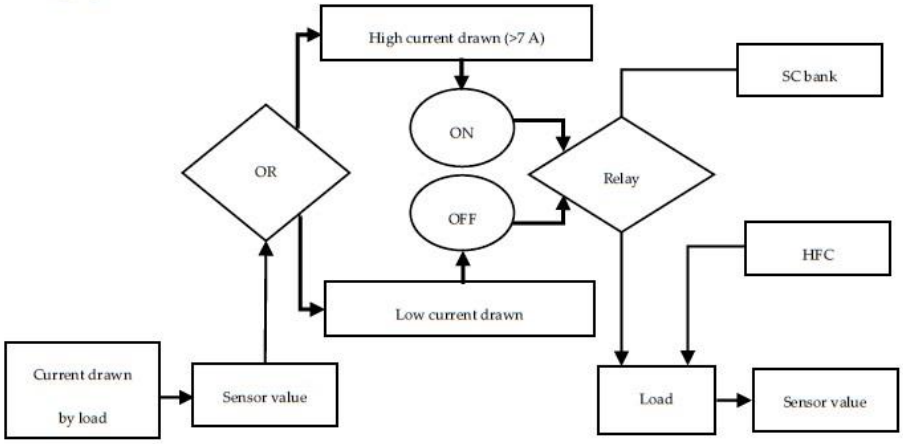


**Fig. 3 – Functional flow diagram.**

## 2.3 Power sources

This research comprises the combination of three power sources in different configurations, in order to assess the effect of each on the output. The research includes the use of an HFC, a SC bank and a LiPo battery. Each of these sources has their respective capacities for the combination, as is explained below.

### 2.3.1 Hydrogen fuel cell

A 1 kW HFC system obtained from BMPower [23] was available for use. It was initially tested with the original full load profile of maximum 1.2 kW. The HFC system has the capability of providing 1 kW at 50 V. It can also be combined with a LiPo battery, used as the buffer battery (it is used to supplement the HFC when the HFC requires assistance). The available HFC system has a controller that determines the use of the buffer battery and controls the operation of the HFC. For purpose of this experiment the HFC will be used in combination with the LiPo battery and existing controller as one system.

### 2.3.2 Lithium polymer battery

The battery pack used to supplement the HFC consists of two 12 s LiPo batteries, each with a weight of 0.4 kg, 50 V rated voltage and energy density 160 Wh/kg. Using these details and Eq. (2.1) (obtained using a process of elimination and Eq. (19.9) from [24]), the capacity rating of the battery pack was determined. Each battery was calculated to have a capacity of 1.33 Ah, thus 2.66 Ah for the battery pack.

$$Capacity(Ah) = \frac{Energy\ density\left(\frac{Wh}{kg}\right) Weight(kg)}{Nominal\ voltage\ (V)} \tag{2.1}$$

### 2.3.3 Supercapacitor bank

Previous case studies suggest the use of a SC bank that can match the capabilities of the existing system it wishes to be combined with [18,21,22,25–29]. The existing HFC system contains a buffer battery that supplements the HFC when required. As the SC bank was also used to supplement the HFC, it is desired that it matches the capacity of the buffer battery.

As calculated, the buffer battery pack has a capacity of 2.66 Ah (maximum voltage 50 V and weight 0.8 kg). If the buffer batteries were to be simply replaced by an equivalent SC bank then these requirements will allow the system to operate in an equivalent fashion without compromising the efficiency thereof [21].

To determine the values of the capacitors, the capacity of the buffer battery pack was converted to the applicable unit in Farad. To achieve this, the capacity rating is first converted to ampere–second, thus converting to Coulomb, using Eq. (2.2) (adapted from Eq. (19.2) in [24]).

$$Capacity\ (C) = 3600\big(capacity\ (Ah)\big) \tag{2.2}$$

Using the capacity rating of 2.66 Ah, the capacity was converted to 9 576 C. Next, the capacitance can be calculated using Eq. (2.3) (Eq. (18.10) from [24]).

$$Capacitance\ (F) = \frac{Capacity\ rating\ (C)}{Voltage\ (V)} \tag{2.3}$$

Using the calculated capacity rating and a voltage rating of 50 V, the total capacitance was calculated to be 191.52 F. The nominal voltage of a SC is 2.7 V, thus 19 cells will be required in series to reach 50 V. In series, the total capacitance can be calculated using Eq. (2.4) (Eq. (6.28) from [30]), which can be rewritten to calculate the capacitance per cell.

$$Total\ series\ capacitance = \frac{capacitance\ per\ cell}{number\ of\ cells} \quad (2.4)$$

This equation is valid under the assumption that all connected capacitors have the same capacitance; thus the required capacitance per cell will be 3638.88 F. The largest SC available is 3400 F, with a rated voltage of 3 V per cell. With these values, only 17 cells will be required, thus reducing the capacitance per cell to 3255.84 F. Therefore, the 3400 F cells will be sufficient. According to the Maxwell datasheet [31], the weight of one 3 V/3400 F SC cell is 496 g, therefore the combined weight would be 8.43 kg, which is far greater than 800 g.

To solve the weight issue, the system was designed to accommodate SCs that only supply the increase in power above 1 kW. Furthermore, a boost DC-DC converter was used to increase the voltage requirements from a lower level to the desired 50 V. This allowed the SCs to be much smaller and to recharge much faster, hence making the system more efficient. From the load profile, the maximum power consumed is ~1200 W, which is above the 1 kW rating of the HFC. It is at these points above 1 kW that the SC bank will be required.

The system was designed such that the SC bank is utilized twice during the load (to be discussed in section 2.4 and indicated in Fig. 5 by the green blocks), with each period lasting 2 s. As SCs have the tendency to provide the bulk of the load, the assumption was made that the average power supplied by the HFC will be ~400 W and the SC bank will need to supply the remainder of the power, namely 650 W for the first instance and 800 W for the second instance.

Calculating the energy requirements, for the first instance of 650 W, 1300 J will be required, and for the second instance of 800 W, 1600 J will be required, giving a total of 2900 J. This value was initially rounded up to 3000 J. It was assumed that this is only 80% of the requirement, thus 100% would require 3750 J.

The maximum duty cycle of a boost DC-DC converter is ~70%, thus the SCs will only be able to be boosted with a 70% increase in the maximum voltage. Using $V_{out}$ = 50 V and a duty cycle of 0.7, $V_{in}$ (the minimum required input voltage) is equal to 15 V.

However, SCs have an allowable voltage drop, for efficient lifetime usage, of 20%, therefore the 15 V will be the 80% SOC of the SC bank, at which the converter will be able to boost the input voltage for the entire 20% discharge of the SC bank; 100% SOC of the SCs will therefore be 18.75 V. To achieve this total voltage, about seven cells of 2.7 V each were required—this value is rounded up to eight cells. The maximum voltage will be 21.6 V and the minimum will be 17.28 V. To determine the required capacitance of the SC bank, Eq. (2.5) is used.

$$C = \frac{2(energy\ (J))}{V^2} \quad (2.5)$$

The 3750 J, calculated earlier, is the energy required at the output of the DC-DC converter. Using the law of energy conservation and the efficiency of the system, the output energy of the converter will be a percentage of the input energy. This percentage is the efficiency of the converter (assumed to be 90%). This 10% difference is due to power losses occurring in a system. Therefore, the required input energy was determined using equation (2.6) (Eq. (6.10b) from [24]).

$$E_{in} = \frac{E_{out}}{\eta} \quad (2.6)$$

For this equation, $\eta$ refers to the efficiency constant of 0.9 and results in a minimum required energy at the input of 4167 J. Using this energy requirement and the minimum voltage of the input (80% of the SC bank maximum voltage—mentioned earlier as the most efficient SC operating range), the total capacitance was calculated and rounded up to 28 F. The minimum voltage of the SCs is used as this will ensure that the SCs have sufficient

energy for the requirement, for the entire range of discharge. Using Eq. (2.4) and eight cells, the capacitance per cell was calculated to be 224 F.

To verify that this value is correct, the energy it can supply was calculated and compared with the energy requirement of the load profile. The input energy was calculated to be 6532 J (with 28 F total capacitance), which is greater than the 4167 J requirement at the input—thus a value greater than 224 F per cell can be used in the system. For this project, the capacitance per cell was chosen to be 360 F, which delivers 10498 J (more than sufficient to account for losses in the system). According to the Maxwell Technologies datasheet [32], each one of the SCs weighs 71.4 g, giving a total of 571.2 g, which is well under the weight of the two batteries of 0.8 kg, hence leaving sufficient weight for the circuitry.

### 2.3.4 Configuration

The power sources were tested in multiple configurations in order to assess how each source affects the operation of the system in response to the load. These configurations were also used to compare the results, to determine which is best suited for the application. Before the SC bank was combined with the HFC system, each individual power source's response to the load was required—this allows for a simpler evaluation of the individual contributions when the sources were combined. Three individual tests were initially conducted – the HFC system, the SC bank and the combination of the two power sources.

It was also desired to determine the effect of the DC-DC converter on the SC bank and the system. Therefore, two additional tests were conducted, in which the SC bank was combined with a DC-DC converter. One final test was conducted to show how the addition of selective switching affects the hybrid system. Furthermore, it was also desired to determine whether the order of the connections affected the operation of the system. Two rounds of tests on the six combinations were conducted (to verify the results obtained from each test). The connections for the respective rounds are shown in Fig. 4 (use was made of two switches to demonstrate the required connections).

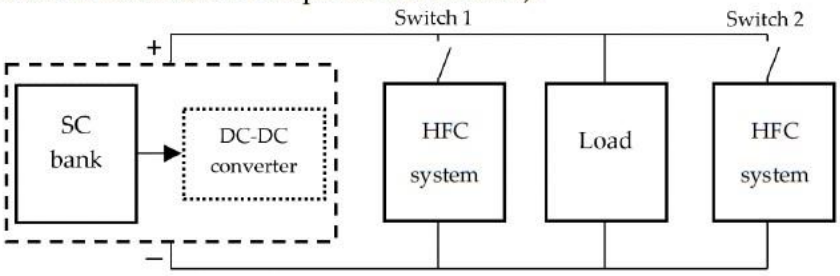


Fig. 4 – Connections 1 & 2: experimental tests.

For round 1 (connection 1) the switch 1 was closed while switch 2 remained open. This connection indicates that the sources are connected in parallel with each other and the load, with the load at the end of the parallel connection. For round 2 (connection 2) switch 1 remained open and switch 2 was closed. This connection again indicates that the sources are connected in parallel with each other and the load, but now with the load between the two sources.

To summarize the six combinations – the HFC and SC were tested individually and then as a combination; the SC bank was combined with the DC-DC converter and tested individually and when combined with the HFC; finally, the HFC and SC (with DC-DC converter) were combined using a relay to control the switching.

## 2.4 Load profile

The load profile used to assess the operation of the different configurations was obtained from an existing hydrogen drone and reduced to a level that can be used by all the power sources. The original load profile is shown in Fig. 5.

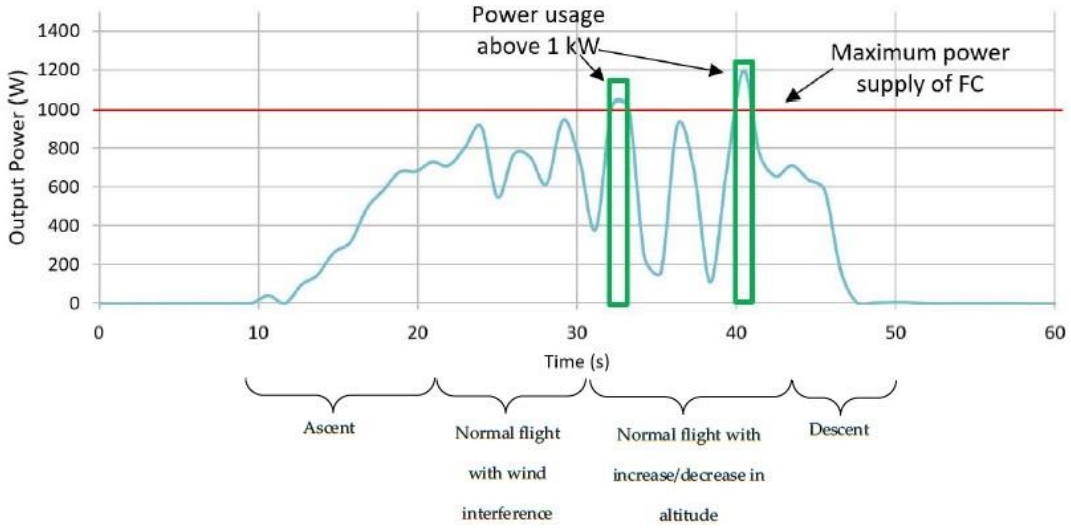


**Fig. 5 – Full load profile (1.2 kW).**

In this load profile there is a horizontal line indicating when the proposed system makes use of the buffer battery to supplement the HFC. This occurs when the system requires more than 1 kW of power to operate. The HFC system (including the buffer battery) provided for this experiment has a rating of 1 kW, however, as the HFC is used for research and experimentation in the HySA laboratory at the North West University, through the years of operation the system has degraded to a point where it is suggested to be used to supply a maximum of 450 W. As the system can supply 50 V, this leaves a maximum current supply of 9 A. While testing the new load profile (450 W maximum) it was discovered that with a maximum demand of 9 A from the load, the HFC system supplied a maximum of 350 W, therefore the load profile was initially reduced accordingly to 350 W.

It is suggested in the case studies [21,22] that the SC bank be used without a DC-DC converter to mainly reduce costs. This project has the future goal of combining SCs into a HFC drone – therefore the experiment is weight and size sensitive. For this experiment it is desired to examine how a DC-DC converter will affect the operation of the SC bank and the entire hybrid system to determine whether it is viable and can be used to reduce the size and weight of the SC bank. Therefore, the point of reference for all the experimentation was chosen to be the SC bank without the DC-DC converter.

The SC bank was designed to have a maximum voltage of 21.5 V. The available HFC has a voltage of 50 V – which is desired to be matched by the SC bank; a smaller HFC is not available for experimentation and the available one is attached to a building supply of hydrogen that is constantly replenished. When the HFC was tested with repetitions of the 9 A (450 W) version of the load profile shown in Fig. 5 it was shown that the HFC has an unvarying supply of the load. For this reason it was decided that the HFC would be replaced with a laboratory power supply (LPS) with a maximum 1.6 A, 21.5 V rating. This replacement allowed the unaided SC bank to match the theoretical HFC voltage whilst still

obtaining usable and comparable results. As of such the load profile was further reduced to a 3 A, 52 W maximum load shown in Fig. 6.

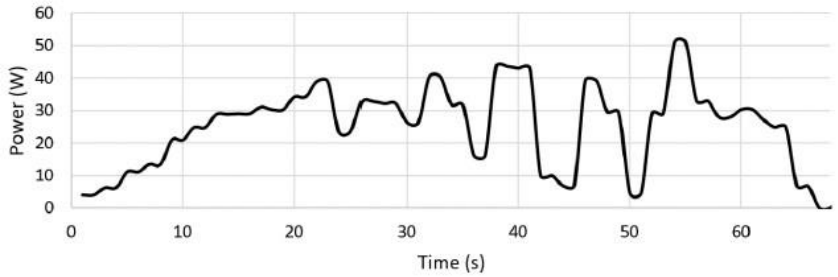


Fig. 6 – Adjusted 3 A load profile.

The SC bank was designed for the full 1.2 kW load profile, as it will allow for an easier transition when a larger HFC system is available, and the DC-DC converter was designed for the 3 A load profile as it is desired to be combined with the available HFC system.

## 3 Simulations

The configurations mentioned above were simulated using Simulink® to assess the validity of the circuit design and proposed experiment as well as to have a basis for comparison against the experimental results. These simulations are provided below. The Simulink® circuit used for the experimentations follows the configuration shown in Fig. 4, with the HFC simulated using a Voltage source block and the SC bank using the Supercapacitor block built in to Simulink®.

### 3.1 Hydrogen fuel cell system

The response of the HFC to the required load is shown in Fig. 7.

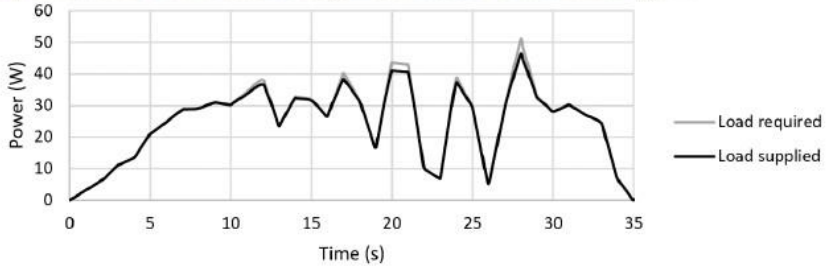


Fig. 7 – Simulated response of HFC system to 3 A load.

From the figure it is evident that the entire load was not provided, however, the HFC managed to supply 99.47 % of the load – this deviation is expected to be provided by the SC bank. In order to determine the duration of the HFC system here and onward, Faradays Law of Electrolysis [33] will be consulted – this loosely states that the hydrogen consumption is proportional to the current drawn. Therefore, to determine the hydrogen consumed, the current drawn for a single repetition will be used in Eq. (3.1).

$$It = \frac{V\rho Fz}{M} \tag{3.1}$$

Using this equation the duration of the HFC system is determined to be 268 s.

### 3.2 Supercapacitor bank - unaided

The response of this system to the load is shown in Fig. 8.

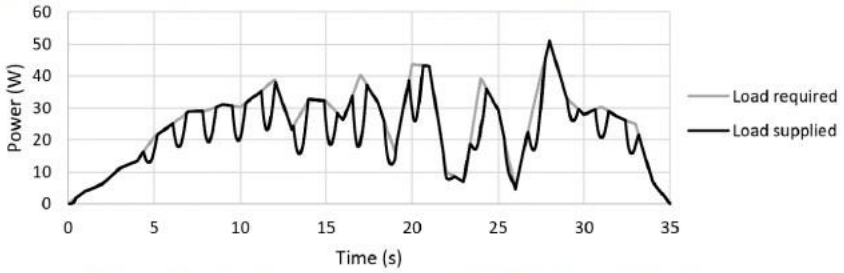


**Fig. 8 - Simulated response of unaided SC bank to 3 A load.**

It is evident from the figure that the load is initially provided whereafter the provision decreases for each repetition according to the depletion of the SC bank. The load was repeated until the SC bank reached the recommended 80% SOC – found to be after 190 s with the required load being provided with an efficiency of 90.69% for this duration. The SC bank achieved a 99.99% efficiency for the first repetition – this is 0.53% better than the HFC.

### 3.3 Supercapacitor bank with DC-DC converter

The response of this combination to the 3 A load is shown in Fig. 9.

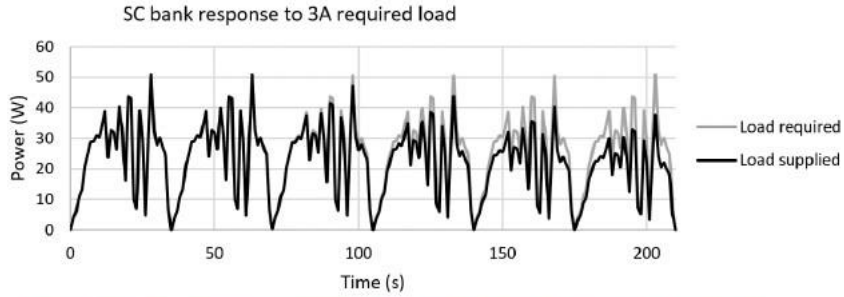


**Fig. 9 - Simulated response of SC bank with DC-DC converter to 3 A load.**

The response shown is that measured at the output of the DC-DC converter. The load was repeated until the SC bank reached 80% SOC – after 186 s. for this duration the load was supplied with 91.58% efficiency. This lack of provision is evident from the figure and results in the assumption that the DC-DC converter does not improve the performance of the SC bank – it decreases the usable time and the measured efficiency.

### 3.4 Hydrogen fuel cell-supercapacitor system – unaided

The response of this combination to the load is seen in Fig. 10.

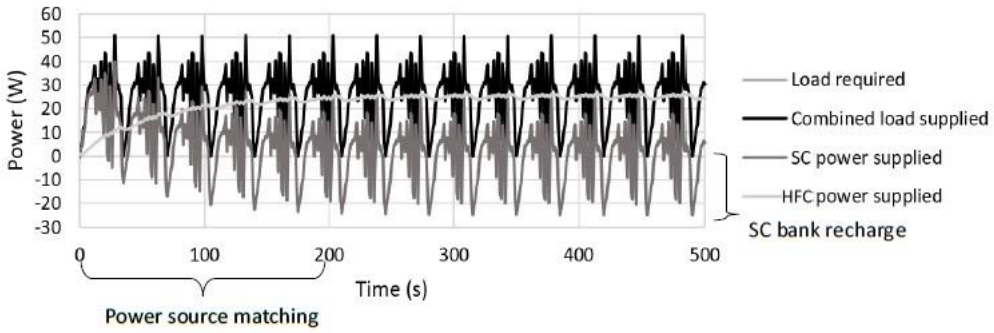


**Fig. 10 - Simulated response of HFC-SC unaided combination to 3 A load.**

The individual contribution of each source as well as the combined contribution to the load is shown for the duration of the load. This combination delivered an efficiency of 99.99% - the required and combined supplied load lie on top of each other in the figure. It is apparent that the HFC is providing the bulk of the load with the SC providing the jumps in load above that which the HFC can supply.

It is seen in the figure that the graph of the power supplied by the SC extends into the negative region of power – this shows that the SC bank is receiving power from the HFC. This is expected as there is no method of blocking the flow of current towards that SC bank in this configuration and as such as it depletes it starts absorbing power in order to recharge. The duration of this system was determined using Eq.(3.1) as 249.75 s. As the HFC system continually recharges the SC bank it will only drop to 80% SOC when the HFC is depleted to the point where it can no longer provide for the SC bank. Therefore the duration of this combination is seen as the duration of the HFC.

## 3.5 Hydrogen fuel cell-supercapacitor system with DC-DC converter

The response of this configuration to the 3 A load is shown in Fig. 11.

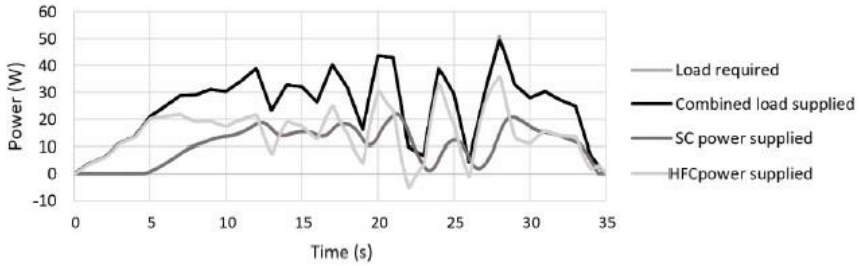


Fig. 11 - Simulated response of HFC-SC-DC-DC converter to 3 A load.

The individual contribution of each source can be seen above with the combined contribution having a 99.91% efficiency in providing the required load. Using Eq.(3.1) the duration of the HFC is determined to be 403 s while the SC bank has a duration of 428.08 s – therefore the system has a duration of 403 s. As the DC-DC converter is bidirectional it blocks the current flow toward the SC bank therefore not allowing it to be recharged by the HFC. It is evident from the figure that the HFC provides the bulk of the load with the SC bank providing the increase in power at the peak requirements of the load.

## 3.6 Hydrogen fuel cell-supercapacitor system with DC-DC converter and selective switching

The response of this system to the load is seen in Fig. 12.

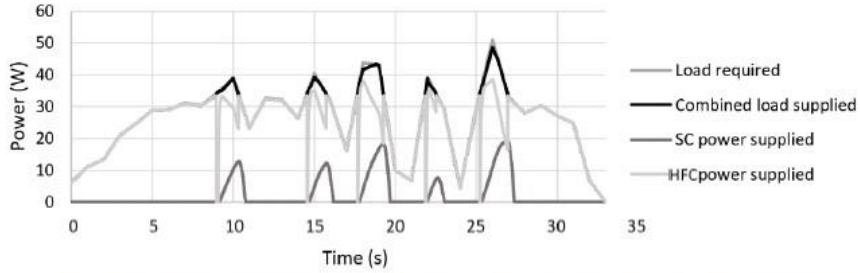


Fig. 12 - Simulated response of HFC-SC-DC-DC converter with selective switching to 3 A load.

For this combination a relay was set to only allow the SC bank to provide power when the power needs exceeded ~35 W. It is shown in the figure that at these points the HFC

initially supplies drops to supply no load – this can be attributed to the SCs very low internal resistance (3.4 mΩ) and willingness to supply the entire load. For the duration of the load – calculated as 293 s using Eq.(3.1) (293 s for the HFC and 2265 s for the SC bank) – the system achieved a 99.66% efficiency.

# 4 Experimental results

## 4.1 Hydrogen fuel cell system

The available HFC system that was used in the experiments is shown in Fig. 13, the dimensions of which can be obtained from the datasheet [23]. This system is supplied by a hydrogen source connected to the building where it is stationed, thus the hydrogen supply was constant.

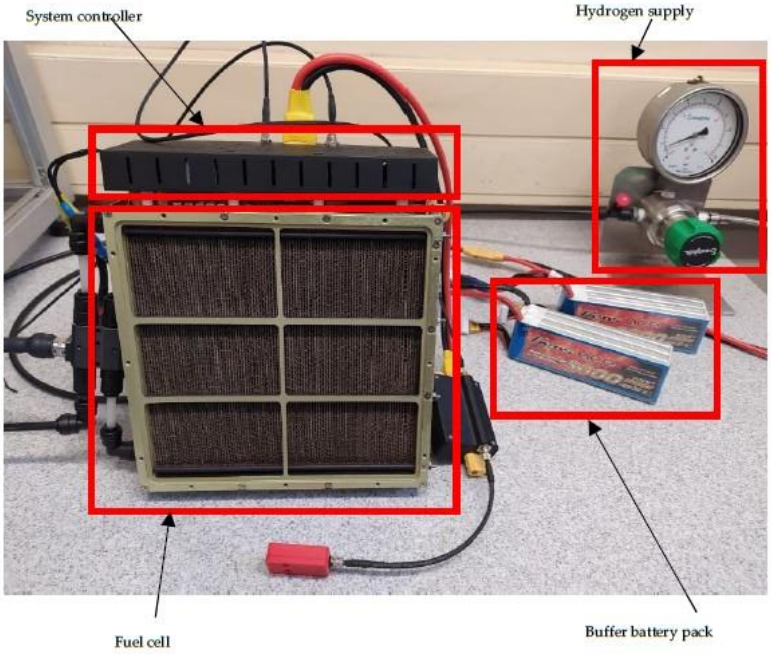


**Fig. 13 – HFC system used for experimentation.**

The available HFC system was tested using a reduced 9 A load as it was degraded, such that it had a maximum deliverance of ~350 W (explanation provided in section 2.4). Therefore, the 1.2 kW load was reduced equivalently and used to test the HFC to determine its response to the load, shown in .

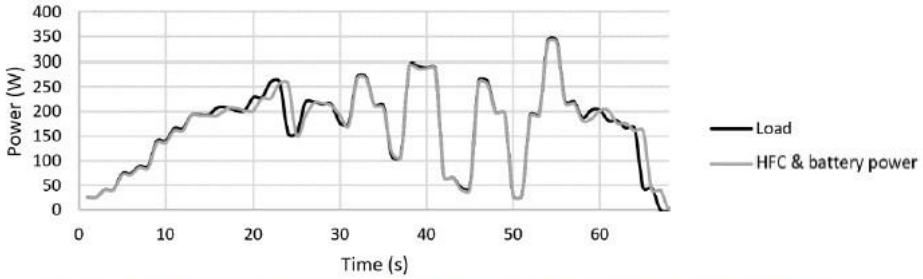


**Fig. 14 – Experimental response of power supplied by HFC system to 9 A load.**

It is evident that the HFC system provided the power required by the load with a calculated efficiency of 99.62%.

It was however desired to combine the SC bank with the HFC system without the use of a DC-DC converter. The requirement here is that the SC bank matches the voltage level of the HFC, or vice versa. A boost DC-DC converter was used with a maximum current capability of 3 A (new load as explained in section 2.4). The designed SC bank had a voltage of 17.28–21.6 V. Thus, to keep within the 3 A constraint, the SC bank can supply a maximum of 51.84 W at its lowest voltage. For this reason, the HFC needs to have a lower capability. However, the available system cannot be reduced to this point.

Hence it was decided that the HFC system be replaced with an equivalent power source. An LPS was selected as it provided the reduced requirements of 1.6 A at 21 V (both the SC bank and LPS were used with a maximum of 21 V, for consistency, throughout). Before the HFC was replaced with the LPS it was tested with its maximum capacity using the 350 W load such that it could be determined that the LPS replacement is justified. Data in Fig. 15 is used for this justification purpose.

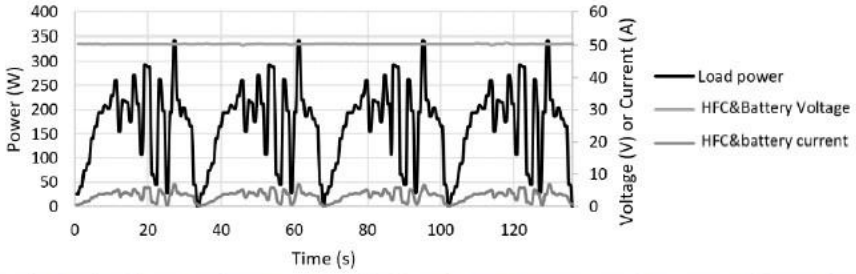


**Fig. 15 – Analysis of voltage and current supplied by the HFC system against power demand of 9 A load.**

It is evident from the figure that the voltage and current supplied by the HFC system, throughout the duration of the load, remained constant. This therefore justifies the use of an LPS as replacement as it will supply the same constant output.

As the SC bank had a maximum current capability of 3 A, the load profile was further reduced to a maximum of 3 A and 51 W for the remainder of the tests. With the replacement of the HFC system, it was desired to see its response to the reduced load of 3 A. Results are shown in Fig. 16.

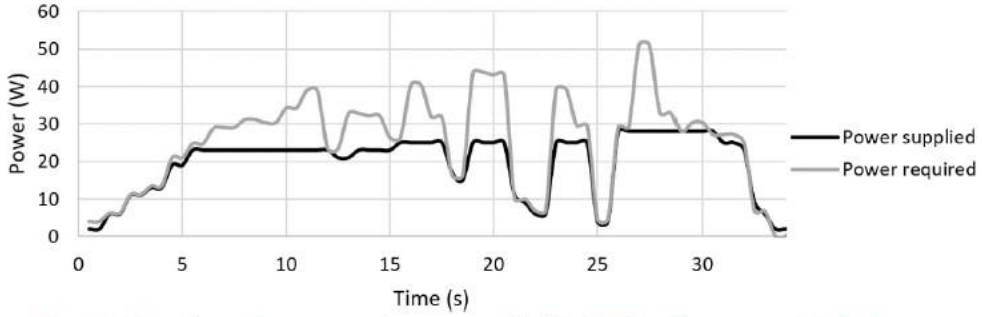


**Fig. 16 – Experimental response of power supplied by HFC replacement to 3 A load.**

It is evident that the HFC replacement can supply a maximum of ~29 W, with a minimum voltage of 17.5 V this gives a maximum current of 1.66 A. With the alterations, this system now had an endurance of 168 s.

## 4.2 Supercapacitor bank

The SC bank was tested under two sets of conditions, with and without the DC-DC converter, to show how the DC-DC converter affected its operation. The system used to conduct the remainder of the tests as well as the SC bank system built (experimental setup used for carrying out tests) is shown in Fig. 17.

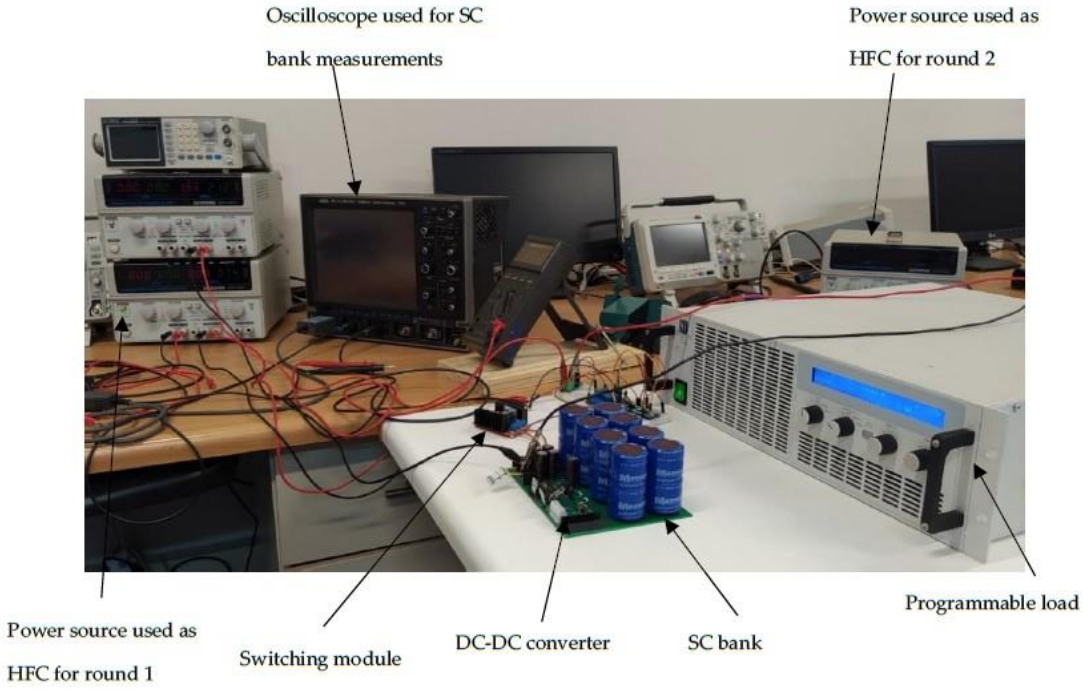


**Fig. 17 – Experimental setup used for testing.**

### 4.2.1 Without DC-DC converter

The SC bank was directly connected to the load and the load was repeated until the SC bank reached its maximum SOC decrease of 20% (at 17.5 V). The response of this connection is shown in Fig. 18.

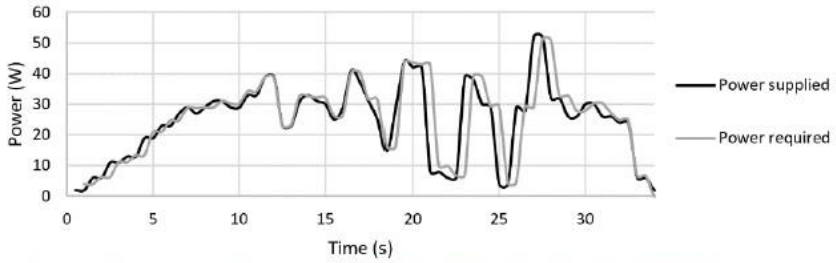


**Fig. 18 – Experimental response of power supplied by SC bank excluding DC-DC converter to load.**

This combination shows a deviation in the power deliverance with a calculated efficiency of 97.21% lasting 130 s.

### 4.2.2 With DC-DC converter

The SC bank was first connected to the DC-DC converter and then to the load. The load was once again repeated until the SC bank reached its 80% SOC value. The response is shown in Fig. 19.

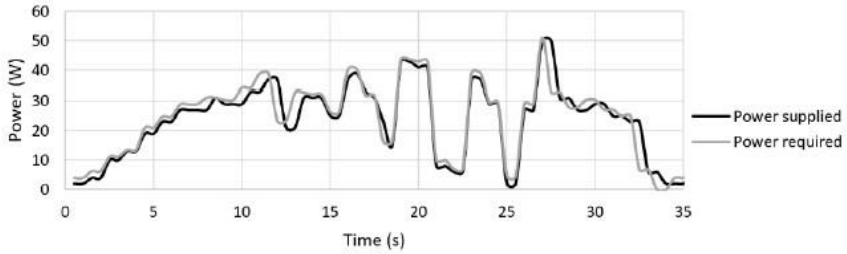


Fig. 19 – Experimental response of power supplied by SC bank including DC-DC converter to load.

This combination shows a similar deviation in the power deliverance but has a calculated efficiency of 96.6% lasting 125 s. The difference can be attributed to the power losses through the DC-DC converter, which is synonymous with its efficiency.

## 4.3 Hybrid combinations

Moving on to the consideration of 'hybrid combinations', the three power sources were combined and then tested in three combinations first, without using the DC-DC converter; second, using the DC-DC converter; and, finally, with a method of selective switching. The two rounds of different configurations described in section 2.3.4 will be discussed in cases where notable variances were observed.

### 4.3.1 Without DC-DC converter

Here, use was made of both connections 1 and 2 (see section 2.3.4), for which similar results were recorded. The results from connection 2 were then used to show the response of the system to the load. See Fig. 20.

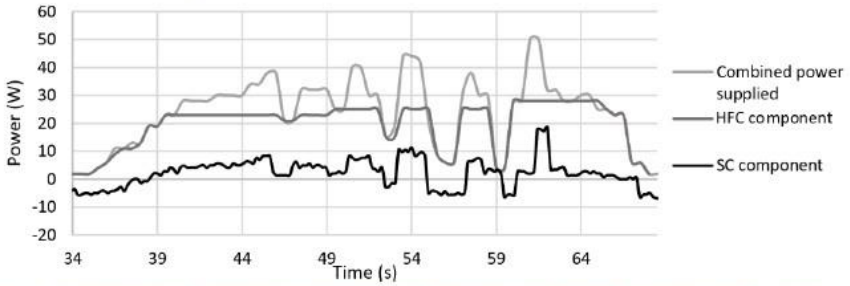


Fig. 20 – Experimental response of individual sources of hybrid system 1 to the load.

The figure shows each individual power source's contribution to the supplied load – where the system was able to provide the required load with a calculated efficiency of 97.09% and an endurance of 160 s. Here, for this combination, the SC bank has a negative power component, which is indicative of the SC receiving power from the HFC replacement. This occurs due to the system having no method of blocking power towards the SC bank; thus, when its voltage dropped below that of the HFC replacement, the SC bank was recharged. This caused the HFC replacement to use more energy to supply both the load and the SC bank.

### 4.3.2 With DC-DC converter

For this configuration, both connections 1 and 2 were used, for which similar efficiencies were recorded, in terms of providing the load. The response of connection 2 is shown in Fig. 21.

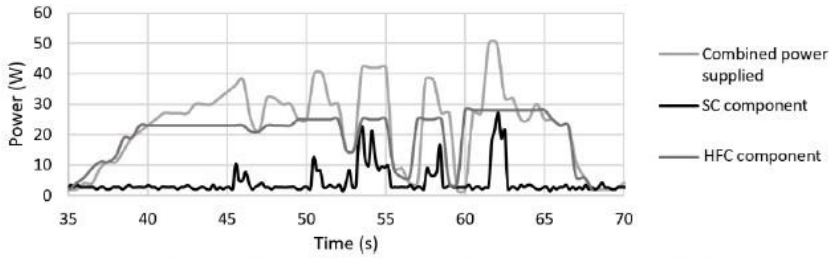


Fig. 21 – Experimental response of individual sources of hybrid system 2 to the load.

It is evident that both sources are supplying the load – with the HFC supplying the bulk and the SC bank supplementing. A calculated efficiency of 96.25% was achieved. No significant difference in the efficiencies of both the connections was observed; however, connection 1 reached a significantly greater endurance of 365 s in comparison to the 214 s obtained from connection 1.

### 4.3.3 With DC-DC converter and selective switching

For this hybrid combination, the SC bank was isolated from the HFC replacement and load for the majority of the load; it was only used when the current requirement exceeded the limits of the HFC replacement (as discussed in section 2.2). For this isolation, a relay was used, with control via an Arduino and current sensor. The response of this system to the load exhibited no notable difference in the two connections. Thus the response of connection 2 was evaluated. See Fig. 22.

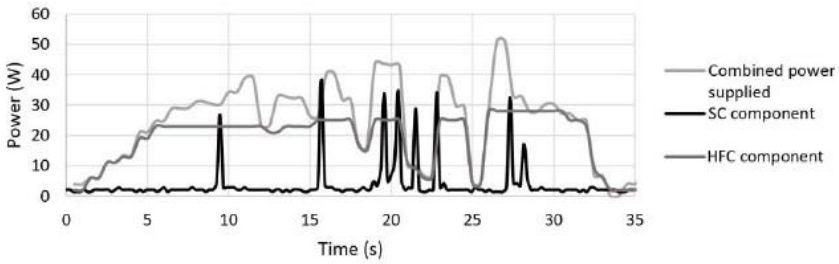


Fig. 22 – Experimental response of individual power sources of hybrid system 3 to the load.

Here, both power sources were used to supply the load and a calculated efficiency of 94.29% was achieved with a measured endurance of 223 s. It is also observed that the HFC supplied the bulk of the load and the SC bank supplemented during peak power demands.

## 5 Discussion

The results obtained from the respective combinations were processed and then combined into Table 1. The content of this table will be used to compare the different combinations to each other as well as to the results obtained through the simulations.

Table 1 – Individual source response

| | | Desired | Simulated | Experimental | Sensitivity analysis (%) |
|---|---|---|---|---|---|
| HFC system | Weight (g) | | | 1400 | |
| | Efficiency (%) | >90 | 99.47 | 76.27 | 23.32 |
| | Power provided (W) | 25.14 | 28.46 | 19.51 | 31.45 |
| | Peak power deliverance (%) | 100 | 98.41 | 67.99 | 30.91 |
| | Energy (J) | 857.14 | 852.60 | 653.74 | 23.32 |
| | Duration (s) | | 268 | 168 | 37.46 |
| SC | Weight (g) | <800 | | 571.2 | |
| | Efficiency (%) | >90 | 99.99 | 97.21 | 2.78 |
| | Power (W) | 25.08 | 23.93 | 24.68 | 3.13 |
| | Peak power deliverance (%) | | 99.99 | 97.79 | 2.20 |
| | Energy (J) | 840.27 | 837.65 | 828 | 1.15 |
| | Duration (s) | | 190 | 130 | 31.62 |
| SC-DC-DC | Weight (g) | | | 700 | |
| | Efficiency (%) | > 90 | 91.58 | 96.66 | 5.55 |
| | Energy at DC-DC input (J) | 933.64 | 657.39 | 850.24 | 29.34 |
| | Energy at DC-DC output (J) | 840.27 | 577.97 | 808.43 | 39.87 |
| | Power provided (W) | 24.76 | 22.67 | 24.13 | 6.42 |
| | Peak power deliverance (%) | | 90.80 | 97.36 | 7.22 |
| | Duration (s) | | 186 | 125 | 32.77 |
| SC-HFC | Weight (g) | | | 1900 | |
| | Combined Energy (J) | 829.54 | 900.18 | 820.26 | 8.88 |
| | SC contribution (J) | 663.63 | 314.70 | 188.39 | 40.14 |
| | HFC contribution (J) | 331.82 | 864.55 | 798.45 | 7.65 |
| | Efficiency (%) | > 90 | 99.99 | 97.09 | 2.90 |
| | Power provided (W) | 24.76 | 24.76 | 24.49 | 1.08 |
| | Peak power deliverance (%) | | 99.99 | 95.30 | 4.69 |
| | Duration (s) | | 250 | 160 | 36.00 |
| SC-HFC with DC-DC | Weight (g) | | | 2100 | |
| | Combined Energy (J) | 840.34 | 771.81 | 811.39 | 5.13 |
| | SC contribution (J) | 504.20 | 304.85 | 115.80 | 62.01 |
| | HFC contribution (J) | 336.13 | 492.46 | 715.76 | 45.34 |
| | Efficiency (%) | > 90 | 99.91 | 96.25 | 3.66 |
| | Power provided (W) | 25.09 | 25.07 | 24.22 | 3.38 |
| | Peak power deliverance (%) | | 99.54 | 95.93 | 3.63 |
| | Duration (s) | | 403 | 365 | 9.43 |
| SC-HFC with DC-DC & selective switching | Weight (g) | | | 2200 | |
| | Combined Energy (J) | 841.41 | 802.40 | 800.55 | 0.23 |
| | SC contribution (J) | 504.84 | 40.28 | 139.97 | 247.49 |
| | HFC contribution (J) | 336.56 | 714.81 | 679.04 | 5.00 |
| | Efficiency (%) | > 90 | 99.66 | 94.29 | 5.39 |
| | Power provided (W) | 25.12 | 25.03 | 23.90 | 4.53 |
| | Peak power deliverance (%) | | 98.60 | 96.92 | 1.70 |
| | Duration (s) | | 293 | 223.43 | 23.74 |

For each combination the weight, power provided, peak power deliverance, energy provided, efficiency and duration has been provided for comparison between the combinations. For combinations with multiple sources, the energy division has been included. The efficiency of each system has been calculated using the power provided

expressed as a percentage of that which was required by the load. The peak power deliverance refers to the system's ability to provide the power required at the two instances mentioned in section 2.3.3, as these were initially used to design the SC bank.

In order to compare the different combinations, a point of reference was required – here, three repetitions of the load was selected. The reason for this selection is that the SC bank without a DC-DC converter has a maximum SOC drop over three repetitions, thus all values from the table have been averaged for three repetitions of the load.

The values of the SC bank in the 'SC contribution' column refer to the energy measured at the output of the DC-DC converter, where applicable. To determine the total energy component provided by each combination that includes the DC-DC converter, the efficiency of said converter is required. As measurements of the SC bank's operation had been recorded, the energy is known at the input of the converter; thus, multiplying the latter energy with the efficiency of the converter gives their contribution to the total energy. The efficiency of the converter was calculated as 94.96%.

The final column refers to a simple sensitivity analysis that has been conducted to determine the percent deviation between the experimental and simulated results. For this, the difference between the results is expressed as a percentage of the simulated results.

The SC bank with converter test shows that the DC-DC converter reduced the efficiency and usable time of the SC bank. Hence, it can be deduced that although the converter can reduce the weight of the system it is questionable whether the decrease in efficiency and usable time will nullify this benefit. This deduction is justified based on the similar difference in efficiencies noted between the HFC-SC combinations with and without the DC-DC converter. It was also noted, in the last three combinations shown in the table, that each addition of a component to the systems led to a decrease in efficiency, attributable to power losses of each component and connecting conductors between them.

It is questionable whether the selective switching is viable as it decreased the efficiency of the system whilst increasing the weight, however, it provided better peak power deliverance and a longer duration. It was mentioned that two rounds of each test were conducted for the HFC-SC combinations and for both rounds all the combinations obtained similar efficiencies and it is thus not necessary to present both results. However, the HFC-SC combination containing the DC-DC converter (without selective switching) obtained a significant variance in the durations between the rounds – round 1 achieved 365 s of operation (with 574 s usable time for the SC bank) whereas round 2 achieved 214 s. This leads to the assumption that the self-regulation of the sources is highly dependent on the order of connection of the sources and can thus be as efficient (if not better) than a method using selective switching.

As the endurance is highly dependent on the usage of the HFC system, to increase endurance the HFC system would need to be used less and the SC bank used more. Therefore, the switching value/point can be adjusted to allow the use of the SC bank at an earlier stage. However, due to the internal resistances of each power source the system decides when each power source is utilized – it is assumed that this endurance is the best that can be achieved with the available power sources.

The first HFC-SC combination shows an improvement in the endurance of the SC bank but a decrease in that of the HFC system – this is attributed to the lack of a current blocking device prohibiting the HFC system from charging the SC bank. When the SC bank is recharged by the HFC system, the HFC system supplies a significantly larger amount of energy in a shorter period of time depleting its capacity faster. This is shown where the

combined energy of this combination is smaller than the summation of the energy provided by the two contributions.

It is also seen that all the HFC combinations with the SC increased the energy supplied in response to the load, not only in the combination but also in the HFC systems' component. Thus, the HFC system (when combined with the SC bank) responds more efficiently to the required load.

For most of the combinations the results obtained for the efficiency, peak power deliverance and duration was seen to be larger during simulations than experiments, with the exception of the SC-DC-DC combination, where only a longer duration was achieved. This is expected as the simulations cannot account for power losses caused by heat and conductor lengths. The results of the simulations were the similar to that of the experiments with where the HFC-SC with DC-DC converter achieved the longest duration and selective switching was found to have minimal benefits; the addition of components resulted in the combinations having a decrease in efficiency as well as peak power deliverance.

For the sensitivity analysis all the values obtained for the HFC system have such a large deviation (> 23%) as the HFC system used for experimentation was of a smaller capacity than that which was required by the load and simulated. This was chosen to be able to see what effect the addition of the SC bank would have. Most of the other categories achieved small deviations (< 10%), which is expected, as the simulations tend to use ideal circumstances which are not applicable during physical experimentation (i.e. power losses due to environmental temperatures, conductor losses, etc.), this argument can also be applied to the deviation shown at the DC-DC input and output and the duration deviations of the different combinations.

The SC contributions in the three SC-HFC combinations are seen to have quite a large deviation, one reason for this could be the difference in connecting conductors between the simulations and the experiments and another could be that the applied DC-DC converter has a larger internal resistance than what was used for the simulations. The latter however does not apply to the difference seen in the final SC-HFC combination, where the experimental contribution of the SCs is far larger than that achieved from the simulations. An explanation for this could be attributed to the relay used during experimentation.

During simulations the relay, as well as the SC bank, will behave ideally, whereas, when used in the experiment the relay causes the SC bank to provide a large burst of energy as soon as the relay closes, which is often larger than that which is required by the load. This is due to the low internal resistance of the SCs and is further justified when comparing Fig. 21 and Fig. 22. In Fig. 21 the SC bank is seen to provide a magnitude of power smaller (and for a period of time longer) than that of Fig. 22.

The large deviation seen for the HFC contribution of the second SC-HFC combination is attributed to the adjustment required by the HFC during experimentation due to the decreased contribution of the SC bank.

Using the results summarized in , a Ragone plot was constructed to present the effect of the SC bank on the individual systems used in this experiment. This plot is shown in Fig. 23. Comparing this achieved Ragone plot to that of Aravindan et al. [8], it is observed that the experimental HFC system utilizes a buffer battery thus affording it a larger power density and lower energy density – therefore lying in a more central position on the experimental Ragone plot as compared to the referenced Ragone plot.

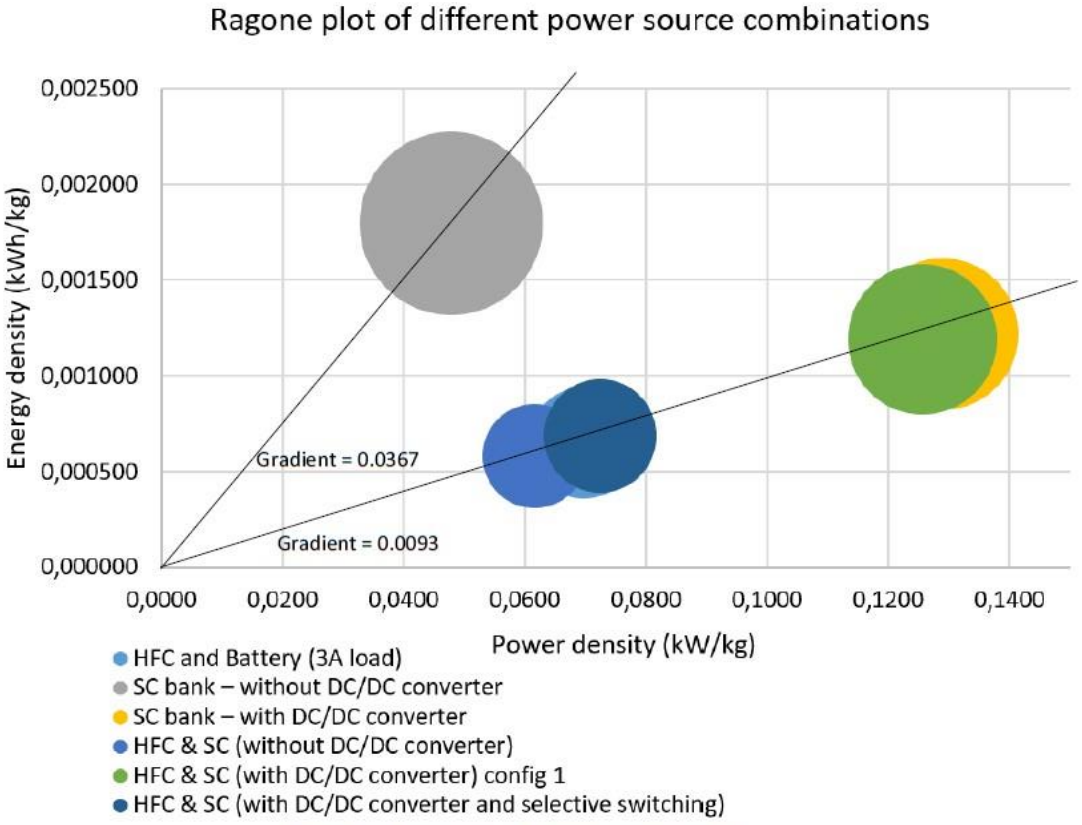


**Fig. 23 – Ragone plot of experimental results.**

A further observation is made that the SC bank (with- and without the DC-DC converter) provides a larger energy density than the HFC system in both Ragone plots – this is firstly due to the HFC system replacement chosen having a smaller capacity such that the effect of the SC bank can better be observed and secondly due to the capacity of the SC bank being designed for the available HFC system and full 1 kW load profile.

The DC-DC converter is seen to significantly improve the power density of the system with a larger factor than the decrease caused in the energy density. The graph contains two diagonal lines whose gradient is determined by dividing the y-axis by the x-axis – this delivers the endurance of each combination. It is noteworthy to bear in mind that these densities are calculated using the weight of each system and therefore the endurance is affected by this weight, with the unaided SC bank having the lowest weight of 0.5 kg.

The three HFC-SC combinations fall on the same gradient thus delivering a similar endurance with respect to the weight variance of each (see Table 1). By simply adding the unaided SC bank to the HFC system, the energy- and power densities of the HFC system experience a considerable decrease. When the DC-DC converter is included in the HFC-SC combinations a noteworthy improvement in the densities of the HFC system is observed.

As mentioned the weight of the system plays a significant role in the calculation of these densities, it is thus understandable that the addition of the SC bank caused a decrease in the densities of the HFC system, however, as the DC-DC converter and switching module add an additional weight to the unaided HFC-SC system, the increase in the densities is of much more interest and is considerably more significant than observed on the graph.

Another noteworthy observation is that of the difference between the densities achieved between the HFC-SC (with DC-DC converter) with and without selective switching.

Without selective switching the addition of the DC-DC converter no longer required the utilization of the HFC to recharge the SC bank, resultantly leading to an increase in the duration of the HFC system and both the densities.

The addition of the selective switching element increased the use of the HFC as the SC bank was only utilized at specified instances of the load – thus leading to a large reduction in the usable time of the combination. As the power and energy density are reliant on the usable duration of the system – these too where reduced.

## 6 Conclusion and Recommendations

Two different storage devices were described and used in various experiments with HFCs: an HFC and SC bank. Six different combinations of these sources were implemented and assessed for their viability. The best combination was found to be the HFC–SC combination with the DC-DC converter and without the use of selective switching, when connected with the load between the two sources. The HFC–SC combination with both the DC-DC converter and selective switching was also found to deliver desirable results; however, it is questionable as to whether the selective switching method is redundant. Furthermore, the DC-DC converter had a negative effect on the efficiency of the SC bank. It reduced the usable time by increasing the energy usage of the SC bank at the converter input whilst decreasing the deliverance of said energy to the required load at its output. The inclusion of the SC bank increased the total efficiency of the power source as a whole and allowed the HFC system to function more optimally to provide energy to the system.

The proposed project implemented a DC-DC converter with the SC bank in order to be able to use a smaller quantity of cells to match the buffer battery. This is to reduce costs and the weight of the overall system as it is designed for application on a drone. The DC-DC converter exhibited an efficiency of >94% and the optimal hybridized storage system obtained an energy density of 1.19 Wh/kg.

The results of the experiments revealed the following:

- The HFC system's response to the load requirements is improved upon the addition of the SC bank.
- The use of a DC-DC converter reduces the efficiency of the SC bank although it improves the efficiency of the HFC-SC combinations (mainly due to its unidirectional flow characteristics).
- The applied selective switching does not offer any significant improvement.
- The usable duration of the system is highly dependent on the order of connection of the power sources.

On completion of the research described, opportunities for further research and aspects to be considered in efforts to achieve further improvements were identified. These include the following.

- As the DC-DC converter is seen to decrease the efficacy of the SC bank, results should be re-examined at a higher power demand to determine whether the efficiency drop increases and whether the benefit of the reduced weight of the system justifies this increase.
- Here, experiments were conducted using an HFC system that already contains and utilizes a battery for supplementation, thus it was not possible to adjust the use of the

battery. It is therefore recommended that an HFC system be considered wherein the use of all three sources can be controlled to further improve/assess the effects thereof.

- To date, the system has only been tested in a theoretical and simulated environment using the load profile of a drone. Its evaluation should therefore be extended, to an actual drone, in order to test the actual operation in a real environment.
- SCs are very useful for storing reverse/negative energy, such as that which is present during braking or when a drone decreases altitude. This was evident in our hybrid test without the DC-DC converter. As this current system was not applied to an actual drone, it is recommended that, if the system is integrated with a drone, this concept be applied – it could lead to a further increase in the usable time. For this application a bi-directional converter could be used that only allows current flow toward the SC bank when the system experiences negative energy from the load.
- The system utilized selective switching when the power exceeded 35 W – this value was seen to be too low to benefit the HFC system and reduce its use. Thus, it is recommended that if selective switching be further investigated that the point of switching be adjusted.
- A mechanical relay was used to apply the selective switching – a solid state Relay could be used to reduce weight and decrease interference in the external circuit caused by the coil.

## Acknowledgements

The authors would like to thank DST HySA Infrastructure Center of Competence for providing the necessary funding and equipment.

## References

[1] Lee J, Kim K, Yoo S, Chung AY, Lee JY, Park SJ, et al. Constructing a reliable and fast recoverable network for drones. 2016 IEEE Int. Conf. Commun., IEEE; 2016, p. 1–6. https://doi.org/10.1109/ICC.2016.7511317.

[2] Yoo S, Kim K, Jung J, Chung AY, Lee J, Lee SK, et al. A Multi-Drone Platform for Empowering Drones' Teamwork. Proc. 21st Annu. Int. Conf. Mob. Comput. Netw. - MobiCom '15, New York, New York, USA: ACM Press; 2015, p. 275–7. https://doi.org/10.1145/2789168.2795180.

[3] Jawad AM, Jawad HM, Nordin R, Gharghan SK, Abdullah NF, Abu-Alshaeer MJ. Wireless Power Transfer With Magnetic Resonator Coupling and Sleep/Active Strategy for a Drone Charging Station in Smart Agriculture. IEEE Access 2019;7:139839–51. https://doi.org/10.1109/ACCESS.2019.2943120.

[4] Lee D, Zhou J, Lin WT. Autonomous battery swapping system for quadcopter. 2015 Int. Conf. Unmanned Aircr. Syst., IEEE; 2015, p. 118–24. https://doi.org/10.1109/ICUAS.2015.7152282.

[5] Rucco A, Sujit PB, Aguiar AP, de Sousa JB, Pereira FL. Optimal Rendezvous Trajectory for Unmanned Aerial-Ground Vehicles. IEEE Trans Aerosp Electron Syst 2018;54:834–47. https://doi.org/10.1109/TAES.2017.2767958.

[6] Fravolini ML, Ficola A, Campa G, Napolitano MR, Seanor B. Modeling and control issues for autonomous aerial refueling for UAVs using a probe–drogue refueling system. Aerosp Sci Technol 2004;8:611–8. https://doi.org/10.1016/j.ast.2004.06.006.

[7] Lu M, Bagheri M, James AP, Phung T. Wireless Charging Techniques for UAVs: A Review, Reconceptualization, and Extension. IEEE Access 2018;6:29865–84. https://doi.org/10.1109/ACCESS.2018.2841376.

[8] Aravindan V, Gnanaraj J, Lee Y-S, Madhavi S. Insertion-Type Electrodes for Nonaqueous Li-Ion Capacitors. Chem Rev 2014;114:11619–35. https://doi.org/10.1021/cr5000915.

[9] Alwateer M, Loke SW, Zuchowicz AM. Drone services: issues in drones for location-based services from human-drone interaction to information processing. J Locat Based Serv 2019;13:94–127. https://doi.org/10.1080/17489725.2018.1564845.

[10] Ruan L, Wang J, Chen J, Xu Y, Yang Y, Jiang H, et al. Energy-efficient multi-UAV coverage deployment in UAV networks: A game-theoretic framework. China Commun 2018;15:194–209. https://doi.org/10.1109/CC.2018.8485481.

[11] Claesson A, Svensson L, Nordberg P, Ringh M, Rosenqvist M, Djarv T, et al. Drones may be used to save lives in out of hospital cardiac arrest due to drowning. Resuscitation 2017;114:152–6. https://doi.org/10.1016/j.resuscitation.2017.01.003.

[12] Loke SW, Alwateer M, Abeysinghe Achchige Don VSA. Virtual Space Boxes and Drone-as-Reference-Station Localisation for Drone Services. Proc. 2nd Work. Micro Aer. Veh. Networks, Syst. Appl. Civ. Use - DroNet '16, New York, New York, USA: ACM Press; 2016, p. 45–8. https://doi.org/10.1145/2935620.2935627.

[13] Shukla A, Xiaoqian H, Karki H. Autonomous tracking and navigation controller for an unmanned aerial vehicle based on visual data for inspection of oil and gas pipelines. 2016 16th Int. Conf. Control. Autom. Syst., IEEE; 2016, p. 194–200. https://doi.org/10.1109/ICCAS.2016.7832320.

[14] Bacco M, Berton A, Ferro E, Gennaro C, Gotta A, Matteoli S, et al. Smart farming: Opportunities, challenges and technology enablers. 2018 IoT Vert. Top. Summit Agric. - Tuscany (IOT Tuscany), IEEE; 2018, p. 1–6. https://doi.org/10.1109/IOT-TUSCANY.2018.8373043.

[15] Ding G, Wu Q, Zhang L, Lin Y, Tsiftsis TA, Yao Y-D. An Amateur Drone Surveillance System Based on the Cognitive Internet of Things. IEEE Commun Mag 2018;56:29–35. https://doi.org/10.1109/MCOM.2017.1700452.

[16] Pan ZF, An L, Wen CY. Recent advances in fuel cells based propulsion systems for unmanned aerial vehicles. Appl Energy 2019;240:473–85. https://doi.org/10.1016/j.apenergy.2019.02.079.

[17] Lee B, Kwon S, Park P, Kim K. Active power management system for an unmanned aerial vehicle powered by solar cells, a fuel cell, and batteries. IEEE Trans Aerosp Electron Syst 2014;50:3167–77. https://doi.org/10.1109/TAES.2014.130468.

[18] Das T, Snyder S. Adaptive Control of a Solid Oxide Fuel Cell Ultra-Capacitor Hybrid System. IEEE Trans Control Syst Technol 2013;21:372–83. https://doi.org/10.1109/TCST.2011.2181514.

[19] Schroth F. Drone Energy Sources – Pushing the Boundaries of Electric Flight. Drone Ind Insights 2017. https://droneii.com/drone-energy-sources (accessed November 27, 2020).

[20] Meacham JR, Jabbari F, Brouwer J, Mauzey JL, Samuelsen GS. Analysis of stationary fuel cell dynamic ramping capabilities and ultra capacitor energy storage using high resolution demand data. J Power Sources 2006;156:472–9. https://doi.org/10.1016/j.jpowsour.2005.05.094.

[21] Bauman J, Kazerani M. A Comparative Study of Fuel-Cell–Battery, Fuel-Cell–Ultracapacitor, and Fuel-Cell–Battery–Ultracapacitor Vehicles. IEEE Trans Veh Technol 2008;57:760–9. https://doi.org/10.1109/TVT.2007.906379.

[22] Thounthong P, Chunkag V, Sethakul P, Davat B, Hinaje M. Comparative Study of Fuel-Cell Vehicle Hybridization with Battery or Supercapacitor Storage Device. IEEE Trans Veh Technol 2009;58:3892–904. https://doi.org/10.1109/TVT.2009.2028571.

[23] BMPower. BMPower Range of products n.d. https://bmpower.us/ (accessed May 18, 2020).

[24] Urone PP. College Physics. 2nd ed. Sacramento, California: Brooks/Cole; 2001.

[25] Xun Q, Liu Y, Holmberg E. A Comparative Study of Fuel Cell Electric Vehicles Hybridization with Battery or Supercapacitor. 2018 Int. Symp. Power Electron. Electr. Drives, Autom. Motion, IEEE; 2018, p. 389–94. https://doi.org/10.1109/SPEEDAM.2018.8445386.

[26] Gao W. Performance comparison of a fuel cell-battery hybrid powertrain and a fuel cell-ultracapacitor hybrid powertrain. IEEE Trans Veh Technol 2005;54:846–55. https://doi.org/10.1109/TVT.2005.847229.

[27] Schupbach RM, Balda JC, Zolot M, Kramer B. Design methodology of a combined battery-ultracapacitor energy storage unit for vehicle power management. PESC Rec - IEEE Annu Power Electron Spec Conf 2003;1:88–93. https://doi.org/10.1109/pesc.2003.1218278.

[28] Schupbach RM, Balda JC. The role of ultracapacitors in an energy storage unit for vehicle power management. IEEE Veh Technol Conf 2003;58:3236–40. https://doi.org/10.1109/vetecf.2003.1286246.

[29] Pede G, Iacobazzi A, Passerini S, Bobbio A, Botto G. FC vehicle hybridisation: an affordable solution for an energy-efficient FC powered drive train. J Power Sources 2004;125:280–91. https://doi.org/10.1016/j.jpowsour.2003.07.018.

[30] Nilsson JW, Riedel SA. Electric circuits. 9th ed. New Jersey: Pearson; 2011.

[31] Maxwell Technologies. 3.0V 3400F Ultracapacitor Cell. Maxwell Technol Inc 2020:1–5. https://www.maxwell.com/products/ultracapacitors/.

[32] Maxwell Technologies. 2.7V 360F Ultracapacitor Cell. Maxwell Technol 2020:2–3. https://www.maxwell.com/images/documents/2_7_360F_ds_3001963_datasheet.pdf (accessed November 27, 2020).

[33] Barker D, Walsh FC. Applications of Faraday's Laws of Electrolysis in Metal Finishing. Trans IMF 1991;69:158–62. https://doi.org/10.1080/00202967.1991.11870915.